The University of Nottingham

Faculty of Engineering

Department of Civil Engineering

Institute of Engineering Surveying and Space Geodesy

The use of oblique and vertical images for 3D urban modelling

Ahmed M. Hamruni

BSc, MEng, MSc

Thesis submitted to the University of Nottingham

for the degree of Doctor of Philosophy

March, 2010

ABSTRACT

Three-dimensional data are useful for various applications such as visualization for planning, simulation for training and environmental studies, presentations, decision making and many more.

The existing methods of texturing 3-D city models use conventional vertical imagery and libraries of generic textures which are sufficient for some applications of 3-D models like training simulation, gaming, and telecommunication planning. However, the needs for photo-realistic, modelling of the complete details, and geometrically accurate 3-D models are growing rapidly in several fields, especially in engineering and cultural heritage documentation. Photorealism and better details can be achieved through using terrestrial imagery but it is a very time-consuming process particularly in large modelling projects. It is possible to improve efficiency by image capture from a moving ground based vehicle but this requires an extra process in the work flow if the initial modelling has been undertaken by aerial photogrammetric processes.

Pictometry imagery has been used for visual inspection especially in life-saving situations due to the fact that the Pictometry aerial imagery contains oblique (angled) images which provide better view and greater detail. The more conventional method of collecting aerial images with for example the UltraCamD, can also provide excellent views of roof tops and some of the building facades when located away from the nadir on the images.

This research explored the geometry of the Pictometry images (vertical and oblique) and the possibility of using this imagery in 3-D modelling to produce photo-realistic and accurate models. In addition, merging terrestrial imagery with Pictometry imagery to get more ground level details has been investigated in this research.

All work has been carried out using the available software packages at the Institute of Engineering Surveying and Space Geodesy (IESSG) and using data provided by Blom Aerofilms Ltd.

The results of the aerial triangulation of different Pictometry blocks showed that high quality image measurements have been achieved for all the image blocks. The use of indirect georeferencing produced good quality coordination of ground points. The use of in-flight control has produced good results with additional parameters which mitigate any effects of systematic errors. Good quality AT results have been achieved using minimum ground control which reduces a lot of field work and hence time and money.

Extraction of 3D geometry for all buildings in the study area has been performed using both vertical Pictometry imagery and UltraCamD imagery. The polygons extracted from the UltraCamD images have been used as a bench mark (BM) to check the accuracy of polygons extracted from Pictometry.

Planimetric and height comparisons of the extracted features from Pictometry system with the BM results have been performed. The results showed that the Pictometry imagery produced good results especially in plan components taking into consideration the differences in the resolution, GSD, and the flying height between the two camera systems.

The results of automatically texturing the models have shown that using the vertical blocks (UltraCamD or Pictometry) produced very good roof textures but on the other hand produced less quality facades. The use of the Pictometry oblique block in texturing has produced very good facades but in some instances not such good quality roof textures.

The successful combining of vertical and oblique Pictometry images provided an excellent opportunity to produce an efficient method of high quality urban model texturing. The integration of terrestrial images of building facades (whose texture needs enhancement) with the combined aerial imagery block has been successfully and automatically performed. The results are much better than the results obtained by manual texturing which not only depends upon the experience and skill of the operator but is also time consuming and laborious.

ACKNOWLEDGEMENTS

In the name of ***ALLAH***, the most Gracious, the most Merciful

Firstly, and most importantly, thanks to ***ALLAH*** for making all this possible, ***HE*** is truly magnificent!

Secondly, I would like to acknowledge the financial support of the Libyan government and Blom Aerofilms Ltd. for providing the aerial photography of test sites.

I am indebted to my research supervisors, Associate Professor Martin J. Smith and Associate Professor Richard M. Bingley, from the IESSG for the advice, support and encouragement received throughout the research. I am also grateful to the internal assessors, Associate Professor Gethin W. Roberts and Dr. David Park, for their useful suggestions and recommendations. Without their constructive criticism, the past 3 years would not have been so productive and successful.

My extraordinary gratitude goes to Dr. Nikolaos Kokkas for his help, support and expert advice on mastering the used software.

Furthermore I would like to thank Dr. Khaldoun Qtaishat, Dr. Ahmad Taha and PhD student El-Said Zahran for all their advice and support, and other members of the IESSG, who helped and talked to me whenever I was stuck.

Finally I would like to dedicate this thesis to my parents, wife and children who I am eternally grateful to for all their patience and support.

TABLE OF CONTENTS

LIST OF FIGURES

LIST OF TABLES

LIST OF ABBREVIATIONS

A set of definitions and terminology explanations are provided for purposes of completeness and to introduce the author's meaning of a number of terms used throughout this Thesis. These are:

2D:	2-Dimensional
3D:	3-Dimensional
AP:	Additional Parameters
AT:	Aerial Triangulation
CAD:	Computer Aided Design
CCD:	Charged Coupled Device
CCPs:	Check Control Points
DEM:	Digital Elevation Model
DG:	Direct Georeferencing
DGPS:	Differential Global Positioning
DPW:	Digital Photogrammetric Workstation
DSM:	Digital Surface Model
DTM:	Digital Terrain Model
EFS:	Electronic field study
EOP:	Exterior Orientation Parameters
GCPs:	Ground Control Points
GIS:	Geographic Information System
GPS PPP:	GPS Precise Point Positioning
GSD:	Ground Sample Distance
IBM:	Image Based Modelling
IGS:	International GNSS Service
IMU:	Inertial Measurement Unit
INS:	Inertial Navigation System
LGO:	Leica Geo Office
LiDAR:	Light Detection And Ranging
LoD:	Level of Detail
LPS:	Leica Photogrammetric Suite
ORIMA:	ORIentation Management software
RBM:	Range Based Modelling
RMSE:	Root Mean Square Error
TIN:	Triangulated Irregular Network
VRML:	Virtual Reality Modelling Language

CHAPTER 1: INTRODUCTION

This chapter reflects the objectives of this thesis. It gives an overview of the related works, the aims, objectives, and a brief description of the thesis breakdown.

1.1 Background and motivation

The primary objective of photogrammetry is to generate spatial and descriptive information from two-dimensional imagery. There is an increasing demand from a growing range of applications for 3D computer digital models of our environment. The application defines the level of detail required in the 3D model. This is comparable to the traditional concept of the scale of mapping required to ensure fitness-for-purpose. In many applications there is no need for a geometrically correct 3D model of an environment as there is only a need to view an area of interest to support a decision making process. A big advantage of the 3D model is its convincing effect on users for a future decision making processes (Tunc et al., 2004). This has major financial benefits as the creation of 3D models is a costly process. However, a geometrically accurate 3D landscape model may be necessary in some cases particularly where for example; there is a need for the integration with engineering design information and for cultural heritage documentation.

Photorealism and high levels of detail can be achieved through using terrestrial imagery but it is very time-consuming process particularly in large modelling projects (Meng and Forberg, 2007). It is possible to improve efficiency by image capture from a moving vehicle (mobile mapping) but this requires an extra process in the work flow if the initial modelling has been undertaken by aerial photogrammetric processes (Smith et al., 2009).

To enable visualization, particularly in urban areas with deep building canyons, the most appropriate viewing angle for 3D modelling is often from the air looking obliquely at the ground and facades of the surrounding buildings. Pictometry vertical and oblique images are an established technique for visual inspection of the landscape as they provide a good view and high

level of detail of not just the roof tops but also many facades of the buildings (Pictometry, 2008).

The more conventional method of collecting aerial images with, for example, the UltraCamD, can also provide excellent views of roof tops and some of the building faces when located away from the nadir on the images. Combining the imagery provides an opportunity to maximise and optimise the capture of 3D urban models from aerial imagery.

The revolutionary Pictometry oblique imagery can be used for texture mapping large models quickly and can enable photorealism. Terrestrial imagery might be combined with oblique imagery in certain areas to give better quality models, particularly when 'ground level' viewing of the models is required.

1.2 Aim and objectives

Pictometry imagery has been used to provide visual inspection of places of interest. The overall aim of this research is to investigate the geometric potential for using Pictometry imagery to provide 3D city modelling and texturing. Most people view the world from the ground, so it is important to have good ground level models. Pictometry vertical and oblique imagery may not be able to produce good ground level 3D models because of its aerial perspective, therefore terrestrial imagery will be considered to fulfil this requirement.

This research aim will be assessed through investigating the following objectives:

1. Basic image orientation and geometry through exploring the aerial triangulation (AT) on vertical and oblique imagery. The effect of using different ground control points (GCPs) and check control points (CCPs) combinations will be explored. In addition, 4 different solutions will be used to assess the quality of AT as well as investigating the use of minimum control.
2. The possibility of combining the vertical imagery (Pictometry or UltraCamD) and oblique Pictometry images in one block through performing AT.
3. The use of oblique imagery alone to extract detailed 3-D models.

4. The use of the combined blocks of vertical and oblique images in texture mapping the models automatically instead of using the vertical block to texture the roofs automatically and then using the oblique block to texture the facades manually.
5. The possibility of integrating terrestrial images with the combined aerial images block and then using the block in automatic texture mapping of the models.
6. The accuracy of the 3D models using bench mark (BM) models extracted from the conventional orthogonal imagery captured by the UltraCamD camera.

1.3 Methodology

To fulfil the above objectives the following research methodology is considered to be necessary:

i. A literature review of principles and the work by others in the different subjects covered during this research; in particular processing of oblique imagery and using this kind of imagery in extracting and texturing 3-D models (all objectives).

ii. Setting up a test site by establishing a good network of GCPs using static GPS to obtain the required accuracy (objective 1).

iii. Creating individual photogrammetric blocks of vertical and oblique Pictometry images and UltraCamD images (objective 1).

iv. Creating combined photogrammetric blocks of Pictometry images, (consisting of 5 different kinds of images which are: vertical images, oblique images taken from south, north, west, and east) and of UltraCamD and oblique images (objective 2)**.**

v. Processing the individual and combined blocks using the available software in the IESSG; Leica photogrammetric Suite software (LPS) and ORIentation Management software (ORIMA), (objectives 1 and 2).

vi. Extracting 3D geometry of buildings and texture mapping the 3D models using vertical and oblique Pictometry imagery as well as the UltraCamD images (objectives 3 and 4).

vii. Using terrestrial imagery to texture facades that need some enhancement after using Pictometry imagery (objective 5).

viii. Comparing the results of using Pictometry imagery with 3D models of the campus extracted from UltraCamD imagery (objective 6).

1.4 Contribution to knowledge

The recent rapid development of multisensor technologies has made it possible to construct detailed 3D city models using multiple small-format digital cameras. The multiple-camera arrangement acquires one vertical and four oblique colour photos simultaneously which can be a cost effective alternative to using terrestrial images in texture mapping.

Oblique images have historically been used for visualisation and interpretation purposes, rather than for metric applications. Exceptions are the military sector and archaeology where oblique images have long been standard for reconnaissance purposes (Smith, 1989). However, until recently digital oblique images were generally outside of the focus of photogrammetrists. They can thus be truly regarded as a new data source for photogrammetry and GIS.

The scientific contribution of this research comes from the creation and analysis of different photogrammetric blocks of images that used the relatively new imaging system, Pictometry, which combines five cameras in one cluster producing vertical images as well as oblique images from the 4 compass directions.

The images are provided with information so that potentially, efficient photogrammetric processing can take place. The quality of the direct measurement of the position and orientation of the images will have a direct influence on the quality of the 'mapping'; 3D ground point coordination. There are a number of issues related to the use of this kind of imagery for mapping purposes, issues such as; camera geometry and calibration, aerial triangulation quality with and without the directly measured parameters and choice of images for feature extraction and mapping.

As yet, there have been no studies reported in the literature investigating the geometry of Pictometry imagery. Therefore, investigating the orientation and geometry of oblique and vertical digital aerial images from the Pictometry system is of crucial importance to assess the potential use of images captured using this system in 3D urban modelling.

A review of the literature did not identify any studies investigating the combining of this type of vertical and oblique images in one photogrammetric block. Automatic texturing of roof tops and facades of buildings will be performed in one step using the combined block of both vertical and oblique images. Furthermore, to take advantage of the conventional well-established UltraCamD imaging system in 3D city urban modelling, images from this system will be combined with the oblique images in one block. In addition, a new approach of integrating terrestrial images with the aerial images photogrammetric block will be introduced. This integrated block will be used in automatic texture mapping of building facades and roof tops.

Research into current methods for 3D modelling has revealed that no critical comparison between the two imaging systems (UltraCamD and Pictometry) has yet been performed in terms of extracted geometry.

1.5 Organization of the thesis

The thesis outline has been chosen to guide the reader through the stages of this research. This thesis consists of 8 chapters which are organized such that the reader is first presented with background theory to provide an understanding of the subject matter; then an outline of the sensors used, study area and data sets; next a demonstration of the work performed to fulfil the aims and objectives of the research; analysis, discussions and then conclusions. A brief summary of the contents of each of the remaining 7 chapters is outlined in the following paragraphs.

Chapter 2 consists of an introduction to the some of the applications of 3D models, as 3D city models have been increasingly applied as a communication language and working tools in a growing number of fields. It then provides comprehensive literature review containing the techniques used for obtaining the 3D models and texture mapping them. A brief description of the concept of 'level of detail' and different levels of detail will be introduced in this chapter. This chapter will also introduce AT and the benefits achieved when performing the AT. Finally, a summary of the chapter contents will be given.

Chapter 3 will highlight some of the benefits of digital photogrammetry. Moreover, this chapter will provide an overview of different kinds of digital aerial cameras available in the market. In addition, it will describe in detail the

characteristics of the data collections systems used to capture the aerial photography used in this research. It will also describe the operating concepts of the Pictometry imaging system and the procedure of performing measurements on oblique images.

Chapter 4 serves the purpose of introducing the test sites used for the trials, the main campus of the University of Nottingham and a small part of Nottingham city centre. In addition, this chapter gives an overview of the data provided for the purpose of this research, which has been collected using the sensors described in the previous chapter.

Chapter 5 presents and analyses the procedures and parameters used to setup the different photogrammetric blocks of different imagery, which will be used to assess the geometry of that imagery, by applying the methodology presented in Chapter one. Furthermore, the AT results and the analysis of these results will be introduced in this chapter. The use of minimum control instead of direct georeferencing and a summary of the chapter will be presented.

Chapter 6 begins with a detailed description of the process followed for buildings reconstruction in this research using Pictometry and UltraCamD blocks. The accuracy of the 3D geometric models will then be discussed. This chapter also describes in detail the texture mapping process using the available photogrammetric blocks. Finally, a summary of the results will be given.

Chapter 7 will explain a new method of integrating terrestrial imagery with aerial images photogrammetric blocks, as using terrestrial imagery is inevitable to overcome the limitations of aerial imagery in texture mapping application scenarios.

Chapter 8 is dedicated to summarize the findings and to suggest improvements as well as identifying and recommending possible areas for further research.

CHAPTER2: BACKGROUND

Site recording and modelling has been an important topic in photogrammetry from its very beginning in the middle of the 19th century. Since then technologies have changed several times fundamentally (Gruen, 2000). The recent rapid development of multisensor and multimedia technologies has made it possible to construct and visualise detailed 3D models of our built environment. Three-dimensional modelling of objects and scenes is an intensive and long-lasting research problem in the computer graphic, vision and photogrammetric communities (El-Hakim and Remondino, 2006).

For 3D city models, the most important features are buildings which have to be acquired in densely built-up areas, centres of cities and towns. In Europe, very complex, highly irregular house and roof patterns are common, many dating back to the late medieval ages. Figure 2.1 shows some of the different roof patterns that are present in the study area. In this case, automated procedures do not give the desired results, and human intervention is urgently needed (Sinning-Meister et al., 1996). Other features that might be included in 3D city models are street-level scenes such as roads, urban vegetation, trees, and cars.

This chapter begins with the importance of 3D models, as 3D city models have been increasingly applied as communication language and working tools in a growing number of fields, and then followed by the techniques used for obtaining the 3D models. A brief description of the concept of 'level of detail' and different levels of detail will be introduced in this chapter. Finally, a summary of the chapter contents will be given.

2.1 Importance of 3D models

The needs for 3D city models are growing and expanding rapidly in a variety of applications in recent years. In a steady shift from traditional 2D-GIS toward 3D-GIS, an increasing amount of accurate 3D city models have become required to be produced in a short period of time and provided widely on the market.

Figure 2.1: Examples of different roof patterns in the study area

The biggest advantage of the 3D model is its mobility and its convincing effect on users for future decision making processes. It has the potential to be shown everywhere and allows people who cannot or do not want to travel to get to know the region (Tunc et al., 2004).

Digital 3D models have some advantages over traditional ways of geospatial data handling (Lerma et al., 2004):

- Due to its digital storage, models can be supplemented and reconstructed into different environments by means of importing and exporting tools.
- Realistic presentations of the model can be produced by using some kind of interactive animation and simulation environments (for example, VRML or X3D).
- Last but not least, digital models can always be updated and rebuilt individually or just be considered as a part of a complex model.

Originally, simulations for propagation of electromagnetic waves (telecommunication planning) were thought to be one of the major application areas. These are used by network operators for the planning of antenna locations, figure 2.2.

3D-data seem to be useful for other various applications such as:

- 3D visualization for city planning, design, monitoring, and general city-related decision making.

- 3D visualization for presentations and public display.
- Geo-referenced search capabilities for locations and/or location related information.
- Precise measurements of distance, lines-of-sight, surfaces and volumes throughout the 3D-model.
- Seamless integration with customized tools and databases such as CAD and GIS.
- Analysis of traffic flow, pedestrian patterns, zoning, land-use and special restrictions.
- Leasing, sales and marketing information analysis of real estate, figure 2.3.

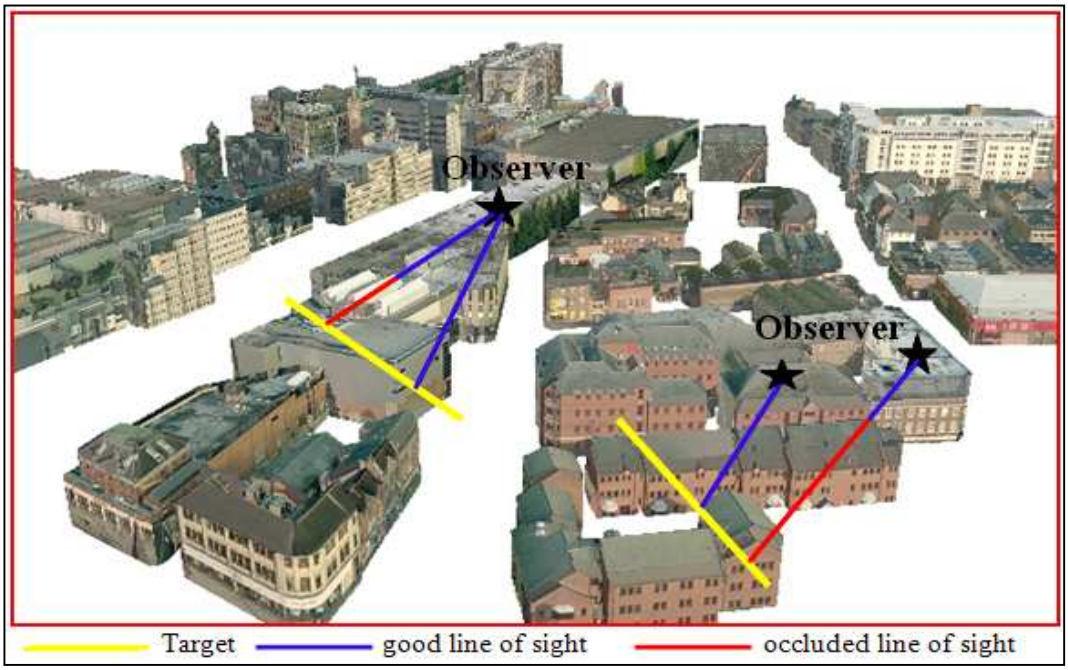

Figure 2.2: Line of sight simulations for planning locations of telecommunication antennae, the 3D model is for part of Nottingham city centre.

Figure 2.3: advertising service provides a standard gray, untextured 3D model, left, or model of your property textured with detailed terrestrial images, adapted and reproduced from Cybercity(2009).

- Applications for planning, managing, monitoring, training and simulation of security-related scenarios such as special events, emergency planning, and crime scenario mapping, figure 2.4.
- Pollution distribution analysis, figure2.5.

Figure 2.4: Different scenarios of simulation training; top left police car in emergency rides, top right driving simulation of truck, bottom left nautical simulation, and bottom right emergency scenario in a tunnel, adapted and reproduced from Bildstein (2005).

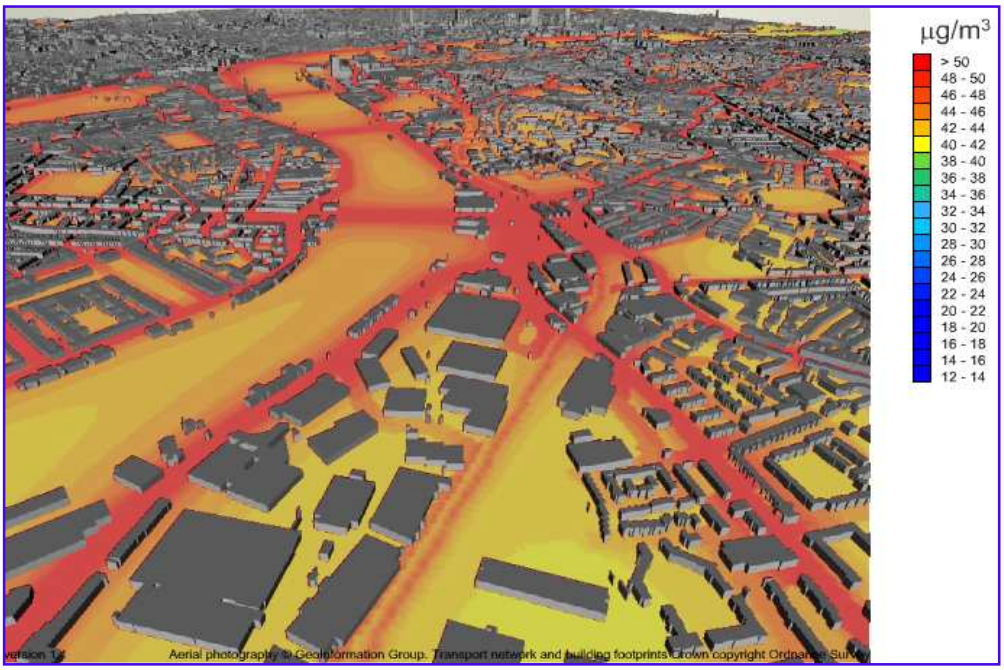

Figure 2.5: map of air pollution in London, adapted from (http://www.londonair.org.uk/london/asp/virtualmaps.asp)

- Customized training and building scenarios based upon the city model.
- Integration with custom 3D indoor models of real estate sites or buildings.
- Cultural heritage documentation, figure 2.6.

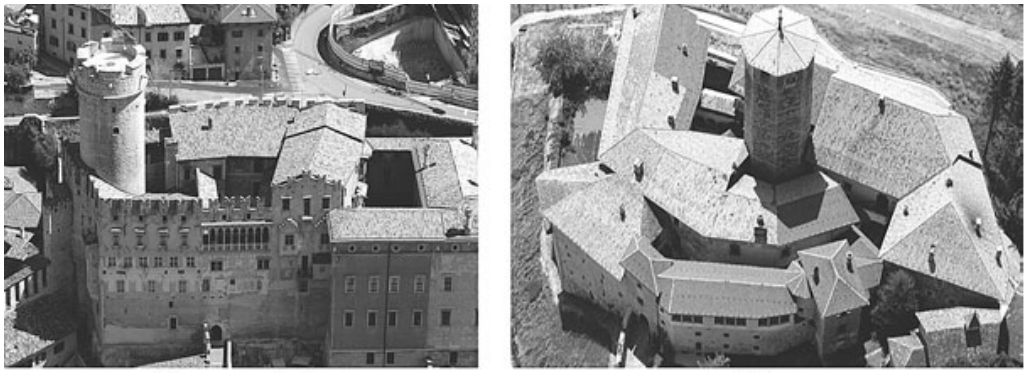

Figure 2.6: Selected castles of Trentino, Italy, adapted from El-Hakim et al. (2007)

- Google Earth and Microsoft Virtual Earth.
- Disaster simulation such as floods, hurricanes and earthquakes, figure 2.7.

Although these application fields share the common demand for 3D information, their special requirements differ considerably with regard to precision, actuality, spatial coverage and interoperability. In other words, what is needed is not one single solution, but rather a number of 3D city models, which can be:

(1) Different resolutions (level of detail) of a city model,

(2) Different updates of a city model, or

(3) Interoperable models of different cities spread over a large region.

While cases (2) and (3) deal with the research issues of spatial-temporal data acquisition and modelling, case (1) focuses on the study of 3D objects in the scale space (Meng and Forberg, 2007).

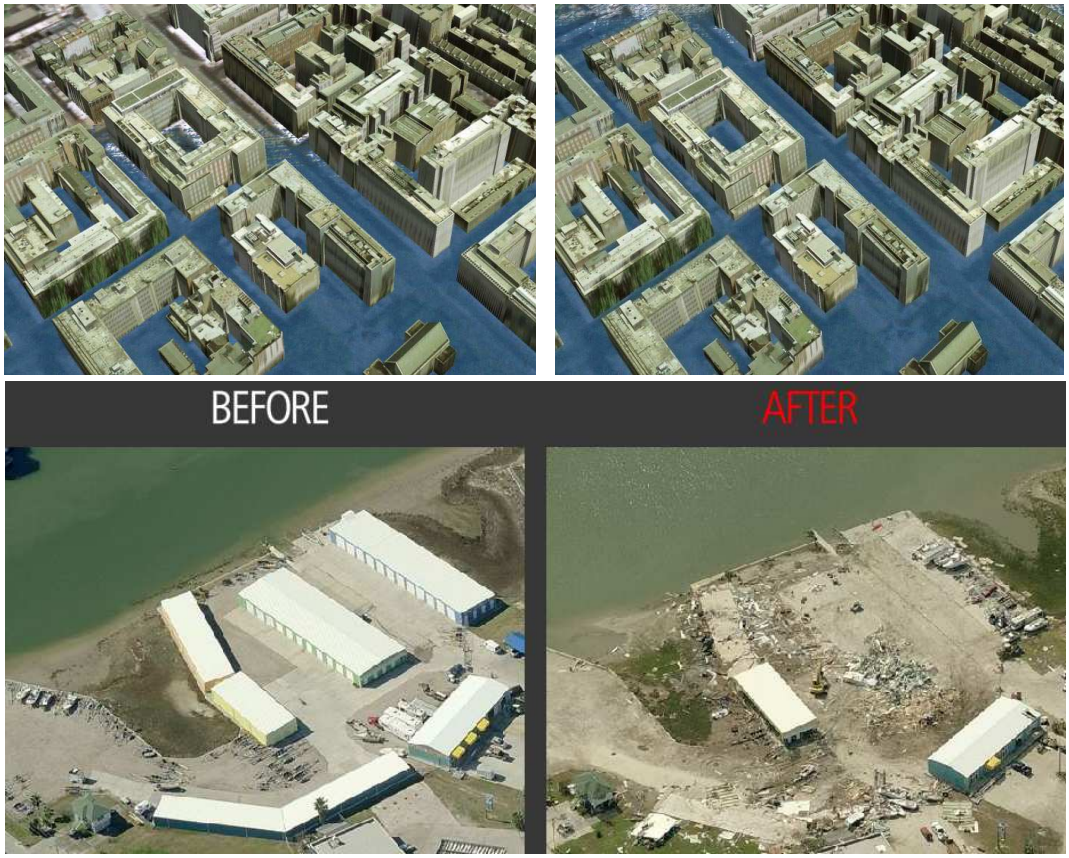

Figure 2.7: Top, visualization of flood analysis in London, UK, flooding levels are 1.8m and 2m left and right pictures respectively, adapted from Kokkas (2008), bottom, buildings before and after hurricane Ike, adapted from Pictometry (2008)

2.2 Reconstruction Techniques of 3D building geometry

In order to generate 3D city models, a semi-automatic or automatic feature extraction procedure is applied to derive the roof structure from the available data source, e.g. stereo aerial images. Once the roof structures are measured, the objects are intersected with the DTM to generate the walls of the buildings.

Traditional reconstruction methods of generating 3D city models had required enormous amount of time for manual work. Ordinary modelling methods of 3D city used to be as following (Tunc et al., 2004):

1. Scan map and get digital image.
2. Trace digital image of map with 3D CAD software resulting in 2D data of buildings outlines.

3. Manually make 3D modelling of buildings with 3D CAD by extruding 2D outlines to building height, and/or modelling manually detailed 3D geometry referring to drawings and photographs also with 3D CAD.

This is a labour-intensive endeavour where engineering plans or drawings plus surveying and/or standard photogrammetry techniques are employed followed by importing the measurements into a CAD system to create a 3D model. The results are often unsatisfactory in appearance and seem computer-generated rather than realistic.

Madani (2004) stated that the procedure steps to generate 3D models can be summarised as following, figure 2.8:

1- Data collection to cover all required details.
2- Generation of 3D points or range images.
3- Registration of the generated 3D points or range images in one coordinate system.
4- Creation of geometric model (usually) at various resolutions for level of detail hierarchy.
5- Texture mapping the geometric 3D model for realistic appearance.
6- Rendering of the final product at acceptable speed.

At the moment it can safely be said that, for all types of objects and sites, there is no single modelling technique is able to satisfy all requirements of high geometric accuracy, portability, full automation, capture of all details, photo-realism and low cost as well as application flexibility and model size efficiency (El-Hakim and Remondino, 2006).

Large-scale 3D urban modelling systems acquire most of their data from ground image sensors and traditional aerial image sensors, aerial active sensors, ground-based laser range-scanning, and existing 2D footprint data from GIS or CAD data. Each of these data sources, figure 2.9, and their corresponding modelling techniques has advantages and disadvantages. For example, images provide texture and colour information with high accuracy, making them necessary for texture data and appealing for extracting small model features. LiDAR data samples, on the other hand, are dense 3D representations of building and terrain surfaces. Fusing these data sources can generate more accurate and automatic urban models.

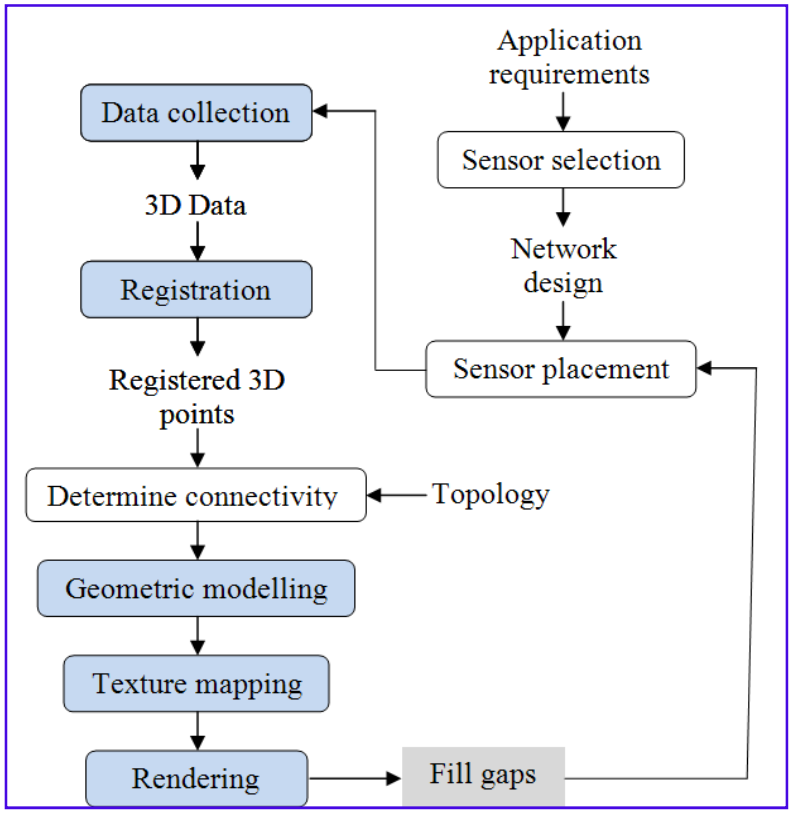

Figure 2.8: Simplified block diagram of the main steps in the creation of 3D virtual environments, adapted from Madani, (2004).

Independent of the sensor (digital camera or laser scanner) used for surveying of an object; the whole modelling process can be divided into three phases: data acquisition, data orientation, and the actual modelling (Ressla et al., 2006).

Regarding the data acquisition, we have nowadays at our disposal a vast collection of appropriate and efficient data acquisition tools: high resolution satellites, large format digital aerial cameras, hyper spectral sensors with several hundreds of channels, interferometric radar from space and aerial platforms, laserscanners of aerial and terrestrial type, partially with integrated cameras, model helicopters with off-the-shelf digital cameras, panoramic cameras and a large number of customer still video cameras. This is augmented by GPS/IMU systems for precise navigation and positioning to make the data orientation more efficient and easier (Gruen, 2005).

Automated and semi-automated algorithms allow us to process the data (modelling) more efficiently than ever before and Spatial Information System technology provides for data administration, analysis and other functions of

interest. In addition, visualization and animation software is becoming affordable at better functionality and lower costs (Gruen, 2005).

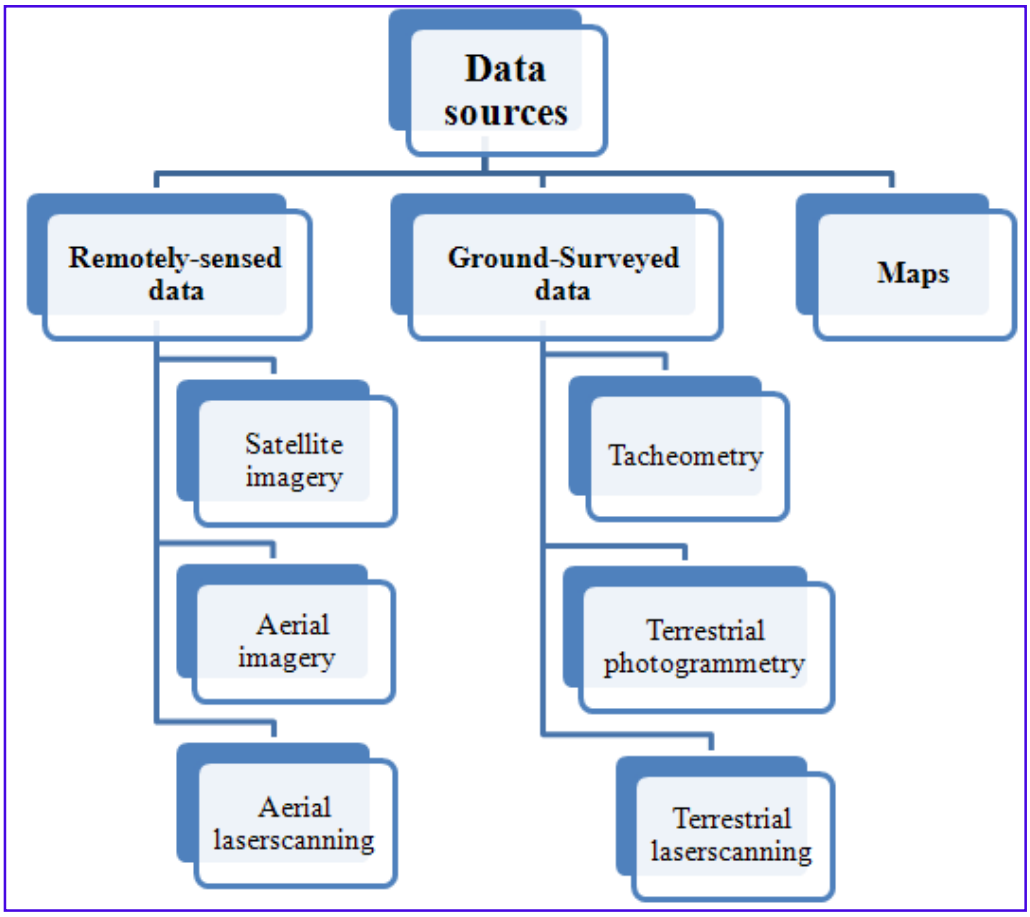

Figure 2.9: Data sources for 3D reconstruction techniques.

A summary of different methods for building reconstruction is now introduced in the following subsections.

2.2.1 Image-based modelling

Aerial and terrestrial images are very appropriate data sources for generation of city models. They allow deriving both the geometrical and the texture models from one unique dataset. The photogrammetric technique is highly scalable, it can adapt to required changes in resolution and accuracy in a flexible way. The processing of new images guarantees an up-to-date model, (Gruen, 2008). Nowadays, photogrammetry and remote sensing are better defined as image-based modelling (IBM) techniques, which allow for the extraction of both geometrical and semantic information from images. IBM is

the most widely used method for geometric surfaces of architectural objects (Debevec et al., 1996), (Liebowitz et al., 1999) and (El-Hakim, 2002) or for precise terrain and city modelling (Gruen, 2000). IBM methods use 2D image measurements (correspondences) to recover 3D object information. IBM or photogrammetry has established itself as the main technique for obtaining accurate 3D information from photography and imagery. The modern approach to 3D modelling by imagery is digital photogrammetry (Leica, 2009b). Photogrammetry is concerned with deriving measurements of the size, shape and position of objects from measurements made on photographs. In its simplest form, a pair of overlapping photographs is used to create a three-dimensional model, which with the use of appropriate instruments can yield quantifiable dimensions of the object.

Traditionally, these dimensions were represented on maps and plans, either as elevations, facades and/or contours (Habib et al., 2004a).

Image-based modelling still remains the most complete, economical, portable, flexible, and widely used approach (El-Hakim and Remondino, 2006).

3D city modelling has been an active research area in digital photogrammetry for more than a decade and a number of methods and systems have been developed for creating 3D city models from digital images and other auxiliary data automatically or semiautomatically. Two major steps involved in generating 3D city models are the creation of building geometry and adding textures.

Image-based approaches use widely available hardware such as high quality cameras and powerful computers. The same system can potentially capture a wide range of objects and scenes. Image-based approaches are also capable of producing realistic models, and those based on photogrammetry have high geometric accuracy (El-Hakim et al., 2004). IBM consists of two major techniques: aerial photogrammetry and terrestrial photogrammetry.

2.2.1.1 Aerial photogrammetry

Aerial photogrammetry is able to economically capture the roof landscape and ground texture of a large built-up area. The limited resolution of 2-D aerial images, the most common source of data, however, does not allow the

detection of small roof elements. Moreover, façade structures can be difficult to acquire as they are mostly invisible from the air.

There are a lot of systems that use widely available aerial stereo images which allow the determination of the third dimension by epipolar matching of different features extracted from both images. Multiview strategies are advantageous in providing redundant information and improving the accuracy of the reconstruction. These systems can be classified into two categories: systems that are extensions of monocular systems for working with stereo images and systems that were designed from the beginning to work with stereo images (Suveg and Vosselman, 2004).

Aerial images may differ from each other with respect to scale, spectral range of recording, sensor geometry, image quality, imaging conditions (weather, lighting), etc. Objects like buildings can be rather complex structures with many architectural details. They may be surrounded by other disturbing man-made and natural objects. Occlusion of parts introduced mainly from vegetation is common, which makes automatic building reconstruction from aerial images a difficult problem, and the geometrical resolution may be limited, figure 2.10.

Figure 2.10: A building in Nottingham University campus with occlusion due to vegetation, Pictometry oblique aerial image.

Occlusion can be reasonably reduced by increasing the overlap, which is achievable nowadays using large format digital aerial cameras, because the more images an object can be seen in, the better its 3D-geometry can be reconstructed. What is more important is that multiple images can reduce problems with occlusion.

Aerial images have several advantages over terrestrial images; for example:

- They provide accurate building footprints and roof heights.
- They can be rectified into orthoimages, which facilitate the merger of multiple images to cover large geographic areas. Orthoimages also facilitate fusion with 2D GIS systems, for integrating the models with rich information databases (Jinhui Hu et al., 2003).

The complexity of aerial imagery, however, is mostly due to the large number of different objects depicted (Mayer, 1999). Nevertheless, such imagery offers highly interesting properties. Compared to ground-based approaches, data capturing is very efficient for large areas, the processing workflow is proven and gives reliable results, and target areas are covered completely with image data regardless of access difficulties or restrictions. The steady technical advances in cameras have enabled spatial resolution to be increasing continuously.

However, aerial images often lack facade information, resulting in models with no visual realism. Integrating facade data is usually a manual process and requires additional sensor data.

2.2.1.2 Terrestrial photogrammetry

Terrestrial, or ground-level, images are very convenient data source. Although this data provides high fidelity ground, vegetation, and building facade detail, it lacks building roof information, and occlusions limit its range. The limited area visible in each image and the calibration needed to stitch images together makes it difficult to construct large urban areas. Terrestrially created models are therefore most useful in aesthetic applications that require 3D models of only a few structures (Jinhui Hu et al., 2003).

Terrestrial measurement is a complementary method for the acquisition of fine details, especially the individual structure points that cannot be observed

from the air. The high precision of this method requires laborious field work since terrestrial details are usually selected and measured on site.

Panoramic images are another convenient and economical data source. Cameras with special lenses or mirror systems acquire the images, or image processing software stitches them together from multiple planar projection images. Examples of such processing software include Autostitch, PanoramaBuilder, Microsoft Image Editor and Photoshop CS4.

Although IBM techniques are sensitive to environmental lighting conditions, noise and occlusions, they can produce accurate and realistic-looking models. However, these techniques remain highly interactive since fully automated methods are still unproven in real applications. The manual interaction needed will inevitably limit the amount of details a model can have (El-Hakim et al., 2007).

2.2.2 Range-based modelling (RBM)

3D model reconstruction from images requires that interest points or edges be visible in the image, which is not always possible. Furthermore, illumination or ambient light problems can affect the extraction of such points and edges; whereas, active sensors such as laser scanners avoid these limitations by creating points on the surface with less concern over light conditions. These sensors have the advantage of acquiring dense 3D coordinates of points automatically (Blais, 2004). In recent years, advances in resolution and accuracy of Synthetic Aperture Radar (SAR) and airborne laser scanners have also shown they are suitable for the generation of DSMs and 3D models (Brenner et al., 2001) and (Maas and Vosselman, 1999). The main advantages of satellite data compared to aerial images are high swath width and ground coverage. However, such data have a relatively low resolution and a low Signal to Noise Ratio (SNR) to deal with 3D reconstruction problems compared to aerial data (Lafarge et al., 2008).

2.2.2.1 Aerial laser scanning

In use since the 1990's, aerial laser scanning based on Light Detection And Ranging (LiDAR) technology can be used for direct acquisition of 3D building surfaces. LiDAR scanning can take place day or night (active system), as long as clear flying conditions are present. The directly available 3D surface

characterized by a point cloud allows for straightforward data processing (Meng and Forberg, 2007). LiDAR has gained popularity as a way to quickly collect 3D information about an urban site. LiDAR scanning of a site produces dense, unorganized points with XYZ coordinates that require further processing to identify buildings, trees, and bare ground (Verma et al., 2006).

A typical LiDAR system is operated from a plane, a helicopter or a satellite. The instrument rapidly transmits pulses of laser which travel to the surface, where they are reflected. The return pulse is collected by a high-speed data recorder. Since the formula for the speed of light is well known, time intervals from transmission to collection are easily derived. Time intervals are then converted to distance based on positional information obtained from ground/aircraft GPS receivers and the on-board Inertial Measurement Unit (IMU) that constantly records the attitude (pitch, roll, and heading) of the aircraft (Kraus, 2007). The accuracy of the LiDAR data is a function of the flying height, laser beam diameter (system dependent), the quality of the GPS/IMU data, and post-processing procedures.

The planimetric accuracy of LiDAR is influenced by the accuracy of GPS location in plan, the accuracy of the IMU orientation and the accuracy to which the deflection angle of the laser beam is recorded. The last two error sources effect a relatively large reduction in accuracy with increase in flying height. The accuracy of the laser ranging component and the GPS height determination are responsible for the height accuracy of LiDAR (Kraus, 2007).

According to Kraus (2007), the generation of building models from LiDAR data is performed using either of the following two methods. The first method starts by forming the difference between a DSM and a DTM. The difference model contains the buildings, vegetation and many other objects lying above the DTM. The second method has some similarities with the first one. However, it uses the ground plans of buildings which are available in 2D GIS database.

LiDAR data poses several challenges in building detection and construction. Most objects in city models are best described by their edges, which are not easily accessible in laser scans and often cannot be derived unambiguously. Some objects of interest do not distinguish themselves through

height differences from their neighbourhood; thus cannot be found in laser data. Other challenges are the presence of noise due to errors in GPS/INS, registration errors, and poor reflectivity properties of some surfaces. In addition, a challenge of surface extraction from LiDAR is the high amount of data to process (Rutzinger et al., 2009) and (Gruen, 2008). LiDAR sensors can only collect data during cloud coverage when the clouds are above the airborne platform. LiDAR sensors also cannot collect data in fog, rain, smoke, or snowstorms. Moreover, where there is dense vegetation, the LiDAR pulses, in most cases, cannot penetrate through the foliage to the ground unless ample openings in the vegetation exist and the spot size of the pulse is small and densely spaced. On the other hand, modern LiDAR systems are capable of receiving multiple returns and thus, the effect of occlusions can be reduced by combining the information from different returns, e.g. first and last returns so buildings can be extracted reliably.

In the last few years, LIDAR and image-matching techniques have been employed in many application fields because of their quickness in point cloud generation. Nevertheless, these techniques do not assure complete and reliable results, especially in complex applications such as architectural surveys. Laser scanning techniques do not allow the correct position of object breaklines to be extracted while image matching results require an accurate editing. For this reason, a combination of LiDAR and photogrammetric techniques is used to overcome such problems (Nex and Rinaudo, 2009).

2.2.2.2 Terrestrial laser scanning

Terrestrial laser scanning or ground-based LiDAR technology is used to capture 3D models of complex and irregular buildings (Frueh and Zakhor, 2004). Compared with aerial LiDAR, It is relatively expensive and requires large storage capacity since the footprint contains many measured points that may not belong to the building structure.

The 3D scanning does not reach as high a precision on structural edges of buildings as close range photogrammetry or terrestrial measurement, but its surface-based working principle allows a precise interpretation of the surface areas to create edges (Böhler and Marbs, 2004).

Laser scanners remain costly, bulky, influenced by surface properties, and impractical in many places. Due to object size, shape, and occlusions, it is usually necessary to use multiple scans from different locations to cover every surface. Aligning and integrating the different scans requires special tools and expertise. Also, scanners produce huge number of points, even on perfectly flat surfaces, yet the points really needed for reconstruction, like corners and edges, are often missed (El-Hakim et al., 2007).

2.2.3 Reconstruction from official cadastral databases and maps

The geometric and semantic attributes of buildings documented in cadastral databases and maps provide rich sources for the derivation of building models of different levels of detail.

Information such as ground plan, the number of storeys and the hypothetical assumptions about the average storey height can easily lead to a block model. Further information such as ridge and eave lines and their terrestrially measured heights can extend the block model to include roof forms (Schilcher et al., 1998b).

An important advantage of seamlessly available cadastral data is that individual building models from different cities can be easily sewed together to form a value-added 3D model covering a large region (Averdung, 2004).

One approach of reconstructing building models from 2D ground plans can be summarised as follows (Brenner et al., 2001):

- Work out (in 2D) from the ground plans how the building can be divided into primitives.
- Select each primitive and determine its dimensions using a measurement process, additional information, e.g. aerial images, can be used here.
- The final step is the assembly of all primitives in a single model which represents the whole building.

The external knowledge about building outlines simplifies several issues of building reconstruction:

- The orientation of the ground plan lines can be used to constrain the normal direction of roof faces (Brenner and Haala, 1998), usually the normal direction will be perpendicular to one of the outline segments.

- Ground plan often reveals information on the structure of buildings. When modelling buildings by constructive solid geometry, buildings can be regarded as combinations of a few components with simple roof shapes (flat, gable, etc.). The shape of building ground plan can be used to derive hypothesis on the partitioning of a building into these building primitives (Brenner and Haala, 1998) and (Brenner et al., 2001).

On the other hand, some drawbacks of using this data source have to be stressed and taken into account; some roof elements, like dormers will not appear in the final model because they are not represented in 2D maps. This roof detail is usually important to the user as city models are mostly shown from an aerial perspective. On contrary some of the small outline elements are irrelevant to roof structures. Furthermore, there are always buildings which cannot be modelled properly or divided into primitives and thus using this method becomes involved and time consuming. Also in many countries the existing maps are out of date.

2.2.4 Combination of different reconstruction methods

From the preceding summary of current modelling techniques, it's obvious that none can satisfy all the requirements of large-scale modelling projects. All the above methods can be combined to construct high-fidelity and photorealistic 3D building models (Beraldin et al., 2005) and (El-Hakim et al., 2004). A digital camera can be integrated with the aerial laser scanning system so that orthophoto mosaics can be directly created.

The combination of image data with the point cloud makes the interpretation of a 3D scene easier and more reliable (Brenner et al., 2003). Likewise, a terrestrial laser scanning system allows the embedding of a camera to record terrestrial images, thus enabling the precise acquisition of both structure lines and surface details of complex buildings. The superimposition of aerial images and cadastral maps supports the reliable reconstruction of standard roof forms and the determination of height for individual buildings. Similarly, the footprint of an aerial laser scanner can be superimposed on the ground plans of buildings to determine heights for the 3D buildings.

Ortiz and Matas (2009) in cultural heritage documentation of Cáceres Wall in Spain used laser scanning for the main geometry capture and a highly

polygon accuracy with total station to control the alignment of the laser scanner data and used digital photogrammetry to capture the data which the laser scanner could not capture. Those parts were the most difficult ones to record because of its location; narrow patios and hidden corners. Erving et al. (2009) and Stamos (2009) used Laser scanning point clouds, images, and vector data from base maps to create 3D virtual model of urban areas.

The challenge of using data from different sources in one virtual model includes many difficulties such as: various coordinate systems, data contents, file formats, levels of detail, and accuracies. These aspects should be considered and taken into account before model construction (Erving et al., 2009).

2.3 Comparison between IBM and RBM

The ultimate goal of all 3D reconstruction methods is to satisfy the eight requirements listed in Section 2.2 by El-Hakim and Remondino (2006). Since this is not an easy task, methods tend to focus on some of the requirements at the expense of the others. The methods may:

- Focus on accuracy without any automation.
- Focus on full automation.
- Try to reach a balance between all requirements.

Common aspects between digital photogrammetric sensors and LiDAR include (Baltsavias, 1999):

- Use of GPS/IMU for georeferencing.
- Methods for processing of raw data, like filtering of large errors, removal of non-DTM objects like buildings, data reduction and compression, and detection of breaklines, are shared between them.
- Laser data regularly interpolated can be treated as images then various image analysis/processing techniques can often be applied to them. Thus, sensor integration and image (or digital signal) processing and analysis are two important topics that unify the two technologies.
- Automatic and semi-automatic processing is possible at some level.

The major differences between photogrammetry and LiDAR are (Baltsavias, 1999):

- Passive vs. Active;
- Generally frame or linear sensors with perspective geometry vs. generally point sensors with polar geometry;
- Full area coverage vs. pointwise sampling;
- Indirect vs. Direct acquisition or encoding of 3D coordinates;
- Geometrically and radiometrically high quality images with multispectral capabilities vs. no imaging or monochromatic images of inferior quality;
- Ability for laser to see objects much smaller than the footprint, small openings below vegetation, power lines, etc.
- Terrestrial laser surveys take longer time than photographic surveys.

All other differences are often a consequence of the above.

Advantages of imaging methods are their high level of details, economic aspects, portability, handling in spatial limited environment and a short data collection time. Disadvantages remain in the post processing when the texture of the object is poor. Advantages of using active sensor systems like terrestrial laser scanners or LiDAR are 3D survey capacities and the 3D surface acquisition. Nevertheless, this technology is not optimal for capturing linear elements and produces a large amount of data which implies to be reduced for further processing. Consequently, in most cases a combination of the above mentioned methods regarding their benefits may be the best solution (e.g. Frueh et al.(2004), Gonzo et al. (2004) and Grussenmeyer et al. (2008)).

Image-based reconstruction techniques also have a number of advantages over range-based techniques, especially for mapping urban areas. Frame images are necessary most of the time for projects as they provide a higher degree of internal geometric quality. Indeed, frame images are more stable (more internal geometric strength) than whiskbroom or push-broom-like sensors which are heavily dependent on the quality of the attitude measurement. The quality of the attitude measurements also affects LiDAR systems. LiDAR systems are also limited in swath and spatial density. Potentially, a 16-megapixel digital camera with a frame rate acquisition of two seconds could provide potential 3D measurements at a rate of four megahertz and at a spatial density of 100 points per square meter. A benchmark on

building reconstruction within the scope of EuroSDR[1] has shown that very similar results can be obtained with both forms of data (Kaartinen et al., 2005).

Nevertheless, Paparoditis et al. (2006) concluded that having both sources of information at hand would of course be the optimal solution. Frame images would provide rigidity to the distorted LiDAR strips through matching and registration techniques, and the LiDAR cloud would help to initialise the image matching processes by reducing search space. This would reduce processing times and allow measurements of higher spatial density. Since both digital aerial images and LiDAR data complement to each other, accurate and reliable building extraction can be achieved by fusing digital images and LiDAR data (Rotternsteiner and Jansa, 2002), (Vosselman, 2002).

The widely used method for extraction of buildings is the one which is based on photogrammetric techniques relying on aerial images. According to Kaartinen et al.(2005) this method is more accurate in determining building outlines. This was the method that had been followed for the extraction of the building models for this research.

2.4 Texture mapping of the 3D models

Once the 3D geometry of the model has been created, the technique of texture mapping of grey scale or true colour images takes place in order to achieve photo-realistic models. So texture mapping is the method of adding detail, surface texture, or colour to the 3D models. There is a strong relation between texture mapping and 3D geometric models as lack of geometry modelling can be replaced by realistic texturing. It is a balance to achieve the best (or most appropriate) model for the intended purpose.

A realistic and accurate model for visualisation is often required. Pollefeys et al. (2000) stated that ‘visual quality of 3D models becomes one of the main points of attention which results in a change in emphasis for the

[1]European Spatial Data Research: A not-for-profit organisation linking National Mapping and Cadastral agencies with Research Institutes and Universities for the purpose of applied research in spatial data provision, management and delivery (source: http://www.eurosdr.net/start/).

requirements of 3D models'. Stamos (2009) concluded that the 'generation of photorealistic 3D content of urban sites at various resolutions and from various sensors is a very important current problem'. Besides resulting in a photo-realistic look, texture also creates the false impression of a higher level of geometric detail, a fact that is exploited in image-based rendering (Frueh and Zakhor, 2004). Varshosaz (2003) summarized the reasons for using real textures in the following points:

• Improved realism and ease of access: incorporating real textures not only increases the realism of the model but also enables the viewing of details, which are absent from the geometric model. Objects can instantly be recognised and accessed as required.

• Improved interpretability: when models are enhanced using real textures, the relationship between objects can easily be perceived. This not only includes features on the facades of buildings such as doors and windows, but also the surrounding buildings and features like telephone boxes, etc.

• Making instant measurements: a geometric model rendered with real textures can be used as a base to perform measurements on objects that may not even be included in the geometric model. The accuracy of the measurements, however, depends on the accuracy of the geometric model and the way the measurements are carried out.

2.4.1 Texture mapping methods

After the reconstruction of the geometric model, image data is often projected onto the geometry to achieve realism. The image information (texture) can be the same image that was used for the geometric modelling or it can come from different acquisition source or session (e.g. external camera in case of laser scanner, terrestrial images in case of aerial city modelling) (Ortin and Remondino, 2008), (Lorenz and Döllner, 2006). There are different approaches and data sources that have been developed to create building textures automatically or semiautomatically.

2.4.1.1 Existing libraries of textures

When texture information of the building facade is not available, it is a common practice to assign a pseudo texture to the building models instead

(Beck, 2003). Figure 2.11 shows some of the pseudo 3D models and textures. Although this method provides a better presentation of the building model, it is not ideal because it does not represent the true characteristics of the building facade. Such pseudo representation of the building facades makes the overall visualization system less realistic and less useful.

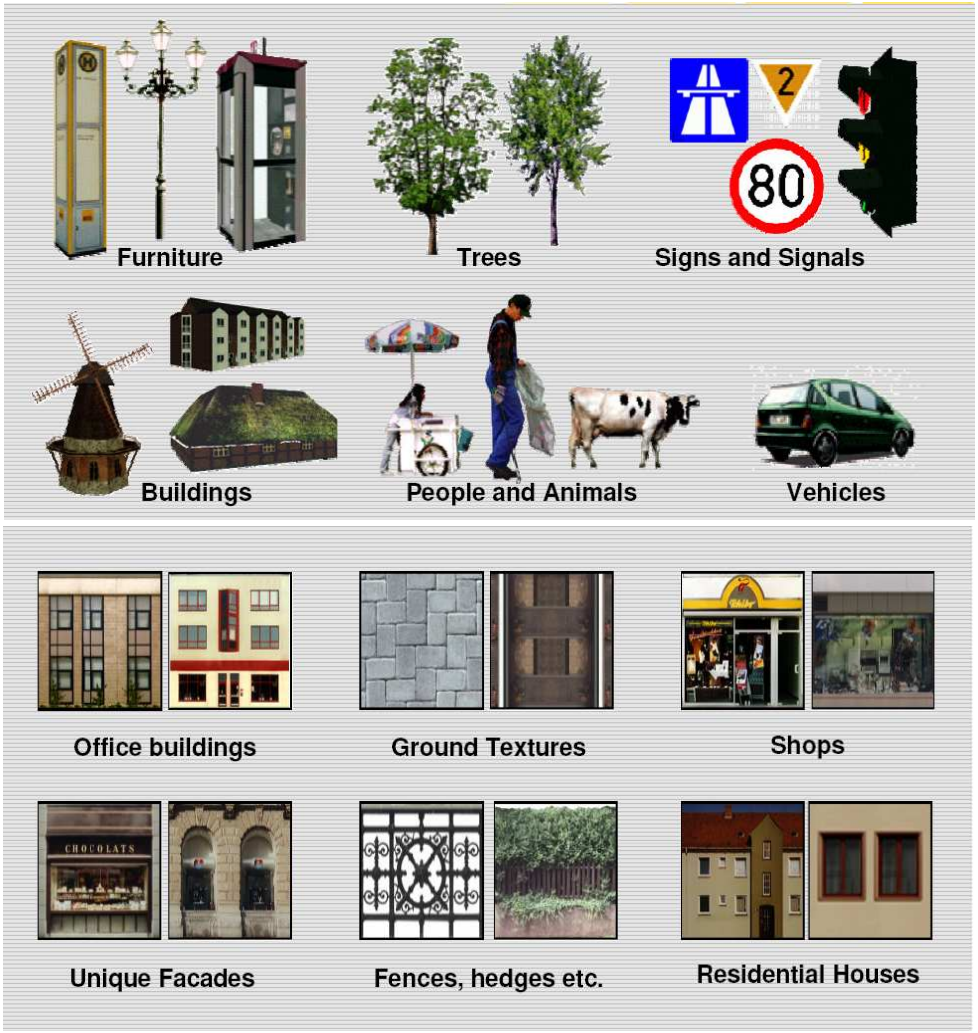

Figure 2.11: Some pseudo 3D models (top) and textures (bottom), adapted from Bildstein (2005).

2.4.1.2 Satellite remote sensing imagery

Remote sensing data can provide limited texture information to the extracted building models as this is restricted by the sensor look angles. Very often, only the building model tops and certain building model facades are textured. Moreover, the building model facades extracted from satellite imagery are pixelated due to the lack of resolution and texture information (Huang et al., 2006), figure 2.12. This is because the represented skew area of

building facade which can be seen from the satellite imagery is relatively small when compared to the actual size.

Figure 2.12: Front and back views of a 3D building model textured using IKONOS imagery, adapted from Huang et al. (2006).

2.4.1.3 Terrestrial imagery

To improve the overall photo-realistic quality and usability, building facades are textured with terrestrial digital photographs taken using commercially available cameras. This may be done using still images of building facades and video recordings of streets. Panoramic photographs or wide angle format photography (technique of imaging that uses specialized equipment and software to capture images with elongated field of view) is sometimes used to texture 3D models as panoramic images provide a highly realistic visualisation to all angles from static viewpoints within the survey area. However, the process of allocating and mapping the appropriate textures from terrestrial images to correct building facade is both time-consuming and laborious. Furthermore, building sides that are not accessible from ground-level are not textured. Jinhui et al. (2003) stated that 'terrestrial images are most useful in aesthetic applications that require 3D models of only a few structures because it lacks building top information, and occlusion limits its range'. The limited area visible in each image and the calibration needed to stitch images together makes it difficult to construct large urban areas. On the other hand, obtaining suitable viewpoints for image acquisition in busy city centres may be problematic due to restrictions on helicopter flight paths or access to rooftops. Hence, building textures are mostly generated from ground-level imagery that often fails to provide optimal facade coverage.

2.4.1.4 Aerial imagery

The more conventional method of collecting aerial images with for example UltraCamD, can also provide excellent views of roof tops and some of the building faces when located away from the nadir on the images (Smith et al., 2009). Several methods have tried to texture building rooftops using vertical aerial images and texture facades by utilizing ground-based images (Brenner et al., 2001). Standard aerial imagery uses a vertical viewing axis, which guarantees optimal resolution for horizontal areas (details of roofs), but depicts vertical elements such as building facades only when available due to perspective effects. Vertical aerial imagery is rarely used as an immediate source for facade texturing. Even when available, the texturing often suffers from comparatively low resolution of image patches of walls and poor depiction of facades. In addition, there are usually too few images available to cover all building sides and in some cases the archive images are black and white and thus are not ideal as texture for photo realistic rendering. Nonetheless, aerial imagery offers highly interesting properties. Compared to ground-based techniques, data capturing is very efficient for large areas, processing workflow is already proven and gives reliable results, and target areas are covered completely with image data regardless of access difficulties or restrictions. Moreover, due to steady technical advances, spatial resolution is continuously increasing.

From a practical point of view, texture mapping is mostly required for the facades of buildings that show, from a pedestrian level of view, the way buildings look in the real world. So in order to provide detailed building facades for both walk-through and fly-through interactive rendering applications, oblique aerial images must be acquired rather than the conventional near-vertical aerial images.

Multiple approaches to facade texturing from vertical aerial images, oblique aerial images, and ground-based techniques have been used. The first approach, by Frueh et al. (2004), uses car-based capturing techniques and aerial imagery to compute a detailed 3D city model of a real city along with a full and realistic texture cover based on multiple kinds of data, such as video, laser scanners, or positioning data. Using vehicles to record photos of the building

facades is more flexible, because the photographer can avoid occlusion caused by other buildings and vegetation. However, the resulting photos are suitable for street views but not for observations from the sky. Moreover, such techniques are expensive for large-scale capturing since it takes long time to drive through the usually dense traffic in the large cities and limited due to visibility problems on street-level. Combining aerial and ground-based textures in one facade can lead to seam between them being clearly noticed, figure 2.13. This is not surprising, since the resolution of the ground-based texture is higher, and ground-based and airborne image acquisitions may be made at different times of the day and even months apart from each other, and thus under completely different lighting conditions. Microsoft and Google Earth use ground-based and airborne image acquisitions as well for texturing 3D city models (ASM, 2008). The building geometry is simple without too many details and the texturing seems accurate if viewed from long distance but the result is not without errors as can be seen from figure 2.14 where the texture mapping of the vertical sides of the buildings has gone completely wrong. Since fine geometric details are not modelled, even when rich texture maps are used, the model will exhibit smooth, flat-looking surfaces and polygonal silhouettes that are easily detected by the human eye.

Furthermore, this technique cannot be used in some smaller cities due to objection of residents as, for example, what was reported by BBC in April, 2009. The report stated that angry residents in Milton Keynes, UK blocked the driver of a Google Street View car when he started taking photographs of their homes; residents said that Street View was an invasion of privacy. Figure 2.15 shows an example of car-based capturing techniques.

An obvious restriction for the car-based systems is they are normally only able to travel on roads; hence the facades on the backside of buildings cannot be captured at all. This necessitates the use of another complementary capturing technique and thus extra costs.

Figure 2.13: Texture-mapped fused model. The arrows indicate the horizontal boundaries between texture from aerial images, i.e. the upper part, and texture from ground-based data acquisition, i.e. the lower part, adapted from Frueh et al. (2004).

Figure 2.14: The 3D model of Philadelphia which has been created by Microsoft is not without problems in texturing, adapted from Microsoft maps.

Figure 2.15: (Left) Street View car with its camera mounted on the roof used by Google Earth to capture home facades, adapted from: http://news.bbc.co.uk/1/hi/england/beds/bucks/herts/7980737.stm, (Right) truck with acquisition equipment that was used by Frueh and Zakhor (2004).

So far, the availability of 3D building models in cities is not dense; the major cities usually have some of their landmarks added, for example London, UK, figure 2.16. Previously, these buildings were just grey 3D boxes but in the last couple of years textured 3D models have become more standardized. Cities such as Hamburg in Germany, Zurich in Switzerland, and Tokyo in Japan are represented by textured 3D building models in Google Earth.

Figure 2.16: Some of London landmarks are represented in 3D on Goggle Earth, adapted from Google Earth.

Nevertheless, lots of buildings are still not textured, which is probably due to difficulties of applying photo-realistic textures to the 3D models, figure 2.17.

Figure 2.17: 3D model of Tokyo, Japan shows only some buildings are textured while the majority are still not textured, adapted from Google Earth.

2.5 Levels of detail (LoD) in 3D modelling

The concept of 'level of detail' has been used in computer graphics since the 1970s, mainly for increasing the efficiency of object rendering and then has been adapted and extended for city modelling (Chikomo et al., 2007). The LoD concept specifies diverse ways of plotting different levels of complexity for a given object, and allows browsers to switch to the view which gives the appropriate version of the object according to the distance from the user. When the distance increases the object's detail (quality) decreases and vice versa (Beck, 2003). Figure 2.18 shows visual effect of 2 successive levels of detail for the Geography building on Nottingham University campus. The left level is the most simplified 3D version of the building structure. It only consists of simple geometrical 3D shapes while the right level is the most accurate version of the building structure; it shows some of the fine details of the roof.

Unlike the 2D topographic maps that have standard official scale series, there are no generally agreed LoDs for 3D buildings (Meng and Forberg, 2007).

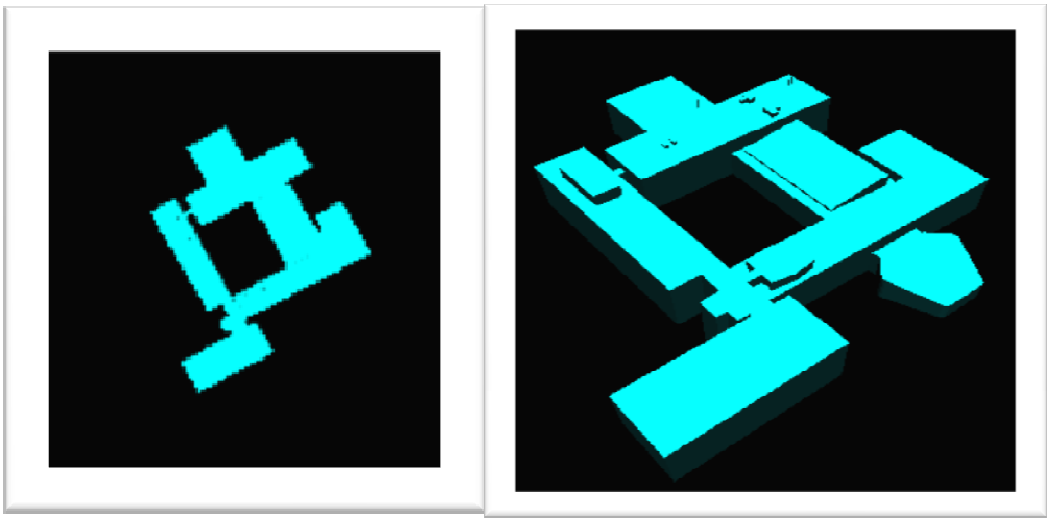

Figure 2.18: LoD refinement of 3D building models depending on the viewing distance: the nearer the building models, the more details they reveal.

In general, three dimensional city and regional models are available in different levels of detail. Usually these are being generated or created from various sources which often are independent of each other (Dietze et al., 2007). For the time being the accessibility of 3D building models worldwide is rather variable. Some regions have been completely covered with redundant 3D data of more than three LoDs (some regions in Europe) and some regions have only access to a very coarse LoD or to a fine LoD for a limited number of buildings. Elsewhere 3D building models are entirely missing (some of the third world countries).

As exemplified in the following list, the currently available LoDs are mainly determined in relation to the resolution of sensor data, the precision of semantic information and the relevant application:

- Gröger et al. (2004) define five LoDs of 3D landscapes:
- LOD0: A digital terrain model with draped orthophoto and classification of land use, figure 2.19.
- LOD1: Popping up of the ground plan to a uniform height, figure 2.19.
- LOD2: LoD1 enhanced with roof textures, roof structures and vegetation features, figure 2.20.
- LOD3: Architecture models with vegetation features and street furniture, figure 2.20.
- LOD4: Indoors architecture models, figure 2.20.

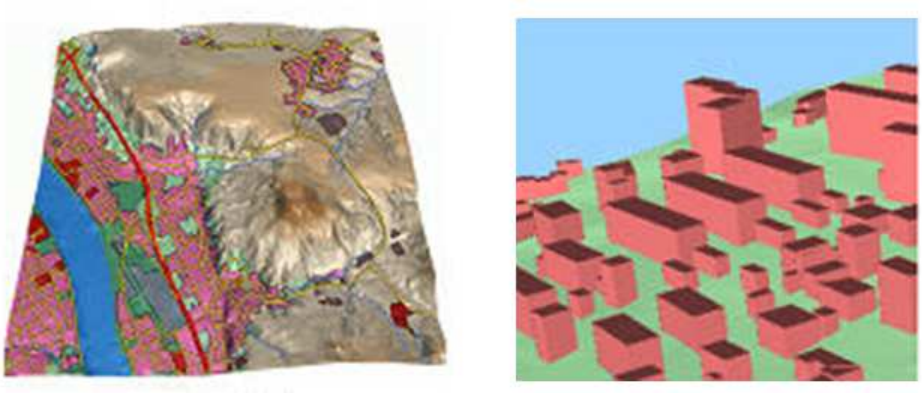

Figure 2.19: Left: LoD0; regional model, 2.5D digital terrain model, right: LoD1; block model without roof structure, adapted from (Kolbe et al., 2005).

Figure 2.20: Left: LoD2; site model with roof structures and added textures, middle: LoD3; detailed architectural model, right: LoD4; interior walkable model, adapted from (Kolbe et al., 2005).

- Chikomo et al. (2007) define five levels of detail ranging from a simple block model up to a walkable model, which contains both internal and external geometric detail, figure 2.21.
- Thiemann (2004) summarises three LoDs for buildings:

- LoD1: aggregated settlement blocks with a uniform height,
- LoD2: block of the individual buildings without roof form,
- LoD3: LoD2 enhanced with a simplified roof form.

- The academy of Netlexikon (www.lexikon-definition.de) suggests five LoDs for individual buildings:

- LoD1: Popping up of the ground plan to a uniform height,
- LoD2: LoD1 enhanced with a texture,
- LoD3: External hull of the building with a roof form and small surface elements,
- LoD4: LoD3 enhanced with external textures,

- LoD5: LoD4 enhanced with internal structures.

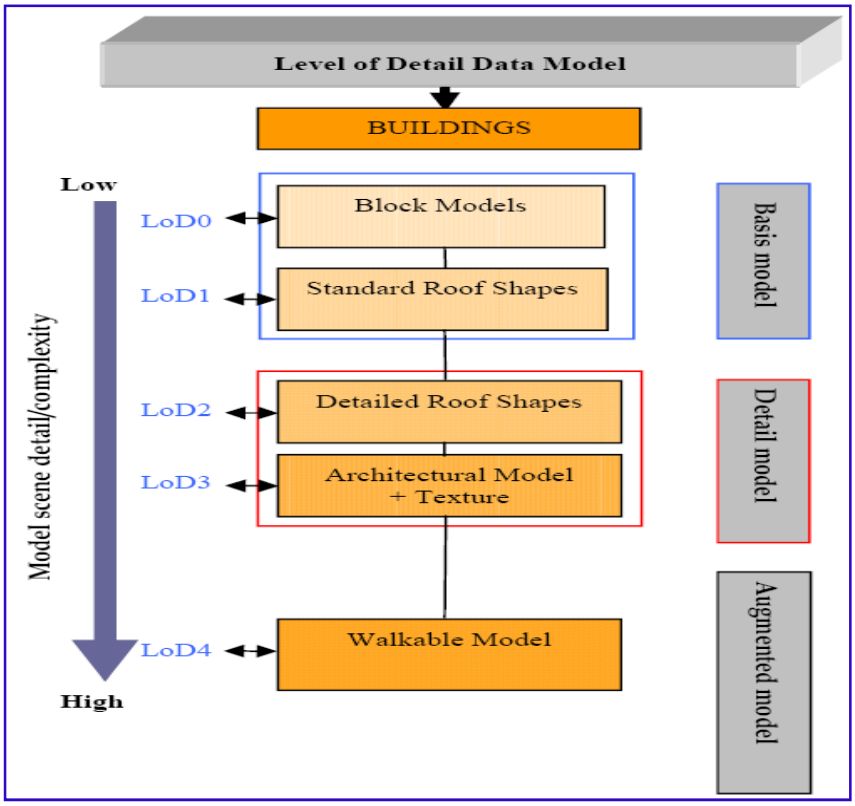

Figure 2.21: Level-of-Detail modelling schema defined by Chikomo et al. (2007)

- In Schilcher et al. (1998a) three LoDs for individual buildings are explained:
  - LoD1: Popping up of the ground plan to a uniform height,
  - LoD2: LoD1 enhanced with a standard roof form,
  - LoD3: LoD2 enhanced with photorealistic textures and small surface features.
- Similarly, three LoDs can be found in Kolbe (2004):
  - LoD1: Popping up of the ground plan to a uniform height,
  - LoD2: LoD1 enhanced with a standard roof form and simulated wall texture,
  - LoD3: LoD2 refined with a detailed roof form, small surface elements and photorealistic textures.

In spite of the differences in the aforementioned definitions of LoD, they all follow the logic of successive refinement from lower LoDs with coarser resolutions to higher LoDs with finer resolutions (Meng and Forberg, 2007).

2.5.1 Characteristics of LoDs

From the above list of different LoD schema the following interpretation of the characteristic of each LoD can be drawn:

- LoD0: automatic production, low-cost and available on the shelf.
- LoD1: Large coverage (large number of buildings), abstraction of buildings, visual simplicity, low-cost, and not always available on the shelf.
- LoD2: Photogrammetric models from aerial photos, high quality geometry, automatic approaches with some human interaction, textures using either aerial or terrestrial pictures, medium to large coverage, reasonably priced, and limited availability.
- LoD3: Modelling of facades from laser scanning data and terrestrial images, limited coverage, expensive and slow production, custom made, and manual design supported by semiautomatic techniques.
- LoD4: Terrestrial Laser Scanning, terrestrial imagery or total station to model interior plans, small coverage, very expensive, slow production rate and time consuming, and too complicated.

2.6 Aerial triangulation

Aerial triangulation (AT) is the major factor that improved the economic feasibility of photogrammetric products. It has been driven by the continuous advances in computing power especially the introduction of digital photogrammetric workstations and automation (Heipke et al., 2002).

AT can be defined as the establishment of vertical and horizontal control points based on a few ground control points. The modern approach through the collinearity equations also determines the position and attitude of each image/exposure, thus it is considered a powerful technique that reduces the number of ground control points required for mapping. The information derived in aerial triangulation is essential in creating digital terrain models, orthophotos, and 3D modelling. Aerial triangulation is undertaken by the combination of resection (used to determine the exterior orientation parameters) and intersection (used to determine the ground coordinates X, Y, and Z of points that appear in the overlapping areas of two or more images, tie

points, based on known interior orientation and known exterior orientation parameters).

2.6.1 Benefits of performing aerial triangulation

For mapping projects having more than two images, the use of space intersection and space resection techniques is limited because it requires long times for processing each image and a lot of GCPs, for example the minimum number of GCPs required to perform space resection for a block of 27 vertical Pictometry images is 81 points. To avoid the above drawbacks, a process is called block triangulation (aerial triangulation) is used.

2.6.2 Georeferencing of images

Image orientation is a key factor in any photogrammetric project as the determination of 3D coordinates from the images requires the orientation to be known. This can be achieved through georeferencing which can be defined as the determination of the exterior orientation parameters of a sensor at the time of recording and the restitution of the scene from the image data (Skaloud and Legat, 2008). The task of Georeferencing is considered one of the most important tasks in photogrammetry. Traditionally it has been achieved indirectly using the well-known method of aerial triangulation. However, with the availability of integrated GPS and IMU, this situation has changed. Direct determination of exterior orientation is now possible. Today, direct and integrated sensor orientation is used for a wide range of sensors including LiDAR and SAR, as well as for digital line scanner systems and aerial cameras (Yastikli and Jacobsen, 2005).

In photogrammetry, the georeferencing methods are divided into direct georeferencing and indirect georeferencing according to different ways in deriving the EOP of images. For direct georeferencing, EOP of images can be determined directly by the integrated inertial and satellite technology comprised of an IMU, a GPS receiver, and a computer. Hence, the EOP are known in direct georeferencing, meaning that the bundles of image rays themselves are fixed in space. Areas with missing object contrast like water surfaces, desert or forests can be bridged without problems using the direct georeferencing. For indirect georeferencing method the EOP of the images are

unknown and need to be determined by relative and absolute orientation techniques. Thus, the bundle of (corrected) rays of each image is allowed to move "freely" to achieve consistency within the image block (via tie points), and the position and orientation of the block is fixed by GCPs. The number of control points needed depends on the methods of indirect georeferencing (block adjustment, stereo-model set-up or mono-image resection). A large amount of control points are required to orient images by the methods of stereo-model set-up or mono-image resection. The determination of control points is expensive and time consuming. Block adjustment can greatly reduce the number of control points. Nowadays bundle block adjustment is popularly used in the photogrammetry field (Skaloud and Legat, 2008), (Jacobsen, 2004).

In the traditional GPS-supported AT, differential GPS (DGPS) positioning technology is used to determine the 3D coordinates of the images' perspective centres at the moment of exposure. This method can significantly reduce the number of GCPs needed. In the DGPS mode, one or more GPS reference stations should be placed on the ground and observed synchronously and continuously together with the airborne GPS receiver during the entire flight mission. The establishment of GPS reference stations for DGPS positioning is not only labour-intensive and costly, but also increases the implementation difficulty of aerial photography.

According to Yuan et al. (2009), in processing of GPS observations, the carrier phase differential technique is used to eliminate or reduce GPS positioning errors, including satellite clock error, satellite orbit error, atmospheric delay error, and so on. Generally speaking, it is difficult to locate a good GPS reference station when the aerial photographic region is large or has difficult access and communication. Moreover, the accuracy of DGPS positioning is relevant to the length of baseline; the longer the baseline, the weaker the correlation between ionospheric refraction error and tropospheric delay error on the ground and aircraft. Due to the need for spatial correlation of atmospheric delay errors, the lengths of DGPS baselines are typically limited to within 20 km if centimetre level accuracy is required with high reliability. When it comes to aerial photogrammetry, this is difficult because the length of

survey areas can be more than 200 km and the distance between the survey area and the airport may be greater.

Due to the above mentioned drawbacks of DGPS, GPS precise point positioning (GPS PPP) is being used nowadays for aerial photography. GPS PPP is a type of absolute GPS positioning which uses International GNSS Service (IGS) precise orbit parameters and clock error products. In their conclusion Yuan et al. (2009) stated that 'GPS PPP eliminates the need to establish GPS reference stations, so only one airborne GPS receiver is mounted on the aircraft. GPS PPP will not only reduce the difficulty and cost of aerial photography, but also increase the flexibility of aerial photography. The performance model of GPS-supported AT can also be replaced by GPS PPP, which makes more extensive applications and plays a very important role in national fundamental surveying and mapping, especially in non-mapped areas, inaccessible regions and on the frontiers'. However, GPS PPP requires very precise orbit products which should be consistent (in terms of accuracy) with sattelite clock file as well as the need to correct for atmospheric errors. Yuan et al. (2009) proved in their experimental results that the 3-dimensional coordinate accuracy of object points determined by GPS PPP in bundle block adjustment are the same as those obtained by DGPS-supported bundle block adjustment. Therefore, GPS PPP can replace DGPS to be applied in topographic mapping.

2.6.3 Bundle Block Adjustment

There are several methods for block triangulation. The bundle block adjustment is the most rigorous and flexible method, considering the minimization and distribution of errors. Bundle block adjustment uses the collinearity condition as the basis for formulating the relationship between image space and ground space (Mikhail et al., 2001). It is considered essential for determining the information required to create orthophotos, DTMs, digital stereo models (oriented images), and extract 3D features.

The bundle adjustment is a computation that processes the photographic measurements to compute X, Y, and Z coordinates of the measured points. To perform this task, the program must triangulate the points, resect the images and perhaps self calibrate the camera.

Resection can be defined as the process of determining the final position and orientation of the camera at the instant of exposure. All the ground points that are known in X, Y, and Z in the image are used in the determination of camera orientation. Space resection techniques can be applied to one image or multiple images. Collinearity equations are used in space resection. The collinearity condition specifies that, for any image, the exposure station, the ground point, and its corresponding image point must lie along a straight line. For every observation (ground point) on every image, a pair of collinearity equations (non-linear observation equations) can be developed as follows:

$$\frac{x}{f} = \frac{[r_{11}(X-X_0)+r_{21}(\mathrm{Y}-\mathrm{Yo})+r_{31}(\mathrm{Z}-\mathrm{Zo})]}{[r_{13}(\mathrm{X}-\mathrm{Xo})+r_{23}(\mathrm{Y}-\mathrm{Yo})+r_{33}(\mathrm{Z}-\mathrm{Zo})]} \quad (2.1)$$

$$\frac{y}{f} = \frac{[r_{12}(X-X_0)+r_{22}(\mathrm{Y}-\mathrm{Yo})+r_{32}(\mathrm{Z}-\mathrm{Zo})]}{[r_{13}(\mathrm{X}-\mathrm{Xo})+r_{23}(\mathrm{Y}-\mathrm{Yo})+r_{33}(\mathrm{Z}-\mathrm{Zo})]} \quad (2.2)$$

Where: x and y are the photograph coordinates (observed)

X, Y and Z are the ground coordinates (observed)

X_o, Y_o and Z_o are the perspective centre coordinates (unknown)

and r_{11}, r_{12}, ……, r33 are the elements of the rotation matrix from the three rotations ω, φ, and κ (unknown), (Smith, 2006).

To solve for the above unknowns (exterior orientation parameters), this requires at least six collinearity equations. Therefore, normally three full ground control points are needed to form the six equations. Redundancy (more GCPs) is recommended to increase the accuracy of the resection and to help detect the blunders. In case of redundancy, least squares adjustment techniques are used to get the most probable positions of exterior orientation parameters.

In a bundle adjustment the resection/intersection is performed simultaneously in a single least squares adjustment process with the image coordinates and control point coordinates considered as the observations, while the exterior orientation parameters of the images and the object coordinates of tie points constitute the unknowns. In some cases, the interior orientation parameters of the camera are also considered as further unknowns (given that they are not precisely known in advance). The linearised least squares observation equations are formed from the collinearity equations typically using Taylor's theory as follows:

$$v_{x=}\left[\begin{matrix} f_x(x,\omega,\varphi,\kappa,X_0,Y_0,Z_0,X,Y,Z)+\frac{\partial f_x}{\partial \omega}d\omega+\frac{\partial f_x}{\partial \varphi}d\varphi+\frac{\partial f_x}{\partial \kappa}d\kappa+\frac{\partial f_x}{\partial X_0}dX_0+ \\ \frac{\partial f_x}{\partial Y_0}dY_0+\frac{\partial f_x}{\partial Z_0}dZ_0+\frac{\partial f_x}{\partial X}dX+\frac{\partial f_x}{\partial Y}dY+\frac{\partial f_x}{\partial Z}dZ \end{matrix}\right]/\frac{\partial f_x}{\partial x} \quad (2.3)$$

$$v_{y=}\left[\begin{matrix} f_y(x,\omega,\varphi,\kappa,X_0,Y_0,Z_0,X,Y,Z)+\frac{\partial y}{\partial \omega}d\omega+\frac{\partial f_y}{\partial \varphi}d\varphi+\frac{\partial f_y}{\partial \kappa}d\kappa+\frac{\partial f_y}{\partial X_0}dX_0+ \\ \frac{\partial f_y}{\partial Y_0}dY_0+\frac{\partial f_y}{\partial Z_0}dZ_0+\frac{\partial f_y}{\partial X}dX+\frac{\partial f_y}{\partial Y}dY+\frac{\partial f_y}{\partial Z}dZ \end{matrix}\right]/\frac{\partial f_y}{\partial x} \quad (2.4)$$

Where:

v_x and v_y .....are the image residuals in the x and y coordinate.

$\frac{\partial f_x}{\partial \omega}, \frac{\partial f_x}{\partial \varphi}, \frac{\partial f_x}{\partial \kappa}, \frac{\partial f_x}{\partial X_0}$,.....are the partial derivatives of the function with respect to the unknown parameters.

$d\omega, d\varphi, d\kappa, dX_0$, ...are the corrections to the approximate values of the unknown parameters (Smith, 2006).

According to Leica, 2009, 'the least squares adjustment is achieved by minimizing and distributing data errors (inaccuracy associated with the input GCPs coordinates, measured tie points and GCPs image positions, camera information, and systematic errors) through the network of observations. The least squares approach requires iterative processing until a solution is obtained. A solution is obtained when the residuals, or errors, associated with the input data are minimized'. The power of the bundle adjustment is its ability to perform the resection, triangulation, and self calibration simultaneously. From the review of the definitions of resection and triangulation, it seems that there is a problem; to triangulate the points, we must know the orientation of images. However, to orient the images, we must know the ground coordinates of the measured points. The bundle adjustment is able to do both at the same time and to perform the self calibration as well. By a block adjustment one can simultaneously get the following:

- The position (X_0, Y_0, Z_0) and orientation (Omega, Phi, Kappa) of each image in a block as they existed at the time of exposure.
- The X, Y, and Z coordinates of tie points collected manually or automatically throughout the block of images. Once the X, Y, and Z

coordinates of tie points are computed, they can be converted to control points.

- The interior orientation parameters associated with a camera or sensor model (f, x_p, and y_p). This process is commonly referred to as self calibrating bundle adjustment (SCBA).
- Additional parameters (AP) characterizing systematic errors within the block of images and observations.
- Most importantly, the results of a block adjustment can provide detailed statistical reports on the accuracy of data.

According to Kraus (2007), Zhu et al. (2008) the advantages of bundle block adjustment over the previous adjustment methods include the following:

- It introduces the direct relation between image and ground coordinates; therefore, it is the most accurate method of aerial triangulation.
- It greatly reduces the number of GCPs.
- It achieves consistent mapping accuracy over the entire block.
- It provides the possibility of incorporating additional parameters in the process of the adjustment, such as interior orientation parameters, field-surveyed observations and so on to compensate for systematic errors.

2.7 Summary

3D city modelling has been an active research area in digital photogrammetry for more than a decade and a number of methods and systems have been developed for creating 3D city models from digital images and other auxiliary data automatically or semiautomatically. Two major steps involved in generating 3D city models are creation of building geometry and adding textures to create photo-realistic building models.

3D building data can be acquired using a variety of terrestrial and non terrestrial techniques. Among others, aerial photogrammetry, aerial laser scanning, terrestrial measurement, terrestrial laser scanning and official cadastral information have been widely applied. Aerial photogrammetry and aerial laser scanning are currently the most used techniques in 3D data acquisition.

Efforts to increase the level of automation became essential in order to meet the increasing demand for 3D models. However, the efforts to completely automate the process from taking images to the output of a 3D model, while promising, are thus far not always successful.

Approaches for texturing facades in large urban environments include car-mounted facade scanning, aerial vertical and oblique images, terrestrial images, random or attribute-based assignment of hand-made typical textures from a library, or selective manual texturing with each having major drawbacks such as need for additional image capturing, lack of realism, or costly manual texture creation.

Using images as texture will not only increase the realism of the model but also enable the viewing of details and creates the false impression of a higher level of geometric detail. The relationship between objects can be perceived easily and reliably when photorealistic models are used in visualization.

In order to accelerate the rendering of complex scenes, objects are modelled at various levels of detail. LoD switching is the practice of displaying different geometric representations of the same object at different times, less detailed representation when the object is farther away and more detailed when it is closer to the observer.

AT is the process of defining the mathematical relationship between the images contained within a block, the camera or sensor model, and the ground. Once this relationship has been defined, accurate imagery and geographic information concerning the Earth's surface can be created. The bundle block adjustment is the most rigorous and flexible method of performing AT, considering the minimization and distribution of errors.

CHAPTER3: DIGITAL AERIAL CAMERAS

3.1 Introduction

Photogrammetry , defined by Mikhail et al. (2001) as "the process of deriving (usually) metric information about an object through measurements made on photographs of the object", involves the techniques of taking photographs, measuring the photographs, and using the measurements to produce maps.

The above three techniques are in continuous advancement and have undergone a remarkable evolution in recent years. This is mainly the result of the recent explosion in information technology and the general development of science and engineering (Madani, 2001). New instruments are introduced to the field of Photogrammetry on continuous basis; this is powered by the improvements in computer technology, especially in increased storage capacity. This chapter will introduce some of the benefits of digital photogrammetry. Moreover, this chapter will provide an overview of different kinds of digital aerial cameras available in the market. In addition, it will describe in detail the characteristics of the data collection systems used to capture the aerial photography used in this research. It will describe the operation concepts of the Pictometry imaging system and the procedure of performing measurements on oblique images.

3.2 Digital photogrammetry

Digital photogrammetry is applied to digital images that are stored and processed on a computer and can be scanned from photographs or directly captured by digital cameras. It is relatively a young field, but fast growing due to improvements of computational power of machines, digital cameras, and storage capacity. This caused a lot of software developments that avoided the use of the mechanical part of photogrammetric plotters, yet still based on the same algorithms as analytical plotters.

Digital photogrammetry (or softcopy photogrammetry as it is called by some authors) has superseded conventional analytical photogrammetry, as the cheaper and more time efficient option. The transition to a digital

photogrammetric environment and the use of digital workstations allowed the automation of some of photogrammetric products such as DSM and orthoimage generation. According to Smith (2006), Paparoditis et al. (2006), Wang et al. (2008), Gruen (2005) and Graham and Koh (2002) some merits of digital photogrammetry are as follows:

- It has brought automation in the areas of interior orientation, relative orientation, DEM generation, image matching, aerial triangulation measurement and feature extraction.
- It has brought new photogrammetric products such as orthoimages and perspective views.
- Compared to analytical plotters, it is considered not expensive.
- It provides several types of viewing systems
- Due to high degree of automation, it can be used by non specialized people.
- The primary data can be accessed immediately after the survey aircraft has landed, or even during the flight.
- The process is free from chemistry and no darkroom or laboratory is required.
- Expensive and time consuming film scanning is no longer required so the photogrammetric production cycle can be reduced.
- Improved image quality as hair, dust, finger prints, scratches, and film deformations no longer pollute the image signal.
- High amount of details can be achieved because the dynamic range of CCD-based digital sensors allows the separation of 2000 to 3000 grey levels whereas a photographic film, even if correctly processed, does not permit the separation of more than 50 to 100 levels. Thus, high accuracy of point measurement can be achieved with digital images, especially in difficult situations such as in shadow areas.
- Digital aerial cameras can be used to produce images with a high degree of image overlap in flight direction at almost no additional costs.

Schenk (1999) stated that 'probably the most significant product of digital photogrammetry is the digital photogrammetric workstation, also called a softcopy workstation'. The role of DPW in digital photogrammetry is equivalent to the role of the analytical plotter in analytical photogrammetry. These digital workstations accommodate images from either a digital camera, which provide purely digital images ready for input into the photogrammetric process, or from a film camera which will require scanning of the negative to create the required digital image, figure 3.1.

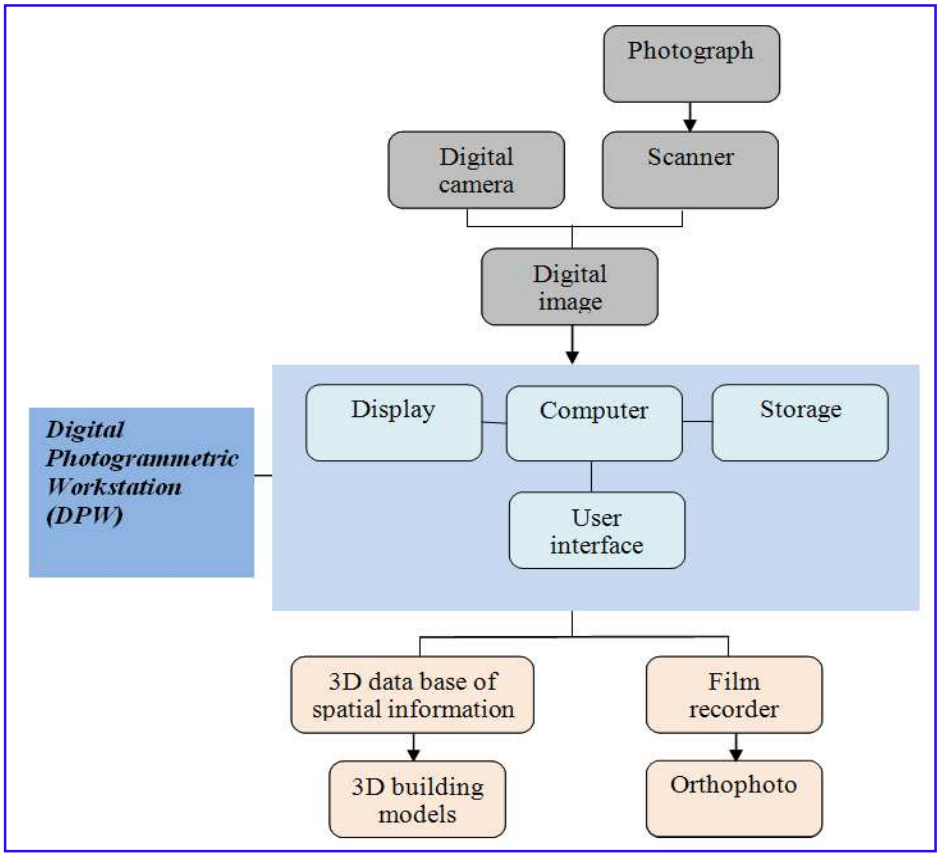

Figure 3.1: Schematic diagram of digital photogrammetry processes with the DPW as the main component, adapted from Schenk (1999).

Digital photogrammetry implies two main tasks: data acquisition and data processing, figure 3.2. As it can be seen from the flow chart, data processing and data acquisition are the major stages of digital photogrammetry. Data processing is carried out in offices and includes processing the images, performing aerial triangulation, extracting DEMs and 3D features, etc. Aerial triangulation is considered one of the major steps in photogrammetric processes and it will be discussed in the fifth chapter.

The majority of photogrammetric operations in the stage of data acquisition involve the use of aerial photographs which are taken with photogrammetric cameras.

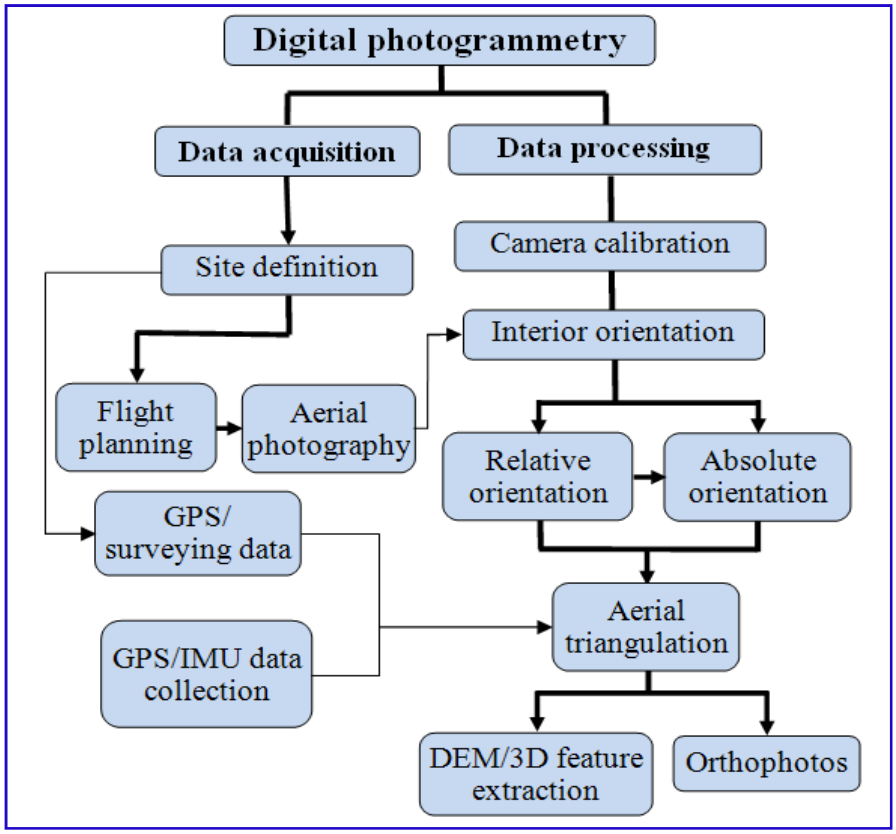

Figure 3.2: Digital photogrammetry tasks

3.3 Photogrammetric cameras

A device that acquires images (the photogrammetric camera), is the most essential part of the photogrammetry system (Moffitt and Mikhail, 1980). Photogrammetric cameras are of two main types: terrestrial and aerial. Terrestrial cameras are mounted on tripods or handheld while aerial cameras are carried onboard aircrafts. Aerial cameras include analogue and digital cameras. According to Habib et al. (2004b) the use of film metric cameras has been the norm in photogrammetric projects. However, the role of digital cameras in such projects has been rising along with its rapid development, ease of use and availability. By now, it can be said that a lot of the aerial photogrammetric single lens film cameras employed by various photogrammetric companies have been replaced by digital ones to benefit from

a fully digital environment. The next section will describe the aerial digital cameras which can be divided into three categories: small, medium, and large format cameras.

3.4 Digital aerial cameras

The transition from the conventional photogrammetric environment to the digital environment did not involve photogrammetric workstations only, but also photogrammetric cameras. Digital photogrammetric cameras have replaced conventional photogrammetric film cameras to achieve a fully digital workflow, beginning from the data acquisition stage, until the final photogrammetric products. Wolf and Dewitt (2000) explained that digital cameras use a two dimensional array CCD mounted at the focal plane of a single lens camera, where the acquisition of an image exposes all the CCD elements and produces the digital image. These digital cameras are classified, according to the amount of pixels they produce in the digital image, into small, medium, and large format cameras. Large format systems are mainly being used by large photogrammetric companies and national mapping agencies, whilst medium and small format cameras are predominantly applied in fields including forestry, agriculture, and disaster management. It is obviously hard to follow the development and availability of new systems from all suppliers, nonetheless, the following sections will highlight some of the available ones in the market.

3.4.1 Large format digital aerial cameras

The digital camera according to Leberl and Szabo (2005) is classified as large format, if it can provide an image with a swath width of 11000 pixels or more. While Petrie and Walker (2007) said that ‘large format cameras are those which produce digital frame images with image sizes of 50 megapixels or more’. Despite the many obvious advantages that large format digital aerial systems have compared to analogue film based cameras, according to Kremer and Cramer (2008) the introduction of these systems did not change two of the main challenges for the producers of aerial images. Firstly, the present day large format digital aerial cameras are of high weight and volume, which forbids the flexible use in smaller and cheaper aircrafts like small single engine

aircrafts and ultra-light aircrafts. Secondly, the relatively high price of those systems is a problem for smaller aerial survey companies and institutions.

Large format digital aerial cameras can be divided into two quite distinct categories (Petrie and Walker, 2007):

1- Individual cameras equipped with individual large-format area arrays producing monochrome (black-and-white) frame images.
2- Systems employing multiple medium-format frame cameras which produce subimages that are combined later using image processing techniques to form a single composite large-format digital frame image.

3.4.1.1 Single large format digital cameras

The large-format single frame cameras use the largest CCD area arrays that are commercially available. Since these arrays are very difficult to manufacture and have low yields, they are extremely expensive. This has restricted their use to reconnaissance cameras built for defence purposes. Recon/Optical is a major supplier of large-format digital frame cameras to government agencies and air forces. These include the CA-260/50 model, which is equipped with a 5k x 10k (50 megapixels) CCD array. Another model is the ‘‘dual-spectrum’’ CA-270, figure 3.3, which allows images to be acquired simultaneously in both the visible and infrared parts of the spectrum, enabling day and night acquisition of digital image data from airborne platforms. Another supplier is BAE Systems, with their ‘Ultra High Resolution Reconnaissance Camera’. This camera uses a 9.2k x 9.2k (85 megapixels) CCD area array (Petrie and Walker, 2007).

Figure 3.3: Recon/Optical CA-270 camera produces large format panchromatic and infrared monochromatic images simultaneously, (source: Petrie and Walker, 2007).

3.4.1.2 Multiple large format digital cameras

Due to the very high price of single large format digital cameras, and since a large field of view is mandatory in aerial photogrammetry due to the strong geometry/high accuracy requirements and for economical reasons; several CCD's can be combined to deliver the large ground coverage.

This approach employs sets of multiple medium format cameras coupled together to form an integrated unit (Petrie and Walker, 2007). The resulting images or sub-images are then rectified and stitched together to form a single large-format digital monochromatic image. These images can then be converted to colour images by using the spectral data acquired by a second set of small-format multispectral cameras that have been integrated into the overall camera system.

Among others, the main four suppliers of this kind of cameras are Microsoft, Intergraph, DiMAC, and Leica Geosystems. Microsoft has produced The UltraCamD and recently UltraCamX, figure 3.4, which was introduced at the ASPRS 2006 Annual Conference in Reno (Petrie, 2006). The UltraCamX retains the same basic design characteristics as the previous UltraCamD (section 3.5). The most important difference is the use of higher density CCD area arrays having pixels that are 7.2 µm in size giving panchromatic image size of 14430 x 9420 pixels or 136 megapixels instead of the 9 µm size which is used for UltraCamD with image of 11500 x 7500 pixels or 86 megapixels.

Figure 3.4: Sensor head of UltraCamX digital aerial camera system with 8 cones and five spectral bands (pan, RGB and NIR), adapted from Schneider and Gruber (2008).

In addition to that, the size of each of the four multispectral images in the UltraCamX has been increased to 4992 x 3328 pixels (16.6 megapixels) while for UltraCamD, it is 4008 x 2572 pixels (10.3 megapixels), figure 3.5, (Gruber et al., 2008) and (Microsoft, 2009).

Another high quality large format camera from Microsoft is the UltraCamX Prime (UltraCamXp) which was introduced at the XXIst ISPRS congress in Beijing, 2008. The UltraCamXp is an enhanced version of its predecessor UltraCamX. It has larger panchromatic image format at 196 megapixels (17,310 across track x 11,310 along track) and a smaller pixel size of 6 µm. Colour and NIR image size has also been increased to 5,770 x 3,770 pixels. According to Microsoft (2009), this camera is the largest format digital aerial sensor ever introduced, so it reduces the number of flight lines, saves time, and lowers cost, without sacrificing radiometric performance.

Another supplier, Intergraph, of large format digital frame cameras has introduced its Digital Mapping Camera (DMC), figure 3.6. According to Dörstel (2003) and Alamús et al. (2006), Intergraph has manufactured first DMC in the beginning of 2003. One of the most important DMC features is the capability to simultaneously capture high resolution panchromatic images of 13824×7680 pixels (106 megapixels) and multispectral images of 3042×2048 pixels (6.2 megapixels) in 4 bands (red, green, blue and near infrared), (Intergraph, 2008).

Figure 3.5: Left; concept of the Microsoft UltraCam large-format digital camera, showing the arrangement of the four lenses mounted along the flight direction and the multiple CCD area arrays that are used to generate the final panchromatic image. Right; the principal components of the Microsoft UltraCamX model with (from left to right) the camera unit with its recessed handles; data storage unit; and user display screen (source: Microsoft, 2009).

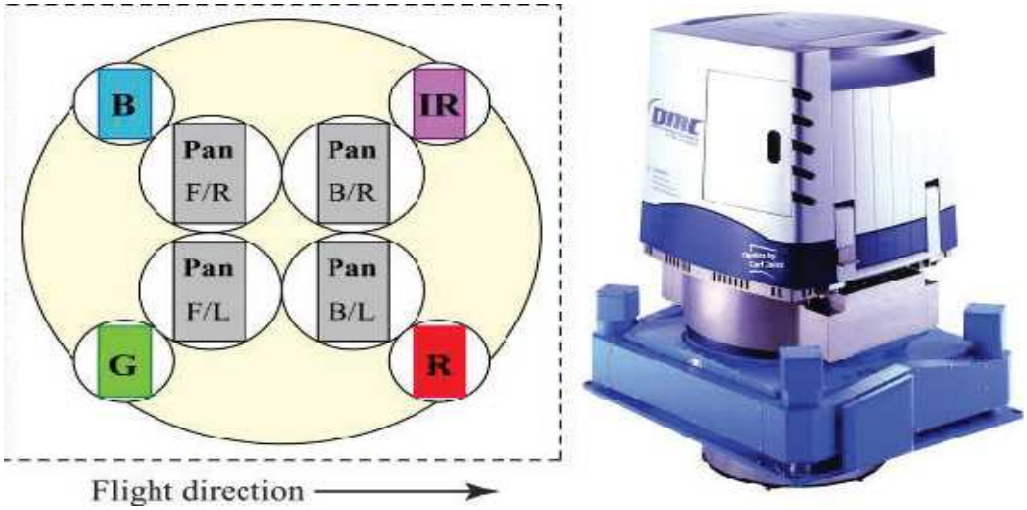

Figure 3.6: Left; Principle of the Intergraph DMC large-format digital camera system comprising four medium-format pan images pointing obliquely outwards in a star-like configuration; and four vertical pointing small-format cameras, each of the latter covering a different spectral band. Right; The Intergraph DMC camera in its current configuration mounted in a T-AS gyro-stabilised mount (source: Intergraph, 2008).

The high resolution image is assembled from 4 views taken with inclined cameras, each covering a quarter of the final image, called virtual image, figure 3.7. The 4 low resolution multi-spectral images are taken by 4 additional nadir looking cameras (one for each colour channel) and completely cover the virtual high resolution image.

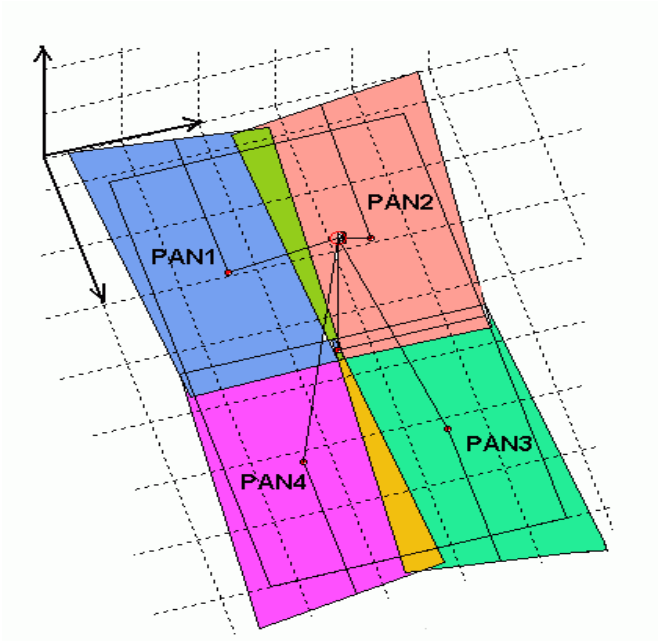

Figure 3.7: Footprint of 4 pan images projected into the virtual image (black), adapted from (Dörstel, 2003).

DiMAC^{WiDE} , announced at the ASPRS 2006 annual Conference, is the DiMAC's large format digital aerial camera that captures a footprint of 10,500 pixels across by 7,200 pixels along the flight line (75.6 Megapixels) with a pixel size of 6.8 μm by using just 2 adjacent camera modules, figure 3.8. The manufacturer claims that this new design decreases the risk of failure, as it contains less number of CCDs and associated components, and minimizes the required post-processing necessary to produce the final colour frame tiff image. Figure 3.9 depicts the side-by-side arrangement of the two vertical images which cover the areas to the left and right of the flight line, as used in the latest configuration of the DiMAC^{WiDE} camera, (Petrie, 2006).

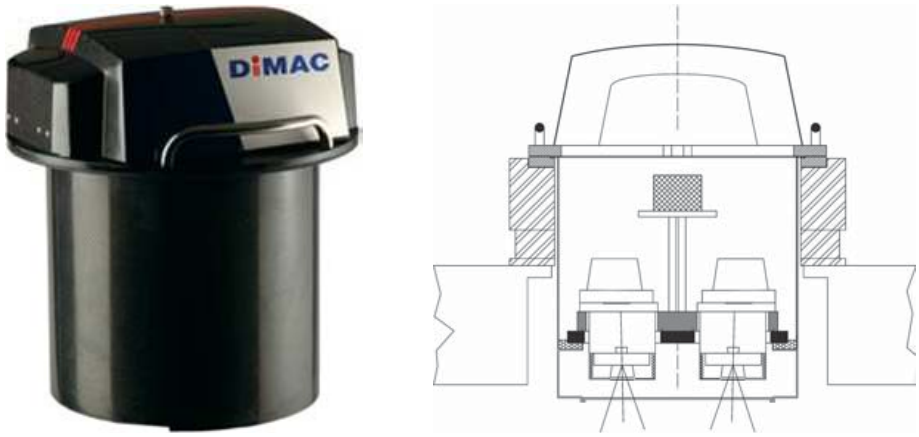

Figure 3.8: Left; DiMAC^{WiDE} large format digital aerial camera, right; schematic diagram showing the two camera modules, adapted from DiMAC brochure.

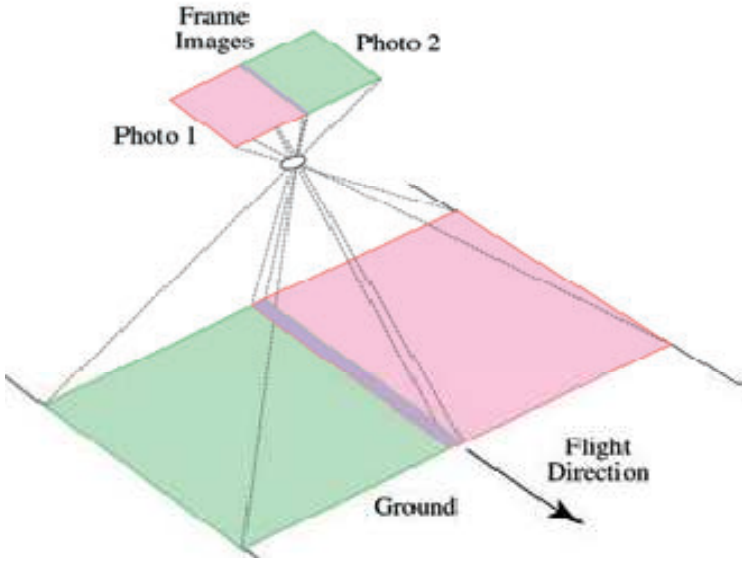

Figure 3.9: Arrangement of the two vertical images which are captured by the two camera modules used in DiMAC^{WiDE} digital camera, adapted from (Petrie, 2006).

3.4.2 Pushbroom scanner sensors

Leica Geosystems developed jointly with DLR- German Aerospace Centre- ADS40 digital imaging system (pushbroom scanner sensor), figure 3.10. This imaging system was introduced at the XIXth ISPRS Congress in Amsterdam in July 2000. According to Fricker (2001), it is the first airborne digital imaging device capable of performance, in terms of resolution and coverage, in a similar range to the established aerial film cameras with their 23 x 23 cm format.

Digital cameras must provide large field of view and swath width in addition to high resolution and accuracy. According to Sandau et al. (2000), the most readily available models of area CCD arrays in mid 1999 are 4k x4k pixels or less whereas a linear array of 12,000 pixels was readily available so that the linear arrays were used instead of multiple area CCD arrays in the ADS40. This imaging system has a pixel size of 6.5 µm, panchromatic line of 2 x 12000 pixels and RGB and NIR lines of 12000 pixels.

The three-line concept used in ADS40 results in three views; forward from the aircraft, vertically down and looking backward, figure 3.10. The imagery from each scan line provides information about the objects on the ground from different viewing angles assembled into strips.

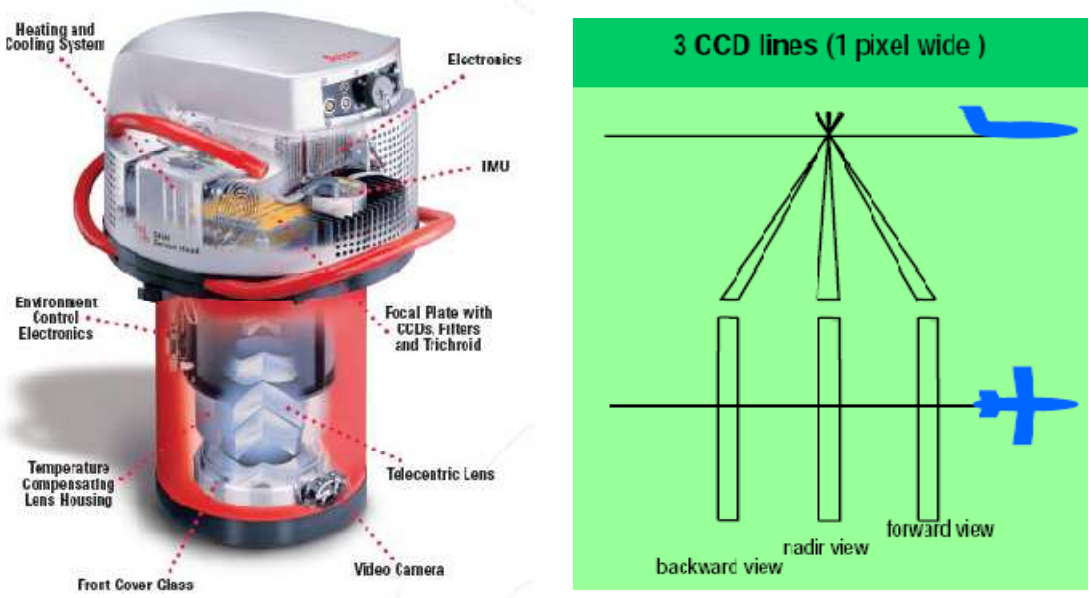

Figure 3.10: Left; the major components of the ADS40, adapted from ADS40 flyer, 2004, right; scanning principle of the three-line digital sensor, adapted from (Sandau et al. 2000).

Fricker, (2001) stated that 'one of the major advantages of the three line airborne digital sensors compared to area array sensors is the acquisition of strip imagery which produces a seamless scene that provides continuous processing in all photogrammetric procedures. Hence, it considerably increases the coverage and reduces the time required to mosaic individual images'.

A scene differs from frame photography in the way that it is scanned continuously rather than taken at a nearly discrete position. All scenes are scanned synchronously which results in seamless strip imagery along each flight line, figure 3.11.

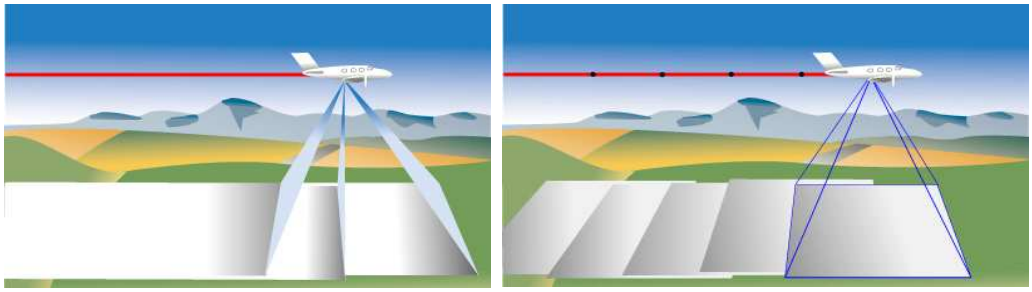

Figure 3.11: Continuous scan of three scenes (left) compared to discrete photos of a frame sensor (right), adapted from ORIMA manual.

Leica Geosystems formally announced the new ADS80 sensor at the ISPRS conference in Beijing in 2008. It is a pushbroom airborne sensor. Some of the differences between the ADS80 and the previous version, ADS40 are: the new Control Unit is smaller, the new system also introduces a new solid state Mass Memory unit which is smaller and weights only 2.5 kg, and has a few different options for data storage modes: single volume, joined volume, and in-flight backup. Furthermore, it contains new periphery equipment, including a new GPS/GLONASS Antenna. Overall, the system weight has been reduced by 26 kg (Leica, 2009a).

These types of large format digital cameras offer great advantages in radiometry and geometry. According to Leberl and Szabo (2005), these cameras are able to collect around 4000 to 7000 gray values for each colour channel. This is much more than the traditional 256 gray values achieved when scanning images, leading to good quality stereo matching. Furthermore, the purely digital aerial images offer excellent geometric performance as well, due

to the perfect edge sharpness achieved by avoiding the traditional film processing stage, as well as the scanning process.

3.4.3 Medium format digital aerial cameras

As stated in the previous subsection, the introduction of large format digital cameras did not solve two of the main challenges for the producers of aerial images; the high weight and volume of them which forbids their use in small aircrafts and their high price which is another problem for small surveying companies.

These reasons have pushed the development of medium format digital aerial cameras. Those cameras do not offer the same high number of pixels per exposure, but they are able to provide good image quality at lower cost and weight (Kremer and Cramer, 2008).

Within the last few years there has been an increase in the number of medium format digital aerial cameras coming to the market. According to Cramer (2005), the medium format digital cameras have image format of 4000 x 4000 pixels or better.

At the XXIst International Society for Photogrammetry and Remote Sensing Congress in Beijing, Vexcel Imaging, Microsoft's Photogrammetry division, announced the UltraCamL, figure 3.12, a smaller, lighter version of the UltraCam large format digital aerial camera system designed to better serve the needs of small mapping firms. The UltraCamL, at a lower price than existing large format systems, is also ideal for larger mapping firms who need to cost-effectively fly small projects or collect digital data in conjunction with LiDAR or other data. The manufacturer claims that it is the highest quality medium format camera available with its panchromatic image size of 9735 across track x 6588 pixels along track (64 megapixels), colour and NIR image size of 5320 x 3600 pixels (19 megapixels) and pixel size of 7.2 μm, (Microsoft, 2009).

From the 2009 annual conference for the American Society for Photogrammetry & Remote Sensing (ASPRS) in Baltimore, Microsoft Imaging announced the availability of the UltraCamLp medium format digital aerial photogrammetric camera. The announcement comes just 8 months after its predecessor, the UltraCamL, was announced. Based on the UltraCamL, the

UltraCamLp features the same advanced technical specifications but boasts an even larger format collection at 92 megapixels (11,704 x 7,920 pixels pan) compared to the UltraCamL 64 megapixel format, making it the largest-footprint medium format camera system on the market and ideal for smaller aircraft and local projects that require a rapid response. This image format capability is made possible through new electronics and a smaller CCD array of just 6 μm (Microsoft, 2009).

Figure 3.12: Sensor unit of the medium format digital camera, UltraCamL, (source: Microsoft, 2009)

In July, 2008 Intergraph introduced the RMK DT, figure 3.13, a new medium format digital aerial camera designed to replace film-based technology for smaller mapping and remote sensing projects and for high resolution engineering projects offering a 6096 x 6500 pixel (40 megapixels), (Intergraph, 2008).

Figure 3.13: Intergraph's medium format digital camera, RMK DT, (source: Intergraph, 2008)

During INTERGEO 2008, in Bremen, Germany, DiMAC introduced the DiMAC^{ULTRALiGHT} which is the smallest of the DiMAC product family and consists of just a single camera module that captures a footprint of 7,200 pixels across by 5,400 pixels along the flight line (38.8 megapixels) with 6.8 μm pixel size, figure 3.14, (DiMAC, 2009).

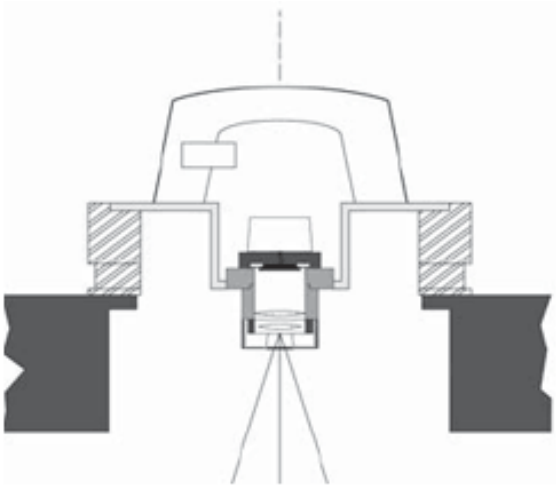

Figure 3.14: Schematic diagram of DiMAC^{ULTRALiGHT} showing only one camera module, adapted from DiMAC, 2009.

Leica Geosystems released the new medium format RCD100 Digital Camera System in March, 2009. It has a Frame size of 7216 pixels x 5412 pixels (39 Megapixels), figure 3.15, (Leica, 2009a).

Figure 3.15: RCD 100 Leica's medium format digital camera, (source: Leica, 2009a).

Another quite interesting technique was proposed by Kremer and Cramer (2008) to avoid using the relatively high price and high weight of large format cameras. It is to combine two or more of medium format cameras (dual or multi-head solutions). This combination of medium format cameras increases

the possible image strip width and therefore reduces the flying time and distance. The system consists of two 39 megapixel medium format cameras, with image format of 7216 x 5412 pixels for each camera, mounted with an oblique angle of +14.8° and -14.8°, respectively. This configuration results in an effective image width of 13650 pixels and still provides a sufficient overlap in between the two neighbouring images, figure 3.16.

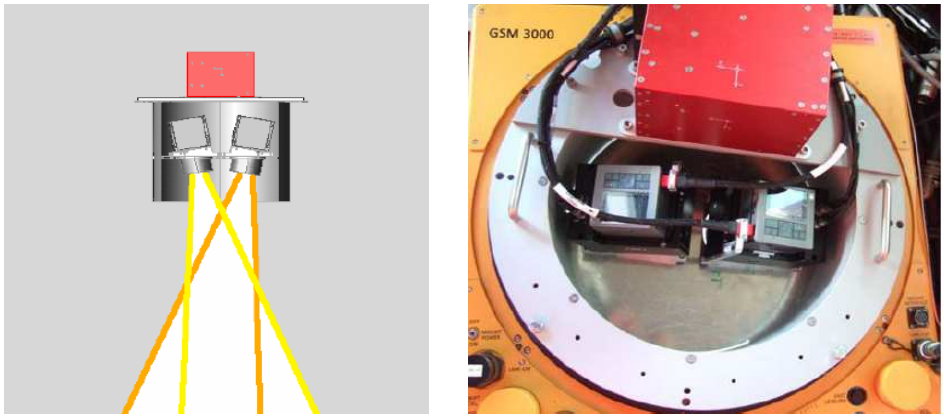

Figure3.16: Left; Arrangement of the two cameras and the IMU in the sensor pod, right; the system installed in the aircraft (Kremer and Cramer, 2008).

3.4.4 Small format digital aerial cameras

Petrie and Walker (2007) stated that 'the small format digital camera has a format size of up to 16 megapixels'. It is normally used for terrestrial photogrammetry purposes, due to the low resolution and ability to cover only a small area, according to Leberl and Szabo (2005). However, due to the advances in technology, especially in the field of small format cameras, this enabled the use of such cameras as digital airborne sensors because of their quite large lens system, as well as the stability and robustness they offer (Cramer, 2005). However, these small format cameras were not designed for photogrammetry i.e. they were not metric cameras, which will require later camera calibration to identify the type of geometry (Smith et al., 2007). The conventional small format digital SLR cameras have been used in many 3D projects, for example, Ortiz and Matas (2009) used a calibrated Canon EOS 400D, figure 3.17, in cultural heritage documentation of Caceres wall in Spain. Nikon D100 and SonyDSC-V1, figure 3.17, were used by Erving et al. (2009) in the test site located in Espoo, Finland. Whereas, Grussenmeyer et al. (2008) used Canon EOS 5-D, figure 3.17, for taking

photos all around the castle in modelling the medieval castle of Haut-Andlau, Alsace, France.

Figure 3.17: Some types of small format digital SLR cameras: top left, Canon EOS400D; top right, Nikon D100; bottom left, Sony DSC-V1; bottom right, Canon EOS 5D (source:dpreview.com/previews).

It is clear from section 3.4 that the aerial digital cameras are advancing rapidly in terms of resolution, for example, what is considered large format in 2006 (76 megapixels for DiMAC^{WiDE}) is considered medium format in 2009 (92 megapixels for UltraCamLp). Table 3.1 provides examples of aerial cameras and small-format cameras available resolutions as of late 2009.

Table 3.1: Available cameras' resolution as of late 2009.

Camera type	**Image format (pixels)**	**Pixel size (µm)**
Large-format aerial camera **(e.g. UltraCamXp)**	17310 x 11310 (196 megapixels)	6
Medium-format aerial camera **(e.g. UltraCamLp)**	11704 x 7920 (92 megapixels)	6
Small-format camera **(e.g. Canon EOS 5D Mark II)**	3750 x 5625 (21.1 megapixels)	6.4
Pushbroom scanner sensor **(e.g. Leica ADS80)**	linear arrays of 12,000 pixels each	6.5

Another quite different development of using small format digital SLR cameras that has come to the market recently is the use of combinations of near-vertical (nadir) and oblique pointing small format digital cameras to generate vertical and oblique (angled) images simultaneously as a plane flies along parallel flight lines in the same way as a traditional vertical survey is undertaken. These cameras are mounted in a single housing in a configuration of three cameras (1 vertical and 2 oblique) or five cameras (1 vertical and 4 oblique).

This concept of multiple cameras mounted together in a vertical and oblique configuration was first seen in the Fairchild T3A aerial (film) cameras of the 1930s, figure 3.18, (Petrie and Walker, 2007). Scheimflug invented an eight-lens camera, figure 3.18, in 1900, viewing oblique into 8 directions (Jacobsen, 2008). This concept is popular among emergency services, monitoring agencies and law enforcement authorities. In this current revival of the old idea, digital cameras are being used instead of film cameras.

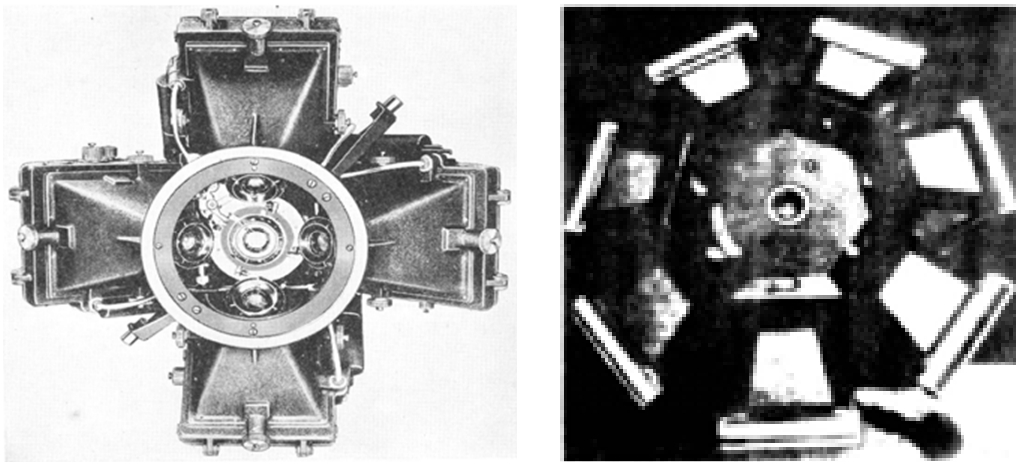

Figure 3.18: Left, the 1934 Fairchild T-3A camera system showing its five-camera arrangement with one vertical and four obliquely pointing cameras, adapted from TRACK'AIR brochure, 2009; right, the 1900 Scheimpflug's 8-lens camera, adapted from (Jacobsen, 2008).

This concept of obtaining oblique images simultaneously with the vertical images is gaining popularity on a daily basis as the oblique images are much easier to interpret by untrained (in aerial photo interpretation) professionals. In addition, multiple image photography using oblique aerial images can be a cost effective alternative to vertical aerial photography, satellite images, and

LiDAR for terrain analysis of relatively small areas. Furthermore, the capital investment in equipment, when using this approach, is relatively small compared to using large format sensors.

This configuration was introduced some years ago by several different companies: Pictometry, MultiVision, COWI Mapping UK, Getmapping, DIMAC and Track'Air. Recently it has also been adopted by several service providers in Europe.

The camera solutions vary from the relatively expensive five camera solution which gives a vertical and four compass point oblique views for every imaging position, for example Pictometry, MultiVision, and MIDAS, to the innovative and cheaper single rotating camera that provides four different angles of view in a single 360 degree rotation (AZICAM) developed by Getmapping (Cassettari, 2007). In addition, DIMAC Systems with its DiMAC^{OBLiQUE}, is using digital camera that includes 6 camera modules, 2 of them performing the vertical acquisition with an image footprint of 10500 by 7200 pixels while 4 camera heads acquire the oblique views at 90° to each other.

A representative system of the five-camera system is the MIDAS system (Multi camera Integrated Digital Acquisition System), figure 3.19, which is recently introduced by Track'Air from the Netherlands. This makes use of five of the Canon EOS-1Ds Mk.I or Mk.II CMOS-based small format digital cameras which produce individual frame images that are either 16.7 or 21 megapixels in size respectively. The MIDAS system also uses the well-known Applanix POS/AV GPS/IMU unit to carry out the measurement of the position and attitude of the platform at the time of the simultaneous exposure of the set of five photos (Petrie, 2006) and (Petrie, 2009).

On the other hand, on June 30th 2009, Getmapping has released details of its 'AZICAM' oblique camera system which was developed in close collaboration with Bath Spa University (GETMAPPING, 2009). It is a single-medium format digital camera mounted on a rotating plate or 'spinner' driven by a precise friction motor to orient the camera for each shot, instead of a normal four camera array used (by the other systems) to take 'North, South, East and West' orientations. The Company is claiming that their system

delivers a wider area of coverage, better image quality and costs less to calibrate and maintain as it is using a single higher-resolution camera. The whole system will fit in an aircraft already configured for a single vertical camera installation.

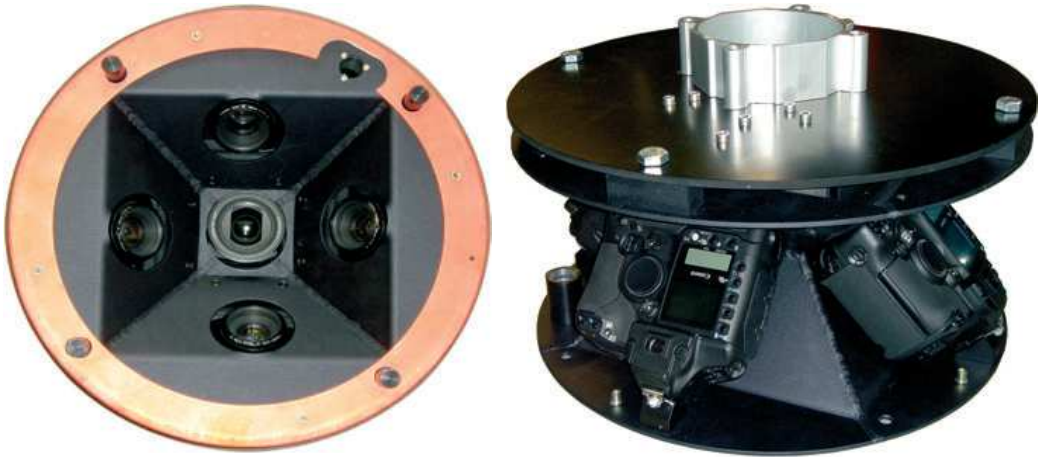

Figure 3.19: The arrangement of the single vertical camera and the four obliquely mounted Canon EOS small-format cameras forming the main part of Track'Air's MIDAS five-camera system as seen (left) from below, and (right) from the side, with the outer cylindrical case having been removed, adapted from (Petrie, 2006).

Pictometry imaging system will be discussed in more details in section 3.6 as it is used to capture some of the images used in this research.

3.5 UltraCamD large format digital imaging system

UltraCamD is an airborne multi-lens large format aerial digital camera that was introduced by Vexcel Imaging (owned by Microsoft since 2006) in May, 2003. It is a metric camera designed to undertake precise photogrammetric applications.

UltraCamD digital camera system delivers large format aerial imagery that is radiometrically and geometrically superior to images captured by conventional film cameras but with significant cost savings on each image. The UltraCamD digital process makes it completely compatible with existing photogrammetric procedures, while increasing productivity (Vexcel, 2007). As some of the digital images provided for this research were taken by Microsoft's UltraCamD large format digital camera system, it is appropriate, in this section, to highlight in some detail the specification and performance of this sensor.

3.5.1 Design Concepts of UltraCamD large format digital camera

Analogue cameras with an image size of 23 cm x 23 cm scanned at 20μm pixel size will produce the equivalent digital image of 11500 x 11500 pixels. Since there are no CCD arrays available with this size in the market, the large format digital images are realized by combination of several smaller format CCD arrays.

UltraCamD consists of four main components, namely the Sensor Unit (SU), the Storage and Computing Unit (SCU), the Interface Panel (IP), and the Mobile Storage Unit (MSU).The sensor unit, figure 3.20, is based on a multi cone concept. The design combines 9 area array CCD sensors of 4008 x 2072 pixels (subimages) and eight cones (camera heads). Four cones for high resolution panchromatic image and the other set of four cones is responsible for the multi spectral channels of the UltraCamD, i.e. red, green blue and near infrared. The optical axes are parallel and the four cones are configured along a straight line. One cone (the master cone) is equipped with four CCD sensors and defines the image coordinate system of each frame, (Gruber and Ladstadter, 2006) and (Smith et al., 2005).

Figure 3.20: Microsoft's UltraCamD large format digital camera showing the sensor unit of the camera which consists of eight independent cameras, so-called cones; the middle four create the large format panchromatic image at a size of 11500 by 7500 pixels. The other set of four cones is responsible for the multi spectral channels of the UltraCamD (source: Vexcel, 2007).

The Camera details are given below:

- Panchromatic, RGB and CIR imagery captured on a single pass
- 11500 pixels perpendicular to the flight direction
- 7500 pixels along the flight direction
- Focal length = 101.400mm
- CCD array sensor size =103.5 x 67.5mm
- CCD pixel size = 9 µm

Each image is captured using four panchromatic lens cones, in a line through the centre of the cone cluster, to create nine overlapping subimages from the 9 medium format CCD sensors of 4008 x 2072 pixels which are then combined into a single seamless large format panchromatic image of 11500 x 7500 pixels, figure 3.21, with embedded photogrammetric geometric information at an accuracy of about ±2µm according to the manufacturer. The multispectral channels are supported by four additional CCD sensors to the sides of the panchromatic cones.

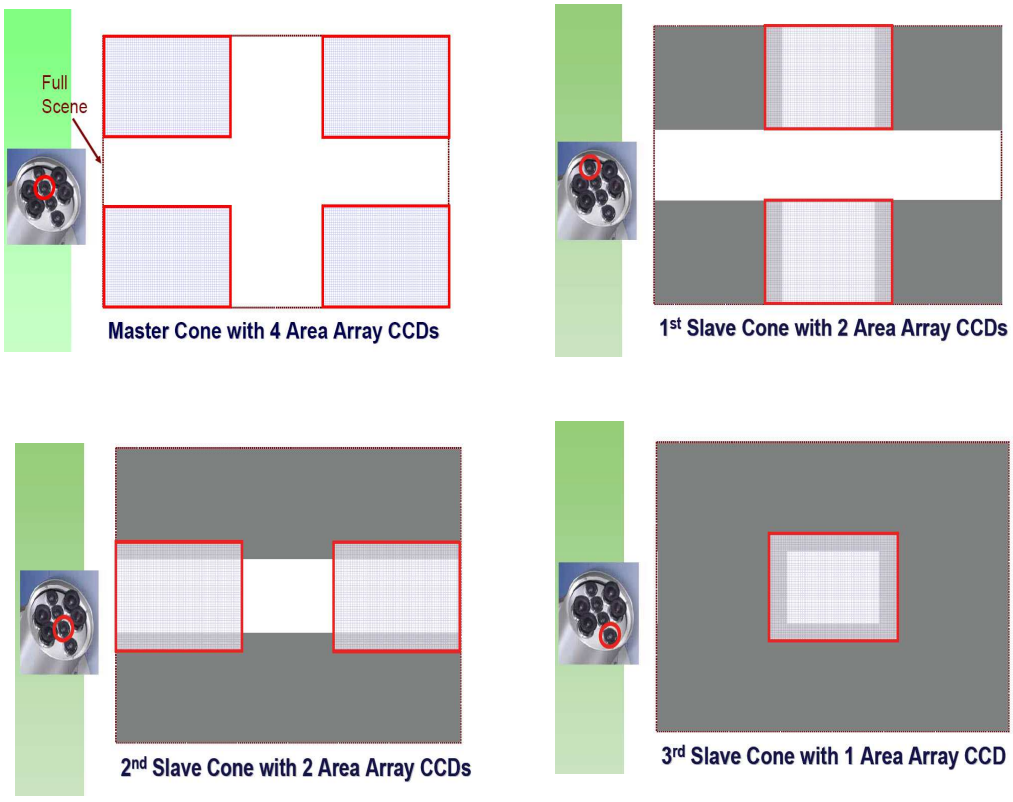

Figure 3.21: The positions of 9 subimages of 4008 x 2072 pixels within the panchromatic cones to create a combined large format image of 11500 x 7500 pixels, adapted from (Qtaishat, 2006).

3.5.2 Stitching process to create a large format image

The master cone is equipped with four CCD sensors and defines the image coordinate system of each frame. The remaining subimages are merged into the master cone's reference by using the tie point at overlapping areas, figure 3.22. Figure 3.23 shows the sequence of exposing the 9 sub-frames to produce a full image with a single central perspective. All the nine subimages are produced by the nine area CCDs from the same effective camera station.

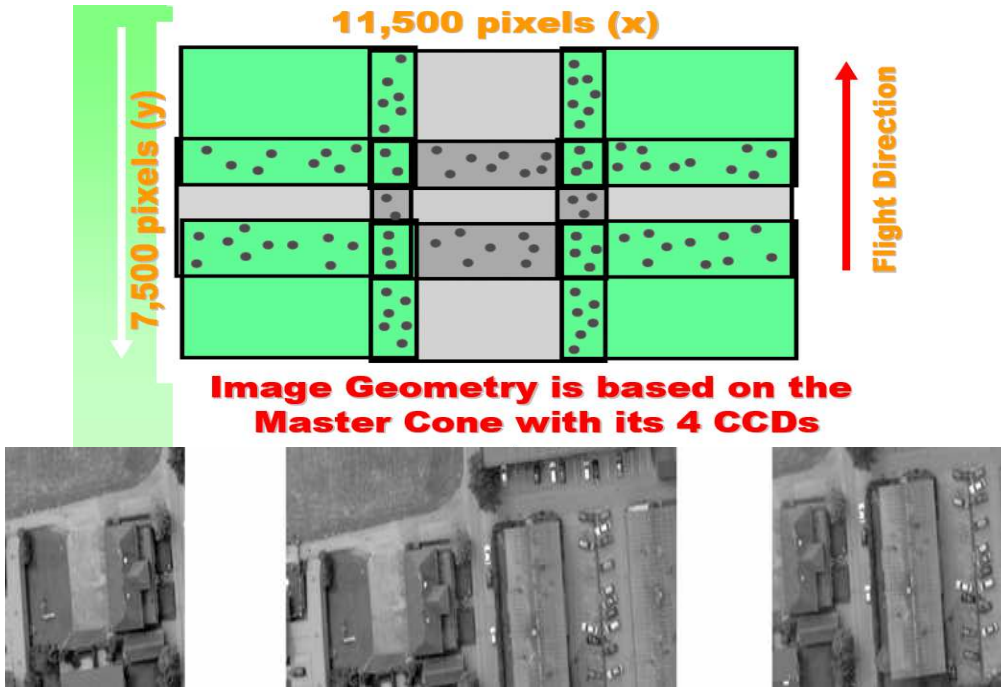

Figure 3.22: Top figure; the 5 sub-images are merged into the master cone's reference by using tie points at overlapping areas, adapted from Qtaishat, (2006). Bottom figure; illustrates the stitching of separate image segments; at the left and right are segments from two component images to be stitched, the centre shows the seam after stitching is completed, source: (Leberl F. and Gruber, 2003).

Most Earth digital imaging sensors, such UltraCamD, provide multispectral images at a lower spatial resolution (10 megapixels) and panchromatic images at a higher spatial resolution (84 megapixels). To get full-resolution colour Images, the panchromatic images are fused with the multi-spectral image in a process called the pansharpening. Pansharpening is a process of transforming a set of coarse (low) spatial resolution multispectral (colour) images to fine (high) spatial resolution colour images, by fusing fine spatial resolution panchromatic (black and white) image. Typically, three low-

resolution visible bands (blue, green and red) are used as main inputs in the process to produce a high-resolution natural (true) colour image. The results have both properties of the input data, namely high resolution and multispectral information. The method of pansharpening is shown in figure 3.24.

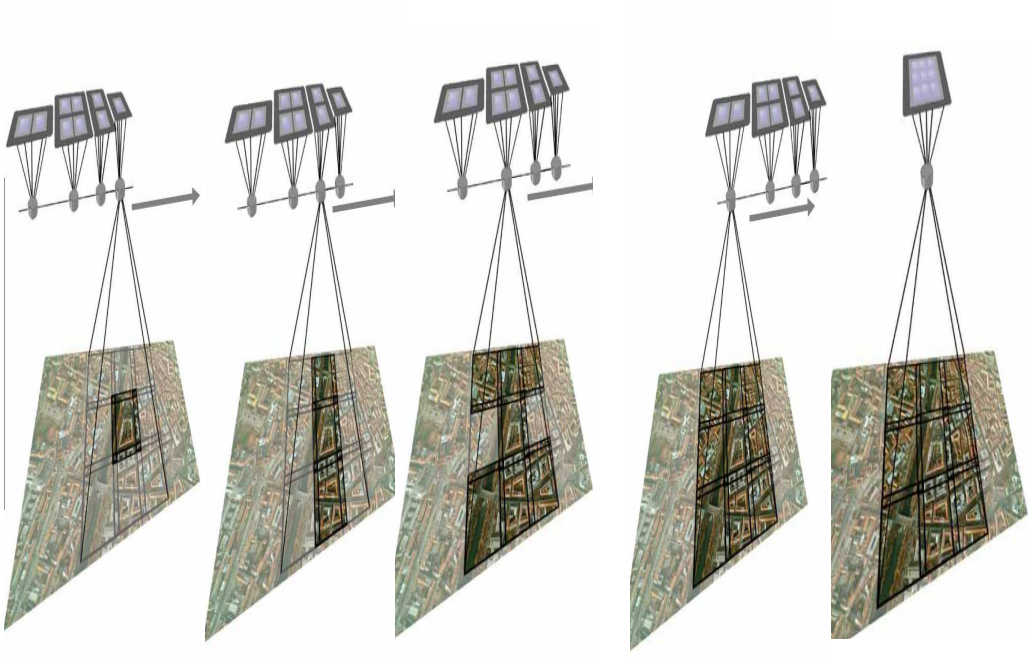

Figure 3.23: All the sub-frames produced by the nine CCDs, adapted from Qtaishat, (2006).

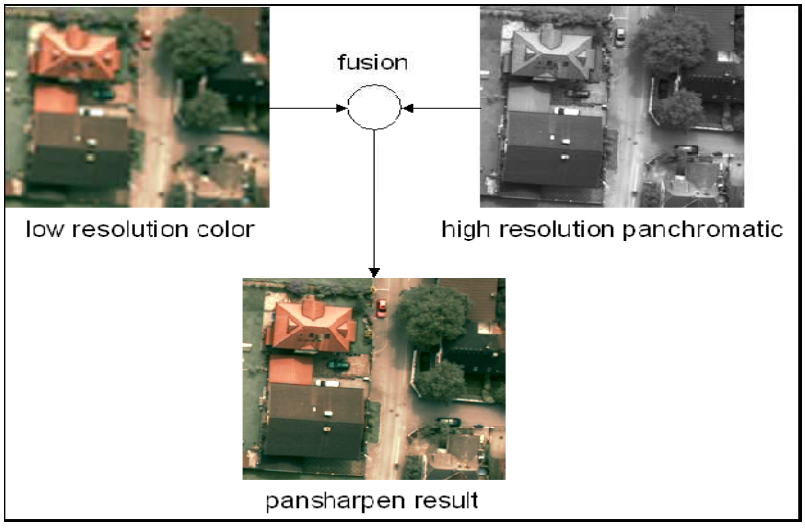

Figure 3.24: Pansharpening process to form high resolution colour image, (Source: http://vexcel.com/downloads/photogram/ultracam/whitepapers/Perko)

3.6 Pictometry digital imaging system

The use of standard vertical images as a topographic background in a GIS is nowadays very common, thus generating a strong demand for current photogrammetric airborne and high-resolution satellite data. Planners, administrative users and the general public use the available vertical images, for example, in Google Earth and other similar services, mainly for orientation and visual inspection of selected features. However, vertical images may not be easily interpreted by everyone. Because of the intuitive nature of oblique images, which appear similar to the common human perspective, these images are very attractive to decision makers, as well as to the general public (Grenzdorffer et al., 2008). At the present time, oblique aerial photography enjoys a much higher profile world-wide than it has done for many years. This is due partly to the activities of the Pictometry Company in the United States and its numerous licensees and competitors who operate multiple oblique cameras world-wide, (Petrie, 2009).

Pictometry is a technology company located in Rochester; New York, founded in 2000 and has introduced to the geospatial market the first imaging systems that used the concept of multiple small format digital SLR cameras to generate vertical and oblique (angled) images of a scene (Pictometry, 2008). The system comprises a single "near-vertical" (nadir) pointing camera and four oblique pointing cameras. Two of the oblique cameras point in opposite directions cross track, while the remaining pair of oblique cameras point in opposite directions along track. The resulting ground coverage of the five cameras takes the form of a cross, figure 3.25.

Due to the capability of the Pictometry system to capture vertical and oblique images from multiple directions, it presents an opportunity to evaluate automatic texture mapping methods for 3D building models. The test site for this research was captured by the Pictometry imaging system. Hence, a detailed description of the Pictometry system will be introduced in the following sections of this chapter.

3.6.1 Pictometry imaging system components

Pictometry digital imaging system has some unique features, compared with other digital mapping cameras/systems. The imaging system consists of a cluster of five digital cameras (one vertical and four oblique), GPS and IMU, and a flight management system. These, combined with a digital terrain model, enable georeferencing of the images so they can be integrated into a geo-spatial environment. According to (Wang et al., 2008), each camera has an array of CCD with about 4900 x 3200 pixels. The five digital cameras are arranged in such a way that four of them look forward, backward, left and right directions at a certain viewing angle respectively and one looks straight down.

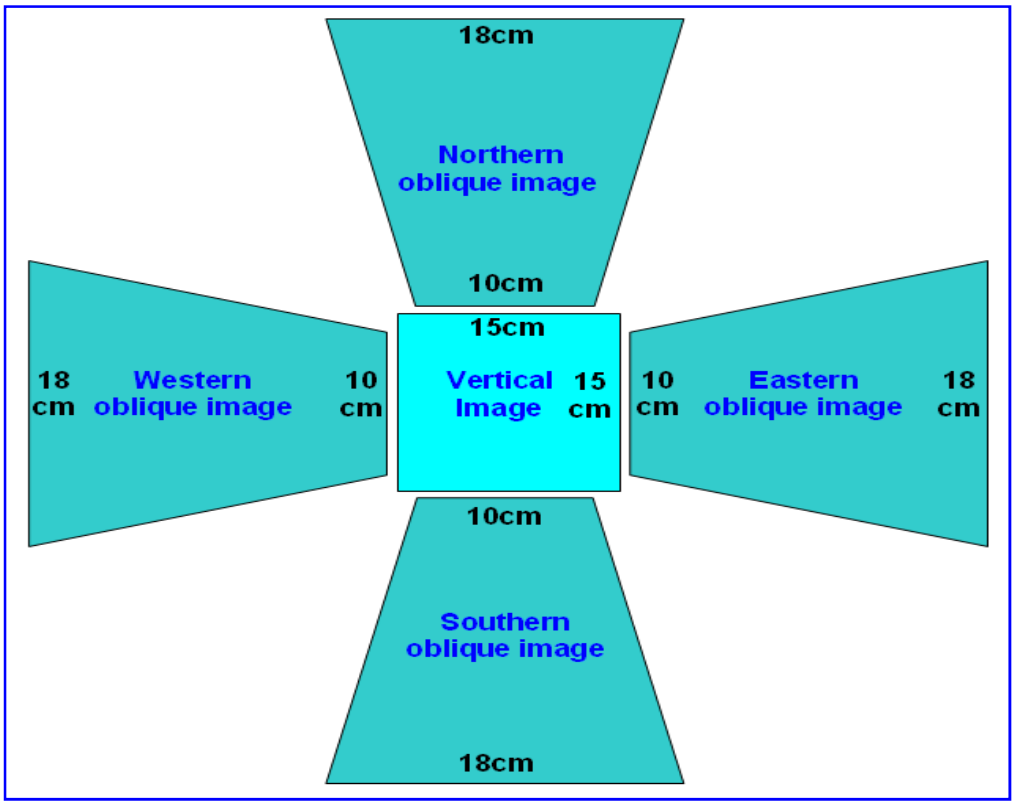

Figure 3.25: Diagram showing the distinctive cross ground coverage of the Pictometry five-camera system producing a single vertical image and four oblique images and the ground sampling distance of each image.

The camera in the vertical direction captures high-resolution vertical images and the other four acquire oblique images at different view directions, figure 3.26. The onboard GPS and IMU provide an accurate position and attitude of each sensor at exposure time, thus the images produced by Pictometry imaging

system are directly georeferenced images. Like traditional aerial images, vertical images provide a vertical view of the terrain surface, while oblique images show the side looking of objects on the ground such as buildings. Aerial platforms currently being used are a combination of Partanavia, Piper Aztec, and Seneca twin-engine aircraft. Each of these uses a standard aerial survey camera hole into which the Pictometry camera system is mounted. Each aircraft contains the five-camera cluster and 400 gigabytes of disk storage and collects approximately 1.1 gigabyte of imagery per square km (Simmons and Karbo, 2007). Furthermore, the Pictometry system comprises a sophisticated viewing and measurement software called Electronic Field Study (EFS) which is used to view the Pictometry images. In addition, EFS can be used to make measurements, navigate, add annotations, and work with shape files.

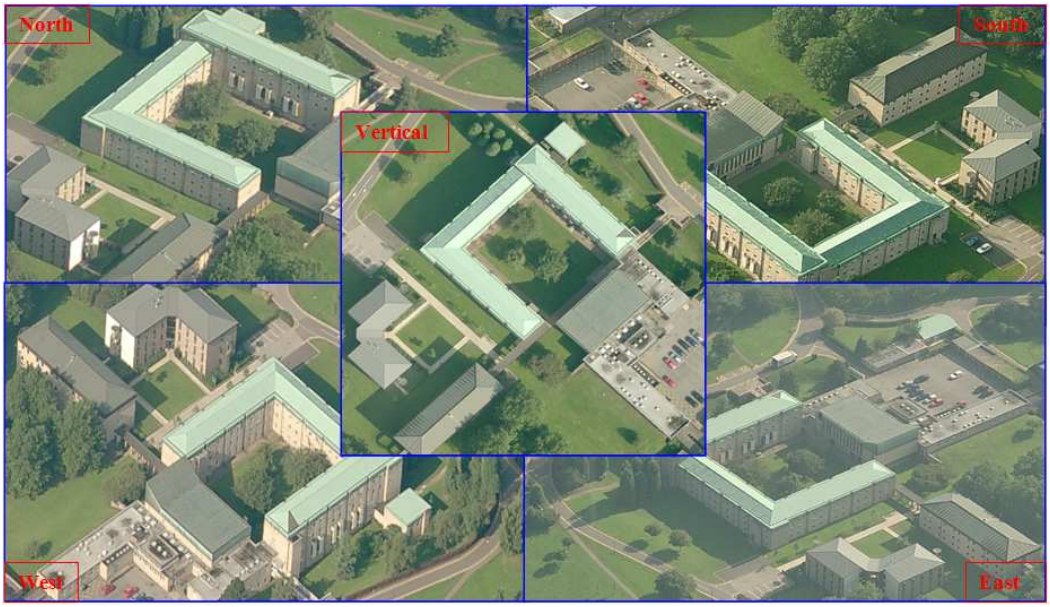

Figure 3.26: The Pictometry system has a five-camera system which can capture a site of interest obliquely (about 50 degrees) from typically the four cardinal points of the compass (North, South, East, and West), in addition to a vertical view. Screen shots of five images of a building in The University campus.

3.6.2 Design principles of Pictometry imaging system

Pictometry system uses medium format digital SLR cameras in a cluster configuration to obtain vertical and oblique aerial images from multiple viewing directions. It captures as many as twelve vantage points, typically with pixel resolution ranging from 15cm to 60cm. Usually, more than 80% of the

total images in an aerial survey are oblique ones covering buildings and other features of interest from multiple angles. These images reveal the front, back, and sides of objects of interest rather than just their tops. Despite the increasing adoption of the system by several mapping firms and local authorities around the world, there have been limited research publications and as a result there is limited information regarding specific details of the system. Figure 3.27 shows the main concepts of the Pictometry system.

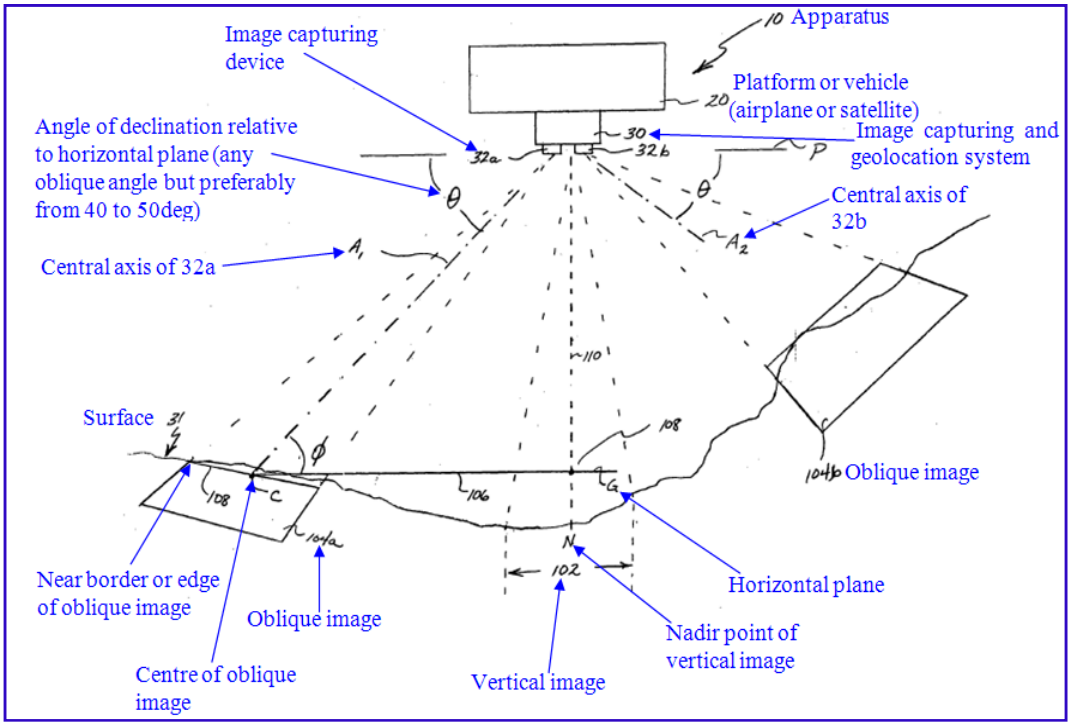

Figure 3.27: Diagram illustrating the platform carrying an image capturing system of the Pictometry imaging system and shows the exemplary vertical and oblique images taken, adapted and reproduced from Pictometry patent EP 1 418 402 A1, 2004.

The feature marked with (20) in figure 3.27 represents an airborne platform in which the image capturing system (30) is deployed. The schematics marked with (32a) and (32b) represent the oblique looking digital SLR cameras. The oblique cameras are mounted to the platform at an angle of declination θ from the horizontal plane (P) pointing at each side of the aircraft. The preferred angle θ used in Pictometry system ranges from 40 to 50 degrees. The image capturing system is illustrated in more detail in figure 3.28.

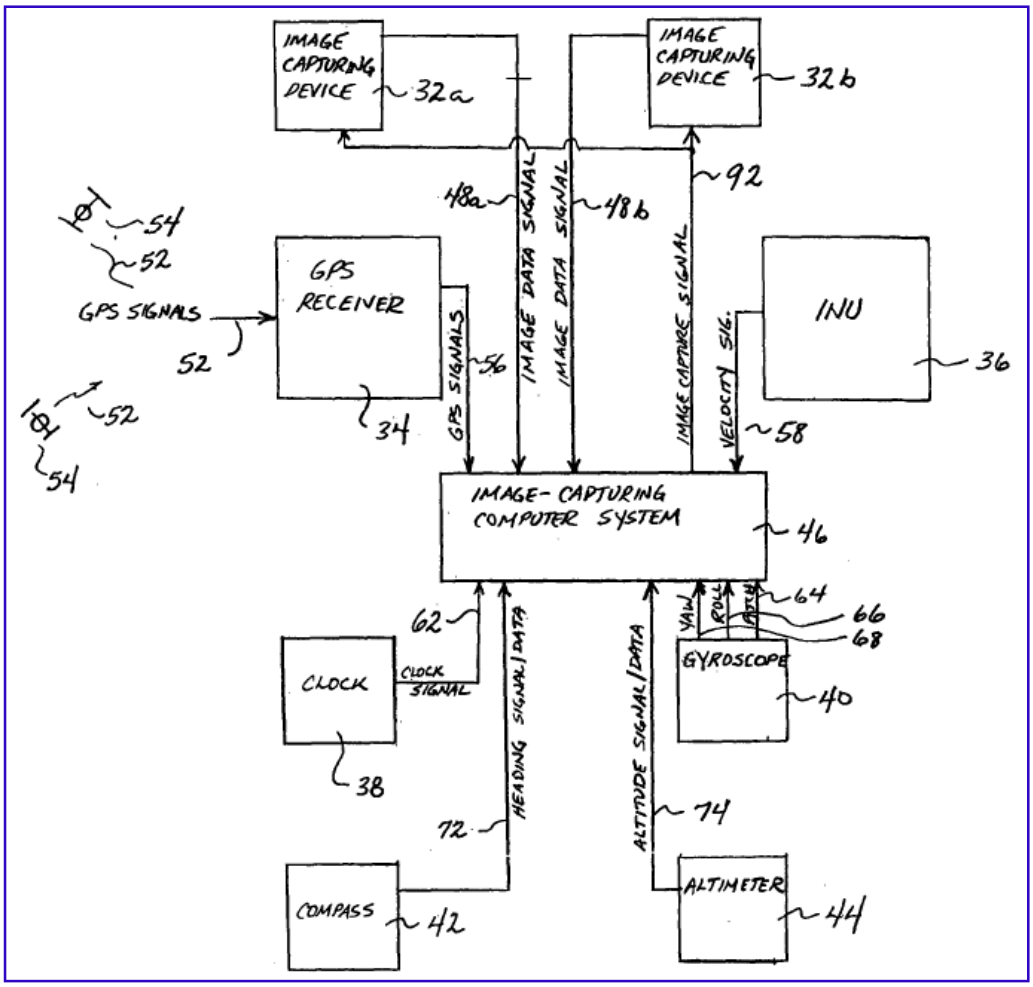

Figure 3.28: Diagrammatic view and the design concepts of the image capturing system, 30 in figure 3.27, adapted from Pictometry patent EP 1 418 402 A1, 2004.

There are some notable features in the above diagram; first, a precise clock (38) is utilized to keep the precise time measurement that is used to synchronize events within the image capturing system (30). The second noteworthy feature is that the system employs a laser altimeter (44) to estimate and store the altitude of the corresponding images captured. All the information from the external components (GPS, INU, gyroscope, etc.) is collected and stored by the onboard image-capturing computer system (46). The image files are stored together with the positional and attitude information. The proprietary software EFS that ships with image data enables further manipulation of the data. The ground coordinates of object points are calculated on the fly for each corresponding pixel using the collinearity condition and a DTM for elevation information. The following notes regarding the system should be made:

- The image capturing system (30) of the present invention can be alternately configured, such as, for example, to derive and/or calculate altitude, pitch, roll and yaw, and compass heading from the GPS and INU signals/data, thereby rendering one or more of the gyroscope, compass and altimeter unnecessary. In figure 3.27, image capturing devices (32a) and (32b) are at an equal angle of declination relative to the horizontal plane (P). However, it is to be understood that the declination angles of the image capturing devices do not have to be equal.
- In figure 3.28, image capturing computer system (46) executes image and data acquiring software that issues a common or single image-capture signal to the image-capturing devices to thereby cause those devices to acquire or capture an image. However, it is to be understood that the present invention can be alternately configured to separately cause the image capturing devices to capture images at different instants and/or at different intervals (Pictometry patent, 2004).

Pictometry imagery consists of orthogonal (traditional straight down images) and oblique images (images taken at an angle of around 50 degrees) which can be taken from two different imaging levels; community and neighbourhood. In this research, neighbourhood images at flying height of 1000m which were supplied by Blom Aerofilms will be used.

3.6.3 Vertical Pictometry imagery

Pictometry imaging system is capable of capturing images at various levels of resolution or ground sample distances (GSD) according to the customer requirements. The first level of detail, referred to as a community level, is taken at a flying height of about 1500-1800m and have an average ground sampling distance (amount of ground covered by one pixel or cell in the raster file) of 60cm/pixel for the vertical images, figure 3.29. The second level of detail, referred to as a neighbourhood level, is significantly more detailed than the community level images. Neighbourhood level vertical images have a ground sample distance of 15cm/pixel and are flown at approximately 600-1000m depending on flying height restrictions in every city, figure 3.30.

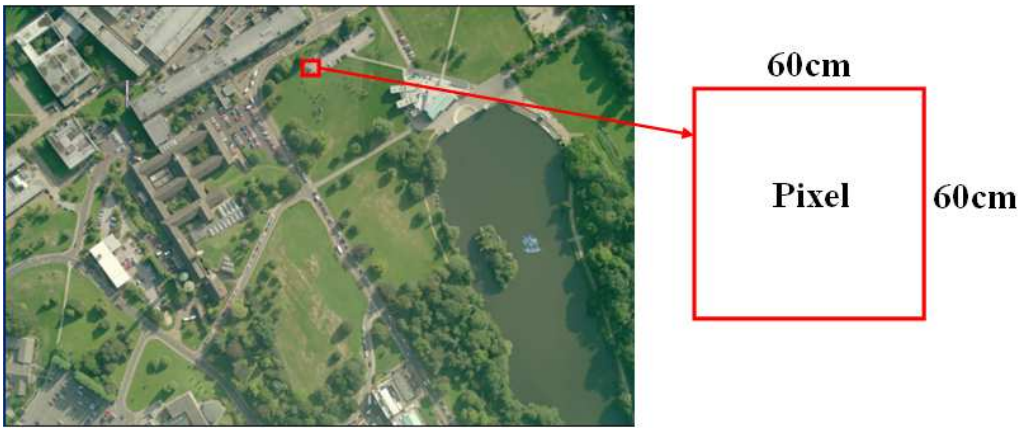

Figure 3.29: Illustration of the ground sampling distance of 1 pixel in vertical community images

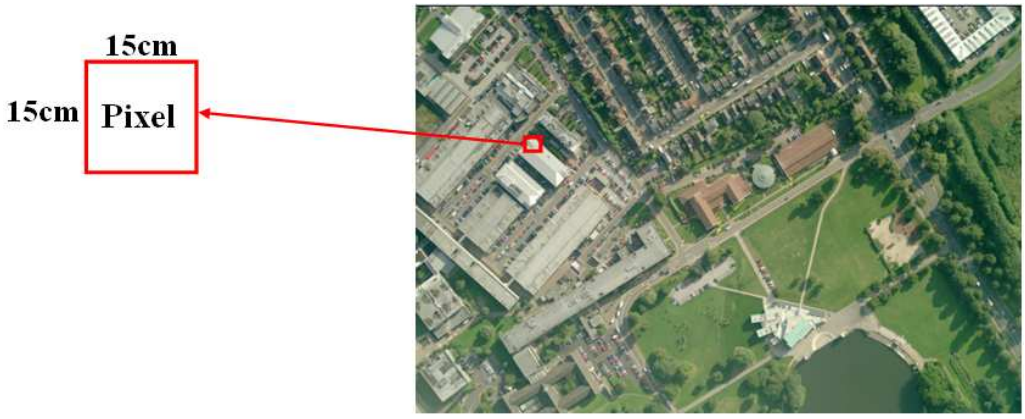

Figure 3.30: Illustration of the ground sampling distance of 1 pixel in vertical neighbourhood images.

The ground sample distance for both types of vertical images (community or neighbourhood) remains substantially constant throughout the image. Vertical images are captured with sufficient overlap to provide stereo pair coverage.

3.6.4 Oblique Pictometry imagery

In the past oblique images were generally taken for visualization and interpretation purposes, rather than for metric applications. An exemption is the military sector were oblique images has been a standard for reconnaissance purposes for a long time (Smith, 1989). Thus oblique images were generally outside of the focus of photogrammetrists mainly due to the difficulties in making measurements and computations. Digital photogrammetry has reduced

some of the difficulties and they now have further potential as a new data source for photogrammetry and GIS (Grenzdorffer et al., 2008).

Because of the intuitive human perception of the oblique view, photogrammetrists' attention has recently returned to oblique images. Oblique aerial photography is fast becoming the new 'must have' image product to complement vertical aerial photography, which is now regarded by many as an essential information asset. Oblique aerial photography, when captured in a systematic way, combined with sophisticated viewing and measurement software tools such as EFS, offers context of features in a more easily understood 3D perspective, with side-on views that are more familiar to many users. The images have many of the features that users expect with vertical imagery such as the ability to take overlapping images and create stereo views, while at the same time providing additional detail. The oblique perspective provides a richer view of the World when combined with traditional vertical aerial photography.

Pictometry oblique images can be taken from two different imaging levels: community and neighbourhood levels. For oblique community level images, the ground sample distance varies from, for example, approximately 45cm pixel in the foreground of the image to approximately 60cm per pixel in the mid-ground of the image, and to approximately 90cm per pixel in the background of the image, figure3.31. Oblique community level images are captured with sufficient overlap such that each area of interest is typically covered by at least two oblique images from each compass direction captured.

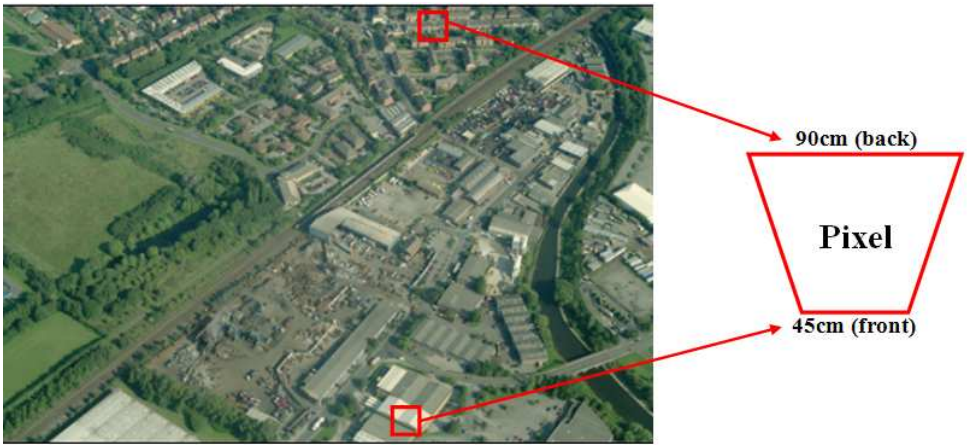

Figure 3.31: Illustration of the ground sampling distance of 1 pixel in oblique community images.

The second level of Pictometry oblique imagery is the neighbourhood oblique images which are taken at a flying height of about 600-1000m. Oblique neighbourhood level images are significantly more detailed than the community level images. They have a ground sample distance of, for example, from approximately 10cm per pixel in the foreground of the image to approximately 15cm per pixel in the mid-ground of the image, and to approximately 18cm per pixel in the background of the image, figure3.32.

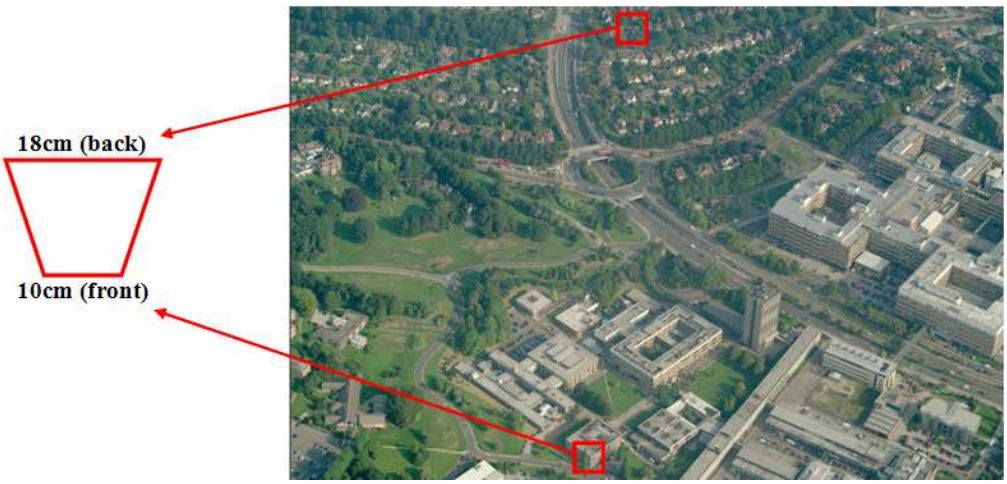

Figure 3.32: Illustration of the ground sampling distance of 1 pixel in oblique neighbourhood images.

Oblique neighbourhood level images are captured with sufficient overlap such that each area of interest is typically covered by at least two oblique images from each compass direction captured, and such that opposing compass directions provide 100% overlap with each other.

It also should be noted that capturing oblique community and/or neighbourhood level images from all four compass directions ensures that every point in the image will appear in the foreground or lower portion of at least one of the captured oblique images, where ground sample distance is lowest and image detail is greatest.

The difficulty has until recently been the cost of capturing film based obliques and georeferencing these for use in a GIS environment. However, the advent of digital cameras for aerial platforms and with digital camera technology changing so fast, in particular the image array size and therefore the area of capture, as well as the development of viewing software where the

oblique imagery is linked to a map or vertical aerial base for reference has overcome one of the major hurdles. The second hurdle is georeferencing of images that have a variable scale/resolution. In the example image shown in figure 3.32 the pixel resolution in the foreground is about 10cm, in the mid scene about 15cm and in the far ground about 18cm. The actual resolutions are a function of the angle the image is taken at, although 45 degrees seems to be the common standard at present. The most innovative solutions such as that generated by Pictometry allow the obliques to be georeferenced based on the aircraft INS and linked through the vertical image or map base to a terrain model.

Georeferencing the oblique imagery extends the benefits of traditional vertical images. This provides a unique perspective view of a locality, allowing users to:

- see each side of a building, structure, or feature, exposing blind spots, exits, and entrances previously impossible to locate on vertical photography,
- measure the height, length, and area of features directly from photography,
- improve the identification of hard-to-see assets and facilities (e.g. lamp posts, telegraph poles, etc.) that can be difficult to distinguish on traditional orthophotography,
- improve the readability of geographical information for non-cartographic skilled people and,
- view GIS data in 3D by draping it on oblique imagery, extending the traditional and more familiar 2D view afforded by most GIS applications, (Pictometry, 2008).

Pictometry supports a variety of applications in planning, property, 3D modelling, change detection, emergency response, insurance, security, navigation and mobile phones, etc.

3.6.4.1 Making measurements on oblique images

The conventional approach of forcing the variously-sized foreground and background pixels of an oblique image into a uniform size to thereby warp the image onto a coordinate system dramatically distorts the oblique image and

thereby renders identification of objects and the taking of measurements of objects depicted therein a laborious and inaccurate task. Correcting for terrain displacement within an oblique image by using an elevation model further distorts the images thereby increasing the difficulty with which measurements can be made and reducing the accuracy of any such measurements (Schultz et al., 2004). Therefore, what is needed is a method and apparatus in photogrammetry that enable geolocation, accurate measurements, and measurement of heights and relative heights of objects within oblique images. Pictometry imaging system provides this through georeferencing of oblique images and using the EFS software.

Generally, through the user computer system, measurements of and between objects depicted in oblique image can be taken by selecting one of the several available measuring modes (distance, area, height, etc) that are provided within EFS. The user selects the desired measurement mode then selects a starting point/pixel and an ending point/pixel on the displayed oblique image. The software automatically calculates the quantity requested by the user. The calculation of, for example, the distance between starting and ending pixels is accomplished by determining the geolocation of each selected pixel on the fly and then the difference between the geolocations of both pixels determines the distance between them. As an example of how the geolocation of a given point within the oblique image is determined, it will be assumed that, for simplicity, the location of the oblique image centre (C) to be determined. As shown in figure 3.27, line (106) extends along the horizontal plane (G) from a point (108) which is directly below image capturing device (32a) to the centre of the image (C). An extension of primary axis (A_1) intersects with centre (C). Angle φ is the angle formed between the line (106) and the extension of (A_1). Thus, a triangle is formed, figure 3.33, having vertices at imaging device (32a), point (108), and centre (C), and having sides 106, the extension of (A_1), and the vertical dashed line (110) between imaging device (32a) and point (108).

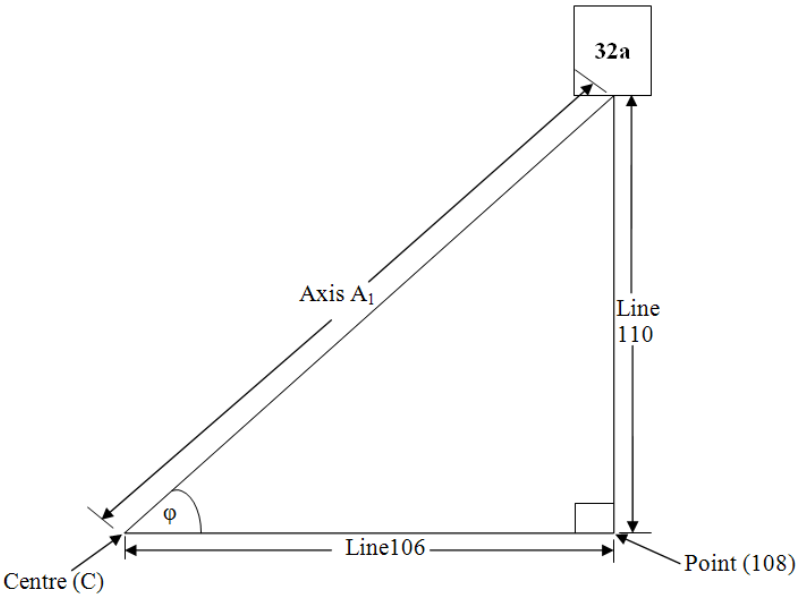

Figure 3.33: Diagram illustrating the triangle formed to calculate the geolocation of the oblique image centre (C).

Since the exact position of the image capturing device (32a) is known at the time of exposure (from exterior orientation parameters) and the length of the triangle side (110) is also known (the altitude of image capturing device), the position of point (108) can be determined. Furthermore, with the length of side (110) and the angle φ are known, the length of sides (106) and (A_1) can be calculated by simple geometry. Moreover, from the position of point (108) and the length of triangle side (106), the exact location of oblique image centre can be determined. Finally, the geolocation of any other pixel on the oblique image can be determined using the geolocation of point (C) and the camera parameters such as focal length, sensor size, etc. Knowing the position of any pixel on the image enables the user to perform any sort of measurement.

It should be noted here that the ground plane is assumed horizontal, flat, or non-sloping plane which typically has an elevation that reflects the average elevation of the terrain. On the other hand, any slope or grade in the surface will result in a difference in the elevation of the nadir point relative to any other point of interest. Thus, referring back to figure 3.27 and figure 3.33, the triangle formed by (106), (110), and (A_1) will no longer be a right-angled triangle. If such is the case, any geometric calculations assuming that the triangle is a right triangle will contain errors. For instance, if the surface slopes

upwards between nadir point (N) and image centre (C) at the edge of oblique image and if the centre (C) is higher than (N) by 10m and with a declination angle θ equal, for example, 50°, the calculated position of centre (C) will be off by about 8.4m if no correction for the change in elevation between the points was introduced. According to the Pictometry patent (2004), corrections are applied to improve the geolocation of points on oblique images by introducing a pre-calculated tessellated or faceted ground plane, see appendix A.

3.6.5 Quality and accuracy characteristics of Pictometry imagery

Despite the widespread use of Pictometry imagery by many organizations in the UK and abroad, there have been very few research efforts to quantitatively analyze the photogrammetric potential of this system. One of the most significant efforts in recent years to evaluate the quality of the direct georeferencing method and the accuracy of the extracted information has been performed by Federal Emergency Management Agency (FEMA) in the USA (FEMA, 2005). The report was an effort to investigate alternative methods for obtaining ground elevation information using different data sources; one of them is the Pictometry system. The data for that specific quality assessment include the following sets:

- 2-view Pictometry of 29 houses in Prince George's County, Maryland compared against a LiDAR dataset approximately equivalent to 60cm contours.
- 4-view Pictometry of 27 houses in Arlington County, Virginia compared against surveyed spot heights at corner adjacent grades.

Accuracy analysis indicated that the average vertical error in top of bottom floor elevations to be 80cm and the overall top of bottom floor vertical accuracy to be 1.90m at the 95% confidence level. When performing the quality assessment, the report highlighted the following potential error sources that may have caused the elevation to be larger than expected:

- Errors in the LiDAR data.
- Errors caused by only having 2-view Pictometry imagery instead of 4-view images to see the buildings from all sides.

- Errors caused by limitations in being able to correctly interpret and measure features with Pictometry imagery.

For the second data set, accurately surveyed spot heights around 27 houses in Arlington County were provided where Pictometry had 4-view imagery available. This would enable sources of the error to be assessed. The average vertical error in top of bottom floor elevations in Arlington County was 48cm and the overall vertical accuracy was 1.53m at the 95% confidence level. The report recognizes that these errors were on the high side partly because these houses were complex split levels on hillsides, and the houses were surrounded by tall trees that blocked many of the aerial oblique views. Of the 27 houses, eight had misidentified the basement or split level to be surveyed for the top of bottom floor, the principal cause for the high error statistic. Pictometry may provide substantially improved results in locations where basements are not an issue (FEMA, 2005).

Despite the above justification, what the report did not mention is that if the inability of the operator to accurately determine conjugate points in multiple images is isolated, the above errors reflect, even partially, the effect of four main error sources in the Pictometry system:

- Errors caused from the performance of the GPS/IMU in the direct georeferencing process.
- Errors due to poor calibration of the individual cameras or lack of calibration as a single cluster of cameras.
- Errors due to the accuracy of the DTM used with Pictometry imagery and the interpolation that takes place when calculating the elevations.
- Errors caused by the non-uniform scale and not constant GSD in oblique images.

One of the most recent evaluation efforts of the Pictometry system was presented by Smith et al. (2008) and by Hamruni et al. (2008). In this research, Pictometry data were obtained over the city of Nottingham by Blom Aerofilms, see chapter 4 for a thorough description of data sets. Smith et al. (2008) and Hamruni et al. (2008) presented results from aerial triangulation using the vertical and oblique images separately and in combination in order to assess the

quality of the block of images for photogrammetric and precision mapping application, see chapter 5 for the AT results.

3.7 Summary

Digital photogrammetry is relatively a young field, but fast growing due to improvements of computational power of computers, digital cameras, and storage capacity. The transition to a digital photogrammetric environment and the use of digital workstations has reduced the cost of photogrammetric products, improved image quality and allowed the automation of some of photogrammetric products such as DSM and orthoimage generation.

The use of large format digital aerial cameras is growing in several applications in recent years such as: mapping, agriculture, industrial inspections, environmental applications, and security applications. The introduction of the large format aerial digital cameras contributed significantly in the reduction of film costs, film development, and costs of scanning aerial photographs. Medium format cameras can be used in small photogrammetric projects where using large format digital cameras can be too costly.

The use of multiple oblique cameras overcomes many of the present limitations of using vertical images to view objects on the earth surface. As a result, numerous digital oblique imaging systems using multiple small format or medium format cameras have been and are being designed and built for use in airborne platforms. At the same time, it is extremely interesting to observe the revival or re-birth of the distinctive configuration of the old Fairchild T-3A film-based five-camera systems dating from the 1930s. This is now being employed in the modern multiple digital camera systems that are being used extensively for the acquisition of high-angle oblique frame images for visualization and interpretative purposes and as a vital component in the construction of detailed and realistic 3D city models.

Oblique imagery, combined with sophisticated viewing and measurement software tools, provides an interesting route into the 3rd Dimension.

CHAPTER 4: DATA SETS AND TEST SITES

4.1 introduction

Any photogrammetric project will involve two main stages: data acquisition and image processing. Data acquisition involves good flight planning to produce good image acquisition. The second stage involves preparing and processing the images and associated data (GPS/IMU) to generate the required product.

This chapter describes the two test sites used in this research, the main campus of The University of Nottingham and a small part of Nottingham city centre. In addition, this chapter gives an overview of the data provided for the purpose of this thesis, which has been collected using the sensors described in section3.5 and section 3.6, and a description of the data acquisition stages, such as: image acquisition and ground control points. This chapter will also include some details on the preparation of flight planning. Even though it is outside the scope of this thesis, it is believed that it is important to have some knowledge of the methodology involved in carrying out such a task.

4.2 Test sites

Images were available covering The University of Nottingham Campus with both Pictometry and the UltraCamD images and formed an ideal test site for the research described. Ground coordinated points have been established and formed the basic ground control for the Pictometry images and UltraCamD images. By combining the two image sets together it is possible to assess the value of using the larger format UltraCamD images with the oblique images for 3D building model texturing. A small area in the city centre of Nottingham will be used as a further application case study, after approving the viability of Pictometry imagery in producing high quality 3D models, where only Pictometry images are available. GPS ground survey has been used to provide independent check points for the evaluation.

The University of Nottingham main campus, figure 4.1, is located just about 3km west of Nottingham's city centre with a total area of about 146 hectares. This study area consists of buildings in various styles ranging from

residential buildings with flat and gable type roofs to industrial buildings with complicated roof details. The topography of the terrain is characterised by rolling hills with dense vegetation and tree clusters presented in many locations.

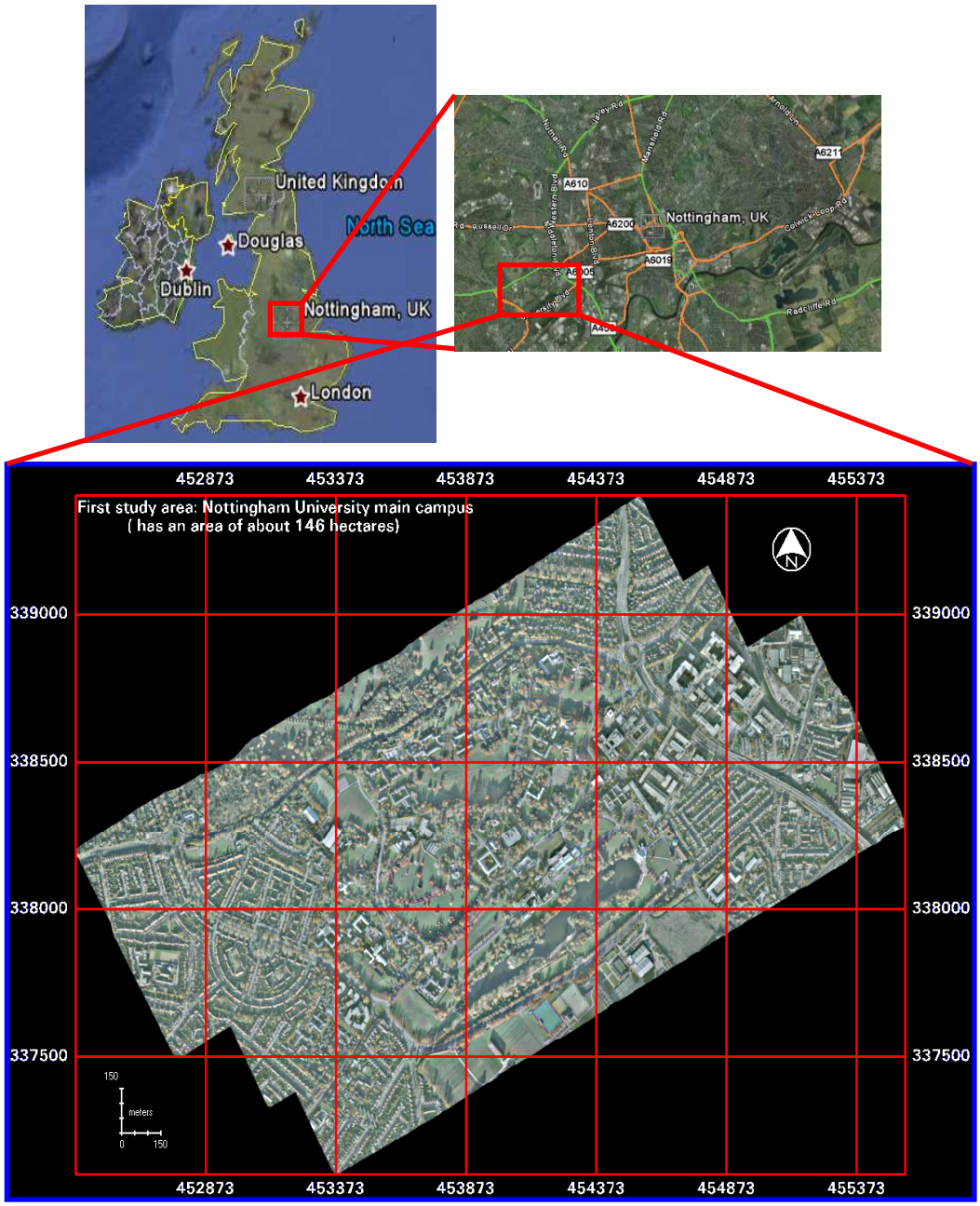

Figure 4.1: A mosaicked image of the first study area; Nottingham University main campus, upper two images adapted from Google Earth.

The second test site, figure 4.2, is located in the Nottingham city centre with an area of about 0.5 km^2. This test site represents a highly built-up area with different types of buildings that range from modern commercial, industrial

and residential building structures and architectures to medieval gothic style architectures. The roof tops of the buildings in this study area are of various types with a lot of details that need to be modelled. This site is relatively flat with light vegetation and trees presented in some areas.

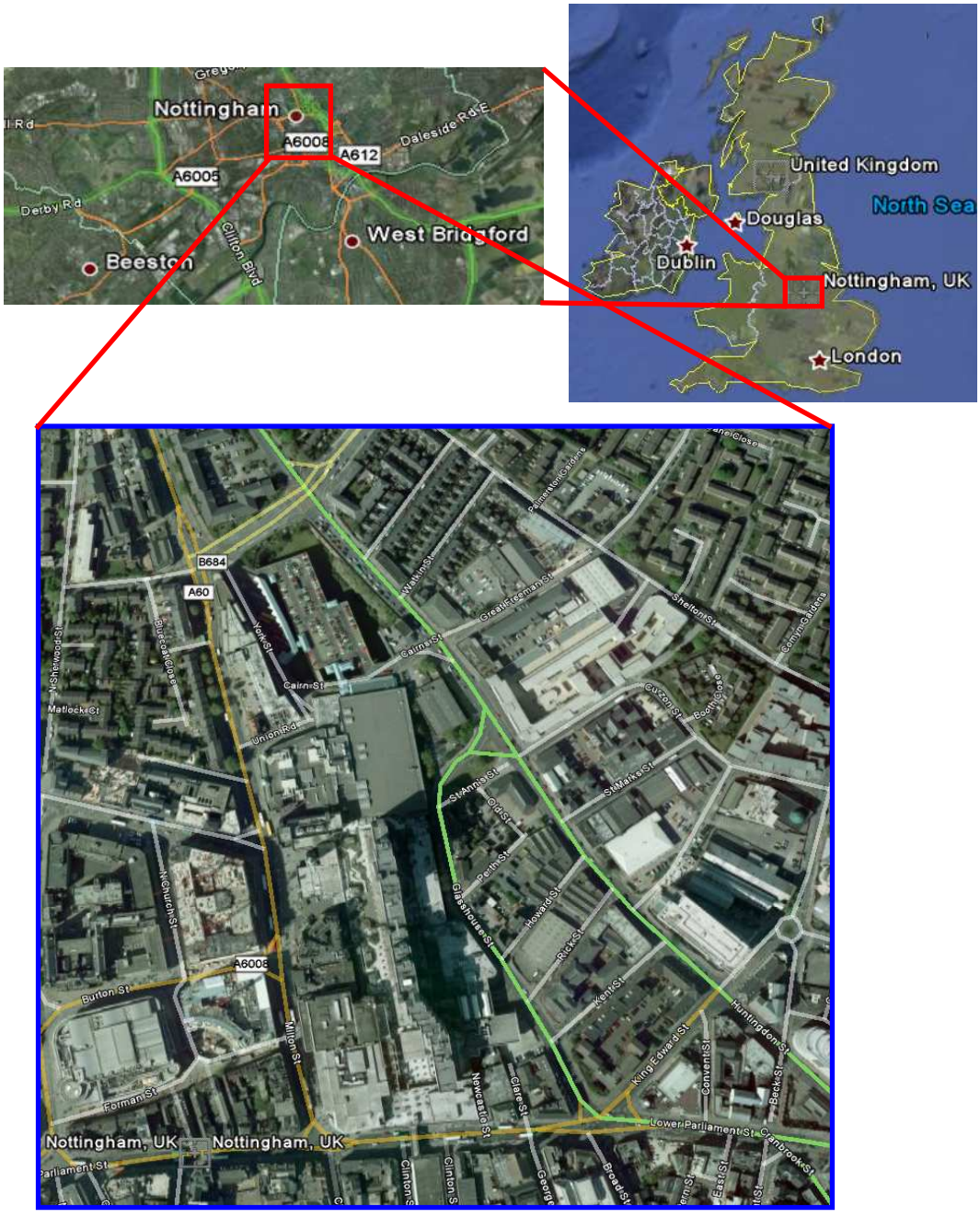

Figure 4.2: The second study area located in the Nottingham city centre, adapted from Google Earth.

This site presents one of the most challenging environments when it comes to urban modelling due to the complexity of building structures and the varied architectural design. Figure 4.3 illustrates the complexity of some of the buildings with pipes and ventilation equipment covering most of the roof top.

Figure 4.3: Example of complex roof tops in the second test site

These buildings provide an excellent opportunity to test the efficiency of the proposed texturing method using the oblique imagery on large and tall industrial buildings. Table 4.1 provides an overview of the test sites, data collected and dates of collecting the data.

Table 4.1: Overview of the test sites and data collected.

Test site	Imagery collected	GSD	Date	GCPs
Nottingham University main campus	Pictometry	10-15cm	September, 2005	41
	UltraCamD	5cm	October, 2006	
Nottingham city centre	Pictometry	10-15cm	September, 2005	8

4.3 data sets

The current research was investigated using data provided by Blom Aerofilms Ltd. through The University of Nottingham. The provided data were raw digital images covering The University of Nottingham main campus and a

small area of Nottingham city centre. The provided data consists of two sets: the first set of data was captured by UltraCamD large format digital camera and the second set was captured by Pictometry imaging system.

4.3.1 UltraCamD images

These images were captured in October 2006 using a Microsoft UltraCamD large format digital aerial camera, and provided in TIFF file format. The flight direction was West-East and reverses covering the whole area of the University campus through 4 different strips, with about 60% forward overlap and 30% side lap. The total number of digital colour images captured was 86. Average flight altitude was about 500m which has led to an image scale of 1:5000 and GSD of about 5cm. The UltraCamD used in this flight mission has a pixel size of 9μm, focal length of 101.400mm and an image format of 11500×7500 pixels (103.5mm x 67.5mm). All the images have been taken on the same day. The camera calibration report for the employed digital camera was also provided; its date of calibration was 19-07-2005, appendix B contains the calibration report of the camera which was provided with the images. In addition to the above, the processed GPS/IMU flight data were provided for all images as a text file in the format of EASTING, NORTHING, ORTHOMETRIC HEIGHT, OMEGA, PHI, and KAPPA. The 'omega' angle is the first rotation about the 'X' axis, the 'phi' angle is the second rotation about the 'Y' axis, and the 'kappa' angle is the third rotation about the 'Z' axis, figure 4.4.

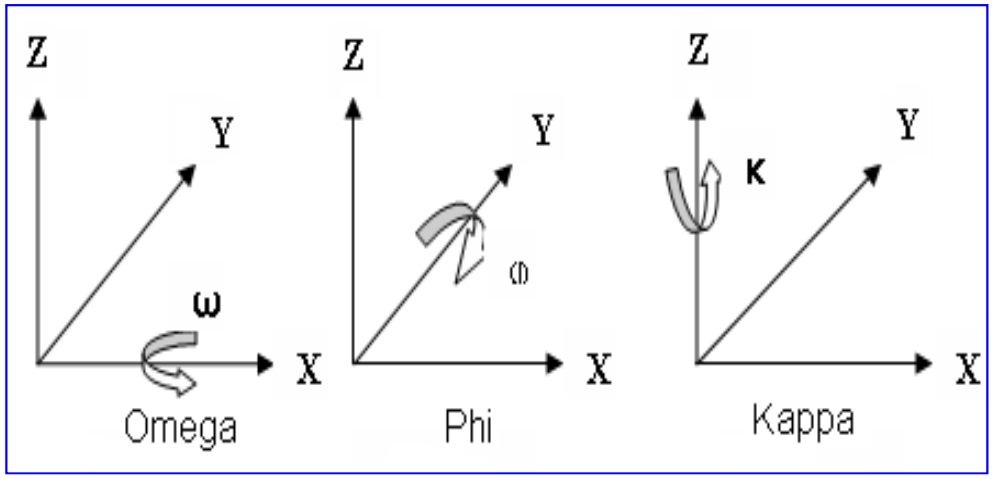

Figure 4.4: Rotation angles around the 3 axes.

One of the main advantages of using the UltraCam D images for this study area is the impressive radiometric quality and ground resolution as indicated in section 3.5 which leads to the potential extraction of very high quality 3D geometry. The extracted 3D geometry from UltraCamD images will be used as a benchmark for the purpose of comparing results of the Pictometry imaging system. The overall quality and ground resolution of the UltraCamD images is indicated in figure 4.5.

Figure 4.5: Subset of an UltraCamD image over Nottingham University test site representing one of the Engineering Faculty buildings of increased roof complexity, the image also shows the high radiometric quality of UltraCamD.

4.3.2 Pictometry images

The second set of images was captured using the Pictometry imaging system in September, 2005. The Pictometry images were provided in a file format of PMI (Pictometry Map Image) for vertical images and PSI (Pictometry Shot Image) for oblique images.

The Pictometry digital images are covering approximately a 2 km^2 region in and around the University main campus with 27 vertical images (3 strips of 9 images each), 12 obliques (3 strips of 4 images each) looking East, 15 (3 strips of 5 images each) looking West, 15 (3 strips of 5 images each) looking

North and 15 (3 strips of 5 images each) looking South. Furthermore, Pictometry vertical and oblique images are available for about 0.5 km^2 in the Nottingham city centre area. The GSD for the oblique imagery is approximately 11 - 15cm. The GSD for the vertical imagery is approximately 10 - 15cm with the flying height between approximately 975m and 1038m for both oblique and vertical images. The pixel size is 9μm with 4008 x 2672 total pixels and a nominal focal length for the vertical camera of 65mm and the oblique cameras of 85mm. The forward overlap for the vertical images varies from 38% to 46% and the side lap from 25% to 36%. The forward overlap of the oblique imagery is approximately from 21% to 47% and side lap 23% to 45%. The oblique images were taken at an inclination angle of about 50° from multiple viewing directions. This makes the building facades in both study areas adequately visible. In-flight GPS and rotation information were available but the quality is not fully known. The calibration of the 5 cameras used to capture images of the study areas was carried out by the data provider between April 5th, 2005 and April 12th, 2005 using the Australis software, see appendix C for the calibration reports.

The overall quality of Pictometry images is characterized in some instances by the presence of haze. The inclination angle in combination with atmospheric scattering and the quality of CCD and lens assembly of the consumer-type cameras adversely affected the quality of oblique images. It is speculated that the cluster of cameras in the Pictometry imaging system consists of typically consumer-type (Canon for example) digital SLR cameras (some details of the system are not available). In spite of the decreased quality of the oblique images, these datasets present an excellent opportunity to evaluate the use of oblique images for automatic texture mapping of building facades alone and in combination with other datasets such as UltraCamD images.

4.4 Ground Control Points

For quality assessment of photogrammetry procedures, it is desirable to have ground control which can be defined as ‘points of known positions and elevations with identifiable images on photographs’ (Wolf, 1983). To produce

topographic and planimetric mapping from stereomodels, the aerial images should be accurately scaled and levelled so as to be georeferenced to a true geographic ground location. To do this, it is necessary to accurately relate the images both horizontally and vertically to the ground. This is usually done by establishing coordinates of specific image points in object space (the ground) with respect to a horizontal datum (horizontal control points), and elevations on vertical level points where the elevation of the point is known with respect to a vertical datum (vertical control points). Nowadays, most control points contain both horizontal and vertical information so they are used for both scaling and levelling.

There are two types of ground control points in common use. Firstly, natural details, which are normally plan or height points and are selected after the photograph has been taken. A plan control is sharp definite piece of detail, such as a building corner, manhole cover corner or white line in a road, while a height control is flat horizontal area near the other detail used for locating position, such as a road junction, corner of car parking or gateway. Secondly, premarks; they are targets that were put in place before photography and they are normally three dimensional coordinated points, with a size selected depending on the photograph scale. Premarks are used in areas that lack natural objects to provide definite images. Sometimes a mixture of natural details and premarks is used.

4.4.1 Number and location of ground control

The density of control points and their optimum location depend on the purpose of photography. Generally, the minimum required number of ground control is two horizontal control points and three vertical control points per stereopair (Smith, 2006). Redundant control is recommended (good survey practice) to enable quality assessment and is usually used to increase the accuracy of the photogrammetry. Heipke (1997) concluded that, In order to be reliably extractable from the imagery, control points should ideally be:

- Geometrically well defined and radiometrically unique
- Visible from various directions and well distributed across the imagery
- Independent of image content and image scale
- Easy to represent in two and three dimensions

- Accessible to determine their object space coordinates

According to Hussain and Bethel (2004), the amount of horizontal control for aerial triangulation differs from the need for vertical control. The horizontal control points are usually needed only along the perimeter of the aerial block and at an average spacing of 3 to 5 models or more. On the other hand, more extensive vertical control is needed in support of aerial triangulation because deformations in the vertical plane can easily occur in large blocks. So it is necessary to provide vertical control points in pairs across the flight line in the first and the last model of each strip. Similar pairs of points are located along the flight line at an average spacing of 3 to 5 models.

By using the process of aerial triangulation along with the availability of an airborne integrated GPS/IMU system (to measure position and attitude of each image) at the image acquisition stage, the number of ground control required for the mapping will be minimized, figure 4.6. Mikhail et al. (2001) concluded that using GPS to determine the exposure station positions essentially makes a control point of each exposure station, reducing control requirements for the block to minimal configurations.

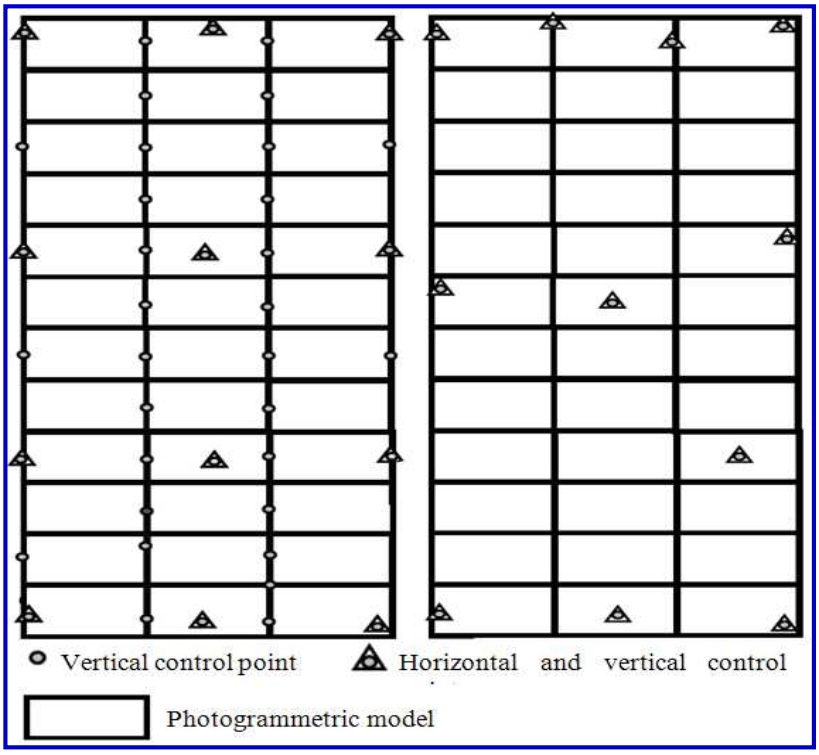

Figure 4.6: Ideal photo control configuration for a photogrammetric block without airborne GPS (left) and with airborne GPS (right). Using GPS reduces the required ground control to minimum, adapted and reproduced from (DOT, 2006).

4.4.2 Collection of GCPs

A total number of 41 coordinated ground points were available for the study area of Nottingham University, figure 4.7. Moreover, 8 coordinated ground points were available for the use in the second study area (Nottingham city centre), figure 4.8. These points were collected using static GPS observation of at least 20 minutes in duration with an estimated accuracy of 5cm which was used as the standard deviation of the ground control points in the triangulations. The 5-cm accuracy was chosen because the baseline length between the chosen GCPs and the reference active station used (over the IESSG) is a few kilometres and by looking at figure 4.9, it can be seen that a 5-cm accuracy can be achieved when observing for a period of about 20 minutes.

Figure 4.7: Locations of the collected GCPs in the Nottingham University test site.

The observation of the GCPs both in the vertical and oblique images was performed manually. Most of the GCPs were easily identifiable due to the good radiometric quality of both image sets. However, some difficulties were encountered while measuring precisely the GCPs on Pictometry images due to the tilt and the apparent differences in scale of oblique images which ranges

from 10cm in the image foreground to 18 cm in the image background as stated in section 3.6.4.

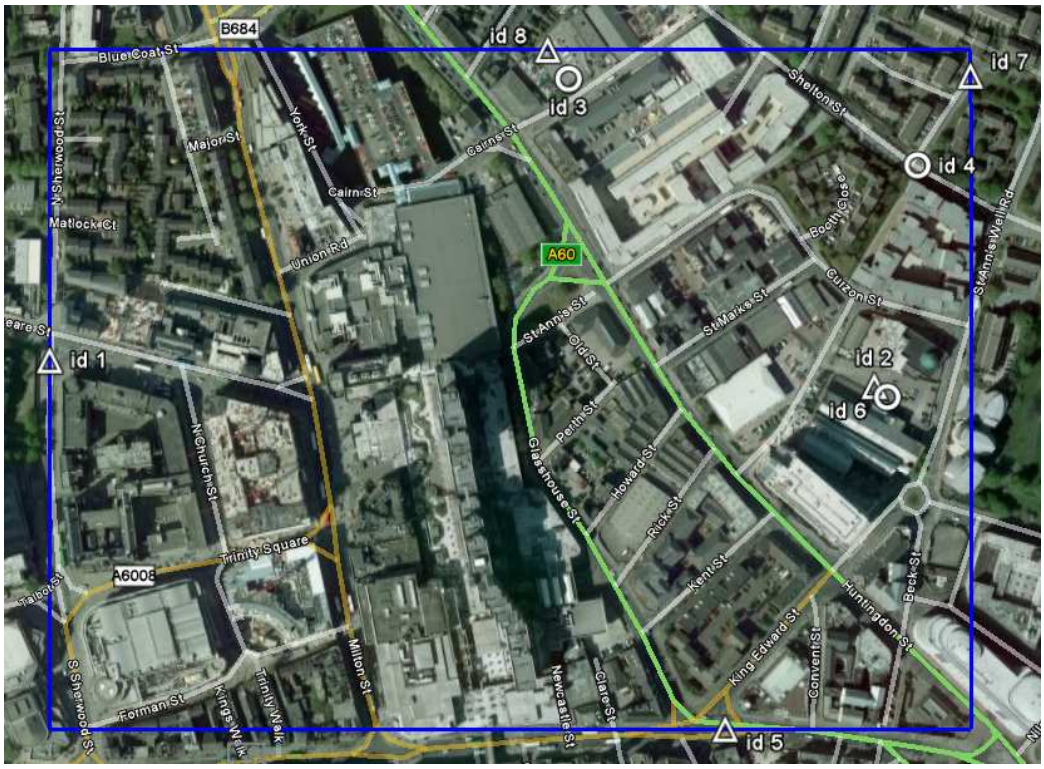

Figure 4.8: Locations of the collected GCPs in the Nottingham city centre test site, the blue square represents the extent of the photogrammetric block, five points used as GCPs (the white triangle) and three points used as check points (the white circle), the image adapted from Google earth.

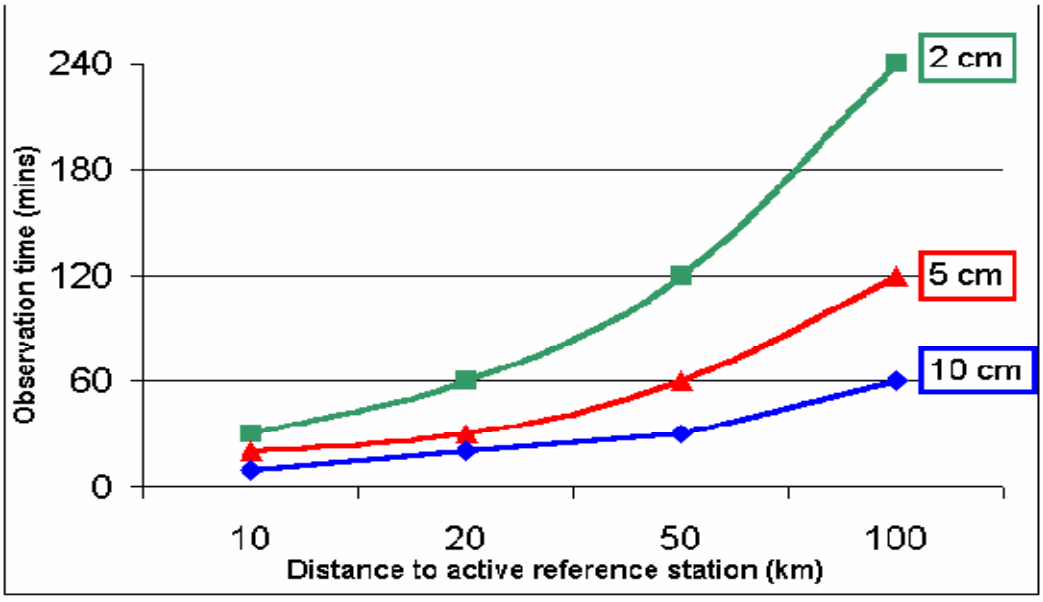

Figure 4.9: Typical GPS observation time as a function of distance to the active reference stations. Adapted from the Ordnance Survey website: ordnancesurvey.co.uk/oswebsite/gps/osnetfreeservices/about/surveying_osnet.html

4.5 Flight planning

A successful project plan is the one that meets the data quality requirements at minimum cost. Flight planning is one of the most important stages in photogrammetric projects, as it describes the strategy of work. Wolf and Dewitt (2000) stated that 'Failure to obtain satisfactory photography on a flight mission not only necessitates costly re-flights, but also in all probability will cause long and expensive delays on the project for which the photos were ordered'. The accuracy requirements set by the user of the photogrammetric data is the most critical factor in the planning stage as it has very big impact on the project's scale and hence on the cost. Therefore, the primary objective of photogrammetric project planning is to determine the smallest image scale which achieves the user's accuracy specifications. In addition, the aim of flight planning is to produce the flight design which shows where the camera exposure centre is for each image, it will also include some specifications that will outline the method of acquisition and other requirements such as the required camera, scale, flying height, forward overlap, side lap, tilt …etc. It will also determine the number of photographs required, the number of strips and the flight lines. This is to insure that every portion of the terrain, project's area, should be imaged from at least two different camera locations to get the stereoscopic viewing required for 3D modelling. This requirement can be achieved by spacing the exposure stations so that a common overlap occurs between images in flight line direction (forward overlap) and in adjacent flight lines (side lap). The forward overlap percentage represents the fraction of an image that is common with adjacent image in the same flight line (strip) while the side or lateral overlap represents such relationship between two images in adjacent strips, figure 4.10.

Forward overlap and stereo coverage can be negatively affected by the flight path of the aircraft. These are most commonly visible in either drift or crab. Drift occurs when the plane deviates from the intended flight line, whereas crab occurs when constant corrections to the flight path cause the images to twist with respect to each other, figure 4.11, (DOT, 2006).

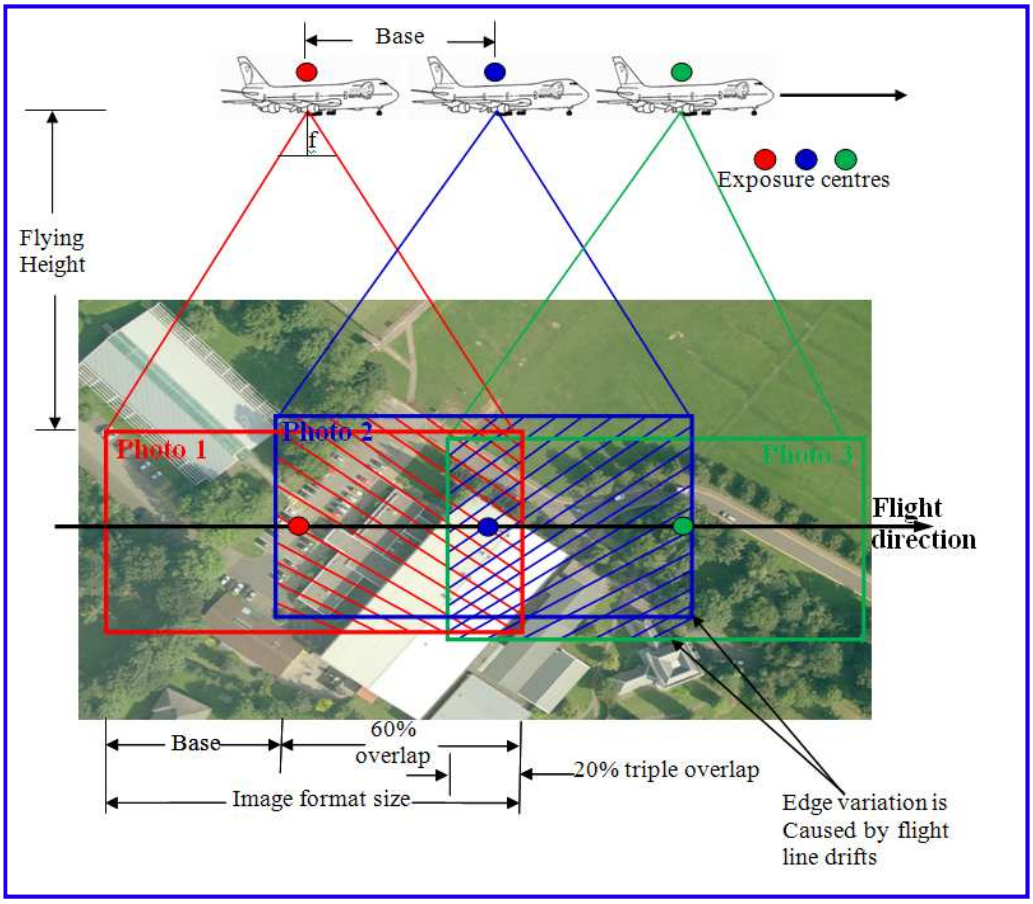

Figure 4.10: A block of overlapping photographs; showing the 60% forward overlap and the 20% triple overlap, the flying height, the base, and the image format size on the ground, this block consists of one strip with three stereo models. To avoid gaps due to aircraft tip, tilt and altitude variation, a standard of 60% overlap should be used.

According to Mikhail et al. (2001), in cases where the user wishes to have imagery with reduced relief displacement for the production of orthophoto or mosaicking, forward overlap of 80% and side lap of 60% should be used.

The scale of the image can be calculated from the following equation:

$$Average\ scale = \frac{focal\ length}{average\ flying\ heigth\ above\ terrain}$$

The ground coverage can be determined from the image format size and the scale factor as follows:

$$Ground\ coverage = image\ format\ size\ x\ scale\ factor$$

The spacing between exposure stations (base) is determined by the following equation considering 60% forward overlap:

$$Base = ground\ coverage(1 - 0.6)$$

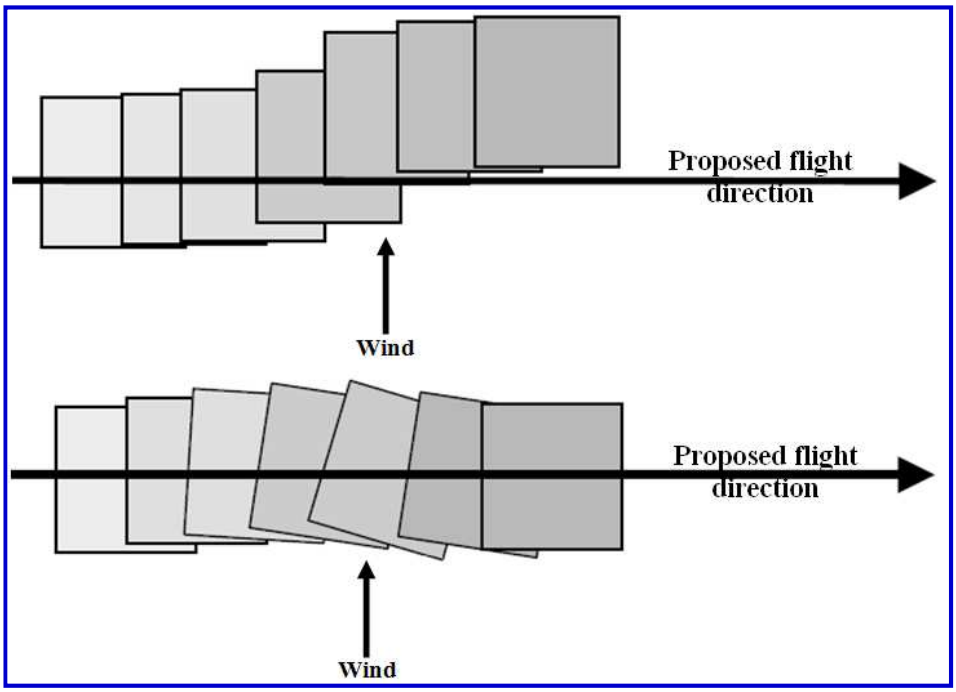

Figure 4.11: Example of drift due to deviation of plane from its proposed trajectory (top) and example of crab because of photo twisting with respect to each other after several corrections of flight path (bottom), adapted and reproduced from (DOT, 2006).

The spacing between strips based on 20% side lap is determined from the following equation:

$$Spacing\ between\ strips = ground\ coverage(1 - 0.2)$$

Number of flight lines (strips) can be determined, assuming that the flight direction will be parallel to the larger dimension of the mapped area to minimize the number of strips and hence the cost, as follows:

$$No.of\ strips = \frac{the\ smaller\ dimension\ of\ the\ mapped\ area}{spacing\ between\ strips}$$

The number of models in each flight line is calculated as follows:

$$No.of\ models\ per\ flight\ line = \frac{length\ of\ the\ mapped\ area}{the\ base}$$

It is important here to note that at least one extra model should be added at each end of the strip because ground control might be located outside the borders of the mapped region. Moreover, to ensure complete coverage of the mapped region, several exposures should be made at the beginning and the end of each strip.

Several changes in the usual workflow for vertical images have to be made when acquiring oblique images. These include flight planning, image processing and image analysis. With regard to flight planning for oblique aerial imaging, several issues have to be considered. First, the GSD is smaller in the foreground than in the background of the oblique image, figure 3.31 and figure 3.32. Second, image scale is not constant throughout the image but it changes with direction. For example, in the background of an oblique image the scale in the direction of view is smaller than the scale in the transverse direction.

According to Grenzdorffer et al. (2008) , the altitude above ground (h_g) and the viewing angle (α_y) across the flight direction have to be defined, figure 4.12. Following the determination of the flying height and the oblique angle, the viewing angle of the lens (β_y) defines the minimum (D_{min}) and the maximum distance (D_{max}) from the aircraft to the area imaged, as well as the image scale for analogue images or the GSD for digital images, (Grenzdorffer et al., 2008).

$$D_{min} = h_g \, tan \, (\alpha_y - \beta_y)$$

$$D_{avg} = D_{max} - \, D_{min}$$

$$D_{max} = h_g \, tan \, (\alpha_y + \beta_y)$$

The minimum image scale factor (m_{min}), average image scale factor (m_{avg}) and maximum image scale factor (m_{max}) are calculated by the following equations:

$$m_{min} = \frac{h_g \, cos \;\; \beta_y}{f \; cos(\alpha_y - \beta_y)}$$

$$m_{avg} = \frac{h_g}{f \; cos \; \alpha_y}$$

$$m_{max} = \frac{h_g \, cos \;\; \beta_y}{f \; cos(\alpha_y + \beta_y)}$$

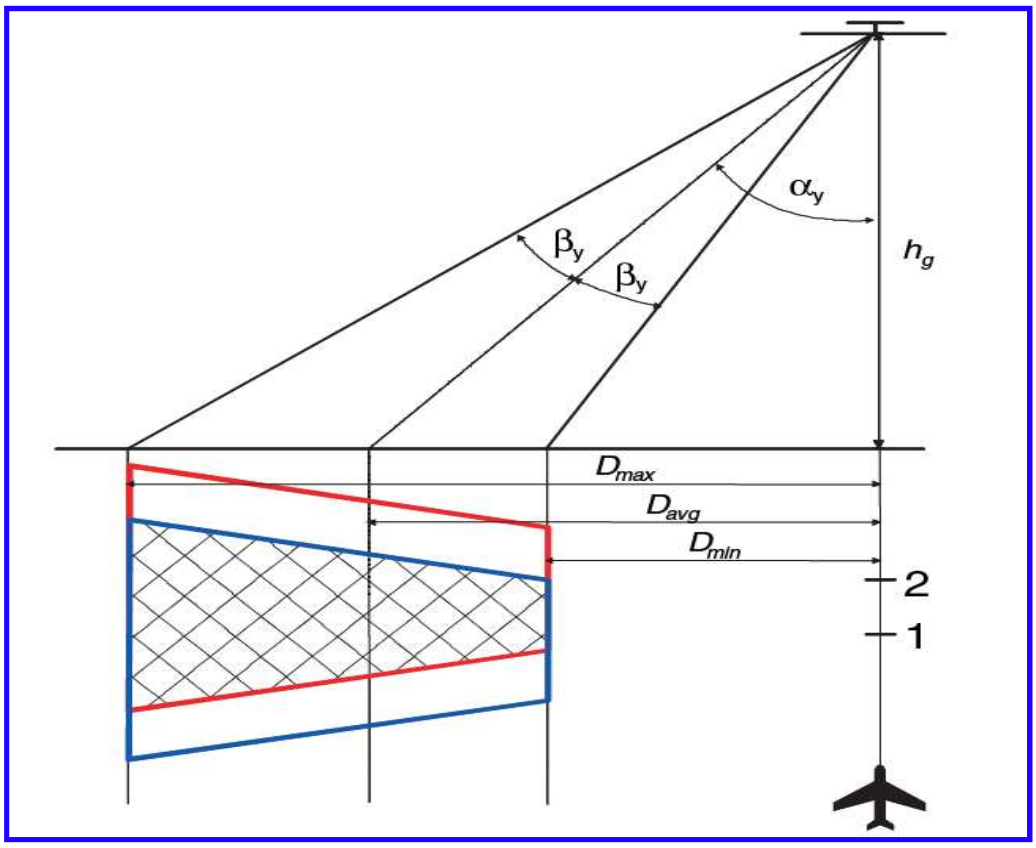

Figure 4.12: Geometry of the oblique images showing the difference in GSD of foreground and background of the oblique image, the viewing angle and the flying height, adapted from (Grenzdorffer et al., 2008).

4.6 Summary

Two test sites used in this research, the main campus of The University of Nottingham and a small part of the Nottingham city centre. These study areas consist of various types of buildings that range from modern commercial, industrial and residential building structures and architectures to medieval gothic style architectures. The provided data for these test sites consists of two sets: the first set of data was captured by the UltraCamD camera and Pictometry system and the second set was captured by Pictometry system only.

The density of control points and their optimum location depend on the purpose of photography. By using the process of aerial triangulation along with the availability of an airborne integrated GPS/IMU system at the image acquisition stage, the number of ground control required for the mapping will be minimized. A total number of 41 coordinated ground points were collected

for the study area of the University campus and 8 points for the study area of city centre. These points were measured using static GPS observation.

Data acquisition in photogrammetric projects involves good flight planning. Flight plans are maps depicting the location of the photo control and the beginning and ending of flight lines upon which aerial photography is to be obtained. The goal of the flight planning process is to produce a flight plan that will provide the best balance between safety, accuracy and economy. Some changes in the usual workflow for vertical images are needed when planning for an acquisition of oblique images because the image scale and the GSD are not constant throughout the oblique image.

CHAPTER 5: AERIAL TRIANGULATION AND GEOMETRY OF PICTOMETRY IMAGERY

5.1 Introduction

One of the primary objectives (section 1.2) of this research and the subject of this chapter is to assess the geometry of the Pictometry vertical and oblique images as well as the UltraCamD images; in particular, investigating the benefits and limitations of integrated sensor orientation and direct georeferencing (the integration of Pictometry camera system with GPS/IMU) in an aerial triangulation. Specifically, it is important to investigate the quality of computed coordinates of the ground points to be confident that integrated sensor orientation can provide coordinates at the required accuracy. This will be done through performing aerial triangulation on different block configurations.

This chapter will introduce the procedures and parameters used to setup the different photogrammetric blocks of different imagery used for assessment as well as the AT results and the analysis of these results.

5.2 Creation of new project and setting up the blocks

Transforming imagery into usable data typically requires several processing steps. The first step in the process is the creation of a new project. Creating a new project is considered one of the most important steps in the data processing stage. It involves setting up the block properties and then beginning processing. The occurrence of any error while establishing the different setup parameters will result in significant time spent on identifying the false parameter or even repeating the entire work. Therefore, this step must be performed with great care to ensure smooth processing throughout the project workflow. This step involves defining project properties such as the type of imagery that will be processed and the coordinate system used. It also involves adding all of the raw data (images) that will be processed to the project. For the purpose of this research, two software packages, LPS and ORIMA, have been used in processing the data to compare the AT results. The following

summarize the details involved when setting up the blocks of both UltraCamD and Pictometry images in both software packages LPS and ORIMA:

- Spheroid name: Airy
- Datum name: Ordnance Survey (OS) Great Britain 1936
- Elevation units: metres
- Scale factor for central meridian: 0.999601
- Elevation type: height
- Horizontal reference coordinate system: Transverse Mercator Projection and OS Great Britain 1936 datum in units of metres
- Vertical reference coordinate system: WGS84 vertical spheroid and WGS vertical datum in units of metres
- Rotation system: Omega, Phi and Kappa
- Photo direction: Z-axis for normal images
- Average flying height: 500 m for UltraCamD images block and 1000m for Pictometry images blocks.

After creating the block file and setting up the block with the above details, the following step will be importing the digital images, and then generating pyramid layers for these imported images. Generating pyramid layers improves the handling of the digital images. According to LPS user manual (2009), the pyramid is a data structure consisting of the same image represented several times, at a decreasing spatial resolution each time. Each level of the pyramid contains the image at a particular resolution. The matching process is performed at each level of resolution, figure 5.1. The search is first performed at the lowest resolution level and subsequently at each higher level of resolution.

This section will also highlight the other general project creation steps that apply to both datasets of imagery: UltraCamD and Pictometry. The steps include the sensor model definition, GCP measurement, tie point generation, and bundle block adjustment.

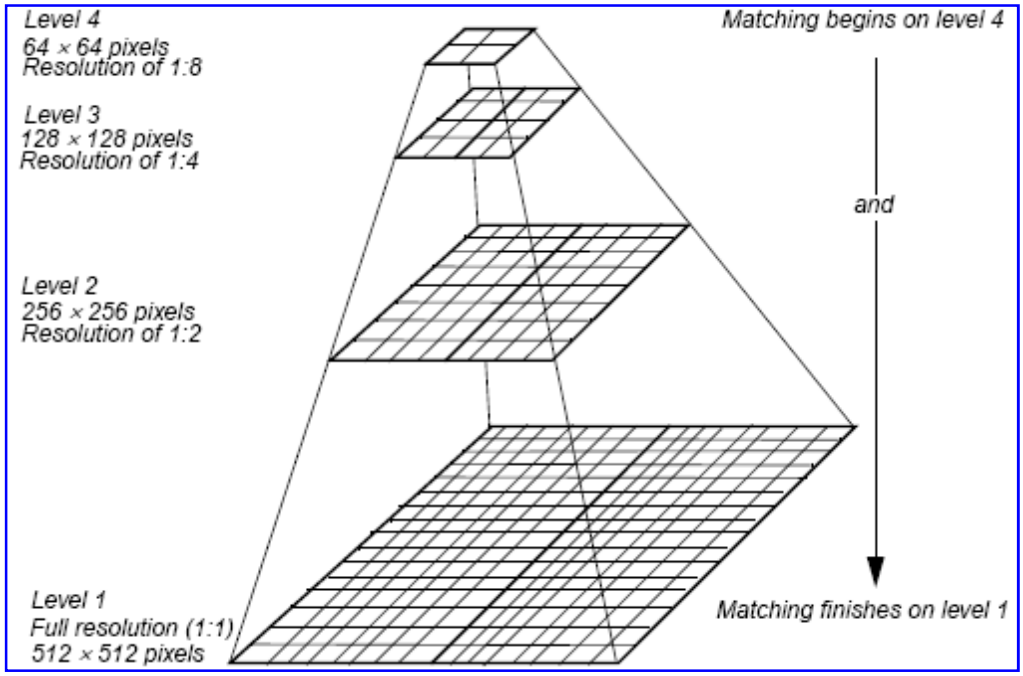

Figure 5.1: Image pyramid layers, adapted from LPS user manual

5.2.1 Sensor Model Definition

A sensor model describes the internal and external properties and characteristics associated with the camera used to capture the provided images. Without this information, value added data layers such as oriented images, 3D feature datasets, DTM, and orthorectified images cannot be derived from imagery.

Internal camera model information, interior orientation (IO), describes the internal geometry including:

- Principal point of autocollimation (p)
- Focal length (f) which is the distance from the principal point to the perspective centre (o),
- Principal point shift (x_p, y_p) which results because of the small deviation from the image coordinate system origin to (p). Figure 5.2 shows the above parameters,

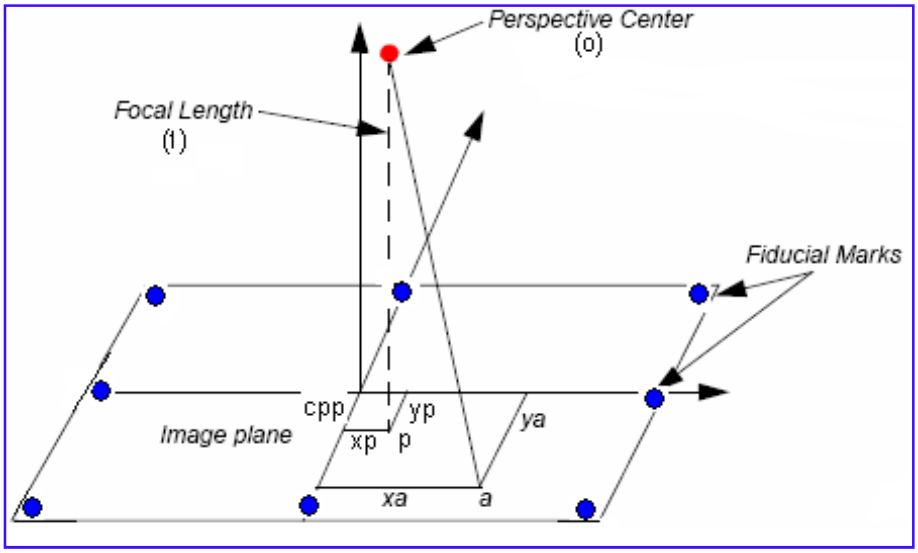

Figure 5.2: The internal geometry of the camera, adapted and reproduced from LPS user manual

- Lens distortion; two types of lens distortion exist: radial and tangential lens distortion. Lens distortion occurs when light rays passing through the lens are deviated, thereby changing direction and intersecting the image plane at positions deviant from the perspective projection (Leica, 2009). Figure 5.3 shows the difference between radial (Δr) and tangential (Δt) lens distortion.
- The physical dimension of the CCD area array.

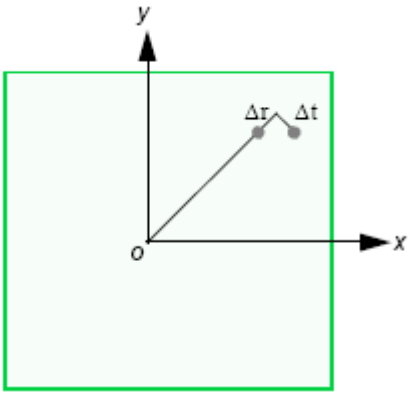

Figure 5.3: Radial and tangential lens distortions, adapted from LPS user manual

For Pictometry images, each set of pictures with different view angle uses a different SLR camera. Despite the lack of information when it comes to the calibration method of the cluster of cameras and the exact camera type,

sufficient information was given for each viewing angle to enable the IO of each camera. This information was given in metadata section accompanying the image files as well as the calibration reports of the individual cameras (see appendix C1, C2, C3, C4). Table 5.1 contains the IO parameters of the cameras used. The idea of IO is to recreate the camera geometry exactly as it was when the image was captured. Since the digital cameras used to capture the datasets of this research do not have any fiducial marks, the physical dimensions of a single CCD detector will be sufficient for the reconstruction of the camera geometry without any need for measuring fiducial marks.

Table 5.1: The IO parameters of the used cameras to capture images used in this research

Camera	**f** (mm)	$\mathbf{x_p}$ (mm)	$\mathbf{y_p}$ (mm)	**Pixel size** (μm)	**Sensor/image format** (mm)
UltraCamD	101.4000	0.0000	0.1800	9 x 9	67.500 x 103.500
Vertical Pictometry	65.0487	-0.3023	-0.2900	9 x 9	24.048 x 36.072
Northern and Southern pointing Pictometry (camera2)	84.7640	0.0606	-0.0767	9 x 9	24.048 x 36.072
Western pointing Pictometry (camera3)	84.8386	0.2548	-0.0652	9 x 9	24.048 x 36.072
Eastern pointing Pictometry (camera4)	84.5753	-0.2303	-0.0447	9 x 9	24.048 x 36.072

It is important to note that camera 2 was used to capture the North and South pointing images. It is also evident from the table that the oblique viewing cameras have similar lens. The presence of significant principal point deviation signifies the use of consumer-type digital SLR cameras, probably available off-the-shelf.

External sensor model information, exterior orientation parameters (EOP), describes the position and orientation of each image as it existed when the imagery was collected. Since the EOP were provided with the imagery, the traditional relative and absolute orientations will be skipped, table 5.2 shows the approximate orientation parameters of the oblique cameras against nadir pointing camera. Knowledge of EOP made possible by integrating GPS/IMU system onboard the aircraft with the aerial cameras. This allows the georeferencing of the images at the time of exposure instead of achieving it

indirectly by using the traditional aerial triangulation. Smith et al. (2006) stated that 'the use of in-flight control systems for controlling blocks of aerial photography is now an established procedure and is regularly being used for production purposes'. The importance of GPS and IMU measurements is increasing as there is greater and greater interest to work without ground control and strive towards direct georeferencing of imagery. In addition, GPS/IMU systems are highly desirable to automate aerial triangulation by giving the image matching algorithm for tie point measurement good starting values.

Table 5.2: Approximate orientation of oblique cameras against nadir reference camera

Camera	**ω** (deg)	**φ** (deg)	**κ** (deg)
Northern camera	50	-4	180
Southern camera	-50	-4	5
Western camera	-8	50	100
Eastern camera	8	-50	-80

5.2.2 GCP Measurement

GCPs are used to establish a geometric relationship among the images in the project, the ground, and the sensor model so that accurate data can be collected from the imagery. Often the GCP has three coordinates: X, Y and Z, which are measured across multiple images. GCPs can be collected from existing vector files, DEMs, orthorectified images, and maps or using ground surveying techniques such as total station or theodolite survey. As stated in section 4.4.2, 49 GCPs were collected (in both study areas) using static GPS observation of at least 20 minutes in duration with an estimated accuracy of 5cm which was used as the standard deviation of the ground control points in the triangulation. It is important to mention here that in some locations of the city centre study area, the observation duration was extended well beyond 30 minutes in order to account for errors caused by multipath and limited open horizon due to tall buildings. The measurement of the GCPs in both UltraCamD images and Pictometry images was performed interactively. These GCPs will serve as orientation points in GPS-supported bundle block

adjustment. Some of the collected GCPs will be used as check control points to independently verify the overall quality and accuracy of the block triangulation results.

5.2.3 Automatic Generation of Tie Points

GCPs measurement is followed by automatically generating the tie points before performing the aerial triangulation process. Tie points can be defined as points with unknown ground coordinates but they can be recognized visually in the overlap area between multiple images. Ideally, tie points should have good contrast in two directions, like the corner of a building or a road intersection and should be distributed over the area of the block. Typically, nine tie points in each image are enough for block triangulation. Figure 5.4 illustrates the ideal placement of tie points.

Tie points are used to position multiple images and strips correctly, relative to each another. Since automatic tie point collection processes multiple images with overlap, minimum input requirements are used to determine the block configuration with respect to which image is adjacent to which image, and which strip is adjacent to which strip in the block.

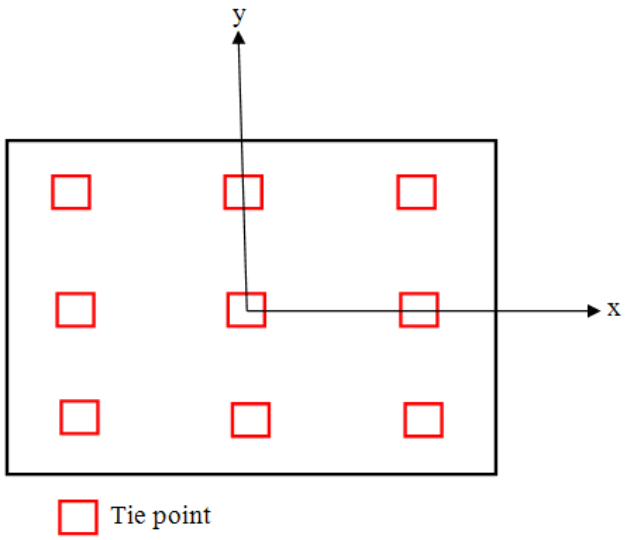

Figure 5.4: Diagram depicts the ideal placement of tie points in a single image.

The minimum input requirements can be the initial exterior orientation parameters (X_0, Y_0, Z_0, ω, φ, and κ) for each image in the block. These can be

obtained from existing traditional aerial triangulation results or airborne GPS and IMU data.

Automatic tie point collection uses digital image matching techniques to automatically identify and measure tie points across multiple overlapping images. The automatic tie point measurement in LPS, which is used in this research, is an area based matching algorithm, utilizing a least squares correlation workflow. Area based matching (signal based matching) algorithm determines the correspondence between two image areas (patches) according to the similarity of their gray level values and geometric differences. Least squares correlation uses the least squares estimation to derive parameters that best fit a search window (candidate windows on the second image that are evaluated relative to the reference window) to a reference window (source window on the first image which remains at a constant location), (Leica, 2009).

Collecting tie points automatically enables easy increase in the number of points on the overlapping areas of the images within the block which gives more data redundancy and therefore better quality of AT results and better minimization and distribution of errors throughout the observations. After the generation of tie points, they should be checked to ensure accuracy. If a point is not as accurate as it should be, one may adjust it with the Select Point tool available in LPS, deactivate it from one or more images, or delete it from all the images on which it exists.

The parameters used to collect the tie points in this research are search size, correlation size, feature point density, least squares size, coefficient limit, and initial accuracy. The default values were used in the generation of the tie points for the UltraCamD images block because they were suitable for the type of terrain in the project, except for the correlation limit which was increased to 0.85 to increase the accuracy by minimizing the chances of generating points of mismatch. However, the function for generating the tie points automatically did not work in the combined block of oblique Pictometry images due to the illumination changes, acquiring the images from different directions, and using different cameras to capture the images. As a result several parameters of tie point generation were changed such as:

- Search size: was increased to give help select more points although it may cause more computation time and more wrong points.
- Correlation size: was decreased to result in larger correlation coefficient and therefore acceptance of more points (may be bad points).
- Least square size: was decreased to increase the number of generated points (bad and good points)
- Initial accuracy: was increased because large value increases the initial search area for possible corresponding points at the initial estimation stage.
- Coefficient limit: was decreased to allow for more accepted correlated points.

Despite changing the above parameters and putting them in different combinations, the automatic generation of tie points did not work and it was limited to the connection of 2 neighbouring images in one strip. Therefore, the tie points for the Pictometry oblique images block were generated manually.

During AT, the assigned statistical weight derived from standard deviation is used to govern the quality of the observation. In this project, static GPS has been used to collect the GCPs which can give cm-level accuracy, so a standard deviation of 5cm for the GCPs has been used. Standard deviation for the EOP has to be assigned properly because assigning big standard deviation causes the final EOP to deviate and vary drastically from the input values. The quality of the EOP was not given, therefore several trials have to be performed to gain experience and knowledge to get the best results during the AT process.

5.3 Aerial triangulation results

The goal of AT is to adjust the image parameters so that the position of a point in one image corresponds to the same position of the point in the other image. When ground control is included, the parameters are adjusted so that the same image point corresponds to the same absolute position on all the overlapping images. There are generally two problems that can happen with simultaneous solution of the bundle block adjustment: first one is failure to converge because of insufficient points to reach the convergence, and second one is high RMS residual error occurs because of mismatching of tie points and/or mislocation or misidentification of control points. This section will give

in detail the AT results of the different blocks used in this research including vertical images blocks of both Pictometry and UltraCamD imagery, combined block of only oblique Pictometry imagery, combined block of oblique and vertical Pictometry imagery, and finally combined block of oblique Pictometry imagery and vertical UltraCamD imagery.

5.3.1 Observation techniques

A total number of 49 coordinated ground points were available. Aerial triangulation for all Pictometry blocks and for UltraCamD block was performed using LPS and ORIMA software packages. Four solutions have been considered; 'float solution', 'constrained solution', 'integrated sensor orientation solution' and finally 'direct georeferencing or only in-flight GPS and IMU' solution.

5.3.1.1 Float solution

In the 'float solution' the interior orientation parameters were kept fixed (the cameras are used exactly as specified in the cameras files) and the initial exterior orientation parameters values were left floating. The projection centre coordinates were assigned a standard deviation a priori of 1000m and orientation angles were given a standard deviation a priori of 360 degrees. EOP were kept floating by assigning them big standard deviations which leads to them having very small weight to minimize their influence on the adjustment. The aerial triangulation trials using this solution were conducted using the in-flight GPS/IMU (EOP) as initial values which allows for adjustment of sensor location and rotation at triangulation. The solution was conducted with and without using the additional parameters.

5.3.1.2 Constrained solution

Statistically constraining the GPS/IMU determined EOP ensures that the final estimated parameters do not deviate drastically from the input values (assuming they are correct) and will optimise the AT solution. The extent of the deviation or fluctuation is controlled by the specified standard deviation values. The quality of the in-flight observations of GPS/IMU is not known for the provided Pictometry imagery. To know the standard deviation a priori that

should be assigned for the EOP, traditional (indirect) AT which is based on GCPs, the measurements of their corresponding image coordinates and the connection of adjacent images and strips by tie points, was performed but without any additional in-flight observations of GPS/IMU to calculate the exterior orientation parameters of the vertical Pictometry block and simultaneously the object coordinates of ground points. The results then are compared to the in-flight determined EOP. This can assist in determination of the standard deviation of EOP (in the case of constrained solution) as the traditional AT provides an independent data for the EOP. The results of the comparison are shown in table 5.3, figure 5.5 (coordinates of images projection centres) and figure 5.6 (orientation angles).

Table 5.3: Results of comparing EOP determined from traditional AT and in-flight determined EOP

	X_o (m)	**Y_o (m)**	**Z_o (m)**	**ω (deg)**	**φ (deg)**	**κ (deg)**
Minimum	-1.937	-1.146	0.154	-0.061	-0.208	0.038
Maximum	2.192	1.625	1.206	1.445	0.123	0.069
RMSE	0.884	0.647	0.648	0.293	0.064	0.053

It is clear from the results that using 1m for the projection centre coordinates and 1 degree for the orientation angles as standard deviation a priori for the EOP in constrained solution is very reasonable. The AT trials using this solution were conducted using the in-flight GPS/IMU as initial values which allows for adjustment of perspective centres and image rotation according to the specified standard deviation. GCPs were used in this solution to define the datum (coordinate system). The solution was conducted with and without using the additional parameters.

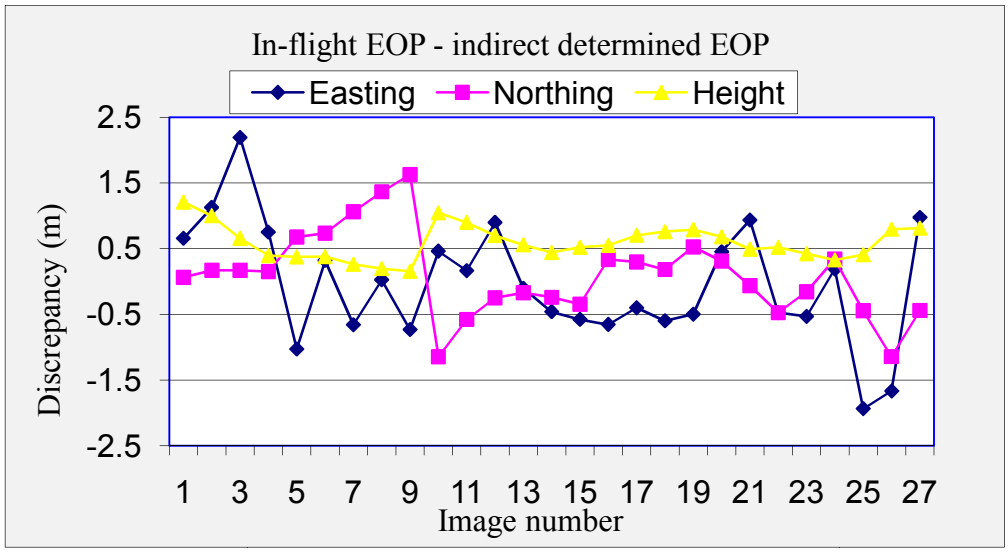

Figure 5.5: Deviation of in-flight determined images positions (X_o, Y_o and Z_o) from traditional AT determined positions.

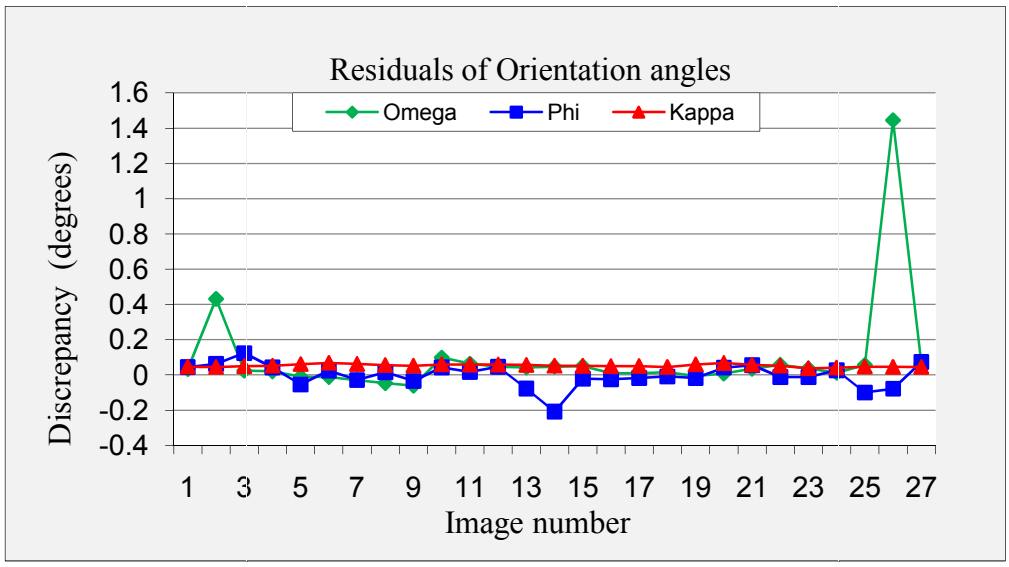

Figure 5.6: Deviation of in-flight determined images orientation (ω, φ, and κ) from traditional AT determined orientation.

As GCPs and GPS positions are used together in this test, the blunder test is capable to identify any blunders and systematic errors.

5.3.1.3 Integrated sensor orientation solution

The integrated sensor orientation is considered one of the GPS-supported bundle block adjustment types in which the 3-D coordinates of ground objects and the EOP of the images are solved together. Here the coordinates of the GPS camera stations, determined by DGPS positioning technology, are treated

as weighted observations for importing into the AT. It requires the determination of image coordinates of tie points, which nowadays is a standard procedure solved by automatic AT. It uses all the available input such as control information in image and object space as well as GPS/IMU observations in a simultaneous adjustment to determine all relevant sensor orientation parameters. This also improves the reliability as the relative relationship of the images is controlled by tie points. For operational blocks usually some check points are measured to check for blunders in the data handling and for quality control of the output coordinates. Figure 5.7 depicts the workflow of triangulating a block of digital images using either integrated sensor orientation or direct georeferencing methods in LPS. The integrated sensor orientation solution follows the blue line when looking at figure 5.7. In this solution the GPS/IMU determined EOP will be treated as initial values and will be constrained (given large weight to maximize their influence on the adjustment). Since no GCPs will be used in this solution and no GPS drift parameters will be used, the datum will be defined through the usage of GPS-derived projection centres. It is important to note here, and in the case of direct georeferencing solution, that any unhandled systematic errors will not be detected and will be pushed into the object points.

5.3.1.4 Direct georeferencing solution

A direct georeferencing system provides the ability to directly relate the data collected by a remote sensing system to the Earth, by accurately measuring the geographic position and orientation of the sensor without the use of traditional ground-based measurements (Mostafa and Hutton, 2001). Direct digital image georeferencing implies the direct measurement of position and orientation of each single image frame at the moment of data acquisition. In principal, this allows immediate map production using the photogrammetric unit (for example, a stereopair of images). Ultimately, this approach totally bypasses the AT step with no GCP requirement except for quality check.

DG is based on an integration of relative kinematic GPS positioning and IMU data by Kalman filtering. GPS and IMU together should be considered as an integrated system so that without one of them suitable results cannot be obtained. Over a short period, IMU provides a very high relative accuracy for

position and attitude information. The absolute accuracy of IMU decreases over time, if no external update measurements are available. GPS can meet these measurement requirements. The high short-term stability of IMU is used to smooth observation noise of GPS and to avoid cycle slips. On the other hand, GPS exhibits high long-term stability therefore its observation is appropriate to compensate the systematic and time-dependent IMU error effects. As a result, GPS/IMU integration provides highly accurate position and attitude (Yastikli and Jacobsen, 2005).

The usual block adjustment is in general an interpolation within the area of the control points. This is different for the direct georeferencing which is an extrapolation from the projection centres to the ground. Extrapolation is sensitive to any source of error requiring a precise system calibration, especially the IO of photogrammetric cameras as well as the attitude relationship between camera and IMU. The focal length determined by a laboratory calibration can change under flight conditions. The change of focal length is important in DG; it corresponds to a scale factor for the height. In traditional block adjustment, the scale is based on horizontal control points and an error in focal length only influences the height difference between the control and the object points (Yastikli and Jacobsen, 2005) and (Jacobsen, 2004).

The direct georeferencing method follows the red setup line when looking at figure 5.7. This method is performed directly after the IO stage by defining the EOP as fixed values without the need for measuring any GCPs, or generating any tie points. However, in order to investigate the quality of such a method, and to have an indication of the internal geometry of the block, it was necessary to measure some check points, and generate tie points. This gave a detailed statistical report through the bundle block adjustment process which outlined the accuracy of the derived data. These check points were the same as those used in the other solutions; they were used as a reference for the absolute check of the derived data. In addition, generating the tie points will insure the elimination of disturbing y-parallax in stereo models which cannot be avoided in a DG solution.

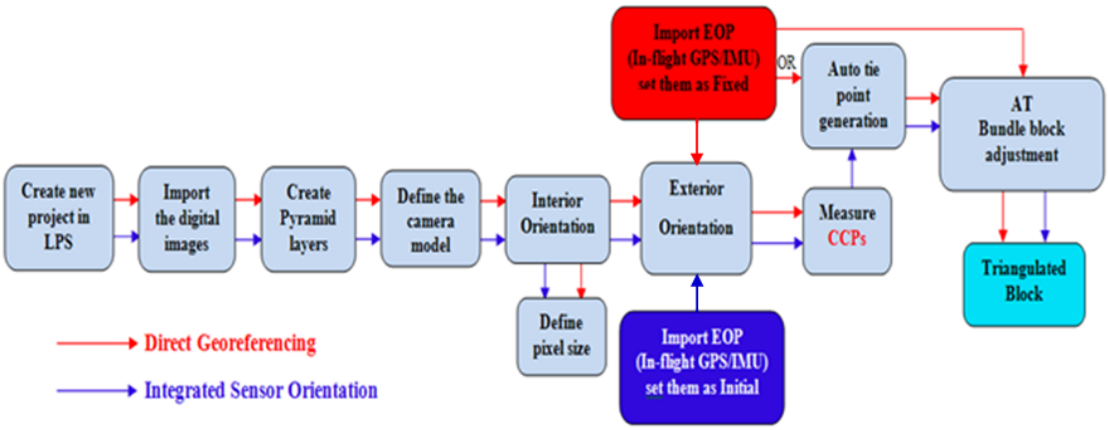

Figure 5.7: The workflow of triangulating a block of digital images using either integrated sensor orientation or direct georeferencing methods in LPS.

This solution, like the others, was conducted with and without using additional parameters. Table 5.4 shows a summary of the used solutions with standard deviation values.

Table 5.4: Summary of the used solutions

Method	**Control**			**Additional parameters**
	GPS	**IMU**	**GCPs**	
Float solution	Large	Large	Small	with and without
Constrained solution	Realistic	Realistic	Small	with and without
Integrated solution	Realistic	Realistic	No	with and without
DG solution	Fixed	Fixed	No	with and without
Small, Large and Realistic: Standard deviation value Small = high weight Large = small weight Realistic = actual estimated value				

5.3.2 Quality of AT

The quality of aerial triangulation is assessed through the comparison of different ground control configurations and different solution types. The configurations of the GCPs and solution types that will be used for the different photogrammetric blocks are as follows:

- **Vertical Pictometry block**: 10 GCPs and 19 CCPs with float and constrained solutions, 29 CCPs with integrated sensor orientation and

only in-flight GPS and IMU (DG) solutions, 1 GCP and 28 CCPs with constrained solution, and finally 2 GCPs and 27 CCPs with constrained solution.

- **Oblique Pictometry block**: 9 GCPs and 22 CCPs with float and constrained solutions, 31 CCPs with integrated sensor orientation and DG solutions, 1 GCP and 30 CCPs with constrained solution, and finally 2 GCPs and 29 CCPs with constrained solution.
- **Combined Pictometry block**: 9 GCPs and 26 CCPs with float and constrained solutions, 35 CCPs with integrated sensor orientation and DG solutions, 1 GCP and 34 CCPs with constrained solution, and finally 2 GCPs and 33 CCPs with constrained solution.
- **UltraCamD block**: 9 GCPs and 24 CCPs with float and constrained solutions, 33 CCPs with integrated sensor orientation and DG solutions, 1 GCP and 32 CCPs with constrained solution, and finally 2 GCPs and 31 CCPs with constrained solution.
- **Combined UltraCamD and oblique Pictometry block:** 9 GCPs and 30 CCPs with float and constrained solutions, 39 CCPs with integrated sensor orientation and DG solutions, 1 GCP and 38 CCPs with constrained solution, and finally 2 GCPs and 37 CCPs with constrained solution.

After the triangulation program is run, the quality evaluation is performed to analyse the results of the bundle adjustment and examine the output. Then the statistical analysis techniques are used to find the quality of the adjustment and to see if there are any bad observations. This operation applies various statistical techniques and provides an indication of the internal and external geometry of the block. The internal geometry includes the RMSE for the GCPs, tie points and image residuals. Since the overall absolute geometric accuracy can only be estimated from independent reference points, The RMSE values of the CCPs compared to the truth value (static GPS survey) will be used to represent the external geometry of the block. A check point analysis compares the photogrammetrically computed ground coordinates of the check points to the original values. The result of the analysis is an RMSE that defines the degree of correspondence between the computed values and the original

values. Residual is the distance between the input (source) location of a GCP (or CCP) and the retransformed location for the same GCP (or CCP). It is a measure of fit or how closely the retransformed location matches the desired output location of a point. Lower residual values (lower RMSE) indicate better results. Residual can be calculated from the following formula:

$$Residual = \sqrt{(x_r - x_i)^2 + (y_r - y_i)^2} \quad (5.1)$$

Where:

x_i and y_i are the source coordinates

x_r and y_r are the retransformed coordinates

The RMSE can be calculated for every GCP or CCP individually and as a total RMSE as follows:

$$\text{RMSE for every GCP(or CCP)} = \sqrt{{r_x}^2 + {r_y}^2} \quad (5.2)$$

Where:

r_x is the residual in X-component which is the distance between the source X-coordinate and the retransformed X-coordinate.

r_y is the residual in Y-component which is the distance between the source Y-coordinate and the retransformed Y-coordinate.

The illustration below (figure 5.8) depicts the relationship between the residual in every point and its RMSE.

$$\text{Total RMSE}_{xy} = \sqrt{{RMSE_x}^2 + {RMSE_y}^2} = \sqrt{\frac{1}{n}\sum_{i=1}^{n} ({r_x}^2 + {r_y}^2)} \quad (5.3)$$

$$\text{Total RMSE}_z = \sqrt{\frac{1}{n}\sum_{i=1}^{n} ({r_z}^2)} \quad (5.4)$$

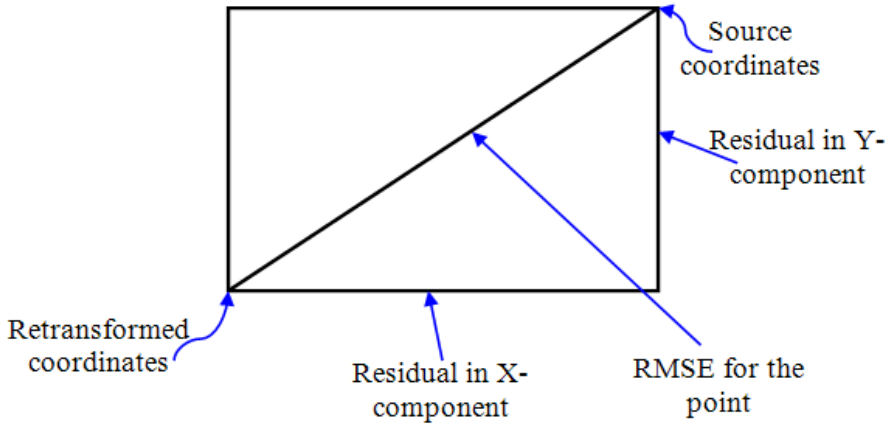

Figure 5.8: The relationship between residual components and the point RMSE

Where:

n is the number of GCPs or CCPs

i is the GCP or CCP number

r_x is the X-Residual for GCP_i or CCP_i

r_y is the Y-Residual for GCP_i or CCP_i

r_z is the Z-Residual for GCP_i or CCP_i

The other measurements of statistical techniques are Sigma0 (from ORIMA) and total image RMSE (from LPS) values. Since errors in the fixed, estimated, or adjusted EOP, GCPs, CCPs, tie point coordinates, and their respective image measurements are reflected in the image coordinate residuals and during the iterative least squares adjustment the values of the new image coordinates are dependent on these parameters, these values provide an indication of the validity of the weights used to compute the AT based on the standard deviation of observation data in the bundle adjustment. In addition, plots of CCPs residuals will be used to evaluate any remaining systematic image errors after performing the bundle block adjustment.

5.3.3 Vertical Pictometry images block

The vertical Pictometry images forming a block (vertical Pictometry block) consists of 27 images (3 strips of 9 images each); see section 4.3.2 for a detailed description of the images.

From the 41 control points available in the study area of Nottingham University main campus, 2 points were excluded from all AT trials due to high

residuals. For the vertical Pictometry images block, the images are in the range of only 29 control points. 10 points were selected as ground control points and 19 as check control points for the first two AT trials while all control points were used as check points for the third and fourth AT trials. The distribution of the control/check points is shown in figure 5.9 as well as the images footprint. This is the final and most correct block. It was created using the EOP that have been provided by Blom Aerofilms. The EOP that are provided with the images as camera-X and camera-Y have systematic error of -100m and +75m respectively which was probably due to transformation errors. Therefore, it was decided to use the EOP provided as camera latitude and camera longitude after converting them to local coordinate system using GridInQuest software. Using camera-X and camera-Y in integrated solution gives very high image residuals and high RMSE for CCPs: 61μm for total image RMSE, 98m for X component, 74m for Y component and 6m for Z component of the CCPs RMSE, figure 5.10 shows the AT result of using the provided camera-X and camera-Y coordinates.

Although a great effort was made to ensure a good distribution of the control points throughout the block, the distribution of GCPs in the vertical Pictometry block was not ideal due to the lack of features that can be recognized or have enough texture and recognizable features in the upper left corner of the block as that area is covered completely by trees. Also, this area is not covered by UltraCamD so this imagery could not be used to provide added GCPs. However, since GPS/IMU data observations are available for each image, the weak control point configuration may not be a problem. The flying height is about 1000m and the nominal camera focal length is 65mm, so the image scale is about 1:15400. The image pixel size is 9μm. The image coordinate measurement standard deviation is set as 0.33 pixels (3μm), which corresponds to a ground space accuracy of 0.046 meters (3 x 15400 / 1000 / 1000). So setting the accuracy of GCPs as 0.05m is very reasonable.

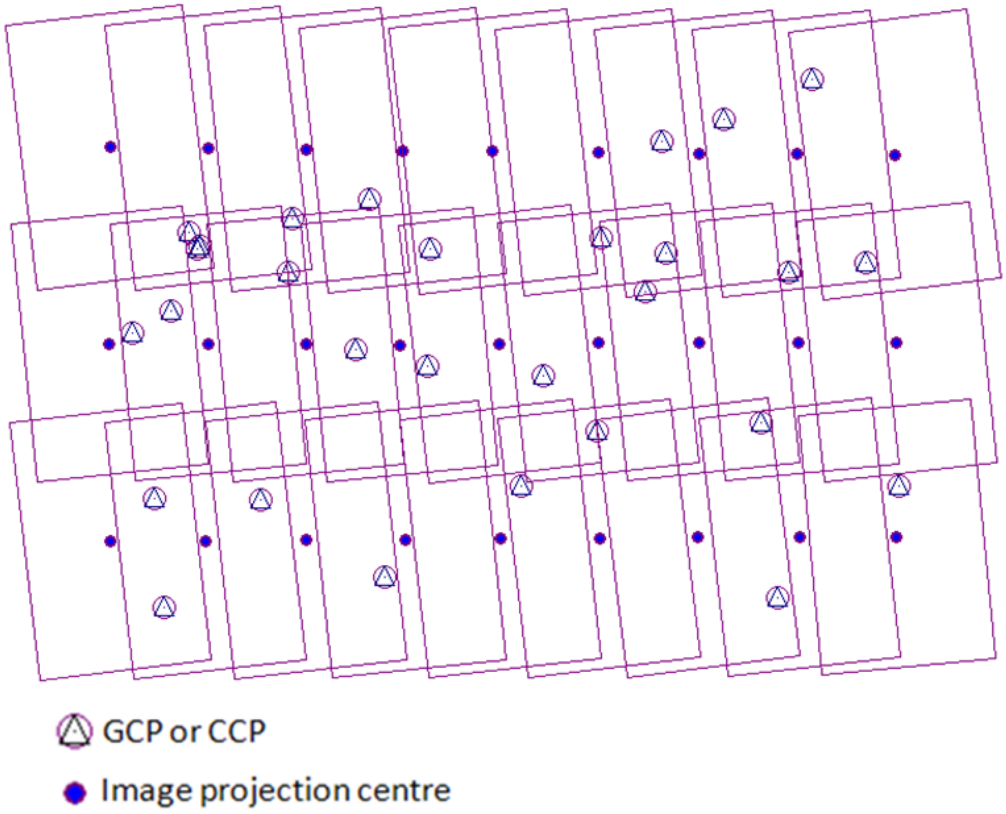

Figure 5.9: The vertical Pictometry images block showing the distribution of control points and images projection centres.

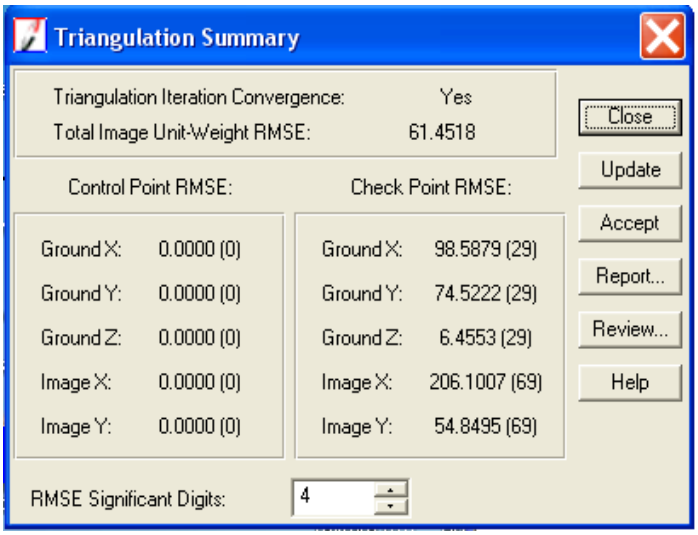

Figure 5.10: LPS AT results of using the projection centres coordinates that contain systematic errors.

A total of 668 tie points were generated automatically using a cross correlation area based matching technique available in LPS. The automatic tie point extraction was generally successful over the block with sufficient tie

point distribution. Blunders and mismatched were identified manually by the operator based on the image residuals. Nine points were excluded due to mismatch. There are 45additional points that show mismatch between strips (between images in different strips). These points were based on shadow and/or on trees. The mismatch in this case is expected because the shadow will not be in the same place as the airplane takes time to come back to the same point and the trees branches move due to wind effects. These points were only excluded from one strip but not completely. The AT results of the 4 solutions are shown in table 5.5 using LPS software and in table 5.6 using ORIMA software.

The results show very good image residuals and fit on the ground control points. The check points show more realistic values of what might be achievable for mapping. When the GSD is 15cm, the accuracy of CCPs in float solution using LPS reach 9.4cm, 8.2cm and 29.5cm on the ground in X, Y and Z components. These are equivalent to 0.63, 0.55 and 2 GSD respectively. As the nominal vertical camera focal length is 65mm and the average flying height is 1000m, this corresponds to 6.1, 5.3, and 19µm in image scale which is 0.68, 0.59, and 2.1pixels respectively. When ORIMA was used, the accuracy reach 4.8, 6.8, and 16.5µm in image scale which correspond to 0.53, 0.76, and 1.83 pixels. The results of both software packages are similar.

Within AT, the use of additional parameters is necessary to overcome remaining systematic effects on the image. Self-calibration is undertaken to fit the physical process of image formation on the assumed mathematical model of central perspective based on the collinearity equations (Cramer and Haala, 2009). The inclusion of the additional parameters (Brown's physical model of 14 parameters) in AT slightly improved the total image RMSE and the RMS of check points for float solution. The additional parameters have improved the Z-component significantly in both LPS and ORIMA. In the constrained solution, the in-flight GPS/IMU EOP used as initial values which allows for adjustment of sensor location and rotation at triangulation but according to the specified standard deviation (1m and 1degree, section 5.3.1.2). The results of AT using this solution are very much similar to those achieved in the float solution except for the Z-component when no additional parameters used in LPS which is almost twice better than that achieved in the float solution.

Table 5.5: Results of AT for vertical block using 4 different solutions in LPS

Solution		**Float**		**Constrained**		**Integrated**		**DG**	
AP		**No**	**Yes**	**No**	**Yes**	**No**	**Yes**	**No**	**Yes**
Total image RMSE(µm)		1.6	1.6	1.7	1.6	2.2	2.1	6.1	2.4
GCPs RMS (no.pts)	***X(m)***	0.025 (10)	0.024 (10)	0.029 (10)	0.025 (10)	-	-	-	-
	Y(m)	0.038 (10)	0.028 (10)	0.040 (10)	0.035 (10)	-	-	-	-
	Z(m)	0.009 (10)	0.006 (10)	0.011 (10)	0.011 (10)	-	-	-	-
CCPs RMS (no. pts)	***X(m)***	0.094 (19)	0.089 (19)	0.086 (19)	0.080 (19)	0.283 (29)	0.278 (29)	0.208 (26)	0.204 (26)
	Y(m)	0.082 (19)	0.076 (19)	0.077 (19)	0.071 (19)	0.447 (29)	0.458 (29)	0.552 (26)	0.460 (26)
	Z(m)	0.295 (19)	0.163 (19)	0.157 (19)	0.147 (19)	0.921 (29)	0.498 (29)	0.644 (26)	0.629 (26)

Table 5.6: Results of AT for vertical block using 4 different solutions in ORIMA

Solution		**Float**		**Constrained**		**Integrated**		**DG**	
AP		**No**	**Yes**	**No**	**Yes**	**No**	**Yes**	**No**	**Yes**
Sigma0 (µm)		1.8	1.6	1.9	1.8	1.9	1.7	1.5	1.4
GCPs RMS (no.pts)	***X(m)***	0.031 (10)	0.022 (10)	0.032 (10)	0.022 (10)	-	-	-	-
	Y(m)	0.037 (10)	0.026 (10)	0.047 (10)	0.036 (10)	-	-	-	-
	Z(m)	0.011 (10)	0.011 (10)	0.015 (10)	0.013 (10)	-	-	-	-
CCPs RMS (no.pts)	***X(m)***	0.074 (19)	0.094 (19)	0.071 (19)	0.083 (19)	0.166 (29)	0.168 (29)	0.335 (29)	0.323 (29)
	Y(m)	0.104 (19)	0.107 (19)	0.111 (19)	0.113 (19)	0.218 (29)	0.481 (29)	0.414 (29)	0.590 (29)
	Z(m)	0.254 (19)	0.182 (19)	0.263 (19)	0.207 (19)	0.401 (29)	0.385 (29)	1.143 (29)	0.790 (29)

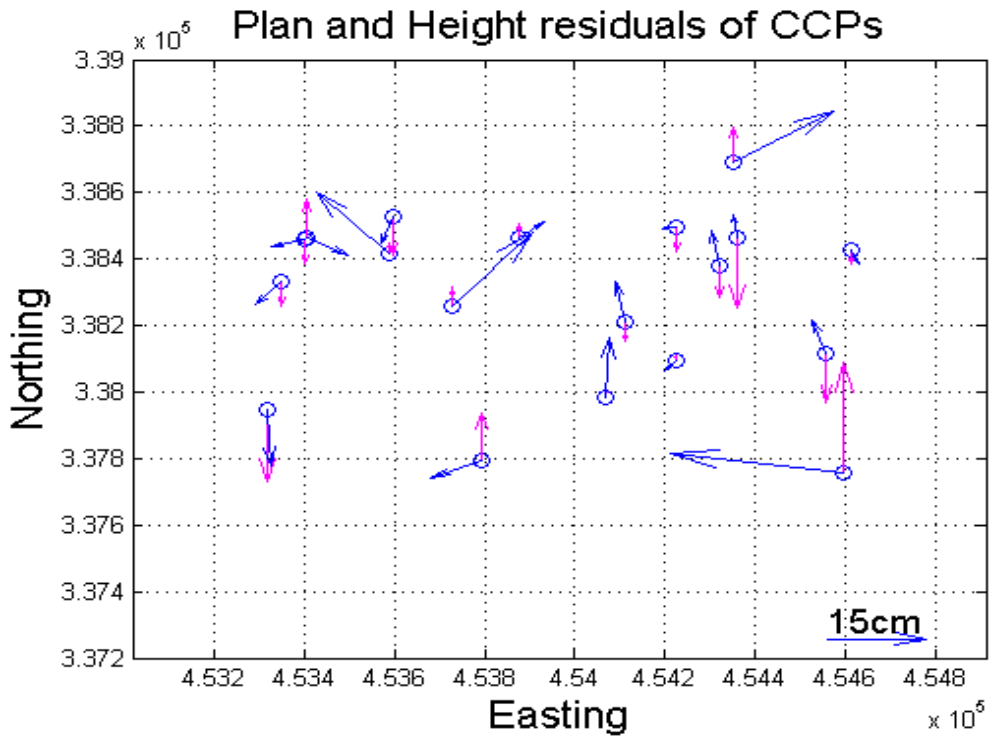

Figure 5.11: Plan (X, Y ground residual component at angle arctan (r_y/r_x)) and height residual vectors for CCPs of constrained solution without additional parameters. Plan vectors are in blue and height vectors are in red.

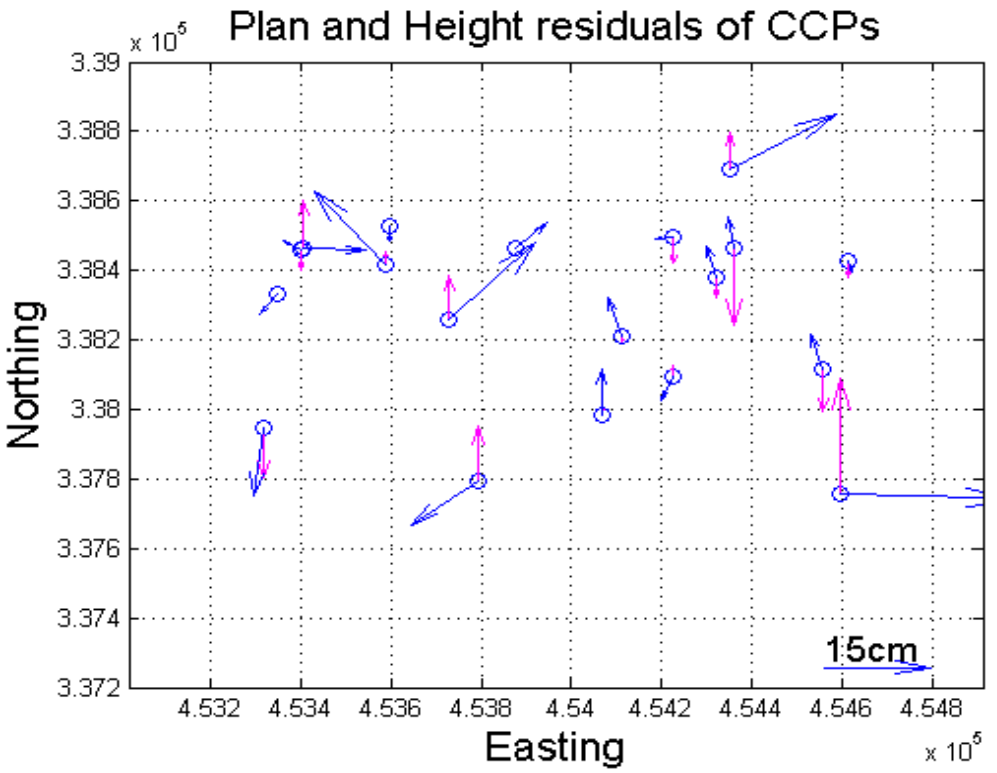

Figure 5.12: Plan (X, Y ground residual component at angle arctan (r_y/r_x)) and height residual vectors for CCPs of constrained solution with additional parameters.

Figure 5.11 and figure 5.12 show the plan and height residual vectors of CCPs for the constrained solution without additional parameters and with additional parameters respectively. The plan residual was calculated using equation 5.2 and the direction of the vector is obtained from the relation:

$$Angle = \tan^{-1}(\frac{r_y}{r_x}) \quad (5.9)$$

The above figures show that the directions of the plan residual vectors are random and not pointing in the same direction which implies that most of systematic errors are eliminated. When examining the lengths of the vectors, it is clear that the vectors' lengths are of different sizes but there is no one vector that has substantially larger length compared to others which may suggest that this point has been badly measured on the image. The introduction of the additional parameters has resulted in a little improvement only in the vertical accuracy. The height accuracy is in the range of 1 to 2 pixels which is a little bit high. This may be related to the uncorrected systematic image errors which reduce the image accuracy and can propagate into object space during AT and leads to a lower vertical accuracy of determined object points. In addition to that, the overlap is not ideal (60%) in this block as the maximum overlap is 46% (see section 4.3.2).

Typically overlap and sidelap lead to the number of observations per point. The more often a point has been observed the easier a blunder can be detected which means better accuracy. Overlap, flying height, and image scale define the intersection angle of rays at a certain point. For this block, about 72% of tie points are 2-fold points (2 intersections), 12% are 3-fold points, and 16% are 4-fold points. Figures 5.13, 5.14 and 5.15 represent the quality of 2-fold, 3-fold and, 4-fold points and table 5.7 summarizes the statistical quality of these points.

Table 5.7: Statistical quality of vertical Pictometry block tie points resulted from constrained solution.

		2-fold points (72%)	3-fold points (12%)	4-fold points (16%)
Max. Residual (m)	X	0.081	0.034	0.031
	Y	0.129	0.034	0.034
	Z	0.427	0.150	0.128
RMSE (m)	X	0.039	0.026	0.023
	Y	0.050	0.026	0.024
	Z	0.236	0.106	0.095

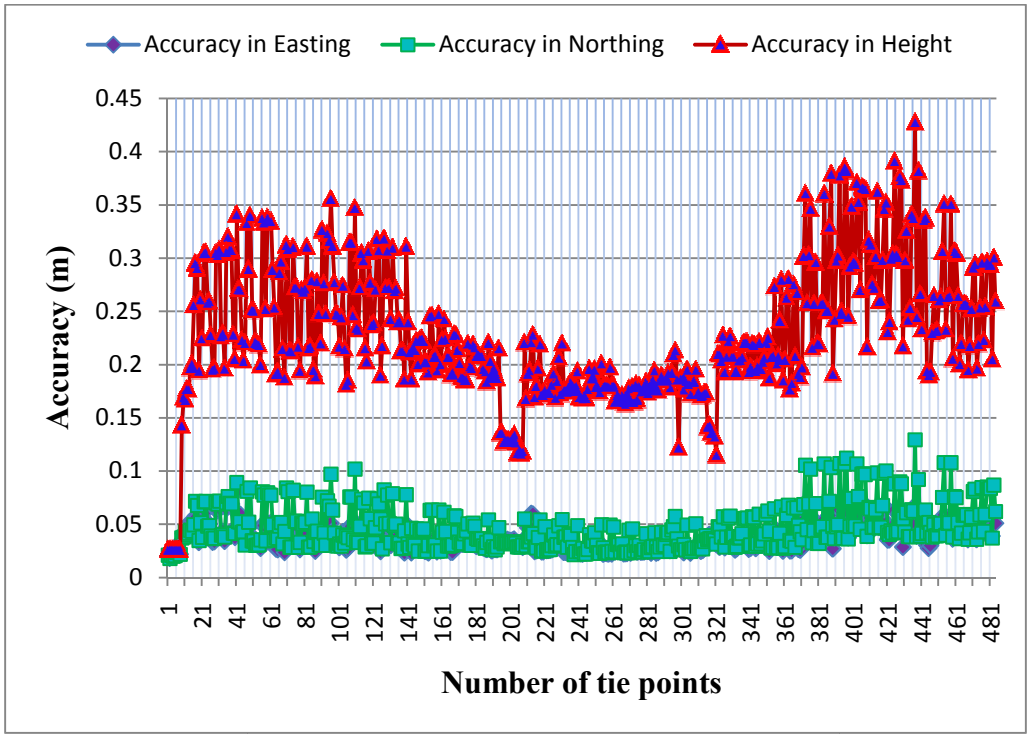

Figure 5.13: Accuracy of 2-fold tie points in the vertical Pictometry block.

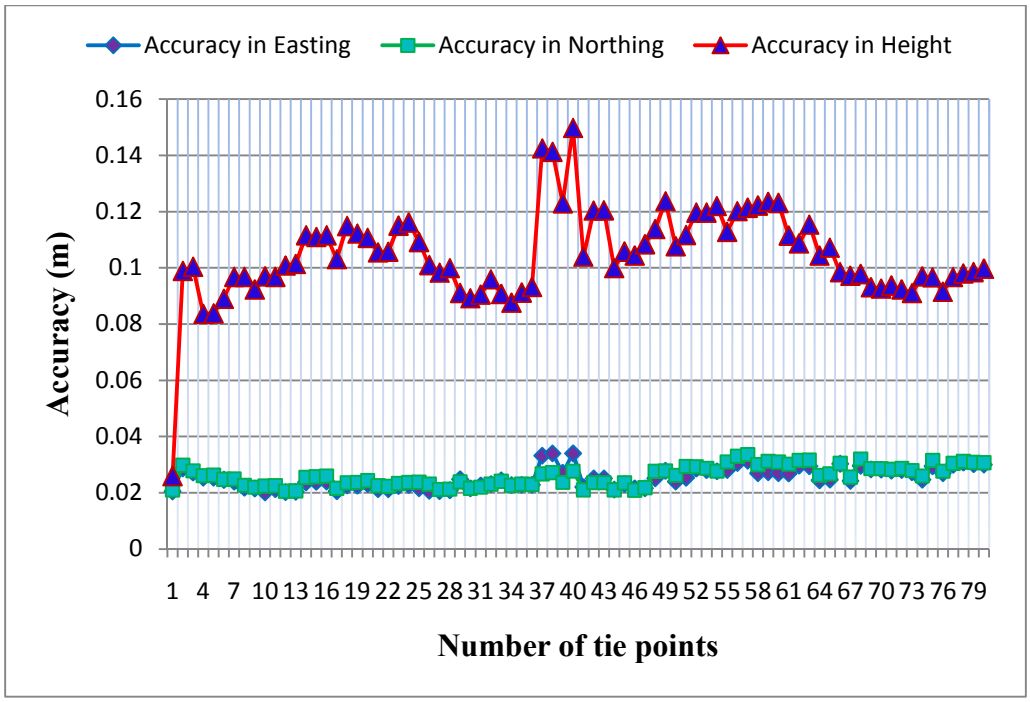

Figure 5.14: Accuracy of 3-fold tie points in the vertical Pictometry block.

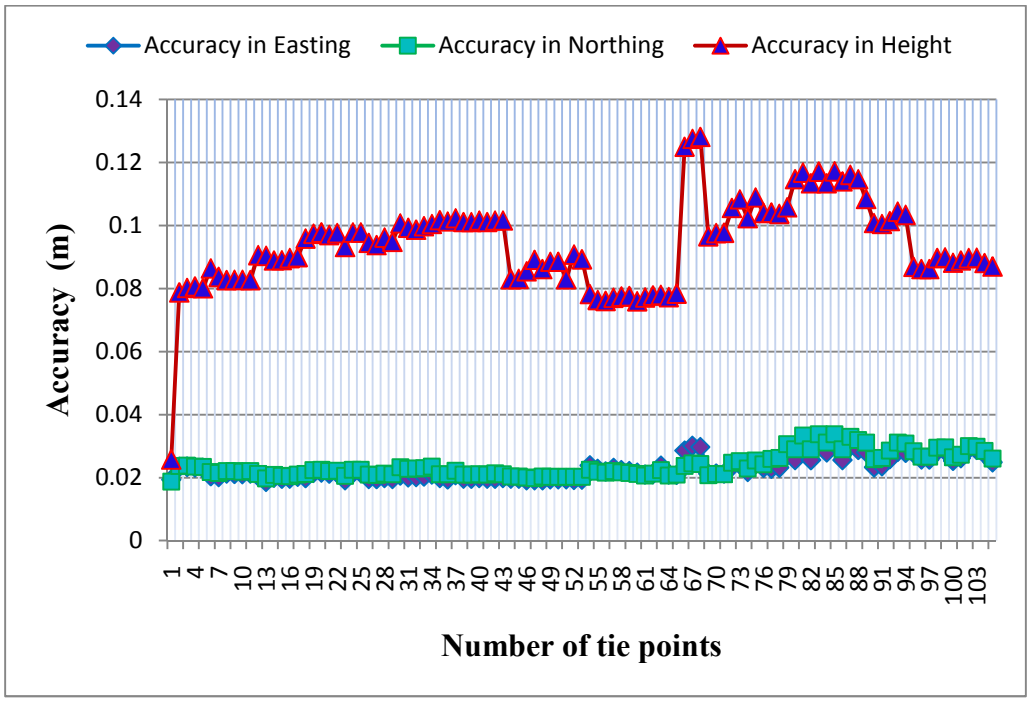

Figure 5.15: Accuracy of 4-fold tie points in the vertical Pictometry block.

It is clear from the above figures that in all cases the multi-ray points are more accurate than two rays per point by a factor of about 2. Moreover, the relatively low height accuracy may indicate small errors that have not been completely modelled. Furthermore, the accuracy of reference point determination (based on static GPS observations) also is of influence.

With regard to integrated sensor orientation and DG solutions, the results show that using direct georeferencing has the potential to be applied with Pictometry imagery although the quality of parameters is not known. The accuracy potential of direct sensor orientation as determined from the best results lies at approximately 20 – 60 cm in X and Y components and 60 – 80 cm in height when expressed as RMS differences at the independent check points. These values are larger by a factor of 2 to 4 when compared to standard photogrammetric results of constrained solution. The fact that the total image RMSE values are larger suggests that stereo plotting in individual models is problematic because of high y-parallax values and that the accuracy of the image coordinates was not fully exploited, because the parameters of exterior orientation were not accurate enough. In contrary to LPS results, ORIMA $sigma_0$ values are very good and even better than that of integrated solution which suggests that 3-D plotting is not problematic. This will be explored by plotting y-parallax for the above solutions because the most sensitive application for the image orientation in terms of accuracy is that of stereo plotting, which relies on models free of y-parallax.

Figure 5.16 shows the y-parallax for direct georeferencing without self-calibration while figure 5.17 shows y-parallax when AP were used. When ORIMA was used the accuracy in object space improved significantly especially in the height which improved by a factor of 3 before applying the additional parameters and by a factor of 2 after the application of AP. Thus, as was expected, integrated sensor orientation overcomes the problem of remaining y-parallax in photogrammetric models and allows for the determination of 3D object space information in much the same way as conventional photogrammetry. Maximum y-parallax when no self-calibration was used is 7.4μm and the standard deviation is 1.16μm. The inclusion of the additional parameters in AT reduced the y-parallax but not significantly; maximum y-parallax now is 7.2μm and the standard deviation is 1.09μm which is equivalent to a drop in y-parallax of only about 6%.

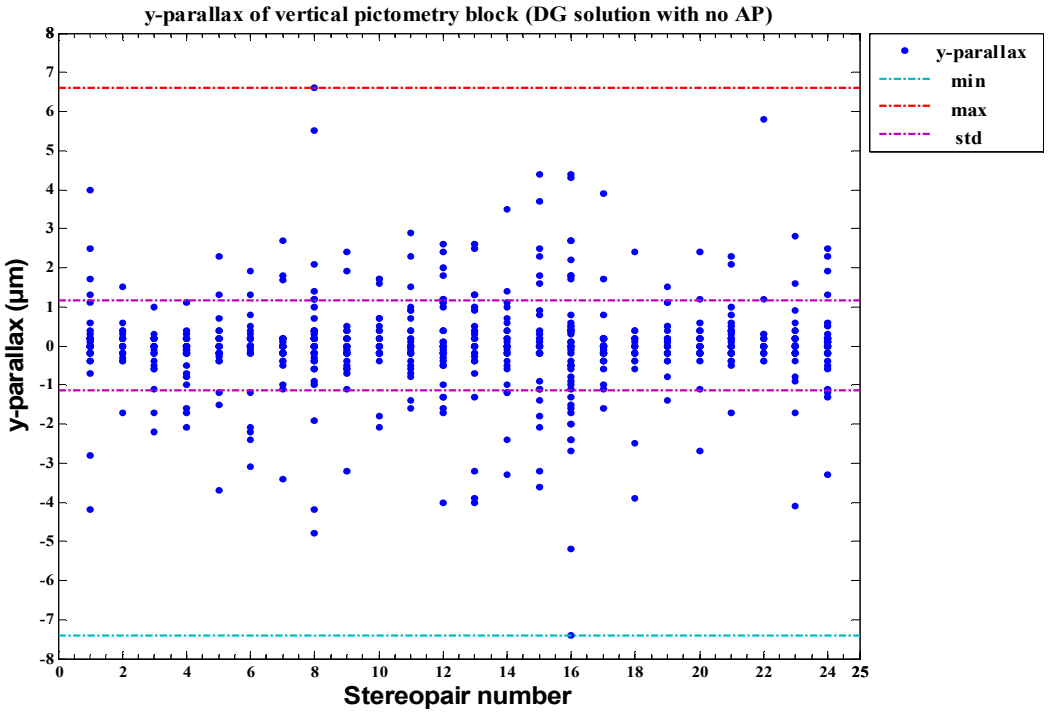

Figure 5.16: y-parallax of vertical Pictometry block in case of DG without AP.

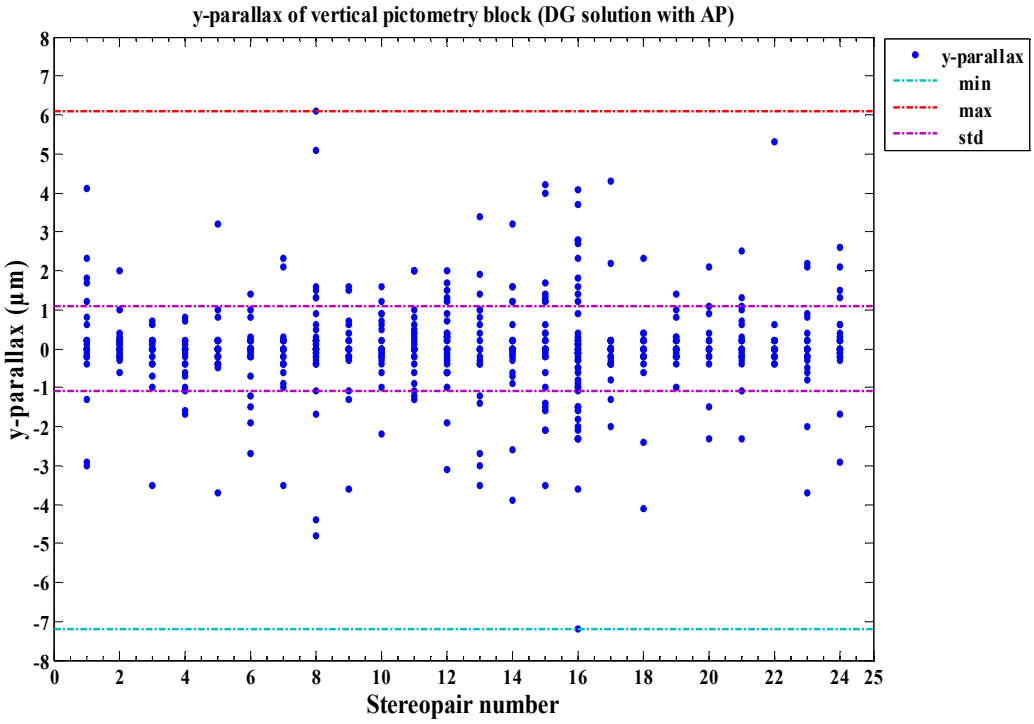

Figure 5.17: y-parallax of vertical Pictometry block in case of DG with AP.

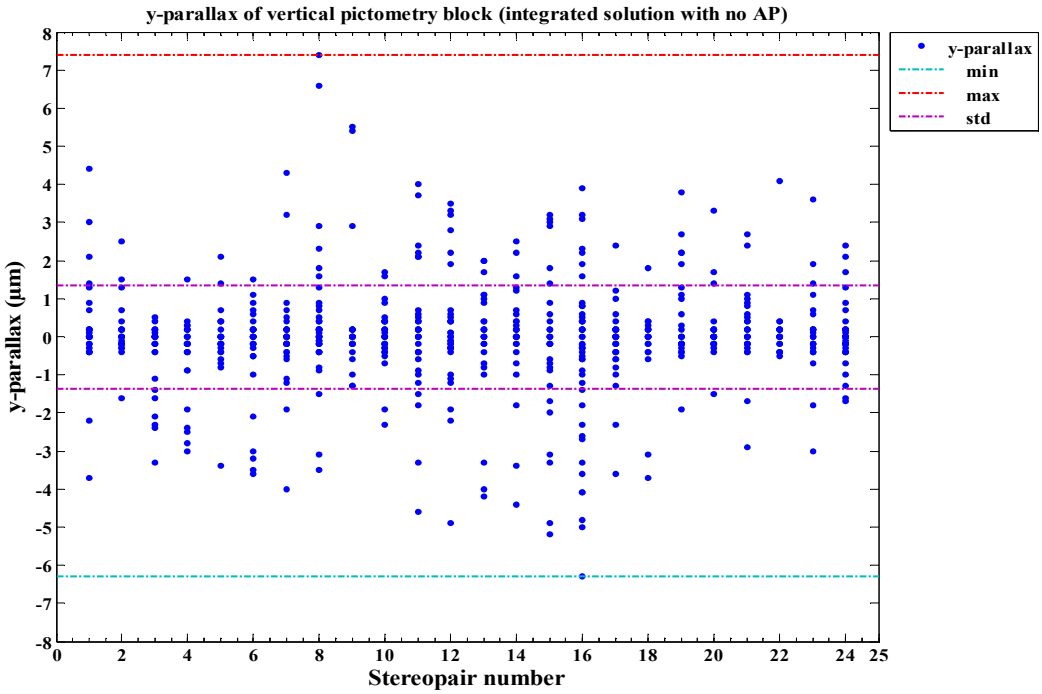

Figure 5.18: y-parallax of vertical Pictometry block in case of integrated sensor solution with no AP.

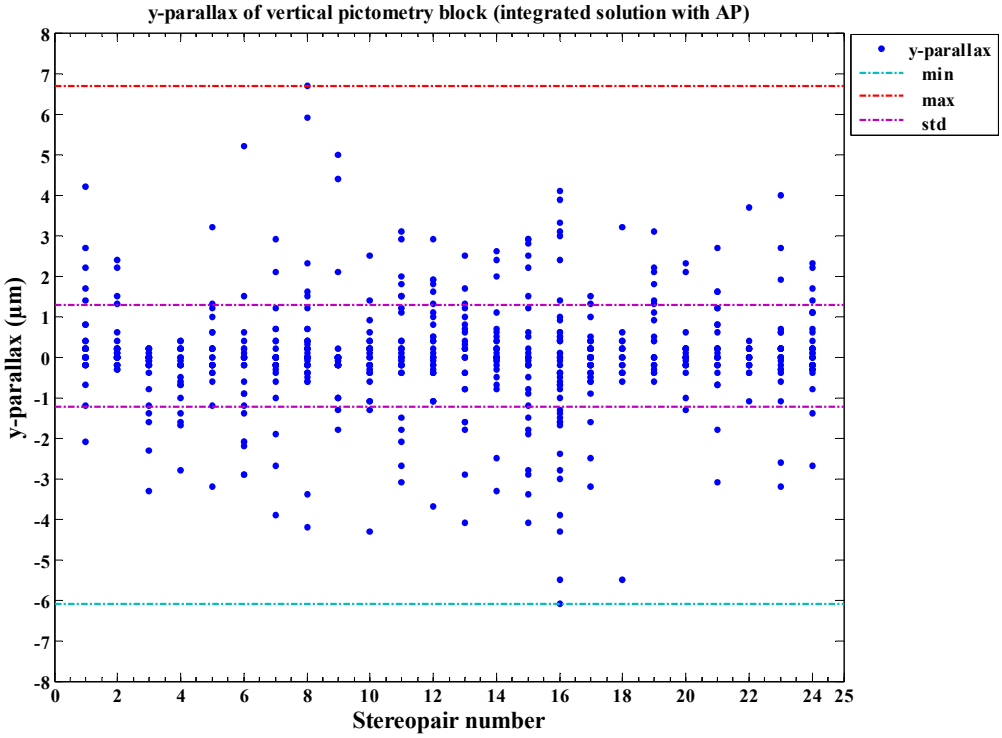

Figure 5.19: y-parallax of vertical Pictometry block in case of integrated sensor solution with AP.

Figure 5.18 and figure 5.19 show y-parallax for the vertical Pictometry block using the integrated sensor orientation solution without using AP model and with using it respectively. The maximum y-parallax has dropped from 7.4 to 6.7µm and the standard deviation has also dropped from 1.36 to 1.29µm which is about 5% drop. In comparison with DG solution, the integrated sensor orientation solution did not improve y-parallax as the figures indicate. The above y-parallax figures were drawn using ORIMA statistical output reports because ORIMA gave better object space accuracy. Table 5.6 shows that $sigma_0$ of DG is less but very close to that of integrated solution which is related to the introduction of tie points in DG solution. Another reason of the improved image space accuracy is stated by Cramer and Haala (2009) as 'the advantage of digital airborne cameras is the good signal-to-noise ratio and the high dynamic range of the collected imagery, which considerably improves the accuracy and reliability of automatic point transfer by image matching compared to scanned analogue images'.

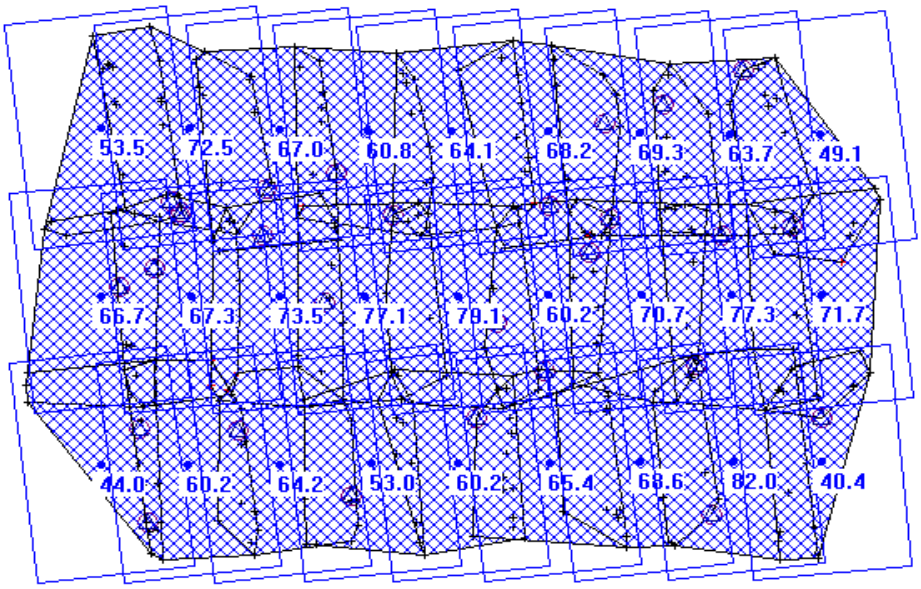

Figure 5.20: The effective footprint in relation to the size of the footprint of the vertical block images.

Figure 5.20 shows a quality check based on tie points. The hatched surface shown above should have no holes in it (in case of finding holes in the surface, additional tie points should be measured). The numbers represent the percentage of the hatched area that corresponds to the effective footprint of the

image in relation to the size of the footprint. For example a value of 75% indicates that the effective footprint covers three quarters of the size of the image footprint. It is clear from figure 5.20 that in this block no holes are found which indicates that there is no need to add more tie points.

It is important to note that during the AT trials of the DG solution, it was necessary to use the blunder checking model within LPS (time-saving robust checking) to get good results. This resulted in elimination of 3 CCPs due to too large residuals they produce. Hence, the number of CCPs of DG solution in table 5.5 is 26 points. In addition, the use of camera parameters (IOP) as fixed for all images or giving them some weight (self-calibration) and including them in AT process (for example same weighted correction for all images), did not change the AT output; the only difference was in the third digit after the decimal point. This implies that the camera is more or less still at the same condition as when it was calibrated and no change occurred under flight condition. Furthermore, several trials have been performed on the constrained solution to check that the given weights (1m, 1deg) for the EOP are reasonable enough. Weights of 0.05m and 0.05deg, 0.05m and 0.01deg, and 0.01m and 0.01deg were tried but the achieved a posterior standard deviation for the independent CCPs was much worse than that achieved when using weights of 1m and 1deg. They were about 20, 50, and 90cm for X, Y, and Z respectively without using AP and 20, 50, and 60cm after applying the AP.

5.3.4 UltraCamD images block

For the block of UltraCamD images, there are 33 control points. 9 points were selected as ground control points and 24 as check control points for the first two AT trials while all control points were used as check points for the third and fourth AT trials. The distribution of the tie points and control/check points are shown in figure 5.21 as well as the images footprint and the camera X-axis. The aerial triangulation trials consist of four different solutions using a combination of different parameters as well as the minimum control solution. In the first trial in-flight GPS and IMU data are used only as initial values without any weighting so that effectively the block is not constrained during the least squares iterations. In the second solution, the EOP used also as initial

values but they were constrained by giving them a weight of 0.1m and 0.1degree for the projection centres and orientation angles respectively.

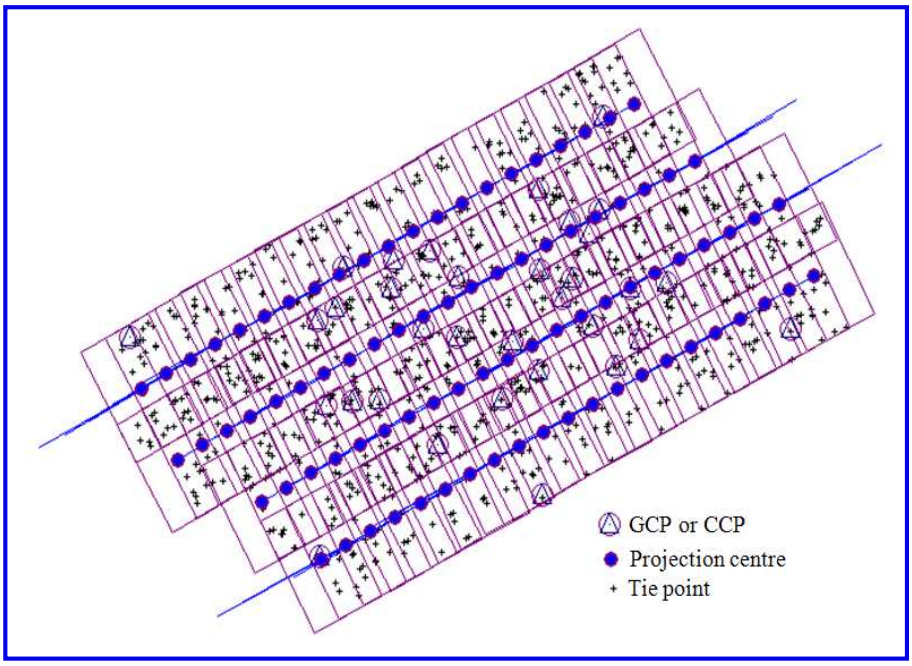

Figure 5.21: UltraCamD images block showing images footprint, distribution of GCPs and tie points, and camera x-axis.

Contrary to Pictometry images, the quality of GPS/IMU positions and attitudes of UltraCamD images was known, hence the assignment of 0.1m and 0.1degree. In the integrated sensor orientation solution, the EOP were kept as initial values but without using any GCPs while in the DG solution the EOP were used as fixed values. As can be seen from figure 5.21, a very good distribution of the control points throughout the block was achievable due to the fact that this block covers more area than that covered by vertical Pictometry block. A total number of 840 tie points were generated automatically using a cross correlation area based matching technique available in LPS. The automatic tie point extraction was generally successful over the block with sufficient tie point distribution. Blunders and mismatches were identified manually by the operator based on the image residuals. It is important to notice here that automatic point measurement (APM) can generate potential blunder points by locating them on the different tops of trees or different rooftops which are not on the ground, figure 5.22. The AT results of

the 4 solutions are shown in table 5.8 using LPS software and in table 5.9 using ORIMA software.

Figure 5.22: Blunders caused by locating tie points on rooftop by APM; the right bottom image shows the AT result before excluding tie point 295 and the left bottom image shows the result after excluding that point.

The results show very good image residuals and fit on the ground control points. The check points show more realistic values of what might be achievable for mapping. The GSD is about 5cm, the accuracy of CCPs in float solution using LPS reach 4cm, 4cm and 9cm on the ground in X, Y and Z components respectively. These are equivalent to 0.80, 0.80 and 1.8 GSD respectively. As the nominal vertical camera focal length is 100mm and the average flying height is 500m, this corresponds to 8, 8, and 18µm in image scale which is 0.89, 0.89, and 2.0pixels respectively. When ORIMA was used, the accuracy reaches 12.0, 8.0, and 17µm in image scale which correspond to 1.33, 0.89, and 1.89pixels. The results of both software packages in most cases are in agreement and very close to each other. For the constrained solution, the AT results are very similar to the float solution results except for the height accuracy before applying the AP technique which was higher when using the ORIMA software. However, after the application of AP model, the results are in agreement in both solutions and using both software packages.

Table 5.8: Results of AT for UltraCamD images vertical block using 4 different solutions in LPS.

Solution		**Float**		**Constrained**		**Integrated**		**DG**	
AP		**No**	**Yes**	**No**	**Yes**	**No**	**Yes**	**No**	**Yes**
Total RMSE (µm)		3.0	2.9	3.1	2.9	3.1	3.0	5.2	4.9
GCPs RMS (no.pts)	***X (m)***	0.062 (9)	0.059 (9)	0.069 (9)	0.059 (9)	-	-	-	-
	Y (m)	0.068 (9)	0.055 (9)	0.056 (9)	0.043 (9)	-	-	-	-
	Z (m)	0.052 (9)	0.020 (9)	0.036 (9)	0.036 (9)	-	-	-	-
CCPs RMS (no.pts)	***X (m)***	0.062 (24)	0.043 (24)	0.067 (24)	0.048 (24)	0.069 (33)	0.058 (33)	0.090 (33)	0.089 (33)
	Y (m)	0.048 (24)	0.037 (24)	0.056 (24)	0.047 (24)	0.103 (33)	0.073 (33)	0.055 (33)	0.055 (33)
	Z (m)	0.118 (24)	0.089 (24)	0.107 (24)	0.109 (24)	0.105 (33)	0.096 (33)	0.123 (33)	0.102 (33)

Table 5.9: Results of AT for UltraCamD images vertical block using 4 different solutions in ORIMA

Solution		**Float**		**Constrained**		**Integrated**		**DG**	
AP		**No**	**Yes**	**No**	**Yes**	**No**	**Yes**	**No**	**Yes**
Sigma0 (µm)		2.5	2.3	2.6	2.3	2.5	2.3	2.5	2.1
GCPs RMS (no.pts)	***X(m)***	0.068 (9)	0.057 (9)	0.067 (9)	0.057 (9)	-	-	-	-
	Y(m)	0.057 (9)	0.060 (9)	0.058 (9)	0.059 (9)	-	-	-	-
	Z(m)	0.097 (9)	0.024 (9)	0.101 (9)	0.024 (9)	-	-	-	-
CCPs RMS (no.pts)	***X(m)***	0.073 (24)	0.064 (24)	0.073 (24)	0.064 (24)	0.065 (33)	0.065 (33)	0.142 (33)	0.072 (33)
	Y(m)	0.033 (24)	0.040 (24)	0.034 (24)	0.038 (24)	0.134 (33)	0.056 (33)	0.107 (33)	0.068 (33)
	Z(m)	0.208 (24)	0.084 (24)	0.212 (24)	0.085 (24)	0.259 (33)	0.217 (33)	0.290 (33)	0.180 (33)

Figure 5.23 and figure 5.24 show the plan and height residual vectors of CCPs for the constrained solution without using AP model and with AP model respectively. The figures show that the residual vectors are pointing randomly which means that most of systematic errors are eliminated except for the upper right vectors (figure 5.23) which point to same direction. This implies that these points still have some systematic errors which have been eliminated when AP was used. Furthermore, the lengths of the vectors are of different sizes and there is no one vector that has substantially larger length compared to others, which may suggest that this point has been badly measured on the image. The introduction of the AP has resulted in a little improvement in the total image RMSE (about 10%) and in plan and height accuracy of GCPs. The substantial improvement was in CCPs (see the scale arrow) especially the vertical accuracy when ORIMA was used. The vertical accuracy has improved by a factor of 4 in GCPs and a factor of 2.5 in CCPs. The height accuracy is in the range of 0.5 pixels for GCPs and 1.5 pixels for CCPs.

Compared to the vertical Pictometry block, it is clear that the accuracy of UltraCamD is much better. It is better by a factor of about 2 to 3. The low checkpoint residuals prove the high geometric quality of the UltraCamD camera system. In addition to the quality of the camera system, the other factors that need to be taken into consideration when comparing the two systems are: the distribution of GCPs is much better for UltraCamD block and the overlap is not ideal for Pictometry block. It is well known that with the increase of image overlap, the number of image intersection rays for each photogrammetric point increases, and the intersection angles will be accordingly larger. Hence, the adjusted block has good geometric stability. The distribution of multiple overlap object points that appear on as many images as possible is better in the UltraCamD block which increases the stability of the block. For UltraCamD block about 10% are 2-fold points, 49% are 3-fold points, 15% are 4-fold points, 18% are 5-fold points,and 8% are 6-fold points. Table 5.10 summarizes the statistical quality of these points.

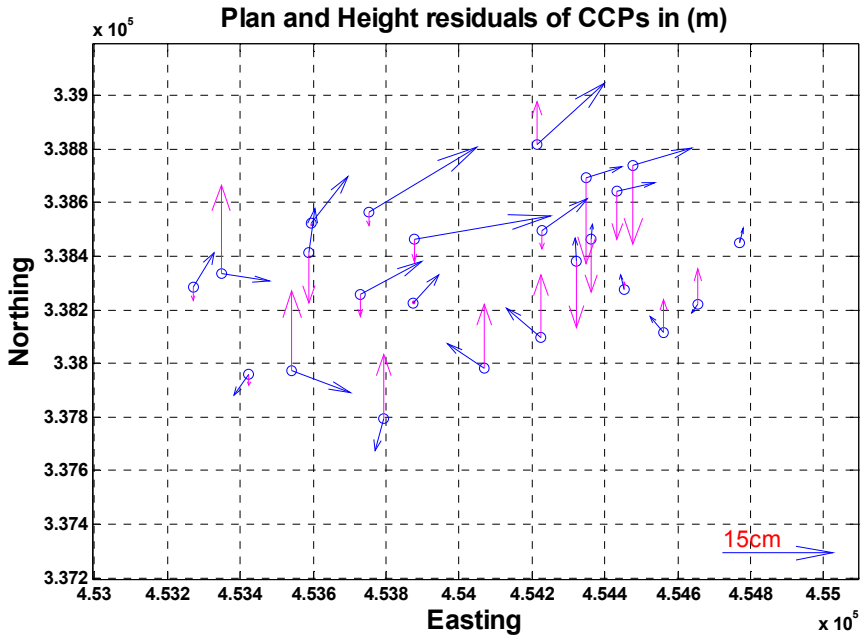

Figure 5.23: Plan and height residual vectors of CCPs for UltraCamD block without using AP model.

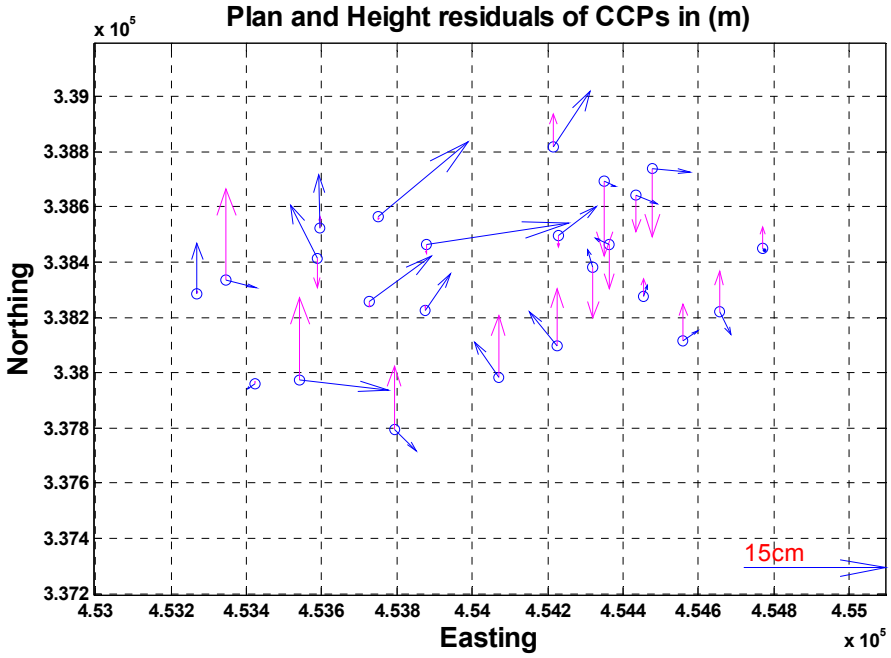

Figure 5.24: Plan and height residual vectors of CCPs for UltraCamD block when AP model was used.

Table 5.10: Statistical quality of multi-ray tie points for UltraCamD block.

		2-fold points	3-fold points	4-fold points	5-fold points	6-fold points
Max. Residual (m)	X	0.076	0.057	0.049	0.044	0.039
	Y	0.073	0.062	0.050	0.045	0.040
	Z	0.192	0.152	0.145	0.124	0.094
RMSE (m)	X	0.048	0.037	0.030	0.031	0.028
	Y	0.050	0.039	0.031	0.031	0.028
	Z	0.135	0.093	0.075	0.072	0.066

Figures D1, D2, D3, D4, and D5 in appendix D depict the quality of 2-fold, 3-fold, 4-fold, 5-fold, and 6-fold tie points of UltraCamD block respectively. Regarding the integrated sensor orientation and DG solutions, the results show that accuracy lies at approximately 5 to 8cm (i.e.1 to 1.5 GSD) in X and Y components and of 10 to 20cm (i.e. 2 to 4 GSD) in the height can be achieved as determined from the best results expressed as RMS differences at the independent check points. These values are comparable to standard photogrammetric results of a constrained solution. ORIMA $sigma_0$ values are very good which suggests that 3-D plotting is not problematic. This will be explored by plotting y-parallax for the above solutions because the most sensitive application for the image orientation in terms of accuracy is that of stereo plotting, which relies on models free of y-parallax. Figure 5.25 shows the y-parallax for direct georeferencing without AP while figure 5.26 shows y-parallax when AP was used. When ORIMA was used the accuracy in image space improved significantly in DG solution (from 4.9µm to 2.1µm when AP model was used). This might be related to the number of AP used which was 14 parameters in case of LPS (Brown's model) and 21 parameters in case of ORIMA. Thus, using the AT result of ORIMA software will overcome the problem of remaining y-parallax in photogrammetric models and allows for the determination of 3D object space information in much the same way as conventional photogrammetry.

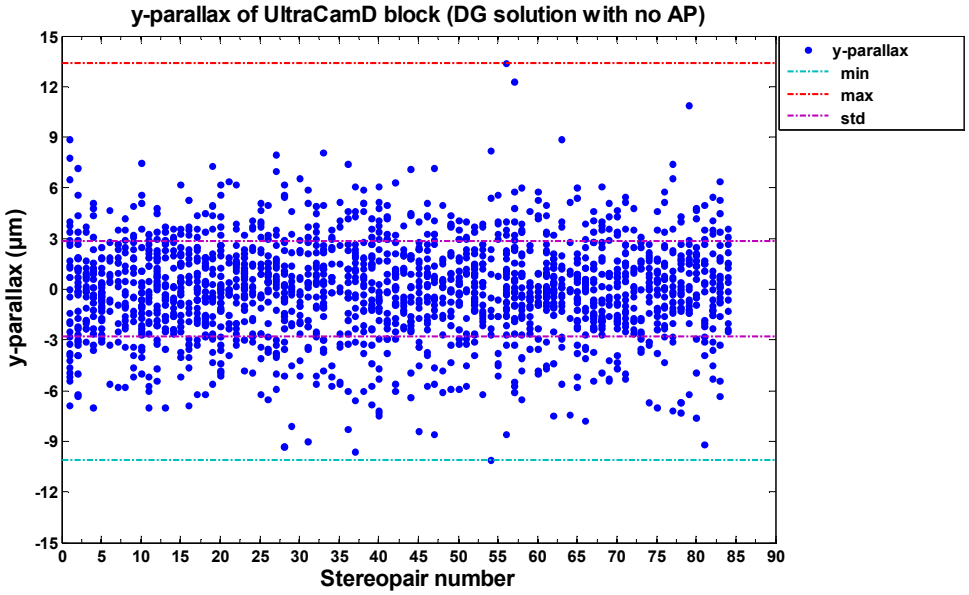

Figure 5.25: y-parallax for DG of UltraCamD block without additional parameters.

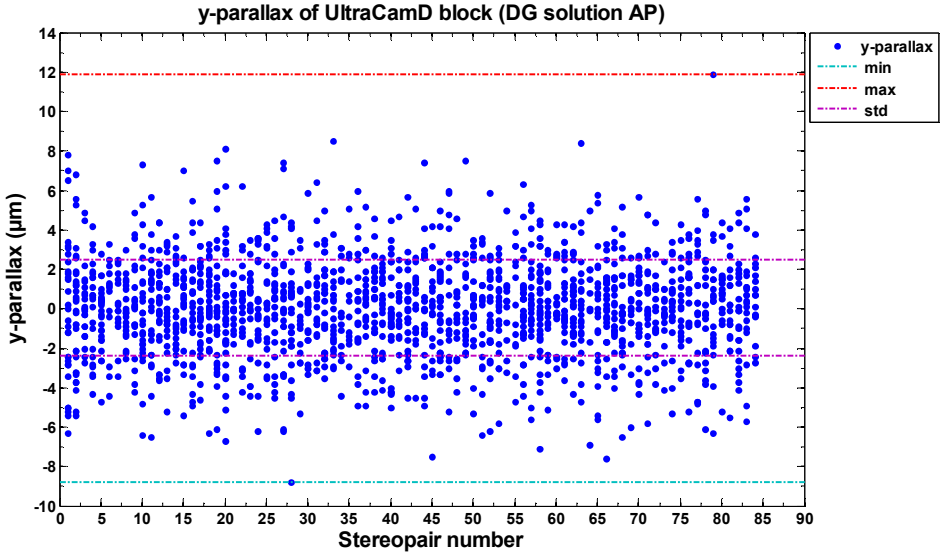

Figure 5.26: y-parallax for DG of UltraCamD block with additional parameters.

Maximum y-parallax when no AP was used is 13.4µm and the standard deviation is 2.83µm. The inclusion of additional parameters in AT reduced the y-parallax; maximum y-parallax now is 11.9µm and the standard deviation is 2.43µm which is equivalent to a drop in y-parallax of about 14%. It is important to note that during the AT trials of the DG solution, when interior orientation parameters were kept fixed, the CCPs accuracy was very low (figure 5.27) so it was necessary to use the IOP as initial values (self-calibration).

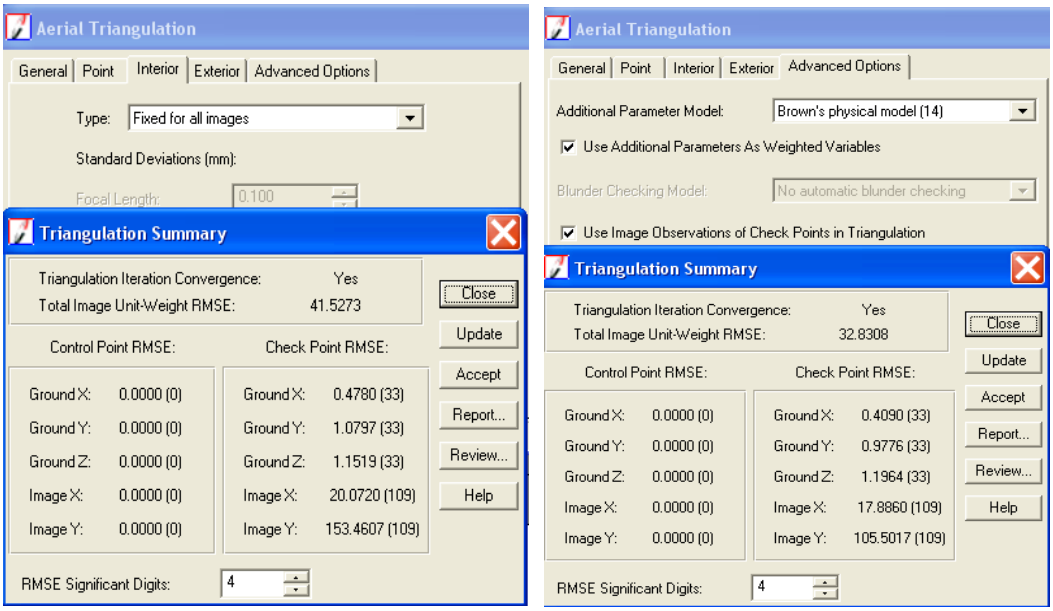

Figure 5.27: AT results when IOP were kept fixed; left figure when no AP used, right figure when AP used.

This indicates that the camera parameters have changed since calibration as the calibration was done in July, 2005 and the imagery was taken in October, 2006. This might be due to atmospheric effects and change in weather conditions between calibration laboratory and real jobsite. Figure 5.28 illustrates the percentage of effective footprint in relation to the footprint of UltraCamD images. No holes in between are found so the addition of more tie points is not necessary.

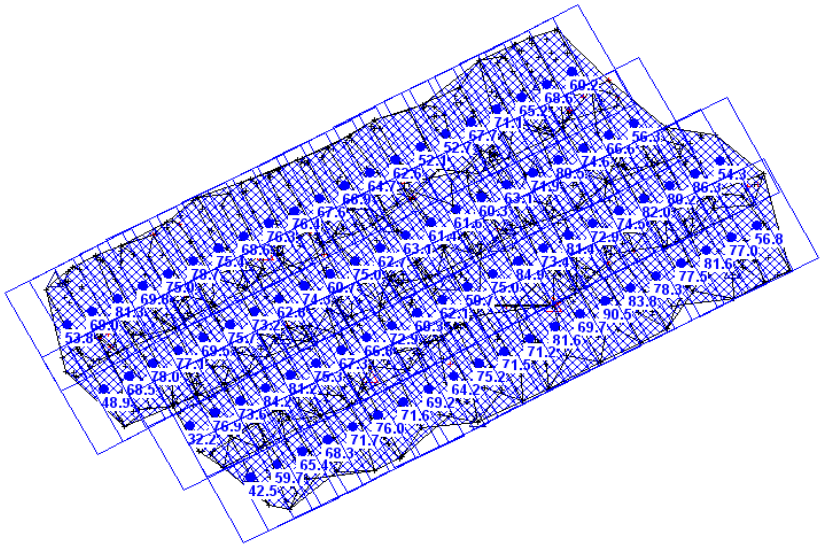

Figure 5.28: The effective footprint in relation to the footprint of UltraCamD images block.

5.3.5 Oblique Pictometry images block

The oblique Pictometry block consists of 57 oblique aerial photographs (photographs taken with the camera axis points between the horizontal and vertical); 12 of them (3 strips of 4 images each) looking East, 15 (3 strips of 5 images each) looking West, 15 (3 strips of 5 images each) looking North, and 15 (3 strips of 5 images each) looking South. For this block, the images are in the range of only 31 control points. 9 points were used as ground control points and 22 as check control points for the first two AT solutions while all control points were used as check points for the third and fourth AT solutions. The distribution of the tie points and control/check points is shown in figure 5.29 as well as the images projection centres and the camera X-axis while figure 5.30 depicts the imagery footprints after the performance of AT.

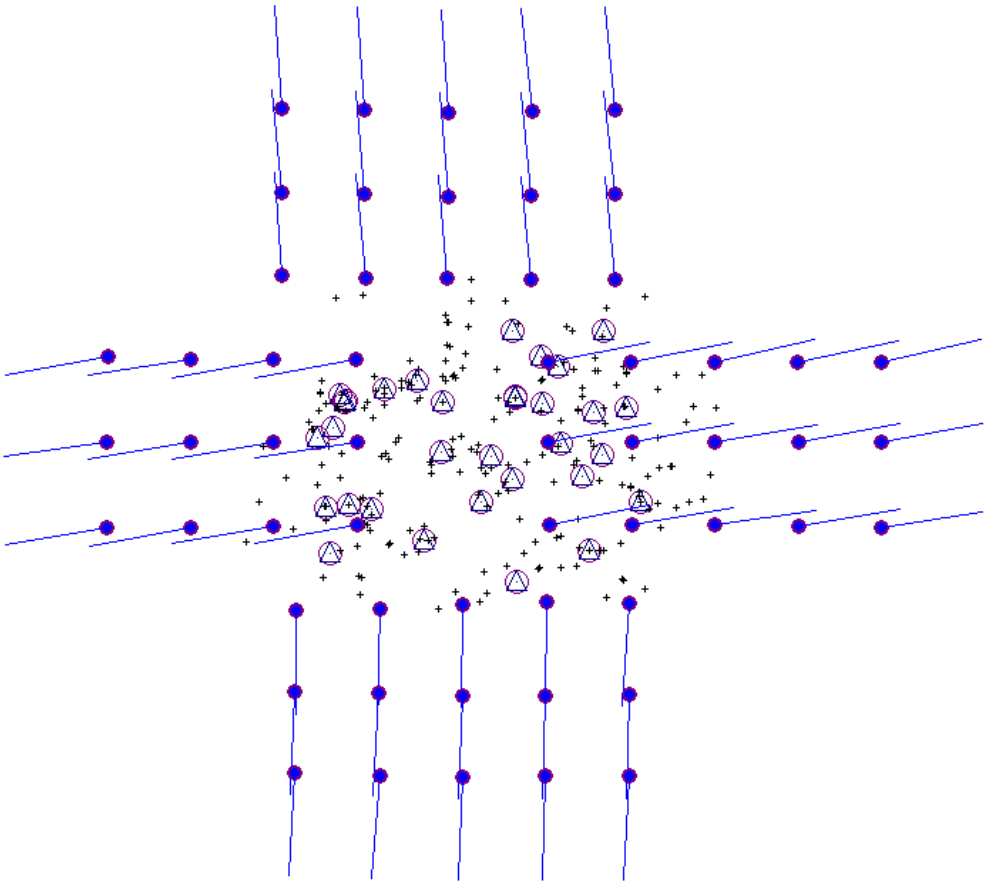

Figure 5.29: Distribution of the tie points and control/check points, projection centres, and camera X-axis for the oblique images block.

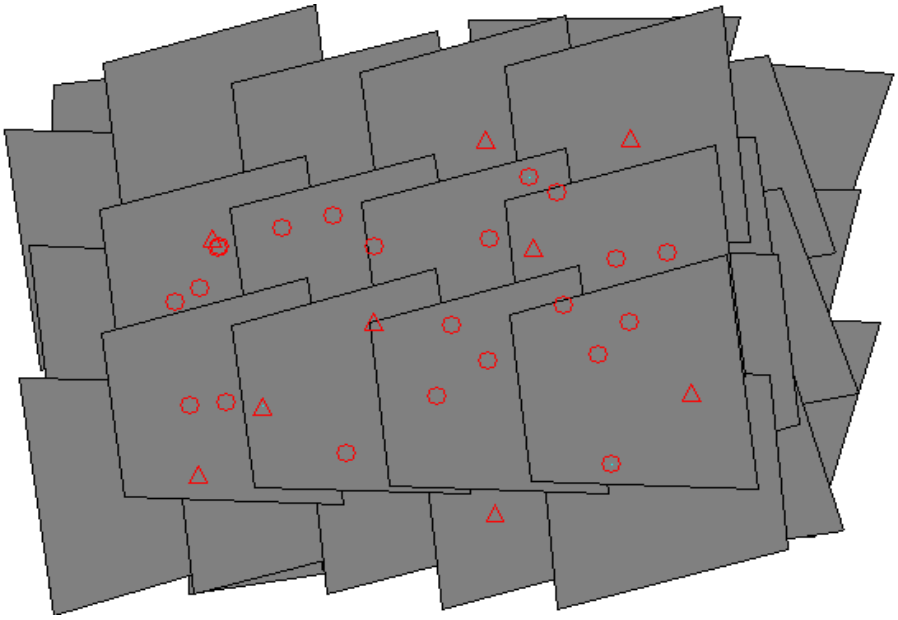

Figure 5.30: Oblique images footprint after performing AT

The observation of GCPs in the Pictometry oblique images was made manually. Most of the GCPs were easily identifiable due to the good radiometric quality of the images. However, some difficulties were encountered while measuring the GCPs on the oblique images due to the tilt and the apparent differences in scale within the oblique images, ranging from 10 cm GSD in the image foreground to 18 cm in the image background.

With images that have large tilts like the oblique images, it is always difficult to produce initial values for the computation. This was apparent when the traditional AT (keeping EOP as unknowns) did not work with this block. The automation of the relative and absolute orientation of oblique images is still an issue of intensive research. Particularly the differences in scale and overlap have to be considered. Labe and Forstner (2006) demonstrated promising results with PFIFF (a digital airborne remote sensing system) oblique images which is based on the use of a single camera. This provides the most flexibility but requires a complex and time consuming flight pattern for the acquisition of oblique imagery.

Tie points for the oblique block were manually observed and the ground control/check points are also the tie points between the blocks. This was necessary because the automatic generation of tie points did not work well with the oblique images due to different illumination and significantly different

views of the target objects/points. The number of measured tie points is 201. While trying to generate the tie points automatically, blunders occurred. Usually a blunder at a particular image point influences the exterior orientation of the image. As the exterior orientation cannot be estimated correctly, all points in that particular image get larger residuals. Figure 5.31 illustrates the smearing effect.

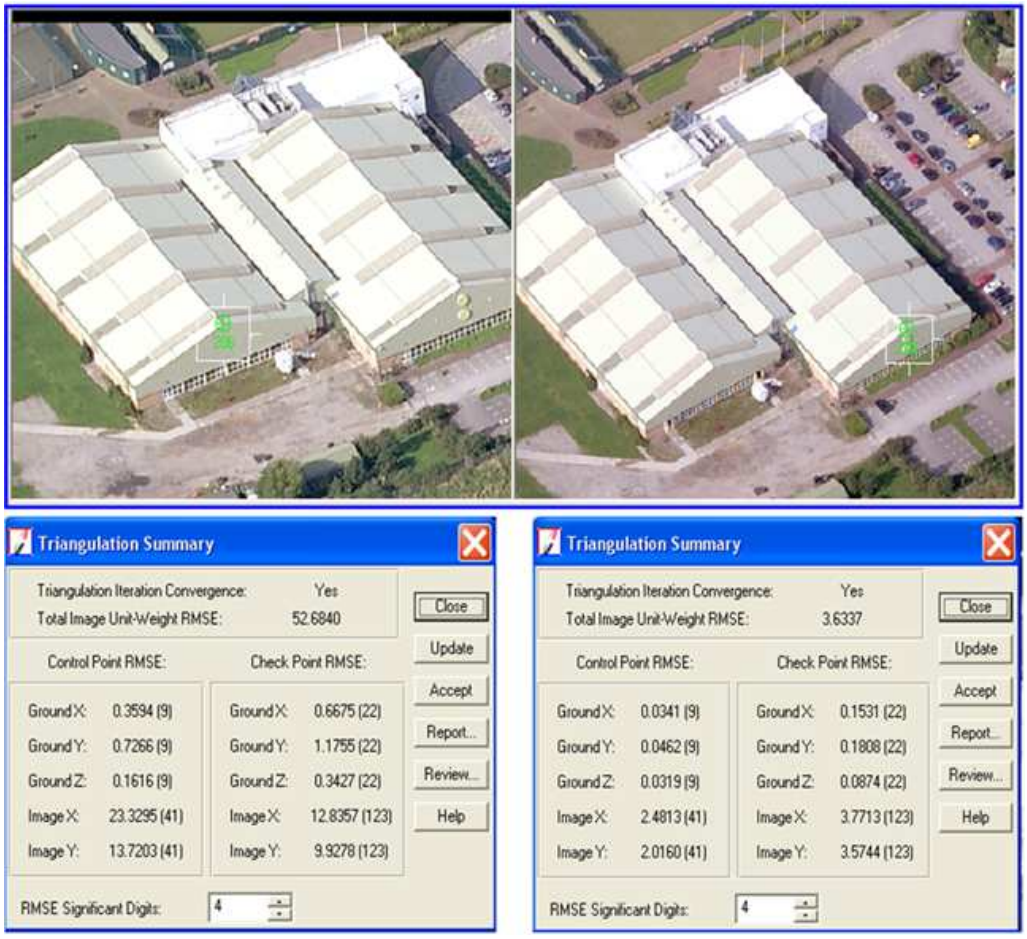

Figure 5.31: Example of mismatching of APM; the upper two images show the location of point 206 in the overlap area of left and right images, the bottom left image is the AT result before excluding point 206, and the bottom right image is the AT result after excluding the mismatched point.

The results of AT for the oblique block using LPS and ORIMA are given in Tables 5.11 and 5.12 respectively. The results show good image residuals and fit on the ground control points. Again, the RMS of CCPs shows the realistic value of what can be achieved in mapping. Including the additional parameters in float and constrained solutions gave a big improvement for the

total image RMSE and Sigma naught (10 to 20%) and a slight improvement for CCPs RMS.

For the integrated and DG solutions, the total image RMSE is almost the same using both software packages in the integrated sensor orientation solution. However, it is again much better when ORIMA was used in DG solution especially when AP model was not used. The RMS of CCPs in case of integrated solution using LPS was a little bit high and ranges from 40cm in Y-component to 78cm in the Z-component. The use of ORIMA has resulted in big improvement in the X-component (from 62cm to 32cm), a little improvement in Y-component (about 5cm), and on the other hand resulted in accuracy deterioration of about 10cm in the Z-component. The use of AP model improved the RMS of CCPs significantly which implies the possible existence of systematic errors before applying the additional parameters. It improved the results by a factor of 2 to 3 in the case of LPS; the biggest accuracy gain was in the height which jumped from 78cm to 28cm. In the case of using ORIMA, the accuracy improved by a factor of 1.5 to 2 and the largest improvement was in Y-component (from 34cm to 16cm). The RMS of CCPs in the case of DG solution using LPS was high and ranges from 35cm in the X-component to 3m in the Y-component. The use of ORIMA has resulted in a noticeable improvement in the Y-component (from 3m to 54cm). Nonetheless, it has resulted in accuracy deterioration of about 30cm in the Z-component and of about 23cm in the X direction. The use of AP model improved the RMS of CCPs significantly especially using ORIMA which again implies the possible existence of systematic errors before applying the additional parameters model. It improved the results by a factor of about 1.5 in case of using LPS; the biggest accuracy gain was in the height which improved from 80cm to 57cm. In case of using ORIMA, the accuracy improved by a factor of about 1.5 to 4 and the largest improvement was in Z-component in which the accuracy gain was 80cm (from 1.13m to 0.33cm).

Figure 5.32 and figure 5.33 show the plan and height residual vectors of CCPs for the constrained solution without using AP model and with AP model respectively.

Table 5.11: Results of AT for oblique images block using 4 different solutions in LPS

Solution		**Float**		**Constrained**		**Integrated**		**DG**	
AP		**No**	**Yes**	**No**	**Yes**	**No**	**Yes**	**No**	**Yes**
Total image RMSE(μm)		3.8	3.2	4.2	3.4	4.9	4.0	10.0	5.5
GCPs RMS (no.pts)	***X(m)***	0.030 (9)	0.021 (9)	0.056 (9)	0.025 (9)	-	-	-	-
	Y(m)	0.061 (9)	0.050 (9)	0.093 (9)	0.060 (9)	-	-	-	-
	Z(m)	0.066 (9)	0.027 (9)	0.053 (9)	0.023 (9)	-	-	-	-
CCPs RMS (no. pts)	***X(m)***	0.159 (22)	0.142 (22)	0.160 (22)	0.144 (22)	0.625 (31)	0.240 (31)	0.348 (31)	0.339 (31)
	Y(m)	0.187 (22)	0.181 (22)	0.192 (22)	0.172 (22)	0.398 (31)	0.169 (31)	2.957 (31)	2.282 (31)
	Z(m)	0.113 (22)	0.076 (22)	0.086 (22)	0.071 (22)	0.781 (31)	0.286 (31)	0.803 (31)	0.567 (31)

Table 5.12: Results of AT for oblique images block using 4 different solutions in ORIMA

Solution		**Float**		**Constrained**		**Integrated**		**DG**	
AP		**No**	**Yes**	**No**	**Yes**	**No**	**Yes**	**No**	**Yes**
Sigma0 (μm)		4.2	3.4	4.3	3.8	4.1	3.7	4.0	3.4
GCPs RMS (no.pts)	***X(m)***	0.039 (9)	0.033 (9)	0.041 (9)	0.038 (9)	-	-	-	-
	Y(m)	0.063 (9)	0.031 (9)	0.076 (9)	0.071 (9)	-	-	-	-
	Z(m)	0.058 (9)	0.041 (9)	0.057 (9)	0.037 (9)	-	-	-	-
CCPs RMS (no.pts)	***X(m)***	0.165 (22)	0.168 (22)	0.154 (22)	0.165 (22)	0.324 (31)	0.173 (31)	0.580 (31)	0.460 (31)
	Y(m)	0.178 (22)	0.194 (22)	0.179 (22)	0.158 (22)	0.344 (31)	0.163 (31)	0.541 (31)	0.257 (31)
	Z(m)	0.111 (22)	0.123 (22)	0.104 (22)	0.090 (22)	0.880 (31)	0.629 (31)	1.128 (31)	0.330 (31)

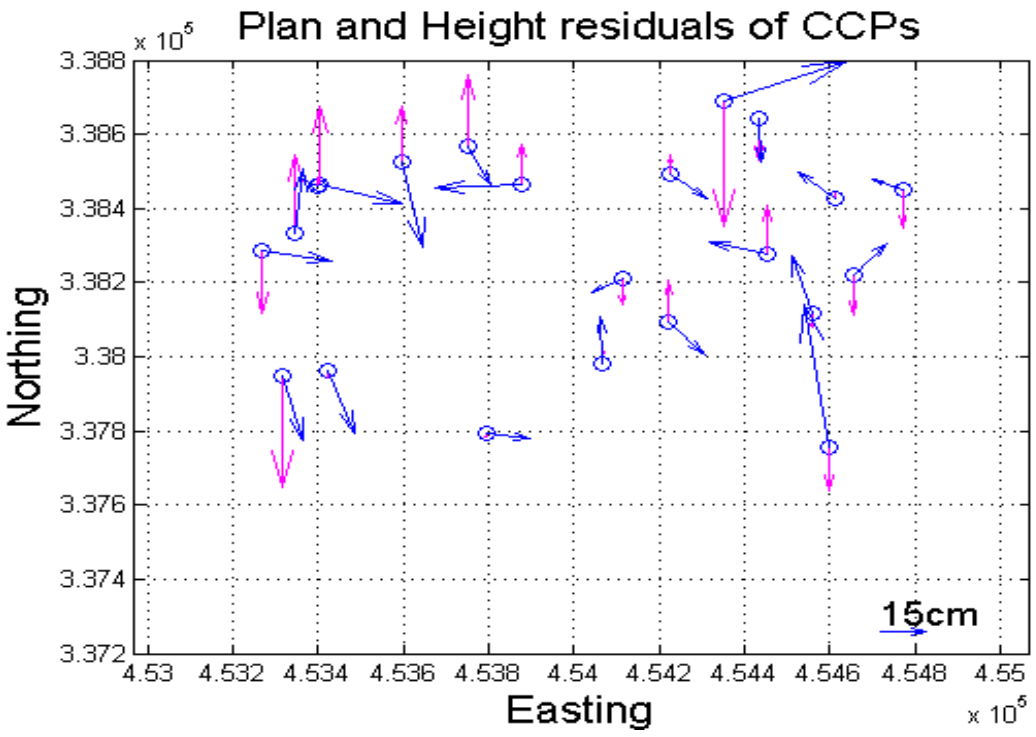

Figure 5.32: Plan and height residual vectors for CCPs of oblique block, constrained solution without AP model.

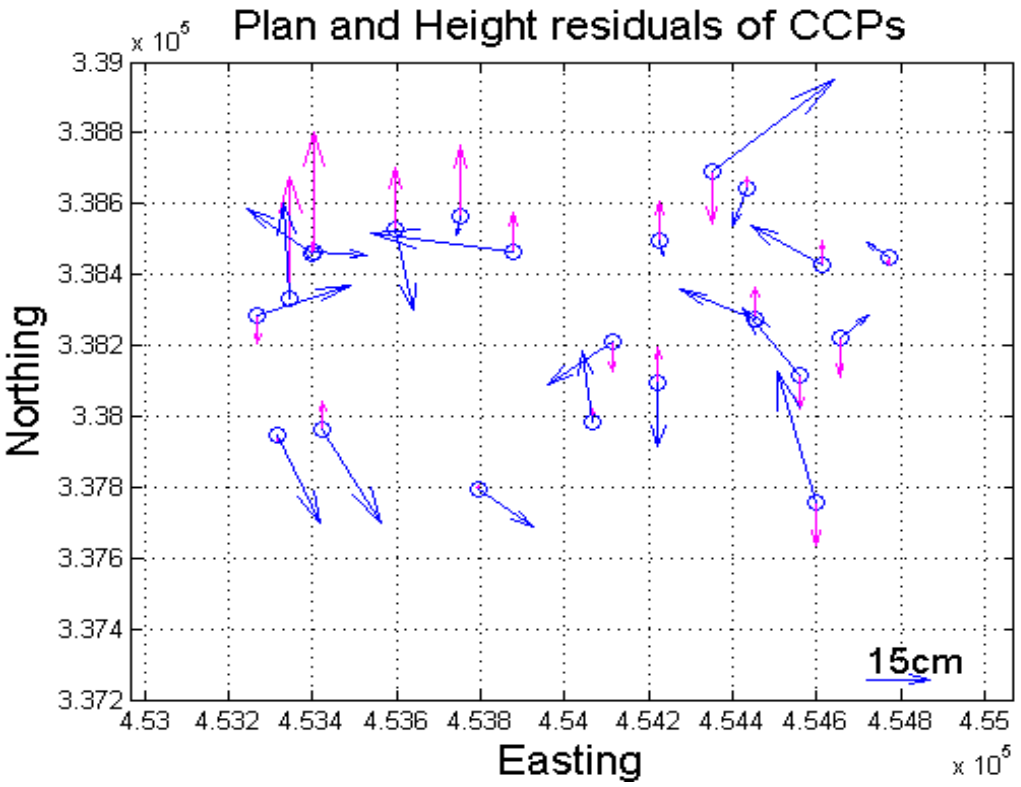

Figure 5.33: Plan and height residual vectors for CCPs of oblique block, constrained solution with AP model.

The figures show that the residual vectors are again pointing randomly which means that most of systematic errors are eliminated. Furthermore, the lengths of the vectors are of different sizes and there is no one vector that has substantially larger length compared to others, which may suggest that this point has been badly measured on the image. The introduction of the AP model has resulted in a reasonable improvement in the total image RMSE (about 10% to 20%) and in plan and height accuracy of GCPs. The use of AP model has brought some improvement in CCPs RMS which can be seen from comparing the residual vectors in both figures (see the scale vector which is directly proportional to residual vectors). The height accuracy of the CCPs is in the range of 7 to 9cm and the plan accuracy ranges between 14 and 17cm.

The lengths of residual vectors are larger compared to the vertical block due to the fact that the residuals in X and Y directions are bigger here. The reason for a relatively high residual may be attributed to the fact that for oblique images there were less tie points as they were generated manually. This may affect the block geometric stability because theoretically the more tie points, the more redundancy we have, the smaller RMSE, and the more reliable exterior orientation parameters. In addition, a high number of tie points makes a very strong connection of the images in the strips and between the strips which increases the quality and accuracy of the triangulated block. On the other hand, the results of the height component in the oblique images block are much better than those in the vertical Pictometry block in all solutions, with only one exception. For the float solution the height accuracy is better by a factor of about 1.5 to 3. The height quality is also better by a factor of 2 to 2.5 in the constrained solution. When direct georeferencing method was used in AT, the height accuracy of the oblique block is better by a factor of 1.5 to 2.5 than that of the vertical block. In case of integrated solution, the height quality is also better in the oblique block when LPS was used but it was worse when ORIMA was used. The improvement of height accuracy of the oblique block is because of using the oblique images which give more intersection rays and therefore good coordinates. In addition to that, the geometry of the vertical block is influenced by the overlap which is less than the ideal 60%. Furthermore, multi-ray tie point distribution is better in the oblique block than

in vertical block. For this block, about 43% of tie points are 2-fold points, 22% are 3-fold points, 8% are 4-fold points, 6% are 5-fold points, 6% are 6-fold points, 3% are 7-fold points, 5% are 8-fold points, and 7% are 9 to 14-fold points. Figures D6 to D13 in appendix D show the quality of multi-ray tie points for the oblique images block and table 5.13 summarizes the statistical quality of these points.

Table 5.13: Statistical quality of multi-ray tie points of oblique block

		2-fold points	3-fold points	4-fold points	5-fold points	6-fold points	7-fold points	8-fold points	9 to14-fold points
Max. Residual (m)	**X**	1.512	0.456	0.195	0.089	0.088	0.084	0.073	0.066
	Y	1.203	0.418	0.325	0.083	0.087	0.078	0.073	0.064
	Z	1.228	0.389	0.262	0.096	0.094	0.085	0.083	0.072
RMSE (m)	**X**	0.416	0.192	0.103	0.074	0.069	0.070	0.062	0.060
	Y	0.470	0.170	0.161	0.070	0.069	0.067	0.060	0.059
	Z	0.525	0.214	0.157	0.080	0.077	0.075	0.068	0.065

As can be seen from the above table, table 5.7 and table 5.10 the accuracy improves significantly with the number of images in which a point appears. Figure 5.34 shows the y-parallax for the DG solution without applying the additional parameters technique while figure 5.35 shows y-parallax when the additional parameters model was used. Again the results of AT using ORIMA software have been used to plot the y-parallax as the $sigma_0$ is better compared to total image RMSE obtained by using LPS. This will help overcome the problem of remaining y-parallax in photogrammetric models and allows for the determination of 3D object space information in much the same way as conventional photogrammetry. Maximum y-parallax when no AP model was used is 16.9μm and the standard deviation is 4.81. The inclusion of AP model in AT reduced the y-parallax to the value of 11.7μm and the standard deviation to the value of 3.14μm which is equivalent to a drop in y-parallax of about 35%.

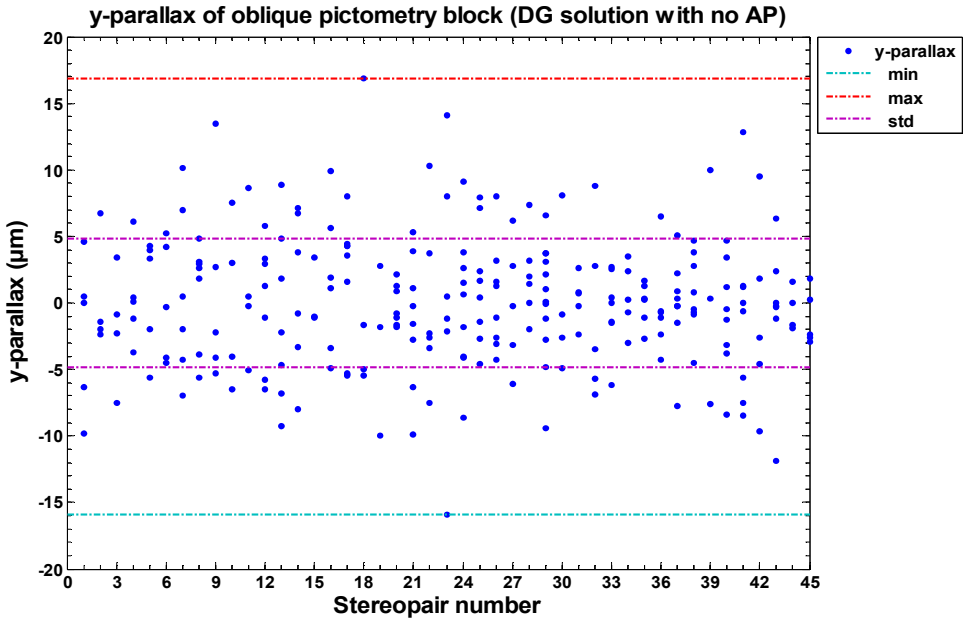

Figure 5.34: y-parallax of oblique Pictometry block in case of DG solution with no AP model.

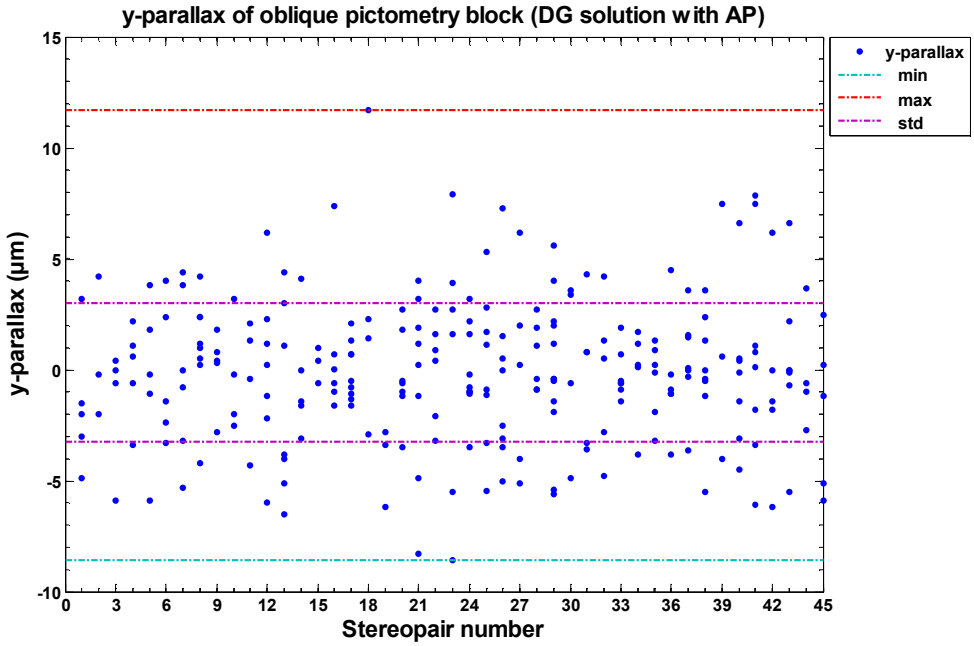

Figure 5.35: y-parallax of oblique Pictometry block in case of DG solution with AP.

According to Heipke et al. (2002), in models with larger y-parallax than 10µm, manual stereo plotting becomes less comfortable and it becomes cumbersome when y-parallax is larger than 20µm. Jacobsen and Wegman (2002) stated that 'as a rule of thumb, y-parallax in a model should not exceed

a maximum of 30µm and the problems with stereo viewing of the floating mark is starting at 20µm'. In this block over 95% of the points have y-parallax of less than 10µm. This implies that stereo plotting using this block in case of using DG rather than the traditional photogrammetric solution will not be problematic.

5.3.6 Combined UltraCamD and Pictometry imagery block

This block consists of two blocks: the UltraCamD images block and the oblique Pictometry images block. It comprises 143 images; of which 86 are UltraCamD images (2 middle strips of 22 images each and 2 edge strips of 21 images each) and the remaining 57 images are oblique Pictometry images: 12 of them looking East (3 strips of 4 images each), 15 looking West (3 strips of 5 images each), 15 looking North (3 strips of 5 images each), and 15 looking South (3 strips of 5 images each). In this block, the images are in the range of all 41 control points. The number of points that was used as ground control points is 9 and the number of points used as check control points is 30 while 2 points were excluded as mentioned before due to high residual they produce. This is for the first two AT solutions while all control points (39) were used as check points for the third and fourth AT solutions. The distribution of the tie points and control/check points is shown in figure 5.36 as well as the images projection centres and the camera X-axis while figure 5.37 depicts the images footprint after the performance of AT.

As can be seen from figure 5.36 and figure 5.37, a very good distribution of the control points throughout the block was achievable due to the fact that this block covers all the study area of Nottingham University main campus. A total number of 1100 tie points were generated. 900 points were generated automatically using a cross correlation area based matching technique available in LPS to tie just the UltraCamD images. The automatic tie point extraction was generally successful over the block with sufficient tie point distribution. Blunders and mismatched points were identified manually by the operator based on the image residuals. The remaining 200 points were generated manually for tying the oblique images as stated in section 5.3.5. The ground control/check points are also the tie points between the blocks.

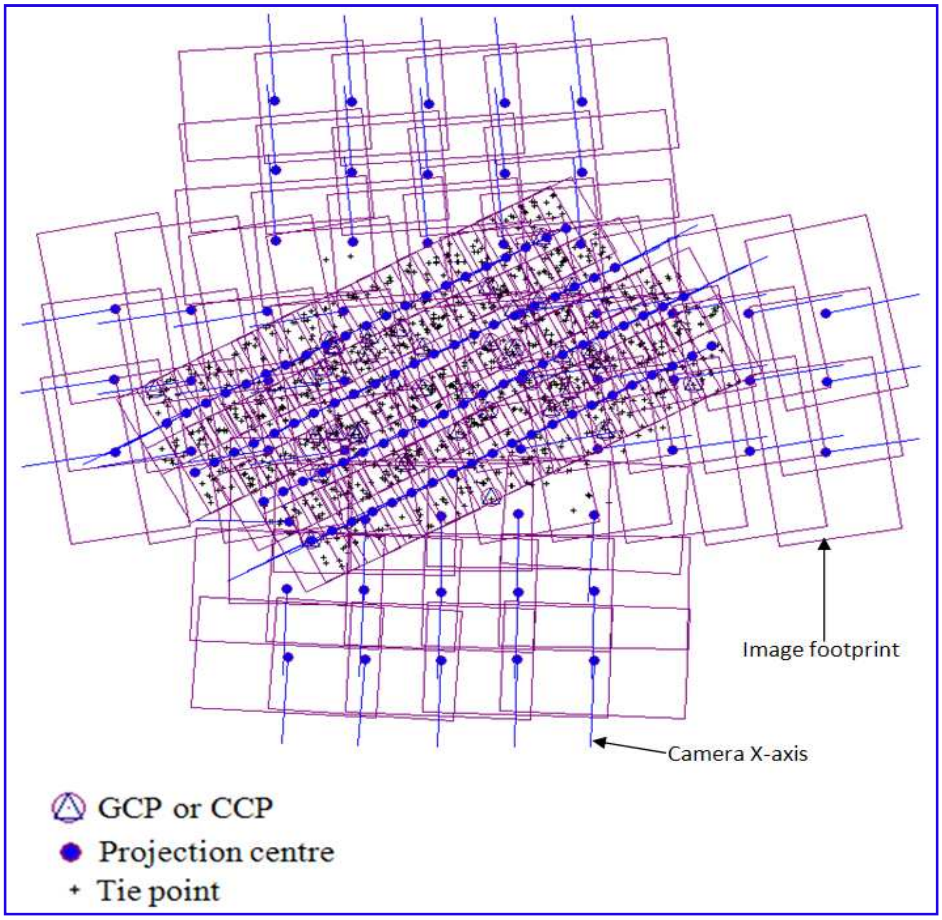

Figure 5.36: Distribution of the tie points and control/check points as well as the images projection centres and the camera X-axis of the combined UltraCamD and oblique Pictometry images block.

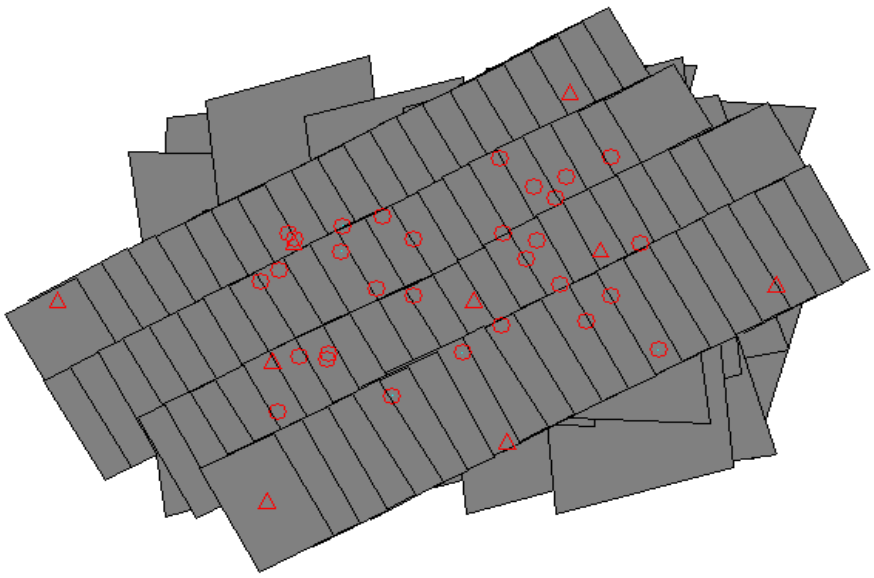

Figure 5.37: The combined UltraCamD and oblique Pictometry images footprint after performing AT.

Trees tend to move in windy conditions, or are difficult to measure accurately as tie point locations. Figure 5.38 shows a typical problem caused by locating tie points on trees.

Figure 5.38: Upper images show the mislocation of tie point 395 by APM, while the bottom left screen shot shows the AT result including the mislocated point and the bottom right screen shot shows the AT result after eliminating the point.

The aerial triangulation trials consist of four different solutions using a combination of different parameters as well as the minimum control solution. In the first trial, in-flight GPS and IMU data were used only as initial values without any weighting so that effectively the block is not constrained during the least squares iterations. In the second solution, the EOP was also used as initial values but they were constrained by giving them a weight of 1m and 1degree for the projection centres and orientation angles respectively. The quality of GPS/IMU positions and attitudes of UltraCamD images was known but those of Pictometry images were not known, hence the assignment of 1m and 1degree. In the integrated sensor orientation solution, the EOP were kept as initial values but without using any GCPs.

The DG solution was not possible in this block because when the EOP set as fixed values, the graphical display function in LPS shows each type of images as one cluster that has the same projection centre (i.e. one cluster of UltraCamD images, and one cluster from each direction of oblique images). In addition, it shows the GCPs, CCPs, and tie points far away from UltraCamD images which should be exactly on top of them as they are vertical images. Figure 5.39 shows the output of LPS graphical display for the combined UltraCamD and oblique images block when performing the DG solution.

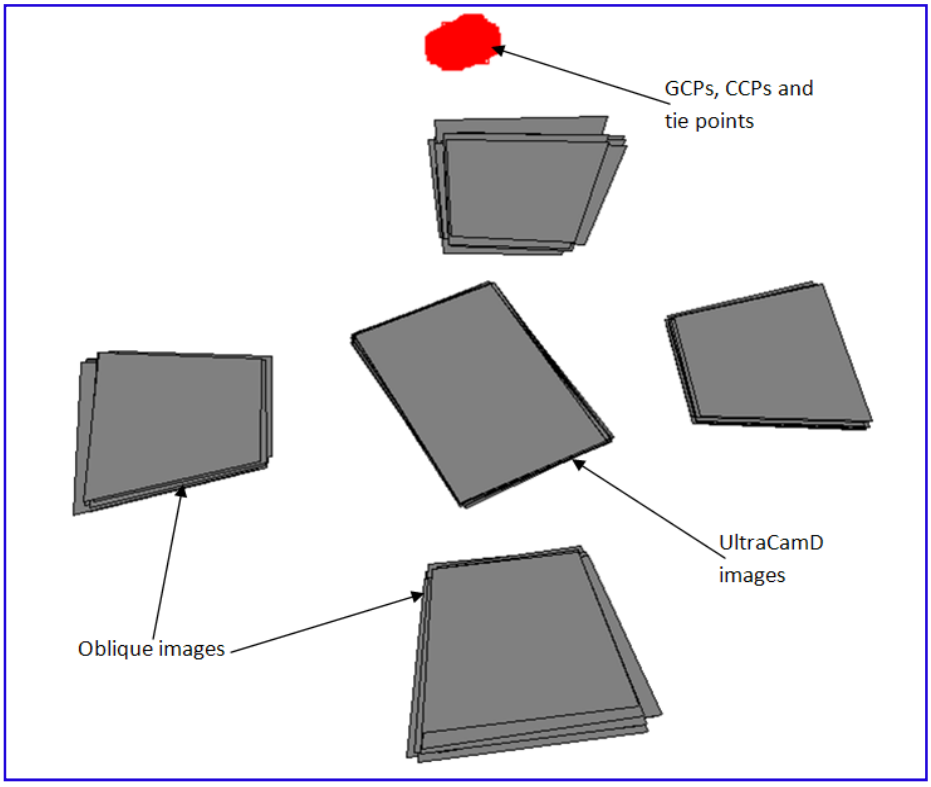

Figure 5.39: LPS graphical display for the combined UltraCamD and oblique images block when performing the DG solution.

The reason behind this might be related to the number of cameras used and the different types of them. Furthermore, different flying height between the two sorties. In addition to that, the quality of the EOP of Pictometry camera system is not known so when setting them as fixed values, they affect the solution. Finally, the software itself could be the reason; it may not support the situation of different cameras with different flying heights as well as setting EOP to fixed values. The results of AT trials are shown in table 5.14 and table 5.15 for LPS and ORIMA respectively.

Table 5.14: AT results of the combined UltraCamD and oblique images block using LPS.

Solution		Float		Constrained		Integrated	
AP		No	Yes	No	Yes	No	Yes
Total RMSE(µm)		3.4	3.3	3.5	3.4	3.5	3.1
GCPs RMS (no.pts)	*X(m)*	0.074 (9)	0.080 (9)	0.087 (9)	0.092 (9)	-	-
	Y(m)	0.055 (9)	0.051 (9)	0.051 (9)	0.049 (9)	-	-
	Z(m)	0.052 (9)	0.035 (9)	0.056 (9)	0.030 (9)	-	-
CCPs RMS (no.pts)	*X(m)*	0.075 (30)	0.074 (30)	0.096 (30)	0.095 (30)	0.442 (39)	0.158 (39)
	Y(m)	0.076 (30)	0.072 (30)	0.083 (30)	0.081 (30)	0.226 (39)	0.198 (39)
	Z(m)	0.091 (30)	0.109 (30)	0.103 (30)	0.080 (30)	0.212 (39)	0.275 (39)

Table 5.15: AT results of the combined UltraCamD and oblique images block using ORIMA.

Solution		Float		Constrained		Integrated	
AP		No	Yes	No	Yes	No	Yes
Sigma0 (µm)		2.9	2.7	3.0	2.8	3.0	2.7
GCPs RMS (no. pts)	*X(m)*	0.076 (9)	0.067 (9)	0.065 (9)	0.067 (9)	-	-
	Y(m)	0.049 (9)	0.040 (9)	0.051 (9)	0.039 (9)	-	-
	Z(m)	0.064 (9)	0.035 (9)	0.065 (9)	0.049 (9)	-	-
CCPs RMS (no. pts)	*X(m)*	0.086 (30)	0.086 (30)	0.090 (30)	0.088 (30)	0.105 (39)	0.114 (39)
	Y(m)	0.059 (30)	0.090 (30)	0.073 (30)	0.089 (30)	0.087 (39)	0.092 (39)
	Z(m)	0.155 (30)	0.109 (30)	0.163 (30)	0.106 (30)	0.297 (39)	0.300 (39)

The results show good image residuals (about one third of a pixel) and fit on the ground control points. Again, the RMS of CCPs shows the realistic value of what can be achieved in mapping. The results of both software packages are in agreement and very close to each other. For the constrained solution, the AT results are very similar to the float solution result except for the height accuracy before applying the additional parameters technique which was higher when using the ORIMA software. However, after the application of AP model, the results are in agreement in both solutions and using both software packages. Including the additional parameters in float and constrained solutions gave a little improvement for the total image RMSE and $Sigma_0$ (3 to 7%) and a big improvement for the height component of GCPs (25 to 50%). The bundle adjustment was computed including fourteen parameters for additional parameters in LPS and twenty one parameters in ORIMA. These parameters, however, had very little effect on RMS of CCPs in plan. Nonetheless, the introduction of AP model has improved the height accuracy of CCPs especially when ORIMA was used. It resulted in accuracy improvement of about 30%.

With regard to the integrated solution, the total image RMSE differs slightly using both software packages. However, it's again better when ORIMA was used. The RMS of CCPs in case of integrated solution using LPS was a little bit high and ranges from 21cm in Z-component to 44cm in the X-component. The use of ORIMA has resulted in big improvements in the X-component (from 44cm to 10cm), in Y-component (from 23cm to 9cm), and on the other hand resulted in accuracy deterioration of about 9cm in the Z-component. The use of AP model in LPS improved the RMS of CCPs significantly in X-direction (improvement of about 65%) and improved the Y-component slightly. On the other hand, the height accuracy was better before applying additional parameters. The use of the 21 additional parameters in ORIMA has resulted in a slight accuracy loss in all directions.

The results of the height component in the combined block are much better than those in the vertical Pictometry block. Table 5.14 and table 5.15 show that accuracy of 0.008% of flying height was achieved. The height accuracy is better by a factor of about 1.5 to 2. Moreover, the height accuracy,

resulted from combining the UltraCamD images with the oblique images in one block, is comparable to the height accuracy of the UltraCamD block. It is almost the same for float and constrained solution but a little bit worse for the integrated solution. This improvement in height accuracy is because of using the oblique images which give more intersection rays and therefore good coordinates.

Figure 5.40 and figure 5.41 show the plan and height residual vectors of CCPs for the constrained solution without using AP model and with AP model respectively. The figures show that the residual vectors are again pointing randomly except for the upper left hand side group of vectors which point to the same direction. This means that some of systematic errors are not eliminated even when the additional parameters have been applied (figure 5.41). This implies that the AP used here are not enough to model all the existing systematic errors in this block. Furthermore, the lengths of the vectors are of different sizes and there is no one vector that has significantly larger length compared to others. This suggests that all CCPs have been correctly measured on the images. The introduction of the AP has resulted in a small improvement in the total image RMSE. The use of additional parameters has brought some improvement in the height accuracy of the CCPs. The height accuracy of the CCPs is in the range of 8 to 10cm and the plan accuracy ranges between 7 and 10cm. The other reason for the height accuracy improvement is the multi-ray tie points distribution which is better in this block than in the vertical block. The reason of this good points distribution is that with the increase of image overlap, the number of image intersection rays for each photogrammetric point increases, and the intersection angles will be accordingly larger. This will result in good geometric block stability. For this block, about 19% of tie points are 2-fold points, 42.8% are 3-fold points, 12.5% are 4-fold points, 14.7% are 5-fold points, 6.5% are 6-fold points, and 4.5% are 7 to 14-fold points. Figures D14 to D19 in appendix D show the quality of multi-ray tie points for the combined UltraCamD and oblique images block, figure 5.42 shows the relation between the number of tie points and the number of images per point, and table 5.16 summarizes the statistical quality of these points.

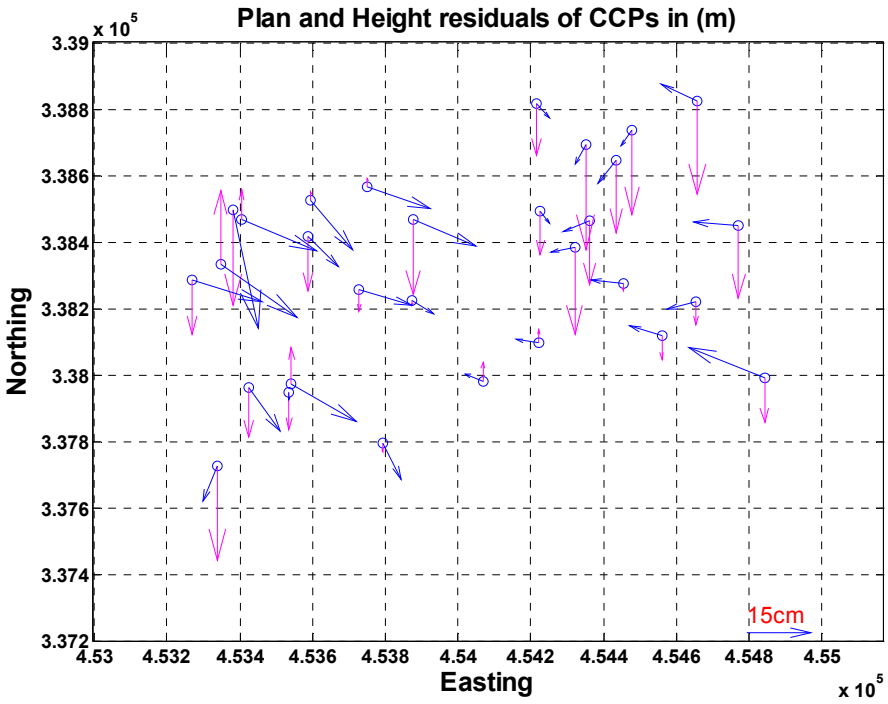

Figure 5.40: Plan and height residual vectors for the combined UltraCamD and oblique images block when no AP model has been used.

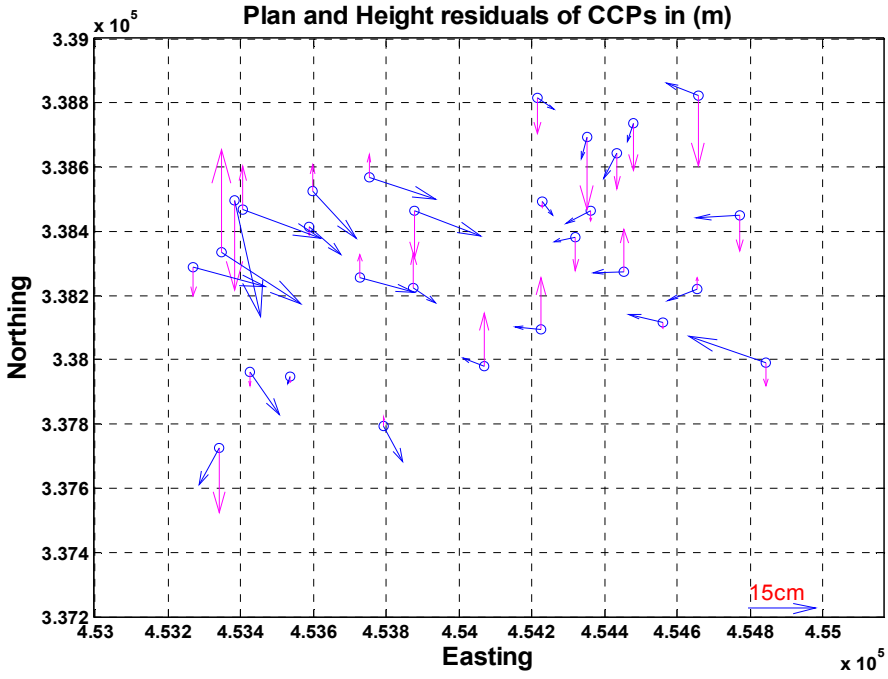

Figure 5.41: Plan and height residual vectors for the combined UltraCamD and oblique images block when AP model has been used.

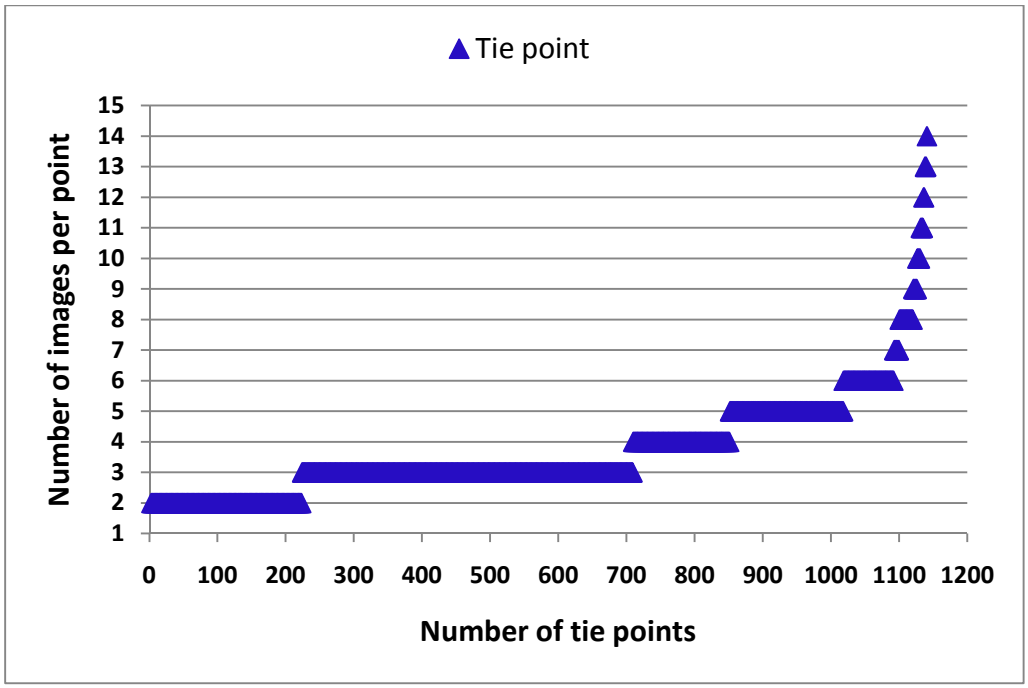

Figure 5.42: The relation between the number of tie points and the number of images per point for the combined UltraCamD and oblique images block.

Table 5.16: Statistical quality of multi-rays tie points of combined UltraCamD and oblique images block

		2-fold points	3-fold points	4-fold points	5-fold points	6-fold points	7 to 14-fold points
Max. Residual (m)	**X**	0.962	0.412	0.167	0.068	0.072	0.051
	Y	0.897	0.365	0.262	0.068	0.065	0.051
	Z	0.905	0.355	0.209	0.116	0.095	0.080
RMSE (m)	**X**	0.246	0.064	0.041	0.034	0.033	0.036
	Y	0.265	0.060	0.056	0.034	0.033	0.036
	Z	0.315	0.104	0.081	0.067	0.061	0.055

Again the accuracy improved significantly with the number of images in which a point appears. Figures 5.43, 5.44, 5.45 and table 5.16 show the relation of number of rays (number of photos per point) and the accuracy of tie points for this block. The overall object point accuracy is as follows: 0.063m in easting, 0.069m in northing, and 0.118m in height. This accuracy is very close to that obtained for the independent check point.

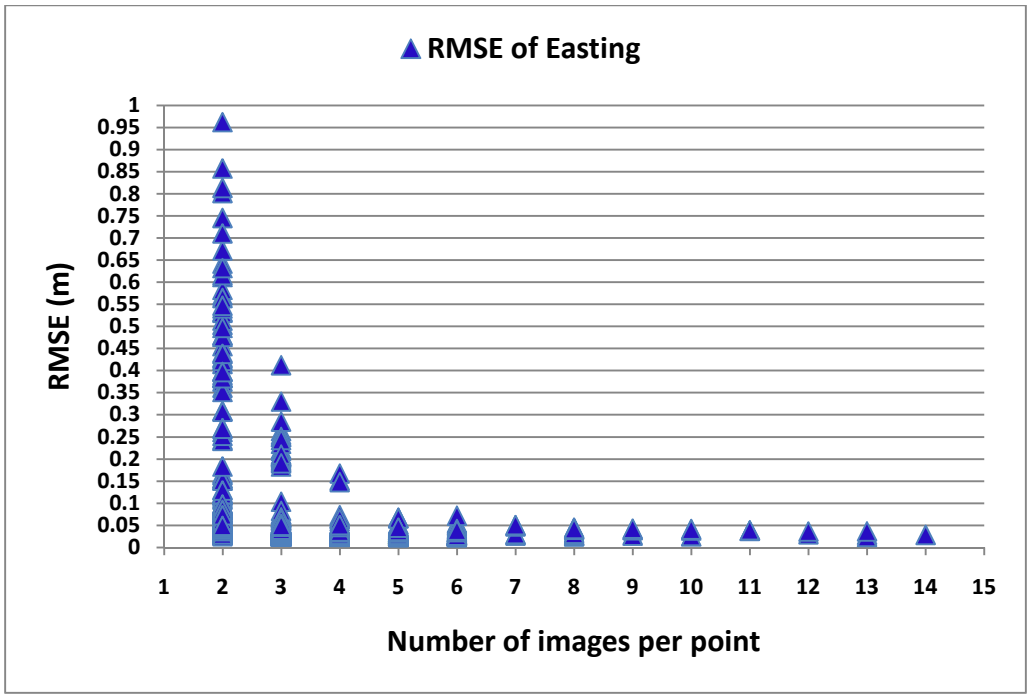

Figure 5.43: Easting RMSE of tie points determined as a function of number of photos per point for combined UltraCamD and oblique images block.

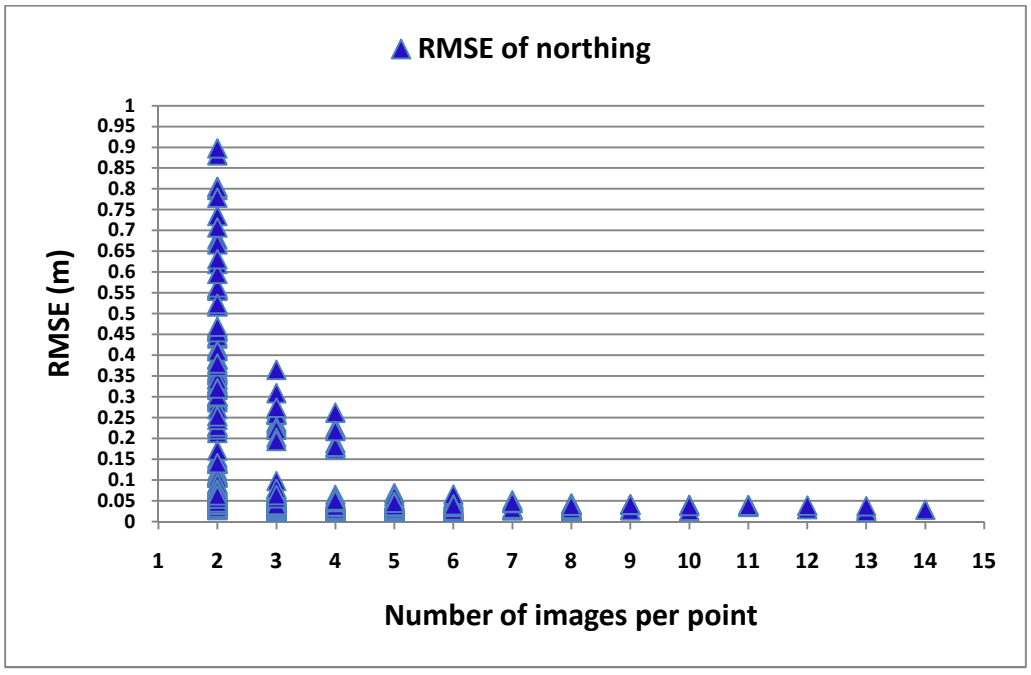

Figure 5.44: Northing RMSE of tie points determined as a function of number of photos per point for combined UltraCamD and oblique images block.

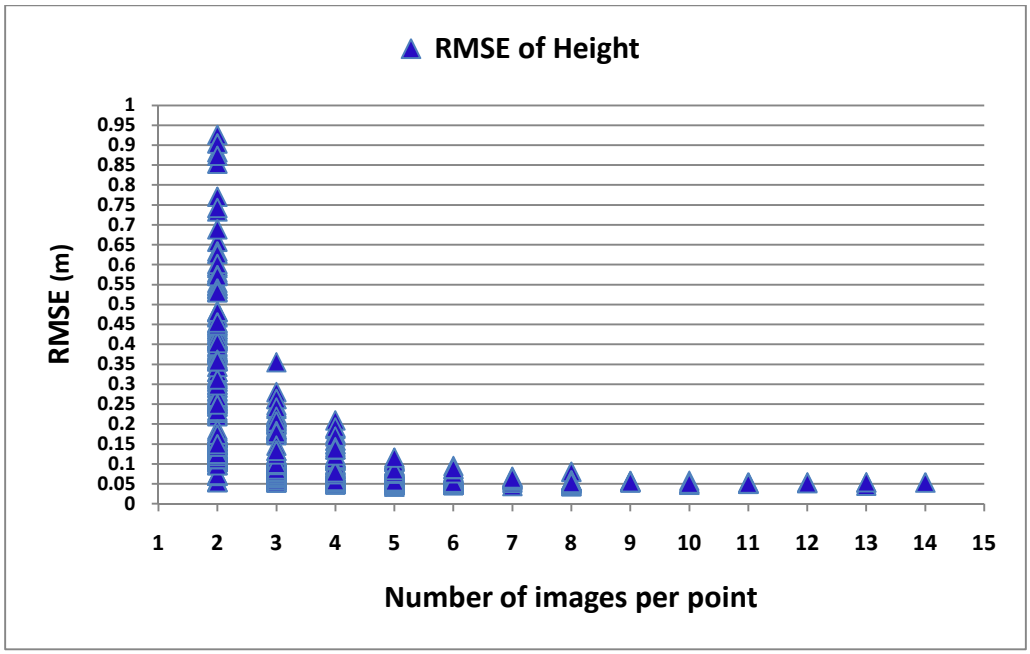

Figure 5.45: Height RMSE of tie points determined as a function of number of photos per point for combined UltraCamD and oblique images block

The results show that height and plan accuracy of tie points in a block adjustment is primarily dependent on the number of images bridged between these tie points. Single points (points lying in two photos only) will be less accurate. The plan accuracy of single points is about 7 times worse than the accuracy of a tie point lying in 6 images and the height accuracy is about 5 times worse than that of a 6-fold point.

To check the benefits of self-calibration on photogrammetric applications and to check the problematic existence of y-parallax for stereo plotting in case of using the integrated sensor orientation solution, x-parallax and y-parallax of the combined block have been calculated and plotted. Table 5.17 shows the statistics of the parallax before and after applying the AP models. In addition, figure 5.46 and figure 5.47 show the plots of x-parallax and y-parallax with and without the application of the AP model.

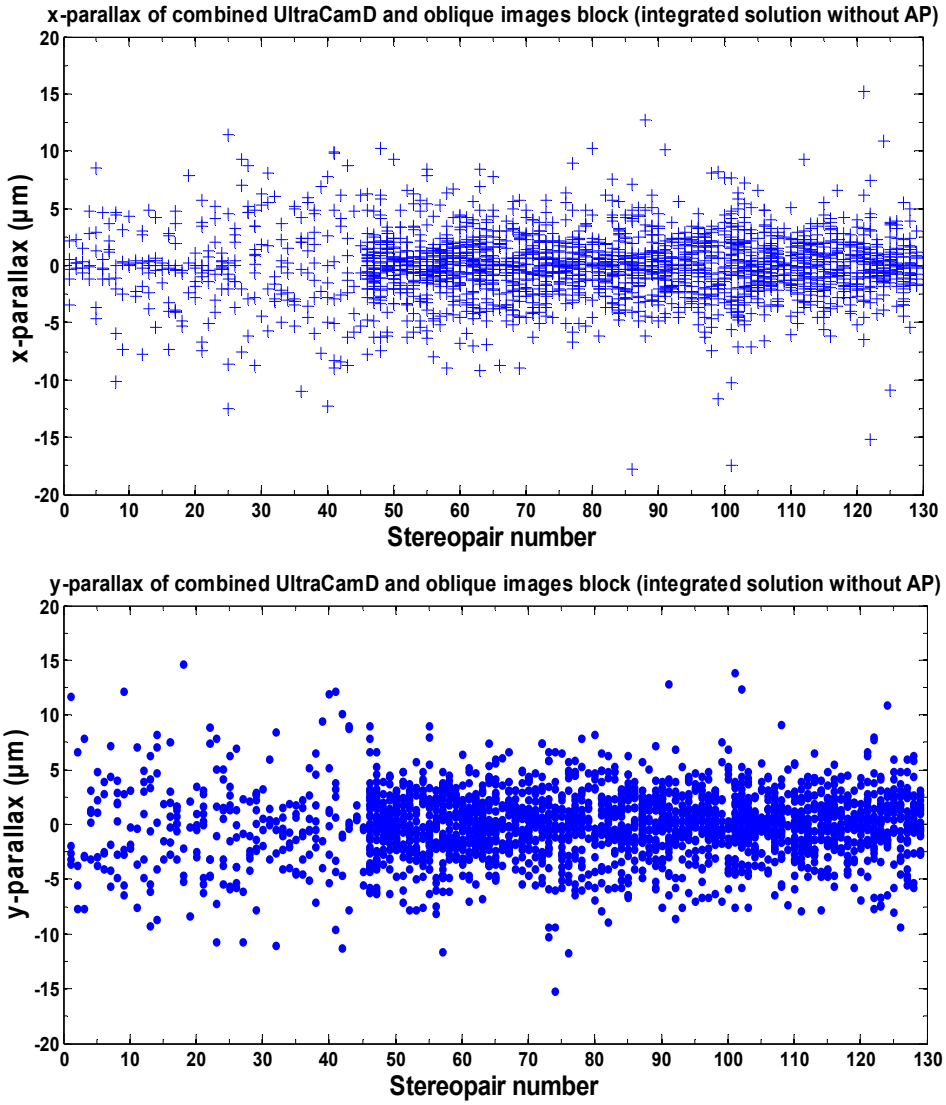

Figure 5.46: x and y-parallax for the combined UltraCamD and oblique images block before the application of the additional parameters model.

Table 5.17: x and y parallax statistics before and after applying the AP.

Parallax	**x-parallax**		**y-parallax**	
Self-calibration	No	yes	No	yes
Min. (µm)	-17.8	-10.9	-15.2	-4.8
Max. (µm)	15.2	10.9	14.7	14.3
Std. (µm)	2.84	2.48	3.13	2.72

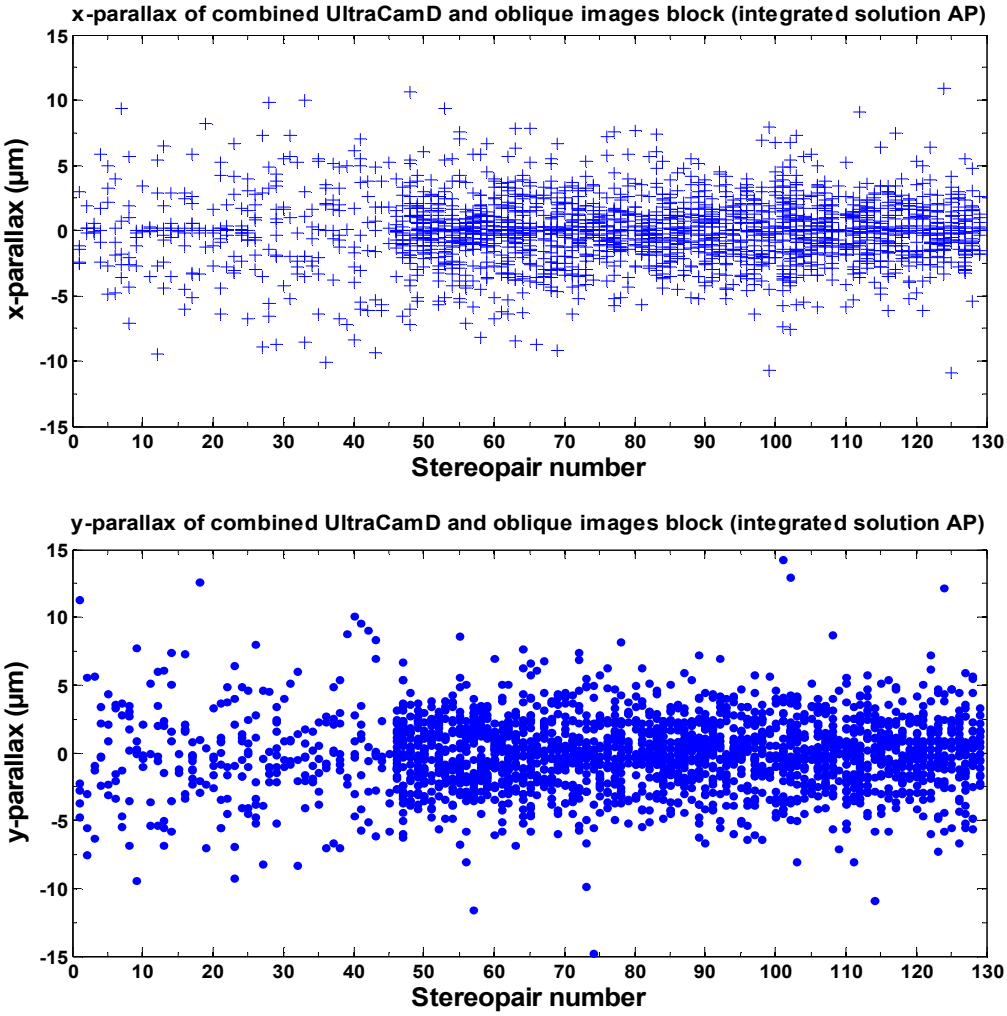

Figure 5.47: x and y-parallax for the combined UltraCamD and oblique images block after the application of the additional parameters model.

The table and the figures above show that a good improvement has been achieved with the application of the AP technique. The standard deviation of x-parallax has fallen from 2.84µm to 2.48µm and that of y-parallax from 3.13µm to 2.72µm. In addition, more than 95% of points have a parallax of less than 10µm (the threshold for comfortable stereo viewing). Thus, using this block with results of integrated solution will not cause any y-parallax problems when manually stereo plotting. This can also help a lot especially that stereo-viewing is an important part of 3D modeling.

Figure 5.48 depicts the percentage of effective footprint in relation to the footprint of UltraCamD and oblique images. No holes in-between are found so the addition of more tie points is not necessary.

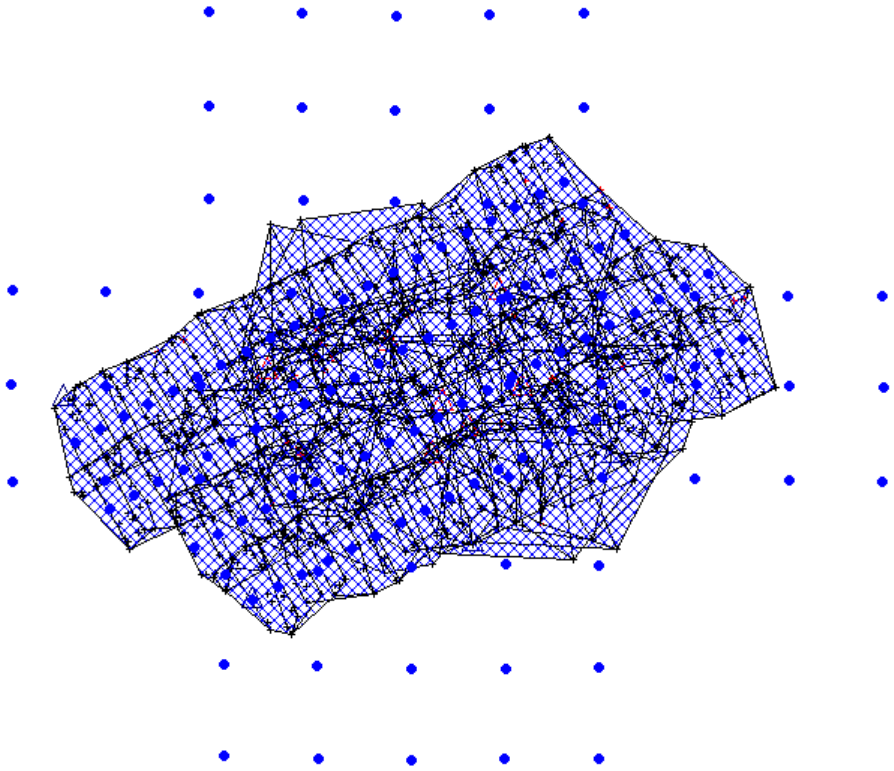

Figure 5.48: The effective footprint in relation to the footprint of UltraCamD and oblique images block.

5.3.7 Combined Pictometry imagery block

This block consists of two sets of imagery: the vertical Pictometry imagery and the oblique Pictometry imagery. It comprises 84 images; 27 of them are vertical Pictometry images (3 strips of 9 images each) and the remaining 57 images are oblique Pictometry images: 12 of them looking East (3 strips of 4 images each), 15 looking West (3 strips of 5 images each), 15 looking North (3 strips of 5 images each), and 15 looking South (3 strips of 5 images each). In this block, the images are in the range of 35 control points with the majority measured on both oblique and vertical images acting as tie points between blocks. The number of points that was used as ground control points is 9 and the number of points used as check control points is 26. This is for the first two AT solutions while all control points (35) were used as check points for the third and fourth AT solutions. The distribution of the tie points and control/check points is shown in figure 5.49 as well as the images

projection centres while figure 5.50 depicts the images footprint after the performance of AT.

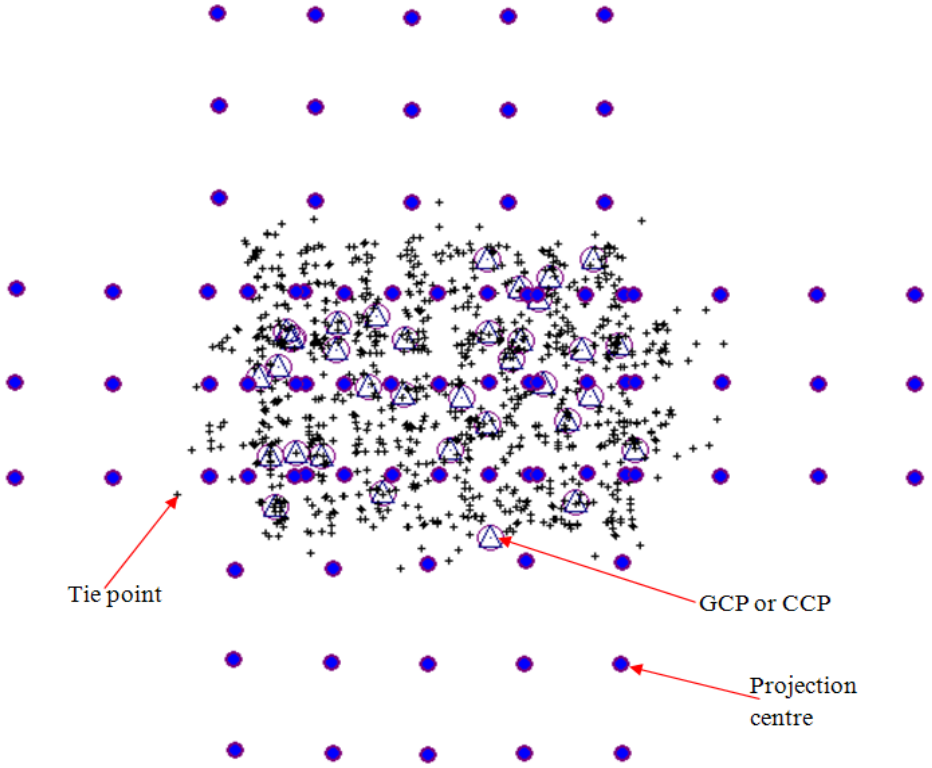

Figure 5.49: Distribution of the tie points and control/check points as well as the images projection centres of the combined Pictometry images block.

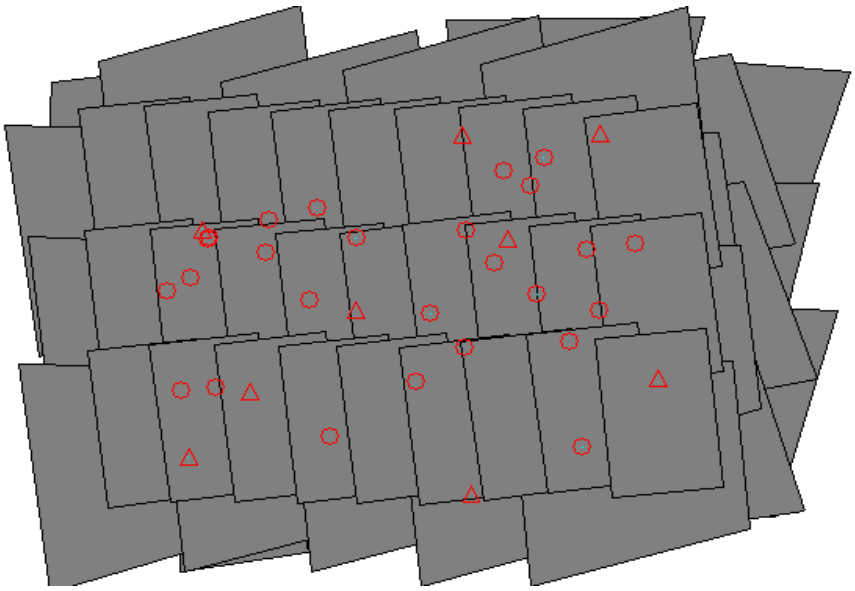

Figure 5.50: The combined Pictometry images footprint after performing AT.

As can be seen from figure 5.49 and figure 5.50, and as stated before for the vertical Pictometry block, the distribution of GCPs in the combined Pictometry block was not ideal due to the lack of features that have enough texture and recognizable features in the upper left corner of the block as that area is completely covered by trees. A total number of 1053 tie points were generated. 852 points were generated automatically using a cross correlation area based matching technique available in LPS to tie the vertical Pictometry images. The automatic tie point extraction was generally successful over the block with sufficient tie point distribution. Blunders and mismatched points were identified manually by the operator based on the image residuals. The remaining 201 points were generated manually for tying the oblique images as stated in section 5.3.5. Most of the blunders and mismatched points were located on shadowy areas of different strips. Shadow movement causes no problem for image matching if only data from one strip is used. However, problems might occur due to the increased time gap while combining image data from different strips. In such cases time dependent shadow movement can result in considerable errors of automatic point transfer, figure 5.51.

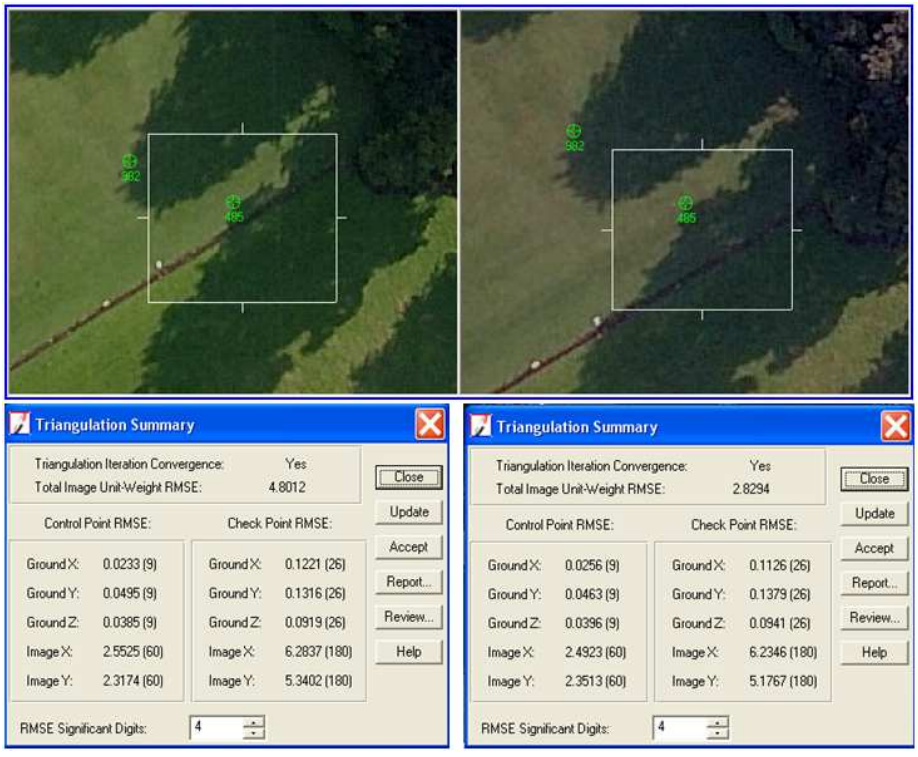

Figure 5.51: Upper images show mislocation of tie point 485 by APM due to shadow movement, while the bottom left screen shot shows AT result including the mislocated point and the bottom right screen shot shows the AT result after eliminating the point.

The aerial triangulation trials for this block consist of four different solutions using a combination of different parameters as well as the minimum control solution. The results of AT trials are shown in table 5.18 and table 5.19 for LPS and ORIMA respectively.

The results show good image residuals (about one third of a pixel) and fit on the ground control points for the first two solutions. Moreover, the results of both software packages are in agreement and very close to each other. Again, the RMS of CCPs shows the realistic value of what can be achieved in mapping. For the constrained solution, the AT results are very similar to the float solution result except for small cm-level differences which are expected due to the fact that in float solution some errors will be pushed into EOP as they were kept floating while in constrained solution there will be a noticeable forcing of the solution on the GCPs. Hence the RMS of GCPs is a little bit bigger in constrained solution. Including the additional parameters in float and constrained solutions gave a little improvement for the total image RMSE and better improvement for $Sigma_0$ (8 to 18%) and a big improvement for RMS of GCPs of constrained solution when LPS was used (from 40 to 50%) and for height component of GCPs and CCPs of both solutions (25 to 40%). In addition, it resulted in a little improve in the other components. When ORIMA was used, the application of the AP resulted in significant accuracy improvement in the height of both GCPs and CCPs of float solution (20 to 60%) and of the X-component of CCPs which improved by 38%. A little improvement was also noticed in most components of GCPs and CCPs of constrained solution. For the integrated and DG solutions, the total image RMSE and $sigma_0$ are surprisingly better in DG solution in both software packages after the introduction of AP model. However, it's again much better when ORIMA was used in DG solution especially when AP technique was not used. The RMS of CCPs in case of integrated solution using LPS was a little bit high in X-component (65cm) and in the Y-component (40cm). The use of ORIMA has resulted in big improvement in the X-component (from 65cm to 17cm), a big improvement in Y-component (from 40cm to 14cm), and on the other hand resulted in accuracy deterioration of about 1.30m in the Z-component.

Table 5.18: AT results of the combined Pictometry images block using LPS.

Solution		**Float**		**Constrained**		**Integrated**		**DG**	
AP		**No**	**Yes**	**No**	**Yes**	**No**	**Yes**	**No**	**Yes**
Total RMSE(µm)		3.3	3.1	3.5	3.2	4.0	3.7	8.1	3.6
GCPs RMS *(no. pts)*	**X(m)**	0.032 (9)	0.031 (9)	0.067 (9)	0.032 (9)	-	-	-	-
	Y(m)	0.044 (9)	0.038 (9)	0.074 (9)	0.044 (9)	-	-	-	-
	Z(m)	0.071 (9)	0.040 (9)	0.056 (9)	0.033 (9)	-	-	-	-
CCPs RMS *(no. pts)*	**X(m)**	0.108 (26)	0.110 (26)	0.137 (26)	0.114 (26)	0.651 (35)	0.286 (35)	0.350 (35)	0.964 (35)
	Y(m)	0.145 (26)	0.141 (26)	0.150 (26)	0.140 (26)	0.400 (35)	0.187 (35)	2.781 (35)	2.268 (35)
	Z(m)	0.123 (26)	0.092 (26)	0.098 (26)	0.083 (26)	0.148 (35)	0.128 (35)	0.754 (35)	0.632 (35)

Table 5.19: AT results of the combined Pictometry images block using ORIMA.

Solution		**Float**		**Constrained**		**Integrated**		**DG**	
AP		**No**	**Yes**	**No**	**Yes**	**No**	**Yes**	**No**	**Yes**
Sigma0(µm)		3.9	3.2	3.9	3.6	3.8	3.3	3.4	3.0
GCPs RMS (no.pts)	**X(m)**	0.028 (9)	0.025 (9)	0.024 (9)	0.038 (9)	-	-	-	-
	Y(m)	0.058 (9)	0.050 (9)	0.064 (9)	0.0577 (9)	-	-	-	-
	Z(m)	0.055 (9)	0.020 (9)	0.057 (9)	0.051 (9)	-	-	-	-
CCPs (no. pts)	**X(m)**	0.232 (26)	0.144 (26)	0.197 (26)	0.162 (26)	0.165 (35)	0.472 (35)	0.614 (35)	0.429 (35)
	Y(m)	0.139 (26)	0.134 (26)	0.136 (26)	0.121 (26)	0.142 (35)	0.152 (35)	0.446 (35)	0.386 (35)
	Z(m)	0.099 (26)	0.078 (26)	0.097 (26)	0.100 (26)	1.009 (35)	0.471 (35)	0.765 (35)	0.602 (35)

The use of additional parameters model improved the RMS of CCPs significantly which implies the possible existence of systematic errors before applying the AP model. It improved the results by a factor of about 2 in case of using LPS; the biggest accuracy gain was in the easting which jumped from 65cm to 28cm. In case of using ORIMA, the height accuracy improved by a factor of 3. On the other hand, the easting accuracy deteriorated a lot (from 16cm to 47cm). The RMS of CCPs in case of DG solution using LPS was high and ranges from 35cm in X-component to 2.80m in the Y-component. The use of ORIMA has resulted in a noticeable big improvement in the Y-component (from 2.8m to 44cm). Nonetheless, it has resulted in accuracy deterioration of about 25cm in the X-component. The use of AP technique improved the RMS of CCPs significantly especially when using ORIMA which again implies the possible existence of systematic errors before applying the additional parameters model. In case of using ORIMA, the accuracy improved by a factor of about 1.5 and the largest improvement was in X-component (from 61cm to 43cm) and in Z-component in which the gain in accuracy was 16cm (from 76cm to 60cm).

The results of the height component in the combined Pictometry block are much better than those in the vertical Pictometry block because of using the oblique images which give more intersection rays and therefore good coordinates. In addition to that, the geometry of the vertical block is influenced by the overlap which is less than the ideal 60%. The height component, when AP model was used, is improved by about 24 to 75% in all solutions compared to that of the vertical Pictometry block. The only one exception is the height in the integrated solution with ORIMA which incurred accuracy loss of about 9cm. Compared to the oblique block, the height accuracy here is almost the same for float and constrained solutions. For the integrated solution, the height accuracy of this block is better by about 16cm in both software packages. This may be related to the high number of tie points here which makes very strong connection of the images in the strips and between the strips. This increases the quality and accuracy of the triangulated block which can be attributed to the increase in data redundancy. On the other hand, for the DG solution, the height accuracy in the oblique block is better by about 6cm and 27cm in case of using

LPS and ORIMA respectively. With regard to the UltraCamD and oblique images block, again the height accuracy for the float and constrained solutions is almost the same. For the integrated solution, it is better by about 15cm when LPS was used but it is worse by about 17cm in case of using ORIMA. Surprisingly, the height quality in this block is comparable to that in UltraCamD block in case of float and constrained solutions. It is almost the same. However, when it comes to the integrated and DG solutions, the height accuracy in UltraCamD block is much better; it's better by about 25 to 53cm. This might be related to the quality of EOP which is better for UltraCamD images.

Now the residual vectors will be examined to check if there are any remaining systematic errors after applying the additional parameters technique. Figure 5.52 and figure 5.53 show the plan and height residual vectors of CCPs for the constrained solution without using AP model and with AP model respectively.

The residual vectors point to random directions which is a good sign of no systematic errors. Also there is no big difference in the vectors' lengths which indicates that all points were measured correctly. Despite the use of the 14-parameters model, it has little effect on the results especially in plan.

The other reason for the height accuracy improvement is the number and distribution of multi-ray tie points which is better in this block than in the vertical block. For this block, about 66% of tie points are 2-fold points (due to the fact that most of these points are on the vertical imagery block which is affected by low overlap), 14% are 3-fold points, 15% are 4-fold points, 1% is 5-fold points, 1% is 6-fold points, and 3% are 7 to 14-fold points. Figure 5.54 shows the relation between the number of tie points and the number of images per point, and table 5.20 summarizes the statistical quality of these points.

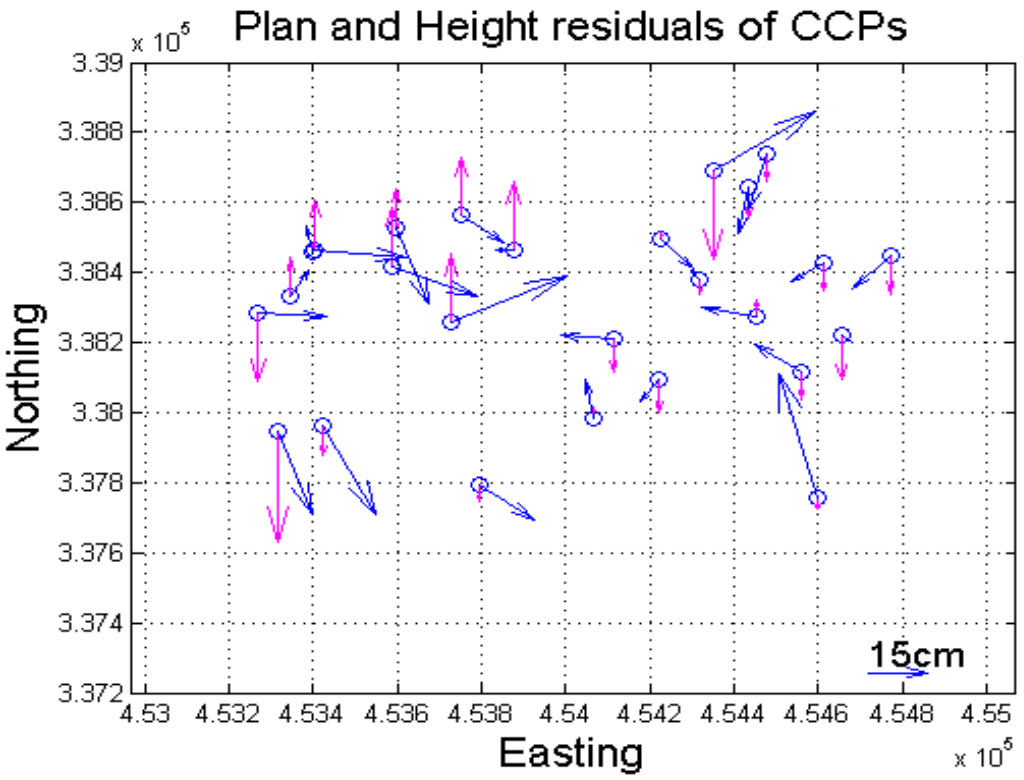

Figure 5.52: Plan and height residual vectors for CCPs of constrained solution without additional parameters for the combined Pictometry block.

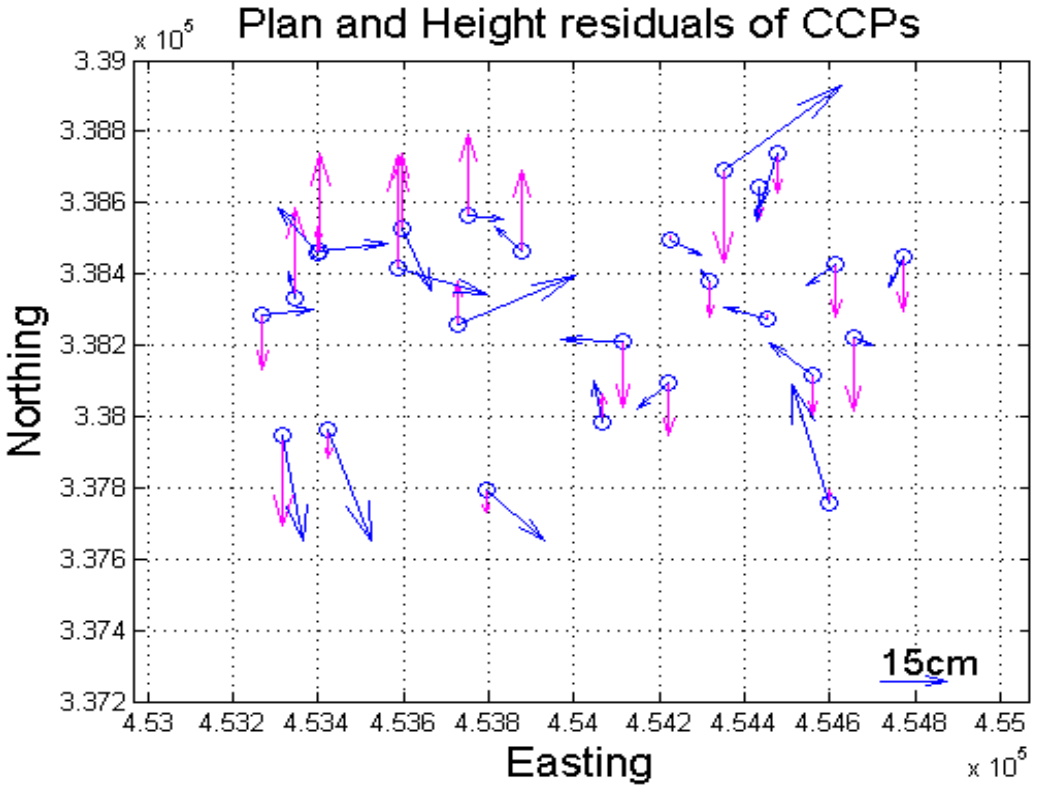

Figure 5.53: Plan and height residual vectors for CCPs of constrained solution with additional parameters for the combined Pictometry block.

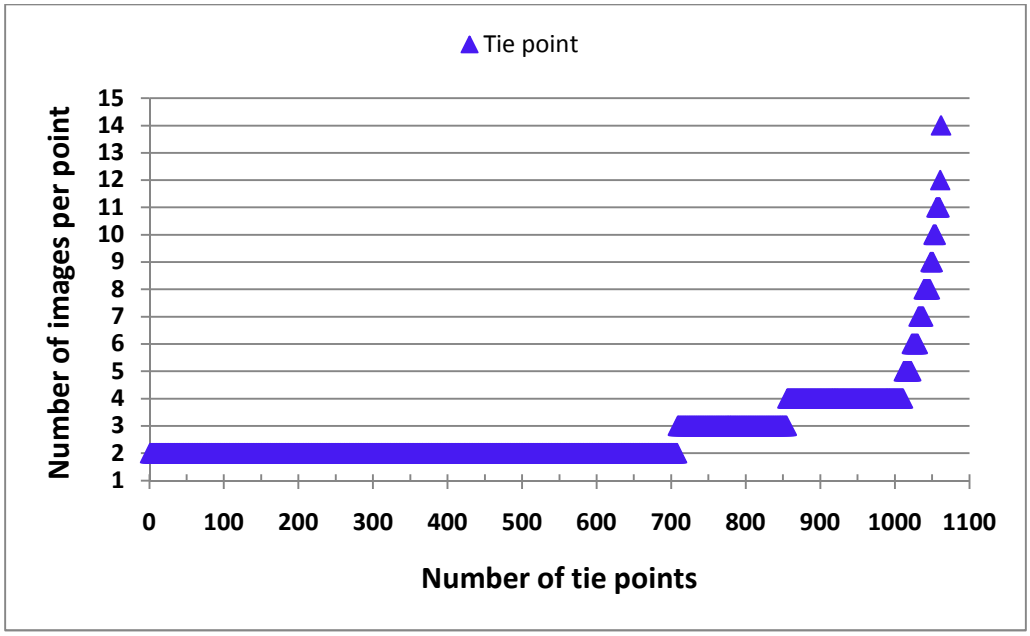

Figure 5.54: The relation between the number of tie points and the number of images per point for the combined Pictometry images block

Again the accuracy improves significantly with the number of images in which a point appears. Figure 5.55, 5.56, and 5.57 show the relation of number of rays (number of photos per point) and the accuracy of tie points for this block. The overall object point accuracy is as following: 0.078m in easting, 0.093m in northing, and 0.312m in height. The plan accuracy is very close to that obtained for the independent check points but the height accuracy is less. The large height RMSE for the tie points is probably showing the effect of the relatively small airbase for the digital cameras compared to the analogue cameras. According to Alamús et al. (2005), it is well known that the point height accuracy is directly related to the base to height (b/h) ratio and also to the point measurement accuracy. This also explains the better height quality obtained from the oblique block, the UltraCamD and oblique images block, and the combined Pictometry images block as the oblique images have a base to height ratio of 0.4 as opposed to UltraCamD images and vertical Pictometry images which have a base to height ratio of only 0.2. Although a smaller b/h ratio geometrically results in lower height accuracy, this accuracy loss is compensated by the higher quality of the digital images and consequently by the higher point measurement accuracy.

Table 5.20: Statistical qualities of multi-rays tie points of combined Pictometry images block.

		2-fold points	3-fold points	4-fold points	5-fold points	6-fold points	7 to 14-fold points
Max. Residual (m)	X	0.930	0.389	0.160	0.071	0.070	0.055
	Y	1.868	0.327	0.265	0.064	0.066	0.049
	Z	1.358	0.354	0.317	0.072	0.070	0.055
RMSE (m)	X	0.147	0.096	0.046	0.058	0.056	0.045
	Y	0.190	0.088	0.060	0.053	0.056	0.044
	Z	0.460	0.223	0.203	0.062	0.061	0.050

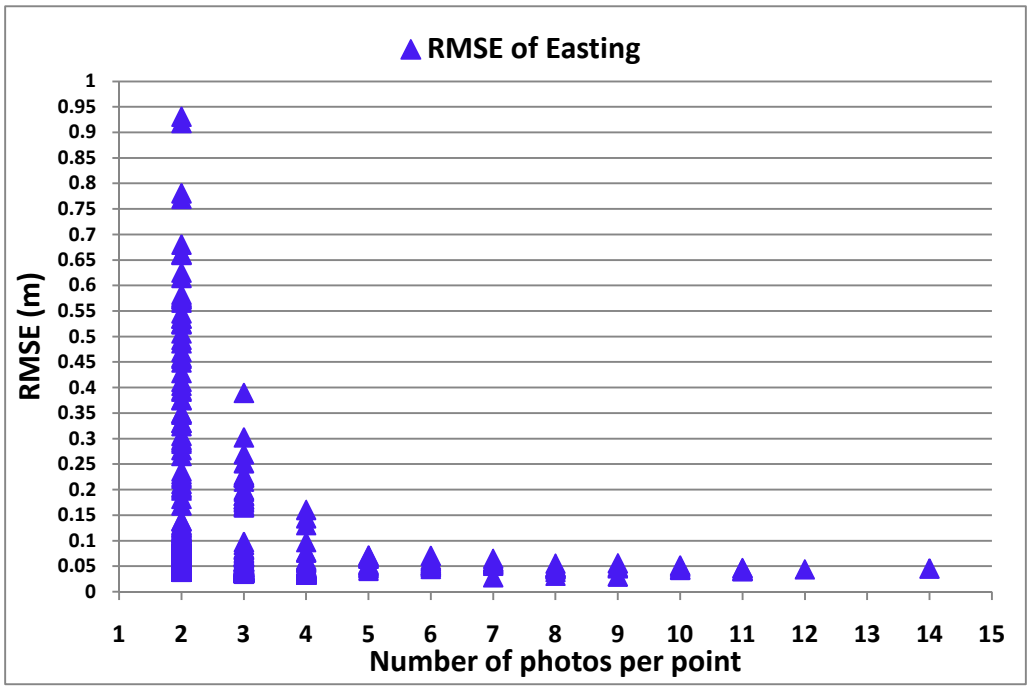

Figure 5.55: Easting RMSE of tie points determined as a function of number of photos per point for combined Pictometry images block.

To check the problematic existence of y-parallax for stereo plotting in case of using the DG solutions, x-parallax and y-parallax of the combined block have been calculated and plotted. Table 5.21 shows the statistics of the parallax before and after applying the additional parameters model. In addition, figure 5.58 and figure 5.59 show the plots of x-parallax and y-parallax with and without the application of the AP model.

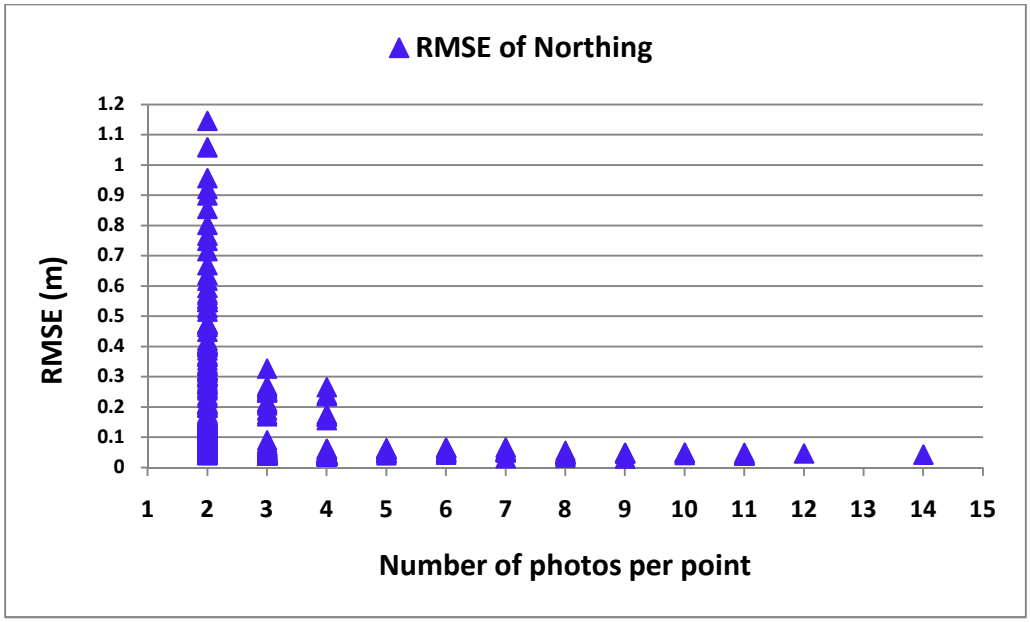

Figure 5.56: Northing RMSE of tie points determined as a function of number of photos per point for combined Pictometry images block.

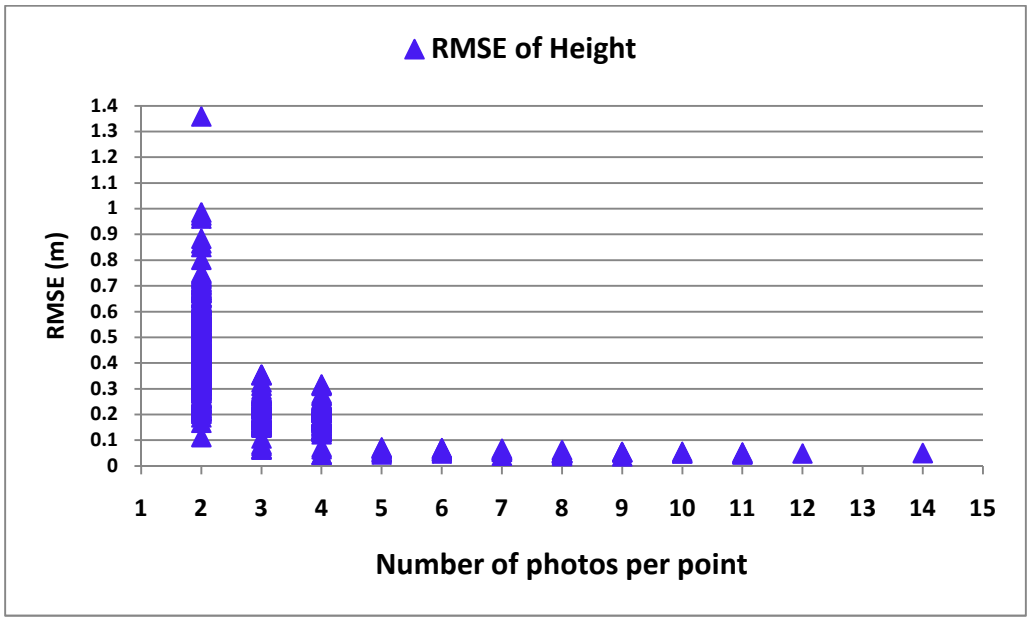

Figure 5.57: Height RMSE of tie points determined as a function of number of photos per point for combined Pictometry images block.

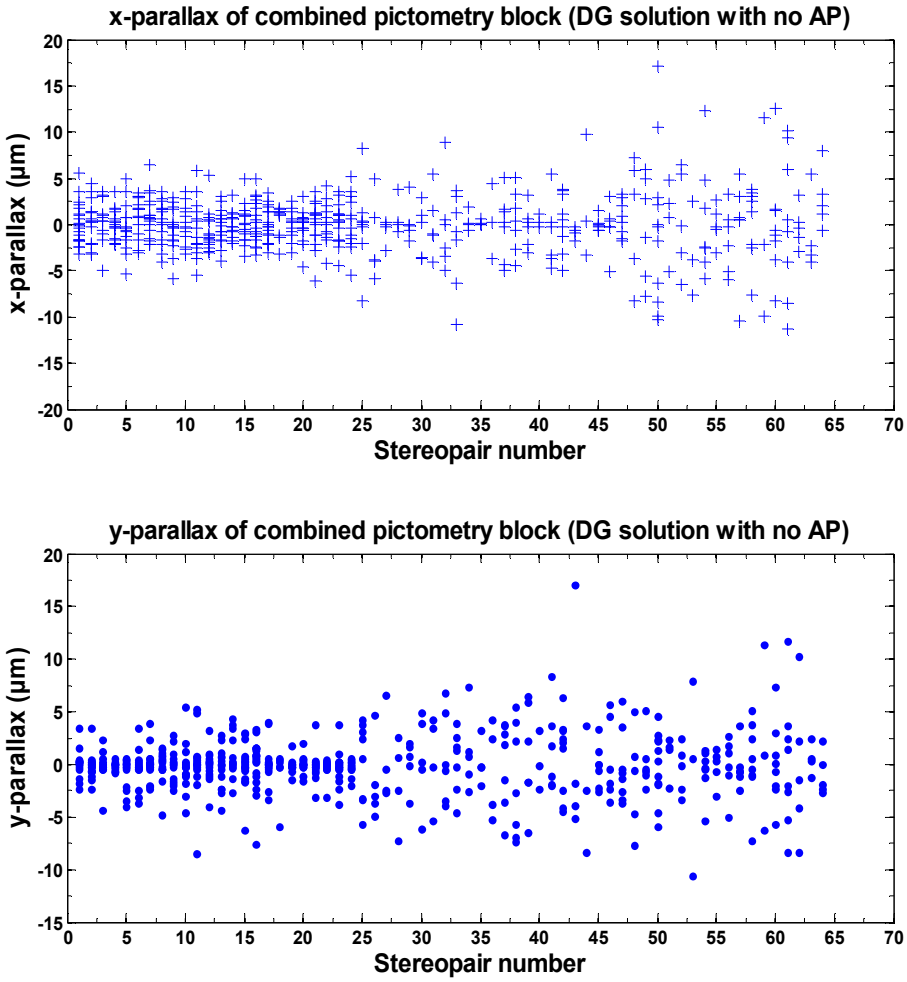

Figure 5.58: x and y-parallax for the combined Pictometry images block before the application of additional parameters model.

Table 5.21: x and y parallax statistics before and after applying the AP model.

Parallax	**x-parallax**		**y-parallax**	
Self-calibration	No	yes	No	yes
Min. (µm)	-11.3	-9.2	-10.6	-8.5
Max. (µm)	17.1	10.3	17.1	10.6
Std. (µm)	3.17	2.60	2.76	2.20

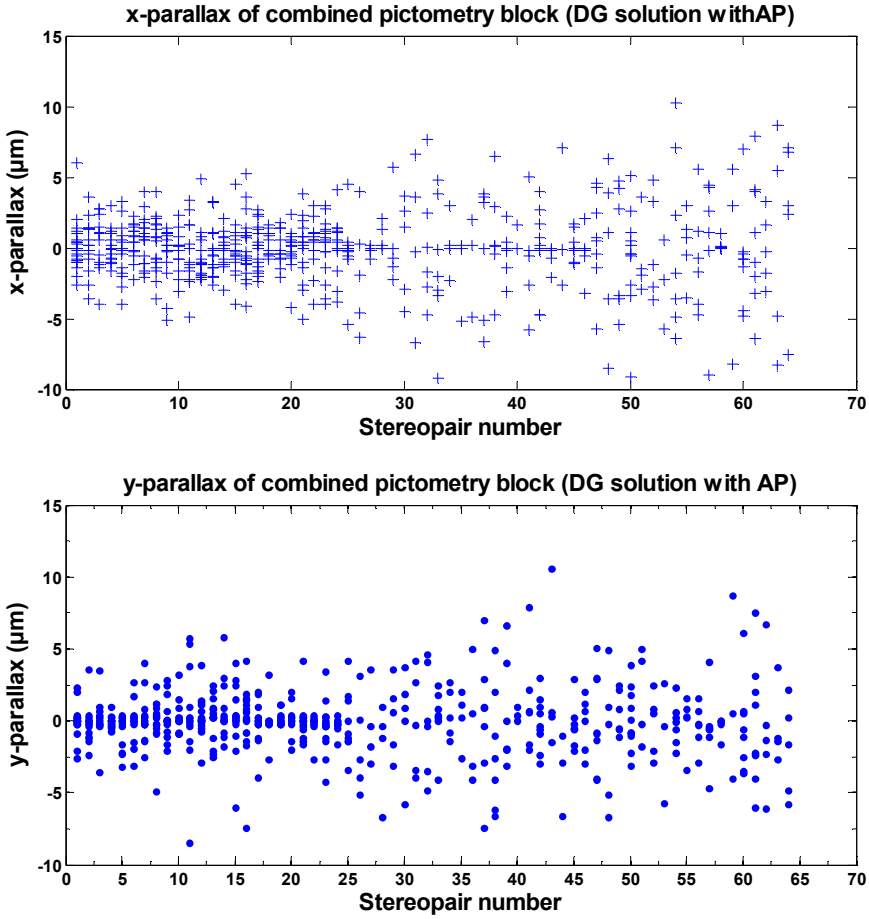

Figure 5.59: x and y-parallax for the combined Pictometry images block after the application of additional parameters model.

The table and the figures above show that a good improvement has been achieved with the application of the AP technique. The standard deviation of x-parallax has fallen from 3.17µm to 2.60µm and that of y-parallax from 2.76µm to 2.20µm. In addition, more than 95% of points have a parallax of less than 10µm (the threshold for comfortable stereo viewing). Thus, using this block with results of DG solution will not cause any y-parallax problems when manually stereo plotting.

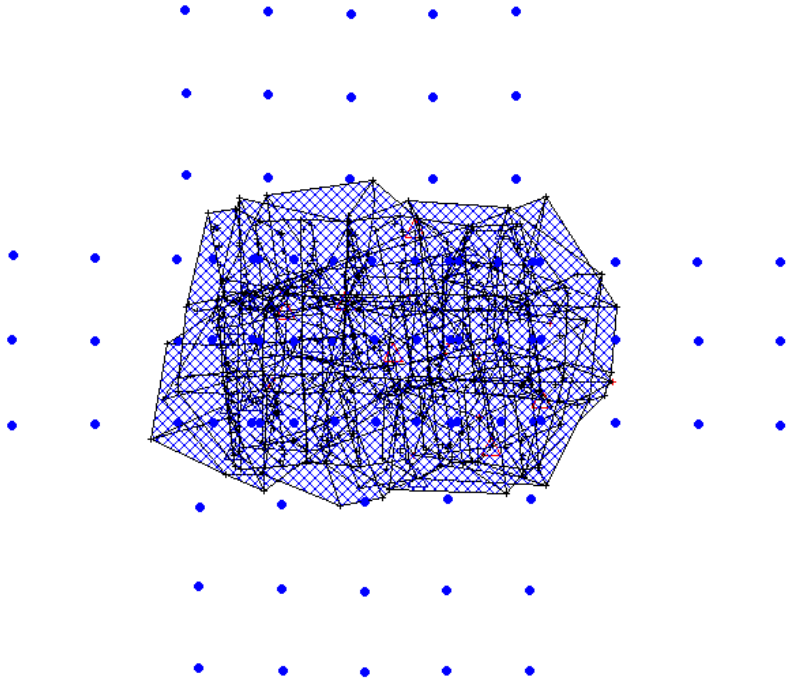

Figure 5.60: The effective footprint in relation to the footprint of the combined Pictometry images block.

Figure 5.60 above shows the percentage of effective footprint in relation to the footprint of the combined Pictometry images block. No holes in-between are found so the addition of more tie points is not necessary. Comparing the effective footprint of this block to that of the UltraCamD and oblique images block (figure 5.48), it is clear that the area covered by the UltraCamD and oblique images block is more and hence the use of only 35 ground points in the combined Pictometry images block whereas all ground points have been used in the UltraCamD and oblique images block.

5.4 Minimum control

With the availability of integrated systems of GPS and IMU, ground control points and hence ground survey can be reduced to the minimum through the use of direct georeferencing for the airborne sensors. But according to Heipke et al. (2002) and Jacobsen and Wegman (2002), the reliability of the results remains a weak point of direct and integrated sensor orientation due to a lack of redundancy in absolute orientation. Systematic errors in the GPS/IMU measurements or changes in the system calibration parameters between

calibration and actual flight may go unnoticed, because they cannot be detected without the introduction of GCP coordinates. Thus, it is recommended to include at least a minimum number of GCPs in the actual project area wherever possible.

Two scenarios have been considered to check the quality of AT in integrated sensor orientation solution with the minimum control; one GCP and two GCPs.

5.4.1 One GCP

One GCP has been used with the integrated sensor orientation solution for the 5 blocks. The results of these tests are shown in table 5.22 (LPS) and table 5.23 (ORIMA). The results show that using one GCP produced high RMS of the control check points when AP model was not used especially when using LPS except for the UltraCamD block which produced very good results comparable to the results of the constrained solution. ORIMA has given better CCPs RMS with one GCP than LPS with only few exceptions like the height in UltraCamD block which was better in LPS. On the other hand, a very significant improvement has been achieved using the AP model ranging from 10% to 70% in LPS except in UltraCamD block in which the application of AP model has no effect on the results. In case of ORIMA, the significant accuracy improvement due to the application of additional parameters was in the height. It improved in some blocks by about 25-55%. In addition, there have been some improvements in plan RMS of CCPs in some blocks with the biggest in the oblique block (about 40 to 50%).

5.4.2 Two GCPs

Tests with two GCPs have been performed to compare the results with one GCP tests and with no GCPs tests in section 5.4. The results of this test are shown in table 5.24 using LPS and table 5.25 using ORIMA.

Table 5.22: AT results of integrated sensor orientation test with 1 GCP for the five blocks using LPS

Block		Vertical		Oblique		Combined Pictometry		Combined UCD/Pict		UltraCamD	
AP		No	Yes	No	Yes	No	Yes	No	Yes	No	Yes
Total RMSE (μm)		2.2	2.1	4.2	3.6	3.9	3.6	3.1	3.0	5.2	4.9
GCPs RMS (no. pts)	X(m)	0.021 (1)	0.035 (1)	0.025 (1)	0.016 (1)	0.023 (1)	0.011 (1)	0.021 (1)	0.003 (1)	0.087 (1)	0.084 (1)
	Y(m)	0.071 (1)	0.059 (1)	0.010 (1)	0.014 (1)	0.009 (1)	0.011 (1)	0.007 (1)	0.001 (1)	0.058 (1)	0.058 (1)
	Z(m)	0.045 (1)	0.021 (1)	0.013 (1)	0.010 (1)	0.009 (1)	0.004 (1)	0.091 (1)	0.009 (1)	0.009 (1)	0.005 (1)
CCPs RMS (no. pts)	X(m)	0.236 (28)	0.213 (28)	0.622 (30)	0.166 (30)	0.609 (34)	0.190 (34)	0.260 (38)	0.205 (38)	0.090 (32)	0.089 (32)
	Y(m)	0.202 (28)	0.272 (28)	0.472 (30)	0.266 (30)	0.398 (34)	0.172 (34)	0.160 (38)	0.121 (38)	0.055 (32)	0.055 (32)
	Z(m)	0.424 (28)	0.300 (28)	0.423 (30)	0.157 (30)	0.351 (34)	0.157 (34)	0.436 (38)	0.134 (38)	0.083 (32)	0.082 (32)

Table 5.23: AT results of integrated sensor orientation test (1 GCP) for the five blocks using ORIMA

Block		Vertical		Oblique		Combined Pictometry		Combined UCD/Pict		UltraCamD	
AP		No	Yes	No	Yes	No	Yes	No	Yes	No	Yes
Sigma0(μm)		1.9	1.7	4.1	3.6	3.6	3.3	2.9	2.7	2.5	2.3
GCPs RMS (no.pts)	X(m)	0.007 (1)	0.006 (1)	0.010 (1)	0.002 (1)	0.001 (1)	0.020 (1)	0.095 (1)	0.086 (1)	0.004 (1)	0.072 (1)
	Y(m)	0.031 (1)	0.023 (1)	0.014 (1)	0.026 (1)	0.005 (1)	0.004 (1)	0.007 (1)	0.003 (1)	0.050 (1)	0.040 (1)
	Z(m)	0.015 (1)	0.006 (1)	0.028 (1)	0.056 (1)	0.060 (1)	0.000 (1)	0.089 (1)	0.058 (1)	0.036 (1)	0.063 (1)
CCPs RMS (no.pts)	X(m)	0.135 (28)	0.144 (28)	0.289 (30)	0.163 (30)	0.248 (34)	0.186 (34)	0.088 (38)	0.085 (38)	0.065 (32)	0.064 (32)
	Y(m)	0.152 (28)	0.318 (28)	0.305 (30)	0.159 (30)	0.205 (34)	0.143 (34)	0.084 (38)	0.081 (38)	0.077 (32)	0.056 (32)
	Z(m)	0.269 (28)	0.277 (28)	0.446 (30)	0.269 (30)	0.490 (34)	0.477 (34)	0.305 (38)	0.236 (38)	0.219 (32)	0.095 (32)

Table 5.24: AT results of integrated sensor orientation test with two GCPs for the five blocks using LPS

Block		Vertical		Oblique		Combined Pictometry		Combined UCD/Pict		UltraCamD	
AP		No	Yes	No	Yes	No	Yes	No	Yes	No	Yes
Total RMSE (µm)		2.2	2.1	4.4	3.7	4.0	3.6	3.4	3.1	5.2	4.9
GCPs RMS (no.pts)	X(m)	0.041 (2)	0.036 (2)	0.175 (2)	0.038 (2)	0.219 (2)	0.044 (2)	0.117 (2)	0.086 (2)	0.076 (2)	0.072 (2)
	Y(m)	0.047 (2)	0.043 (2)	0.101 (2)	0.038 (2)	0.101 (2)	0.039 (2)	0.072 (2)	0.047 (2)	0.048 (2)	0.049 (2)
	Z(m)	0.040 (2)	0.017 (2)	0.067 (2)	0.008 (2)	0.086 (2)	0.020 (2)	0.070 (2)	0.033 (2)	0.031 (2)	0.020 (2)
CCPs RMS (no.pts)	X(m)	0.155 (27)	0.147 (27)	0.185 (29)	0.162 (29)	0.170 (33)	0.107 (33)	0.224 (37)	0.199 (37)	0.090 (31)	0.090 (31)
	Y(m)	0.138 (27)	0.132 (27)	0.264 (29)	0.165 (29)	0.172 (33)	0.127 (33)	0.109 (37)	0.116 (37)	0.056 (31)	0.056 (31)
	Z(m)	0.498 (27)	0.256 (27)	0.283 (29)	0.095 (29)	0.205 (33)	0.107 (33)	0.199 (37)	0.190 (37)	0.086 (31)	0.083 (31)

Table 5.25: AT results of integrated sensor orientation test with two GCPs for the blocks using ORIMA

Block		Vertical		Oblique		Combined Pictometry		Combined UCD/Pict		UltraCamD	
AP		No	Yes	No	Yes	No	Yes	No	Yes	No	Yes
Sigma0(µm)		1.9	1.7	4.1	3.7	3.6	3.4	2.9	2.7	2.5	2.3
GCPs RMS (no.pts)	X(m)	0.017 (2)	0.007 (2)	0.012 (2)	0.032 (2)	0.068 (2)	0.043 (2)	0.072 (2)	0.035 (2)	0.027 (2)	0.061 (2)
	Y(m)	0.026 (2)	0.027 (2)	0.063 (2)	0.044 (2)	0.013 (2)	0.033 (2)	0.064 (2)	0.049 (2)	0.027 (2)	0.033 (2)
	Z(m)	0.013 (2)	0.002 (2)	0.018 (2)	0.050 (2)	0.042 (2)	0.100 (2)	0.407 (2)	0.058 (2)	0.193 (2)	0.039 (2)
CCPs RMS (no.pts)	X(m)	0.118 (27)	0.134 (27)	0.479 (29)	0.160 (29)	0.152 (33)	0.176 (33)	0.117 (37)	0.116 (37)	0.061 (31)	0.065 (31)
	Y(m)	0.140 (27)	0.209 (27)	0.284 (29)	0.151 (29)	0.143 (33)	0.153 (33)	0.079 (37)	0.069 (37)	0.062 (31)	0.055 (31)
	Z(m)	0.299 (27)	0.361 (27)	0.263 (29)	0.153 (29)	0.206 (33)	0.155 (33)	0.264 (37)	0.118 (37)	0.228 (31)	0.077 (31)

The use of 2 GCPs improved the accuracy of AT with no additional parameters significantly in all blocks. The gain in accuracy of CCPs was in the range of about 15 to 70% with the exception of Z-component in the vertical block (LPS) which slightly worsen and the X-component in the oblique block (ORIMA) which significantly deteriorated (about 20cm). The introduction of AP technique has improved the results slightly in X and Y components. However, it improved the results significantly in the height (about 20 to 50%). Again the accuracy of UltraCamD block is almost the same as that when one GCP was used, and surprisingly it is only within a few centimetres of the accuracy obtained from float and constrained solutions. This implies that the in-flight obtained EOP for the UltraCamD block are of high quality as a result of correct GPS/IMU data processing.

Overall, the above 2 tables show that the results of AT are better in the case of using 2 GCPs with no AP than using only 1GCP. When AP model was introduced, the RMS of CCPs improved a lot in both cases (1 and 2 GCPs) especially in the height.

The comparison of the AT results presented in section 5.4 with the minimum control results shows that the results of constrained and float solutions with no AP are much better than the minimum control results which is expected. In the mean time the AP results are slightly better. In the vertical Pictometry block, using minimum control has improved the height accuracy by a factor of about 2 to 2.5 compared to integrated and DG solutions. The accuracy of using minimum control in the integrated sensor orientation solution in oblique block is comparable to that of float and constrained solutions. On the other hand, using minimum control has improved the accuracy significantly compared to integrated sensor orientation and DG solutions especially in height which improved up to 6 times. The same is true for the combined Pictometry block, the UltraCamD and oblique images block, and UltraCamD block in which the height has improved by a factor of 3, 4, and 3 respectively.

The minimum control can be used instead of only DG solution. It gives better results and in the meantime it is a cost effective way as surveying ground control points in the field is time consuming, labour intensive and therefore

expensive process. However, with minimum control all this will be reduced to the minimum.

5.5 City centre block

The city centre block consists of 15 images; 3vertical and 12 oblique images (3 obliques looking north, 3 obliques looking south, 3 obliques looking east, and 3 obliques looking west). The number of GPS-surveyed control points for this block is 8 and the number of tie points is 543. The control points is the tie points between the individual blocks. Figure 5.61 shows the area in Nottingham city centre covered by this block and figure 5.62 shows the images footprint and the tie points' distribution.

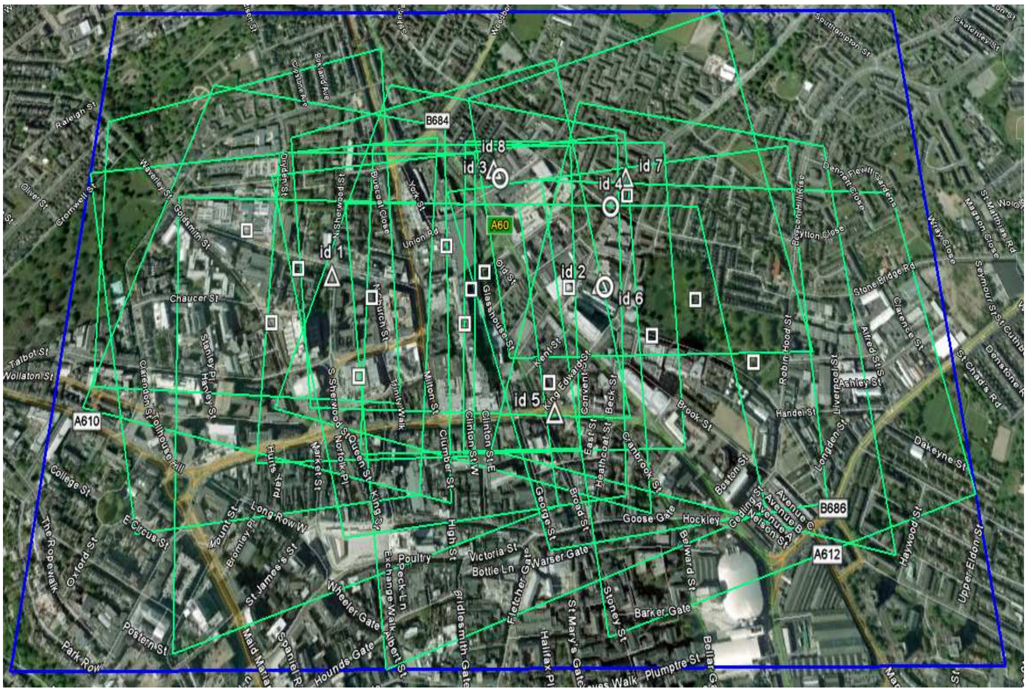

Figure 5.61: Nottingham city centre area covered by city centre combined Pictometry block, the image is adapted from Google earth.

The AT for this block was performed using the constrained solution in only LPS software as the geometric quality of Pictometry imagery has already been proven in section 5.4. Therefore, comparison of AT results from different software packages is no longer necessary; hence ORIMA was not used with this block. The given a priori standard deviation for EOP is the same as previous Pictometry blocks (1m and 1 degree). The AT was conducted with

and without using the additional parameters. The best results of the trials performed are shown in table 5.26.

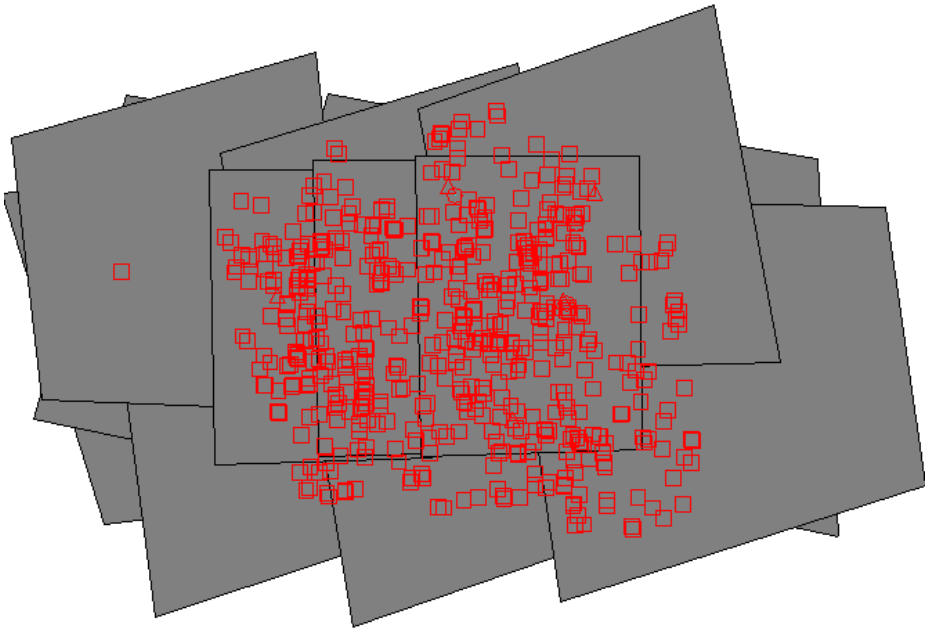

Figure 5.62: The combined Pictometry city centre images footprint after performing AT as well as the distribution of tie points.

Table 5.26: AT results for the city centre combined Pictometry block using LPS

AP		**No**	**Yes**
Total image RMSE (µm)		2.9	2.4
CCPs RMSE (m) (no.pts)	**X**	0.140 (3)	0.121 (3)
	Y	0.136 (3)	0.099 (3)
	Z	0.080 (3)	0.089 (3)

As can be seen from the above table, the AT results of this block are almost the same as those for the UltraCamD and oblique images block (section 5.4.6) and for the combined Pictometry block (section 5.4.7). Again using the oblique images improved the height accuracy due to the multiple intersection rays they produce. Introducing the Ebner's orthogonal model of 12 parameters (Ebner, 1976) improved the accuracy in plan but the height did not benefit from using self-calibration model.

5.6 Summary

Conducting AT requires several processing steps. The first and most important step in the process is the creation of a new project. This involves internal and external sensor model definition, GCP measurement, automatic tie point generation, and bundle block adjustment.

The AT was conducted using four different solutions for the vertical images blocks of both Pictometry and UltraCamD imagery, combined block of oblique Pictometry imagery, combined block of oblique and vertical Pictometry imagery, and finally combined block of oblique Pictometry imagery and vertical UltraCamD imagery.

Since the sigma0 (or total image RMSE) of the block is by itself not a valid indicator of errors or deformation within the block, the overall absolute geometric accuracy was estimated from independent reference points; the RMSE values of the CCPs compared to the truth value (static GPS survey) was used to represent the external geometry of the blocks. In addition, plots of CCPs residual vectors were presented to examine the possible existence of any remaining systematic errors after the solution. Moreover, y-parallax plots were also presented to investigate the problematic existence of y-parallax which affects the stereo viewing which is very important for the 3D modelling stage of the project.

Comparison between the raw EOP values and the calculated EOP values after performing the traditional AT show that there were significant positional and attitude deviation of the order of up to 2m and 1degree for Pictometry imagery, hence the assignment of 1m and 1degree as a priori standard deviation for the in-flight position and attitude. This reflects the non-optimal GPS/IMU quality.

The results of all blocks have shown that the use of indirect georeferencing produced very good quality coordination of ground points. In addition, high quality image measurements have been achieved. The check points show more realistic values of what might be achievable for mapping. Special care was given to the integrated sensor orientation and DG solutions as using these solutions compared to conventional photogrammetry demonstrates a significant decrease in time and thus cost for photogrammetric processes

because the use of automatically measured tie points is a cost effective way of generating ground control points. On the other hand stereo plotting is not always possible using direct sensor orientation due to the sometimes large y-parallax in individual models. This can be improved by a combined adjustment based on the direct sensor orientation together with image coordinates of tie points and not using control points. The results of direct sensor orientation have shown that height accuracy of 0.06% of flying height and plan accuracy of 0.02% of flying height can be achieved for the vertical Pictometry images block. Combining of oblique images with vertical images in one block has given a very good improvement for the height quality which reached 0.02% of flying height. Furthermore, the introduction of the image coordinates of tie points in the solutions reduced the y-parallax to the acceptable levels.

Investigating the distribution of the CCPs residual vectors, there is no noticeable pattern that might indicate the existence of systematic errors except for small patches in the upper left hand side of the combined UltraCamD and oblique images block which point to the same direction. This means that some of systematic errors are not eliminated even when the additional parameters have been applied.

From examining the AT results of the five photogrammetric blocks, the following conclusions can be drawn:

- The total image RMSE of all blocks was less than third of the pixel size of original imagery except for the DG solution which was about half of a pixel.
- Manual generation of tie points between different oblique images was necessary due to quite different image scale, different view directions, different cameras used, and different illumination conditions.
- Statistically constraining the EOP and GCPs (if their accuracy is known) will optimise the AT solution. This is to eliminate the absorption of any errors in control and tie points into the calculated orientation parameters and hence reduce the accuracy of solution.
- Ideally the more GCPs in the project the better, as their huge number ensures better geometric stability of the block and high redundancy.
- Quality of DG is fully dependent on the quality of directly measured EOP.

- The quality of object point coordinates in DG is dependent on the number of image rays used for object point determination. A large image overlap providing strong block geometry positively influences the point accuracy since multiple image rays can compensate remaining errors in the orientation parameters. From the object point accuracy mentioned in section 5.4, the higher accuracy corresponds to blocks with high overlaps while lower accuracy is expected from object points in 2-3 folded points.
- The quality of object point determination increases if appropriate standard deviations are assumed for the GPS/IMU exterior orientations.
- The use of integrated sensor orientation results in a significant accuracy improvement compared to results from DG with fixed EOP.
- The inclusion of AP model resulted in good accuracy improvement in most of the cases and in only minor additional accuracy in the other cases.
- With the increase of image overlap, more object points are automatically recognised, and the corresponding image points per object point increase significantly, which significantly increases the redundancy of the adjustment system. This can greatly improve the coordinate accuracies of all photogrammetric points.
- Generally, the higher the pixel resolution, the better the measurement accuracy of the image coordinates. The pixel size of aerial digital imagery is usually less than 10 μm. Thus, aerial digital imagery has very high geometric accuracy in photogrammetric point determination.
- The accuracy of a solution increases with the increase of the base to height (b/h) ratio.
- The reliability of the results remains a weak point of direct and integrated sensor orientation solutions due to lack of redundancy in absolute orientation. Systematic errors in the GPS/IMU measurements may go unnoticed, because they cannot be detected without the introduction of GCP coordinates. Thus, it is recommended to include at least a minimum number of GCPs in the actual project area wherever possible.
- In addition to the accuracy, it is safe to say that the blocks are reliable because of existence of relatively high number of redundancy (1301 for vertical Pictometry block, 990 for oblique Pictometry block, 2685 for

combined Pictometry block, 3450 for UltraCamD block, and 4649 for combined UltraCamD and oblique images block) which helps in detecting the blunders and bad measurements as they provide check on each other.

Overall, the aerial triangulation has shown that strong image geometry can be achieved from both image types to create high quality 3D urban geometric models. The successful combining of the vertical (Pictometry or UltraCamD) images and the oblique images in one block provides an excellent opportunity to produce an efficient method of high quality automatic texture mapping for the derived 3D city models.

CHAPTER6: 3D MODELLING OF TEST SITES

This chapter begins with a brief description of the most used representation of a 3D object. This is followed by detailed description of the process followed for building reconstruction adapted in this research using Pictometry and UltraCamD blocks. The accuracy of the 3D geometric models will then be discussed. This chapter also describes in detail the texture mapping process using the available photogrammetric blocks. Finally, a summary of the results will be given.

6.1 Introduction

The use of 3D data has become very important in many applications. Hence, there is an increasing need for realistic, accurate, and affordable 3D city models. The representation of a 3D object can be any of the following types (Rottensteiner, 2001):

1- Point cloud: the object is just described by the vertices
2- Wire frame model: the object is described by vertices and edges, figure 6.1.
3- Surface model: object is described by vertices, edges and faces, figure 6.1.
4- Volumetric model: the object is described by vertices, edges, faces and volumes, e.g. a set of volumetric primitives.

Of the four model representations, the surface model is the most applicable both for visualization and for mathematical analysis in GIS packages. Compared with wire frame models, surface models add the important definitions of faces (called patches) and each of which may consist of several polygons. Compared with the volumetric models, surface models allow the representation of irregularly shaped objects in a much easier way (Ressla et al., 2006) and (Song and Shan, 2004).

The method of representation of the 3D buildings in this research will be the surface model as the faces are required for texture mapping process. It is produced from a 2-stage process; extraction of 3D geometry (section 6.2) followed by texture mapping of the 3D models (section 6.4).

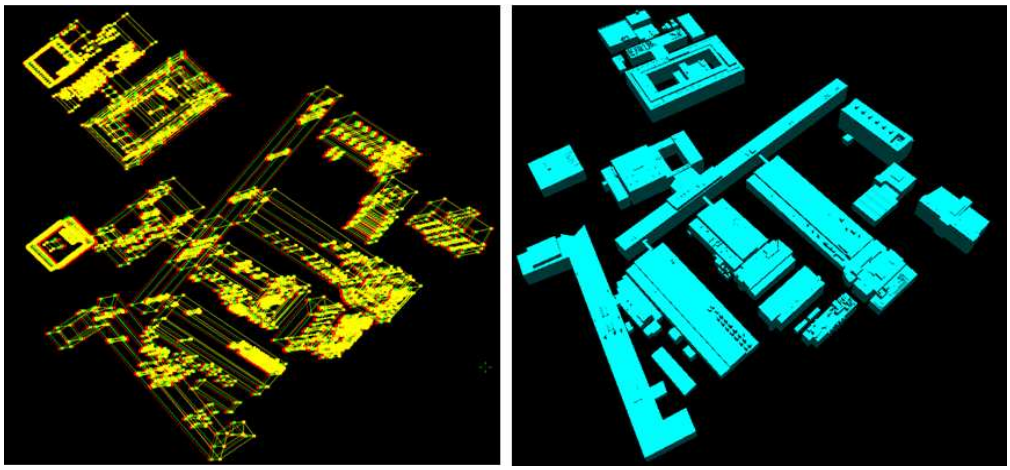

Figure 6.1: Wire frame model (left) and surface model (right) of some of Engineering buildings in Nottingham University.

6.2 Extraction of 3D geometry

Building modelling requires different processes which can be summarised as follows:

- Digitizing (extraction) of roof outlines; this involves digitizing the small roof details in 3D polygons first then digitizing the main roof outline in a different polygon taking into account different elevations of the roof which should be digitized as separate polygons.
- Extrusion of the digitized polygons of each building as a whole (one polyhedral) to ground to create the building facades.
- Exporting the extruded 3D polygons as 3D shapefiles to another software for texturing.

The software that will be used to perform the above stages is Erdas Imagine 9.3 Stereo Analyst. Stereo data collection techniques used in Stereo Analyst provide very good accuracy due to the following reasons:

- Sensor model information (internal and external) used in Stereo Analyst were derived from block AT. This eliminates the errors associated with sensor position and orientation as required for accurate 3D information.
- During the block AT, systematic errors associated with raw imagery are considered and minimized by using the self-calibration technique.
- The collection of 3D information using stereo viewing techniques is not dependent on a DEM as an input source. Changes and variations in depth

perception can be perceived and automatically transformed using sensor model information and raw imagery. Therefore, DEMs containing error are not introduced into collected 3D data.

6.2.1 Extraction of 3D geometry from vertical Pictometry block

A true stereo effect is achieved when two overlapping images (a stereopair) of a common area captured from two different vantage points are rendered and viewed simultaneously. The stereo effect (ability to view with measurable depth perception) is provided by a parallax effect generated from the two different acquisition points. In photogrammetry, stereoscopic depth perception plays a vital role in creating and viewing 3D representations of the surface of the Earth. According to Leica (2009b), the availability of 3D information in a stereo model is possible by the presence of what is referred to as stereoscopic parallax. Parallax (sometimes called disparity) can be simply defined as the difference between the photo coordinates in each photo of a certain point in a stereo pair.

There are two types of parallax: x-parallax and y-parallax. The x-parallax is measured along x dimension (the base that is connecting the two images' perspective centres) and it is used for height determination. The amount of x-parallax is influenced by the elevation of a ground point. Since the degree of topographic relief varies across a stereopair, the amount of x-parallax also varies. Figure 6.2 shows a building with varying x-parallax.

The y-parallax is measured along y dimension (perpendicular direction) and it causes difficulty in viewing the stereopairs. The y-parallax is influenced by: unequal flying height between adjacent images, large differences in photographic orientation between overlapping images and errors in camera model information, figure 6.3.

Although tremendous progress has been made, the main workload of 3D city model generation is still building digitizing. The first step in digitizing the buildings (using Stereo Analyst) is to create a new feature project then the second step is to choose a feature class that will be digitized (buildings for this study). The last step is to select the photogrammetric block that contains the stereo models which will be used for digitizing the buildings.

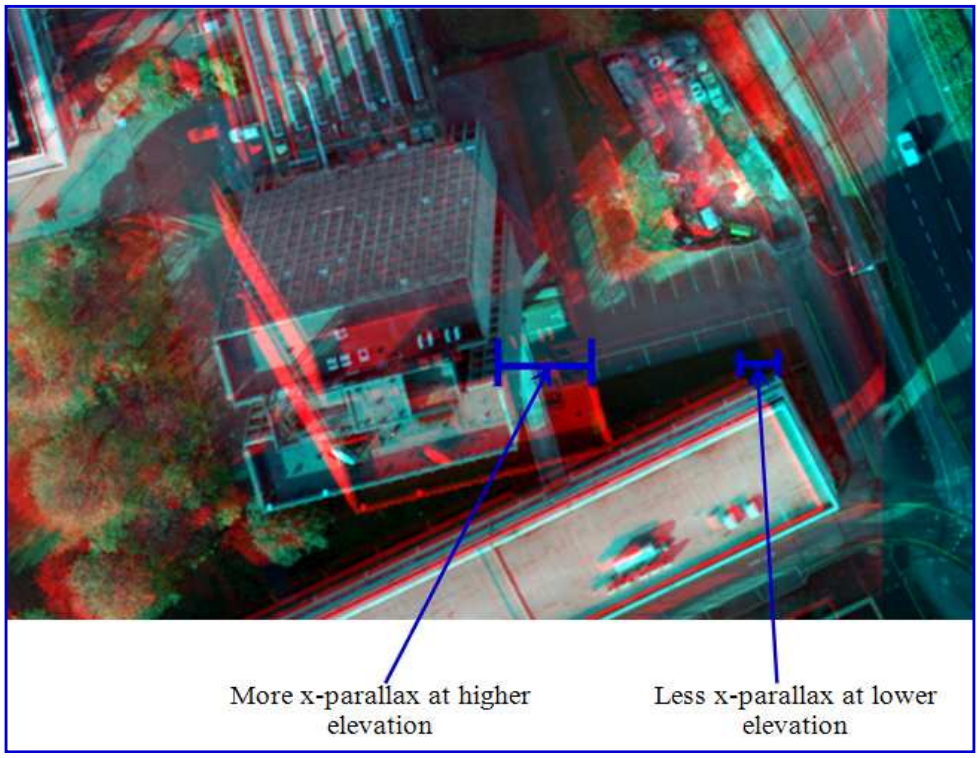

Figure 6.2: Different x-parallax according to elevation of building: Tower building with high x-parallax and Coates building with less x-parallax.

Extraction of 3D geometry for all buildings in both study areas has been performed using vertical Pictometry imagery. It should be noted though that due to the small forward overlap, it was not possible to digitise all the available buildings in both study areas because of lack of stereo coverage.

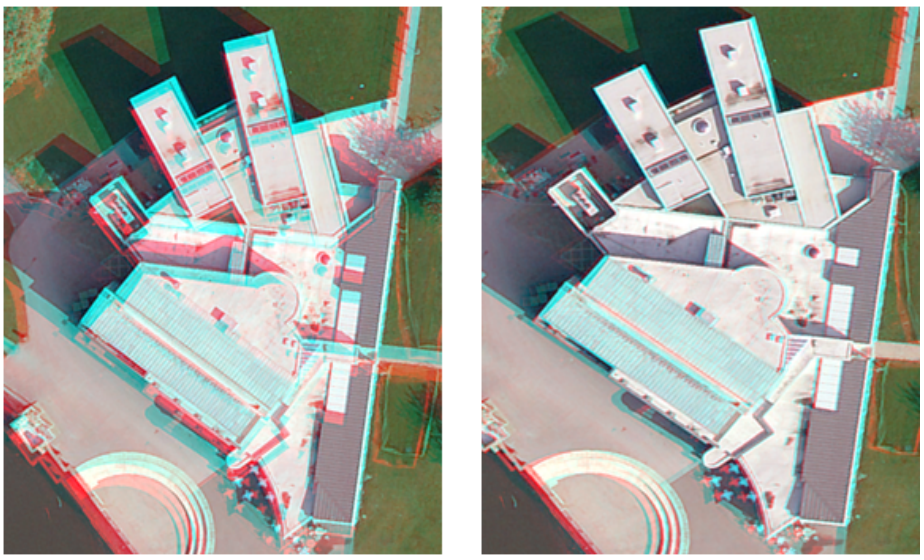

Figure 6.3: Arts centre building with y-parallax (left) and with no y-parallax (right).

The 3D building reconstruction is a difficult problem, mainly due to the complexity of the buildings. Urban environments are very dense and composed of many types of buildings. Hence, it makes digitizing difficult. Therefore, the automation of building reconstruction is obviously an important factor when it comes to efficiency and costs. The success of automation in this field depends on many factors and is a hot topic in research (Ortin and Remondino, 2008). Progress is slow and the acceptance of results depends on the user specifications. Moreover, the image scale plays an important role in automation. Potentially, the smaller the scale the more successful automation will be. On the other hand, Gruen (2008), Khoshelham and Li (2004) and Flamanc et al. (2003) stated that despite the great deal of research that has been carried out on this topic, in commercially available digital photogrammetric software, object extraction functionality is restricted to manual or semiautomated measurements together with the capability of attribute data acquisition. The automated building reconstruction is still a challenging problem. Commercial systems assist the human operator in measuring 3D objects in combination with registration of attribute data in a semiautomated mode. Fully automated approaches are not sufficiently robust and do not achieve the high success rates required for practical applications.

Cavagna et al. (2009) and Khoshelham and Li (2004) concluded that the reasons of causing automated reconstruction of building objects from aerial images is one of the most complex problems in photogrammetry and computer vision are:

- Airborne photography places several obstacles in the way of automatic object recognition, including noise and low contrast of images (the result of distant photography).
- Atmospheric effects and poor illumination.
- Objects of interest are not of fixed shape and size; buildings appear in a variety of shapes and sizes and roofs can be very complex, figure 6.4.
- Occlusion, shadow, undesirable small objects on building roofs (such as antennas or skylights) and vegetation are other examples of complexities involved in the task of automated reconstruction of buildings from aerial images.

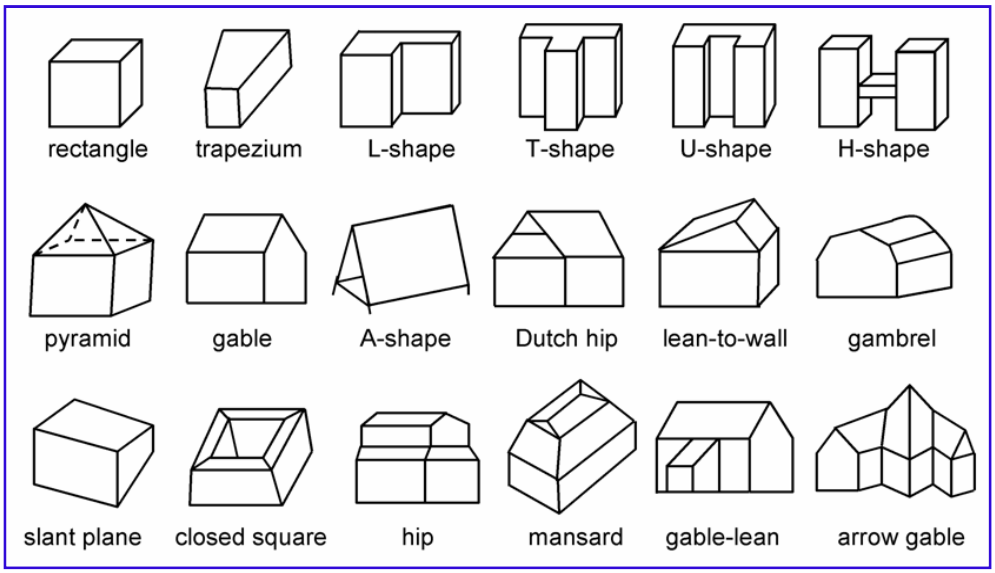

Figure 6.4: Types of ground plan in the top row and roof types in the middle and bottom rows, adapted from Meng and Forberg (2007).

Due to the above reasons, extraction of 3D building geometry in this research will be performed in a semi-automatic mode. After choosing the building feature class, the floating cursor (provided by Stereo Analyst at the user interface) should be adjusted such that the measuring mark on each image is placed on the corresponding point. When the images are viewed stereoscopically the two measuring marks will be seen as a single floating mark. The floating mark is adjusted when the two images are aligned together using the x-parallax, figure 6.5. Each feature will have a different elevation and therefore the floating mark will need to be continuously moved. Then, one corner of the roof is chosen and the floating mark is placed over it making sure that the x-parallax is adjusted accordingly. The digitizing of the roof can now be performed by left-clicking on the first node and continuing to the other corners of the roof. On the last node double click to close the polygon, figure 6.5 shows a collected feature.

For efficient building modelling, it is preferable to first digitize all the small roof details (dormers, chimneys, ventilation equipment etc.) using 3D polygons and then digitize the main roof outline as a separate polygon. Roof levels with different elevations must be digitized as separate 3D polygons even if they share a common boundary. It is important to note that during digitizing, different stereo pairs will have to be selected to plot details of the entire roof.

Figure 6.5: x-parallax has been adjusted for point of interest (left) so that the measuring mark on each image is placed on the corresponding point of left and right images (middle). Right image shows extracted polygons for several buildings in the Nottingham city centre.

Once all the 3D polygons of a particular building have been collected and in order to create the building facades, all the roof polygons then should be extruded onto the ground level to create the polyhedral model. Extrusion turns points into vertical lines, lines into walls, and polygons into blocks. This can be done easily in Stereo Analyst by placing the floating mark on the ground surface next to the building that will be extruded and then x-parallax has to be adjusted to get the correct elevation of the ground. After that, create a selection box enclosing all the features to be extruded using the available tool in Stereo Analyst. Select the '3D Polygon Extend tool' and double click on the ground (where x-parallax has been adjusted) to create a 3D building from an existing roofline by extending the shape to the ground level, figure 6.6.

In addition to the extraction of 3D geometry of buildings in Stereo Analyst, it allows attributes to be collected automatically with attribute tables. Both spatial and non-spatial attribute information associated with a feature can be input during collection as attribute tables for specific features can be opened during digitizing.

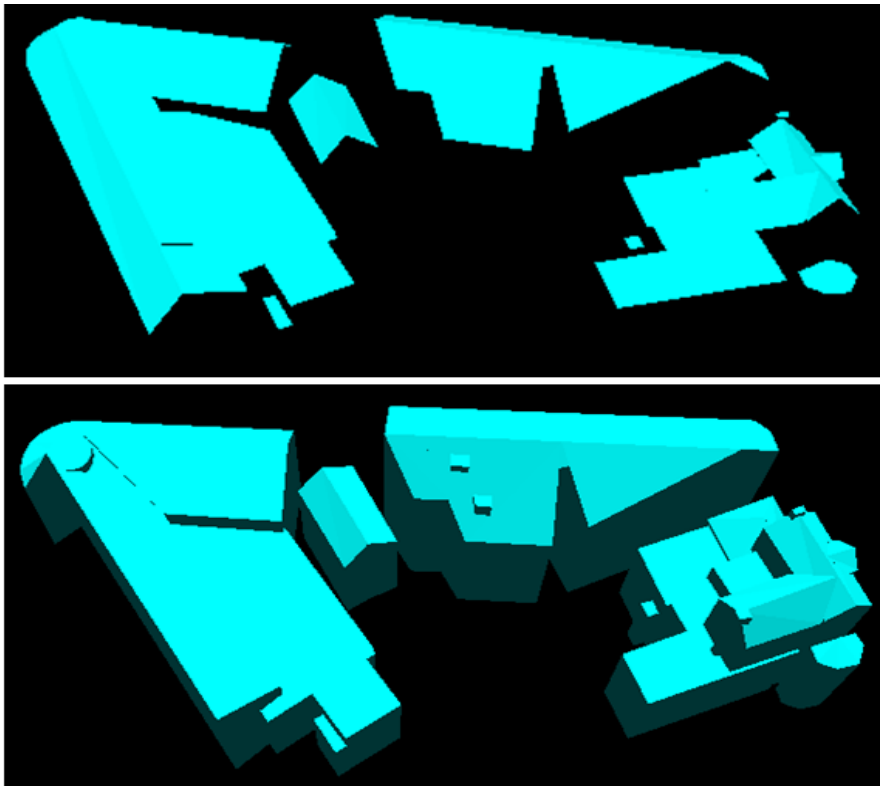

Figure 6.6: Roof outlines of several buildings in Nottingham city centre (top) and the same buildings after extrusion to the ground level (bottom).

6.2.2 Extraction of 3D geometry from UltraCamD block

The extraction of 3D geometry for buildings in the first study area (University of Nottingham main campus) has also been performed using UltraCamD images block. For the second test area (Nottingham city centre), UltraCamD images are not available so only Pictometry images have been used. The reconstruction of 3D building models from UltraCamD images follows the same procedure as in section 6.2.1.

From the previous chapter, it is evident that the accuracy of UltraCamD block is strongly related to the imaging system used (UltraCamD camera). As a result, the polygons extracted from the UltraCamD images block will be used as a bench mark (BM) for comparison of accuracy of those extracted from Pictometry images block due to the following reasons:

- The flying height of UltraCamD mission was about 500m compared to 1000m of Pictometry mission.

- The ground sample distance of UltraCamD images is 5cm while that of vertical Pictometry is 15cm on average.
- High image sharpness which improves the efficiency of the feature extraction process.
- All GCPs have been measured on stereopairs using the vertical Pictometry block, oblique Pictometry block, and UltraCamD block. The results have been compared to the truth value (GPS coordinates) to check the performance of each set of images on stereo models measurement.

It is important to mention here that Arias and Gomez-Lahoz (2009) emphasised that to compare the precision of two cameras, it is necessary to have them working under similar conditions. However, this is not the case here as the aim of the comparison is to find the stereoscopic measurement accuracy of both imaging systems compared to the true values.

The measurement of GCPs in stereomodels was carried out five times and the average of the results was taken. This was done because measurement on stereomodels depends heavily on the operator ability. Due to circumstances, the choice was to use only one operator several times hence the repetition of the stereo measurements 5 times. The number of stereoscopically measured GCPs was only 37 points as 8 points are in the second test site where there are no UltraCamD images and the other 4 points are outside the first test area and can be seen only in UltraCamD images. As the Aerial triangulation results are generated from multiple rays, they do not truly reflect the quality of measurement in a stereo model. So Table 6.1 shows a summary of the results and figure 6.7, figure 6.8, and figure 6.9 show the deviation of the true GCPs coordinates from the stereopair observed photogrammetric coordinates on vertical Pictometry, oblique Pictometry, and UltraCamD blocks respectively.
Table 6.1 shows that the RMSE of the difference between true coordinates and stereopair coordinates of UltraCamD block is better than that of vertical Pictometry block by a factor of 2 in X and Z components and factor of 3.5 in Y component. Furthermore, the RMSE of stereoscopic measurements on UltraCamD images is better than that of oblique images by a factor of 2 in the height, 3 in easting and 4 in northing.

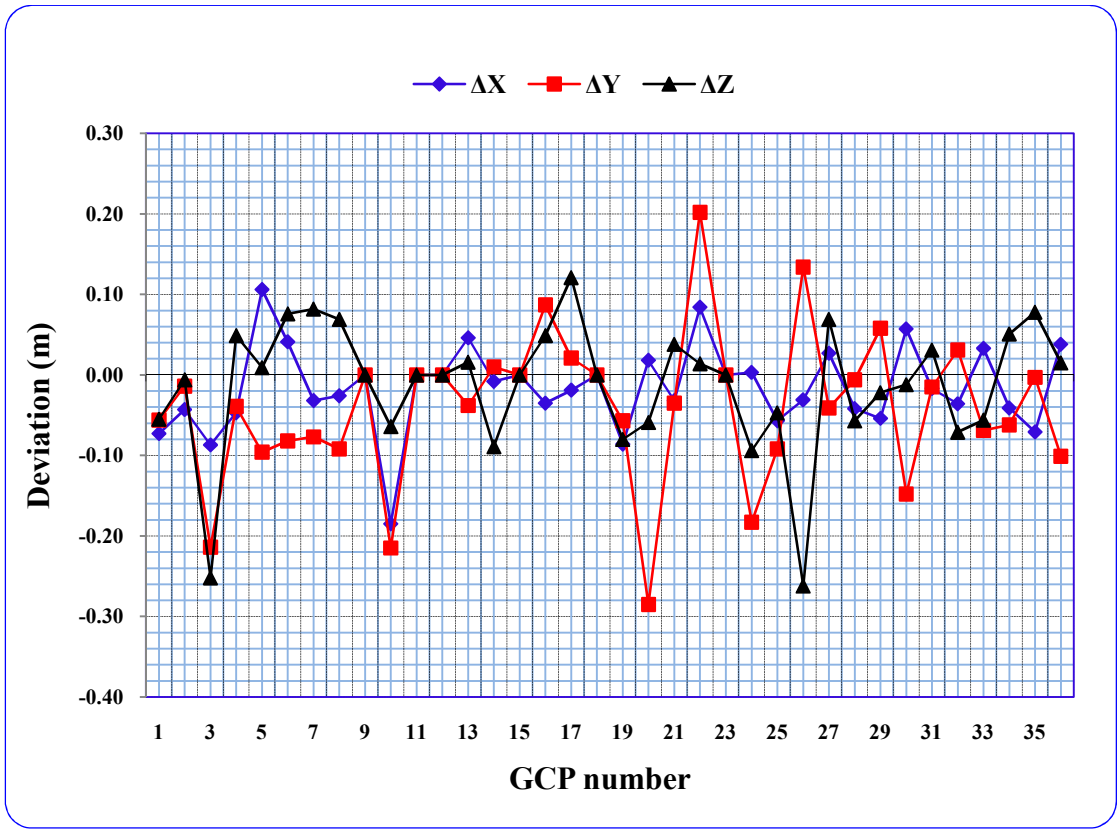

Figure 6.7: Discrepancy between the measurements of GCPs on stereomodels of vertical Pictometry block and true values measured by static GPS.

The stereoscopic measurement accuracy in X and Y (planimetric) is affected by the image scale factor and the image measurement precision. The image measurement precision is a function of the image pixel size and the ground sample distance. The image scale factors for UltraCamD, vertical Pictometry, and oblique cameras are 5000, 15400, and 11800 respectively. Although the pixel size for all cameras used in this research is the same (9µm), the measurement precision of object/target is better in UltraCamD as it has smaller GSD (see section 4.3.1 and section 4.3.2). This explains why UltraCamD planimetric results are much better than those of vertical and oblique Pictometry cameras.

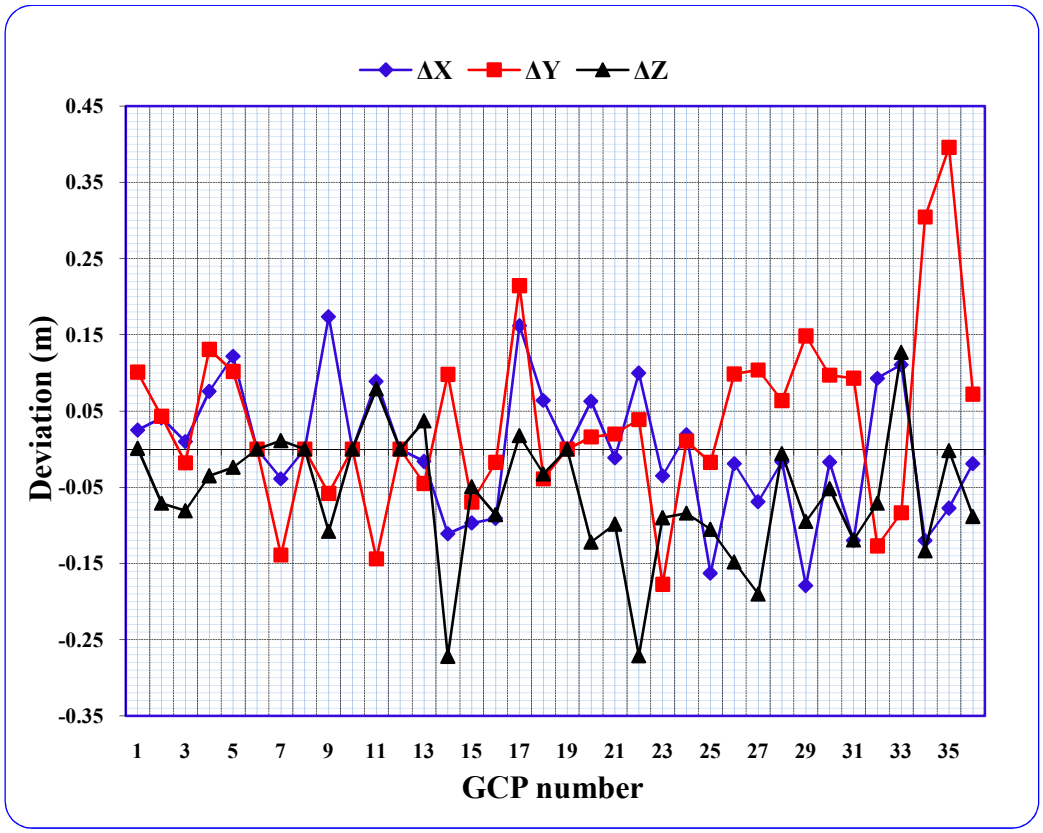

Figure 6.8: Discrepancy between the measurements of GCPs on stereomodels of oblique Pictometry block and true values measured by static GPS.

Table 6.1: Results of comparing stereopair observed photogrammetric coordinates to 37 ground measured points in 3 blocks

Block		Vertical Pictometry	Oblique Pictometry	UltraCamD
Min.	X(m)	-0.185	-0.179	-0.129
	Y(m)	-0.285	-0.177	-0.056
	Z(m)	-0.262	-0.272	-0.099
Max.	X(m)	0.106	0.174	0.092
	Y(m)	0.202	0.396	0.066
	Z(m)	0.121	0.127	0.103
St.dev. of mean	X(m)	0.058	0.093	0.036
	Y(m)	0.101	0.126	0.029
	Z(m)	0.088	0.086	0.042
RMSE	X(m)	0.061	0.092	0.036
	Y(m)	0.113	0.130	0.032
	Z(m)	0.090	0.110	0.050

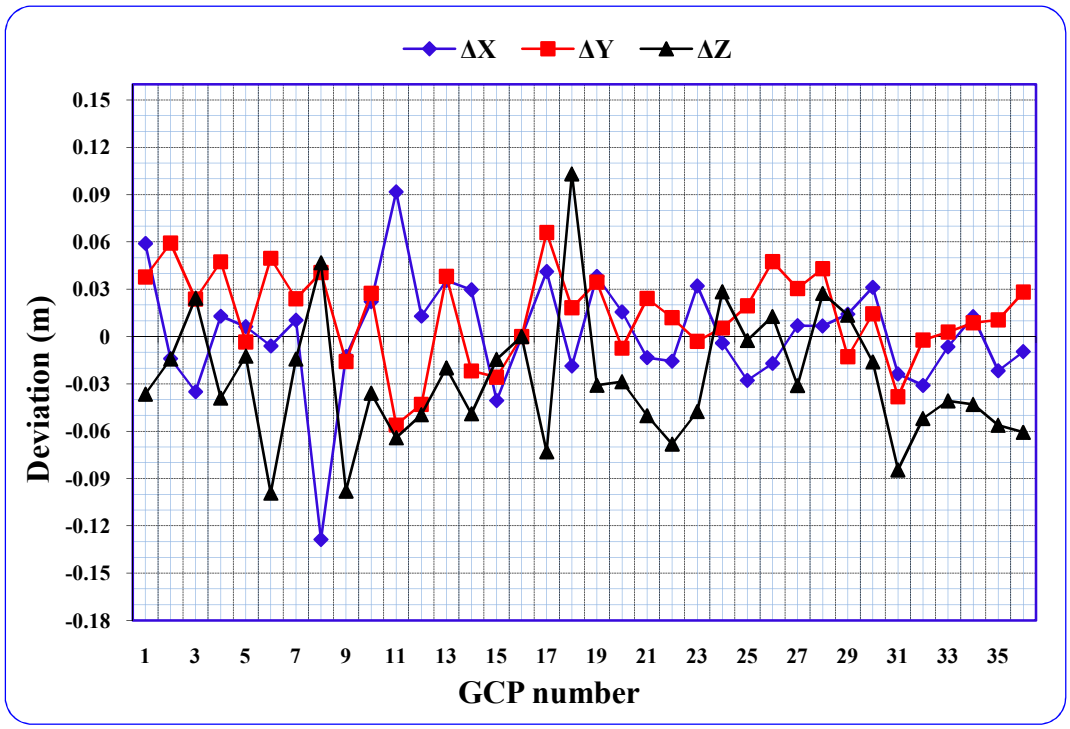

Figure 6.9: Discrepancy between the measurements of GCPs on stereomodels of UltraCamD block and true values measured by static GPS.

The accuracy of stereo measurements in height depends on the image measurement precision and according to Arias and Gomez-Lahoz (2009) on the ratio between focal length and image base, f/b. The image base, b, is a function of the along-strip overlap and the along-strip image size. The ratio f/b affects the accuracy of height. The higher this value, the worse is accuracy of height. Table 6.2 shows the ratios f/b for the different cameras in this research.

Table 6.2: Ratios f/b of aerial photogrammetric cameras using maximum overlap

Camera	Focal length, f (mm)	Image width (mm)	Max. overlap	Base, b (mm)	f/b
UltraCamD	101.4	67.5	60%	27	3.76
Vertical Pictometry	65	24.048	46%	13	5
Oblique camera	85	24.048	47%	12.75	6.67

As can be seen from table 6.2, the ratio f/b of UltraCamD is smaller than that of the other cameras. This and the better image measurement precision of UltraCamD explain its better performance in height.

Figure 6.10 illustrates the digitized building outlines of the first study area using vertical Pictometry block as well as the 3D extruded models of the same

area. Furthermore, figure 6.11depicts the 3D models of the same area but using UltraCamD images block. Comparing figure 6.10 with figure 6.11, it is apparent that some buildings do not exist in the 3D model created by Pictometry block (identified by red arrows in the UltraCamD model, figure 6.11). This was because of the forward overlap in the vertical Pictometry block which was between 38 and 46%. The vertical Pictometry block was used to create a mosaicked image of the Nottingham University main campus to check the effect of not ideal overlap on photogrammetric products. Figure 6.12 depicts the mosaicked image and the models outlines which extracted from the vertical Pictometry block.

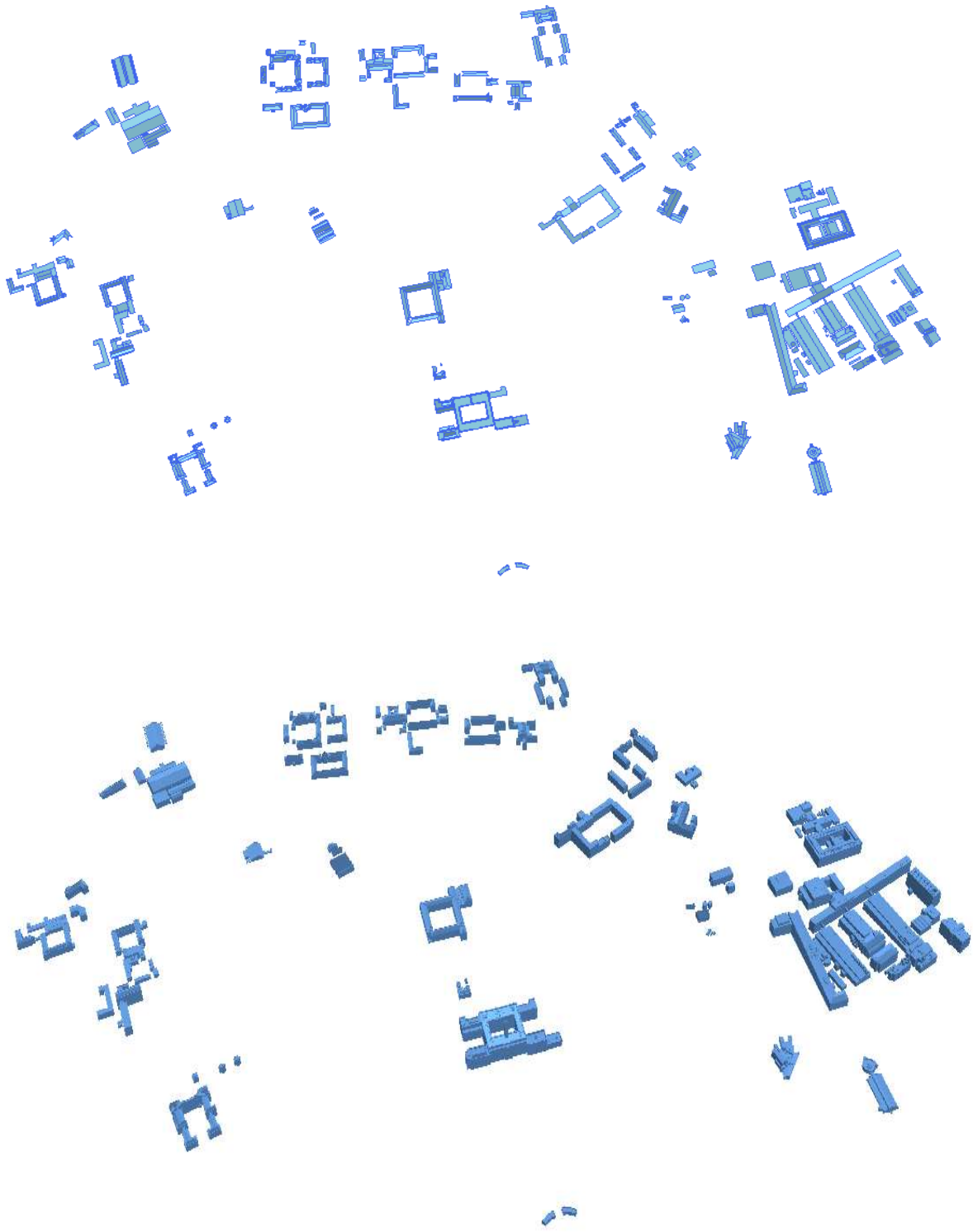

Figure 6.10: Building outlines (top) and 3D extruded building model for first study area (bottom) using vertical Pictometry block.

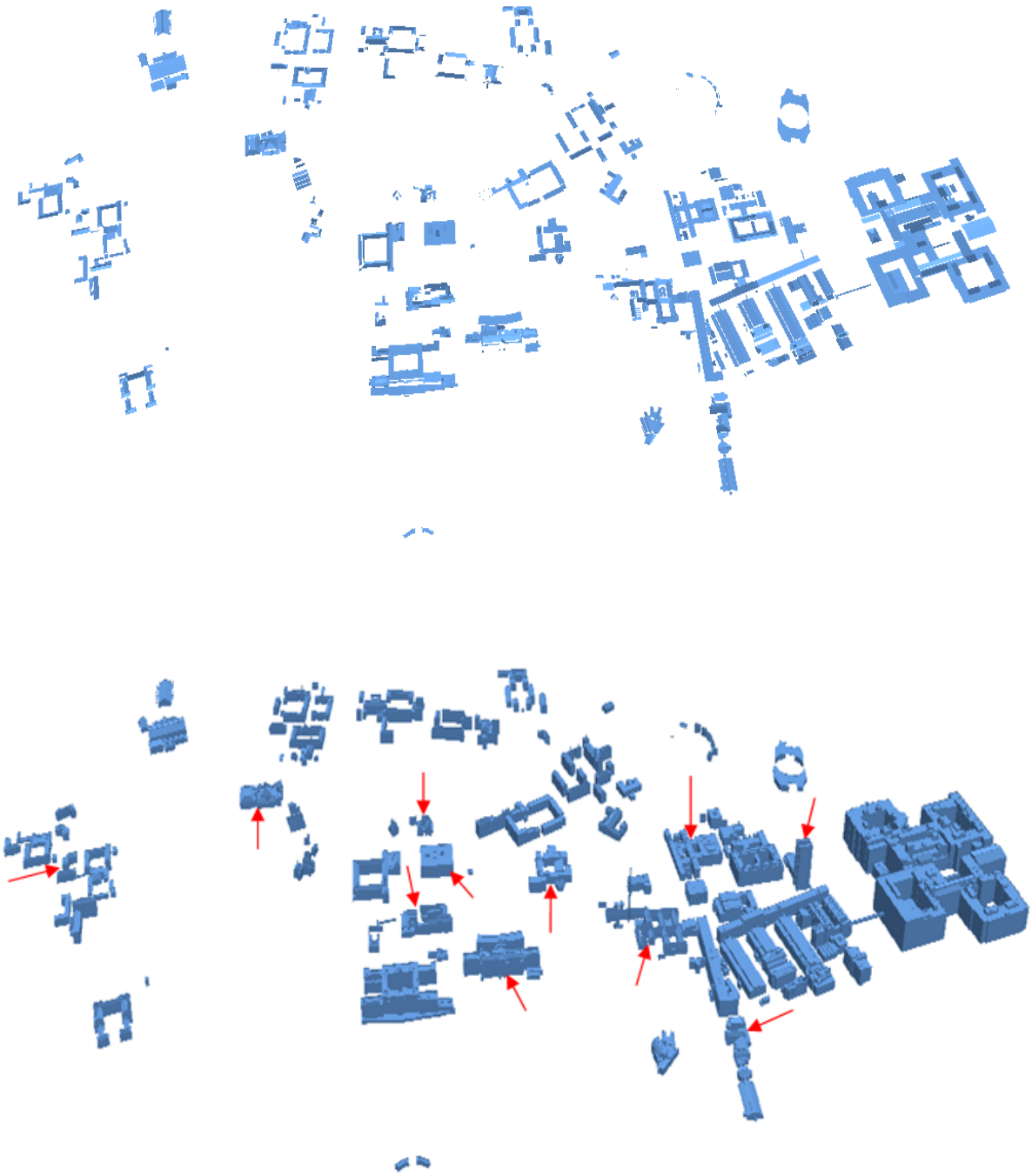

Figure 6.11: Building outlines (top) and 3D extruded building model for first study area (bottom) using UltraCamD block, red arrows show the missing buildings in the 3D model from vertical Pictometry block.

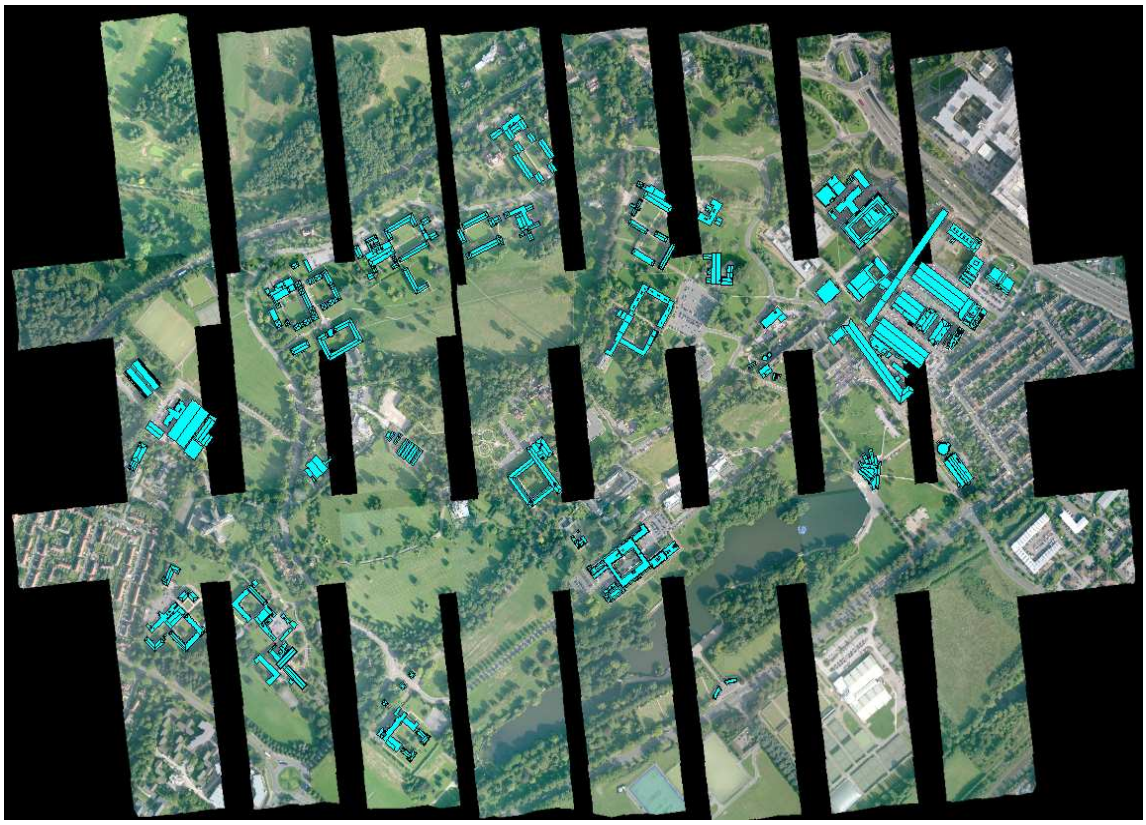

Figure 6.12: A mosaicked image (from Pictometry imagery) of the University main campus showing the gaps caused by low forward overlap (less than 60%) and the digitized buildings outlines.

It is clear from figure 6.12 that the forward overlap was neither enough to create a mosaicked image of the whole area nor to digitize all buildings in the campus. On the other hand, the side lap was in the ideal range (25 to 36%) which contributed in digitizing a lot of buildings.

Figure 6.13 shows the digitized building outlines of the second study area (Nottingham city centre), using combined Pictometry block of this area, as well as the 3D extruded models of the same area.

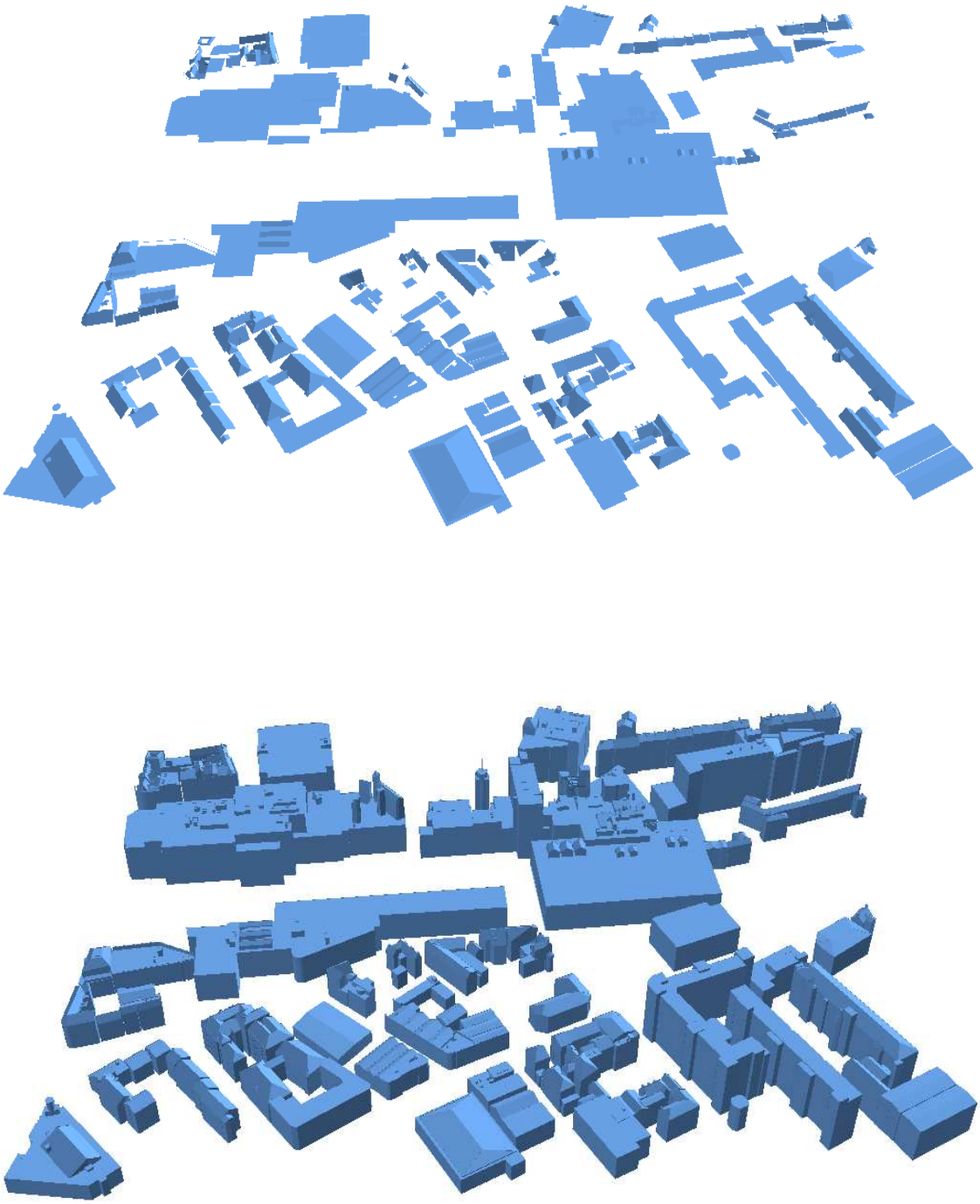

Figure 6.13: Building outlines (top) and 3D extruded building model for second study area (bottom) using vertical Pictometry block.

Figure 6.14 shows the 3D building models after exporting them as KML file to be displayed on Google Earth. They are matching in position on top of their actual places in Google Earth.

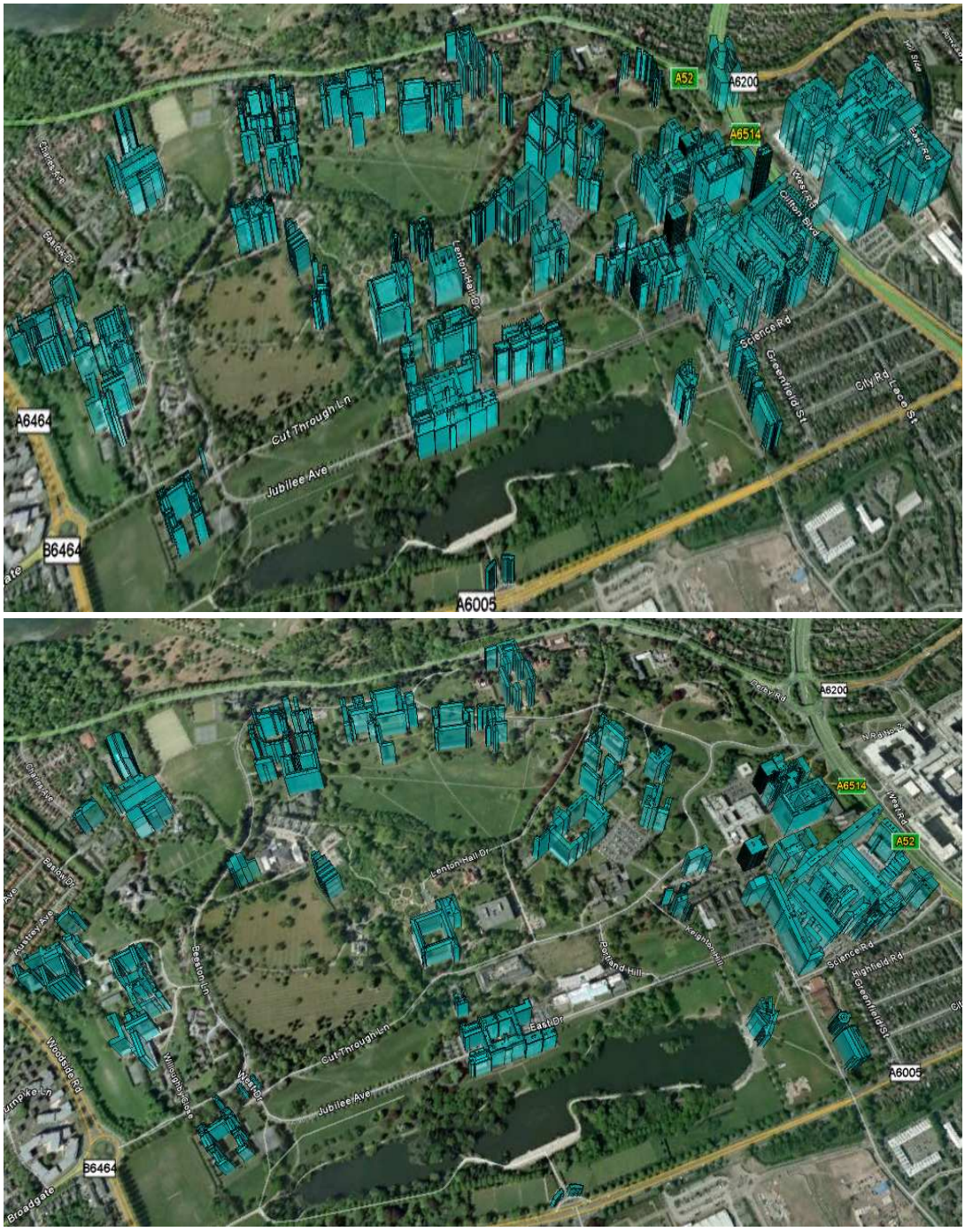

Figure 6.14: 3D building models matched their places on Google Earth; 3D models of UltraCamD block (top) and 3D models of vertical Pictometry block (bottom).

When reconstruction of 3D models was performed, simplification (excluding some of the small roof details) was needed to decrease the amount of data for later visualization purposes especially for UltraCamD block. Simplification is usually based on the LoD required for the purpose of

identification and navigation at street level and from bird's-eye view of the model.

6.2.3 Extraction of 3D geometry from oblique imagery block

Extraction of 3D geometry from the oblique images was not possible because some roof outlines cannot be seen due to the tilt of the oblique images as can be seen in figure 6.15.

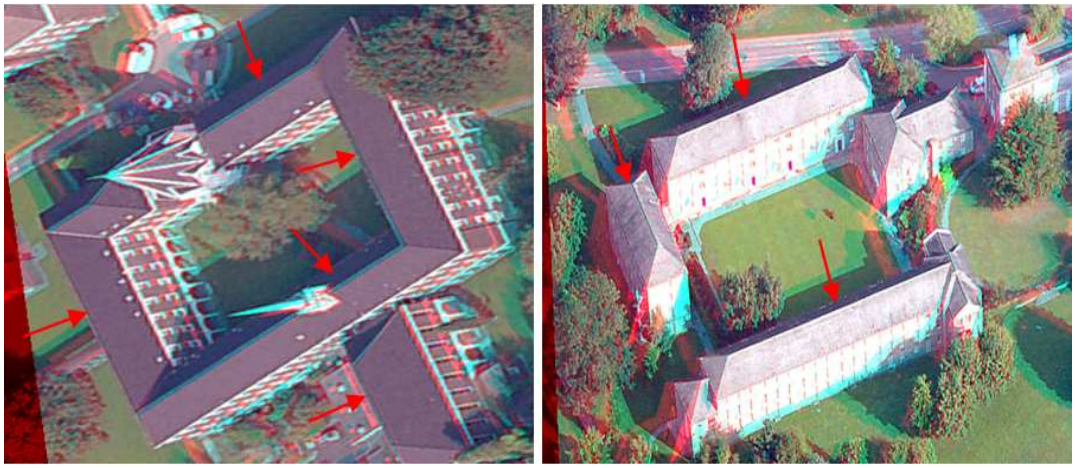

Figure 6.15: Some blind (dead ground) roof outlines in Pictometry oblique images identified by red arrows.

However, the availability of oblique imagery during digitization provided additional information for the interpretation of geometry by allowing each building to be seen from different angles. This is especially proven to be very beneficial where objects are partially obscured or where vertical displacement makes the building footprint is difficult to identify in vertical imagery block. Oblique images were also of a great benefit in helping the interpretation of building outlines where differences in building height required digitizing of separate polygons.

6.3 Accuracy of 3D models extracted from Pictometry imagery

The accuracy assessment of the 3D models reconstructed from vertical Pictometry imagery will be performed qualitatively and quantitatively.

6.3.1 Qualitative evaluation of the Pictometry 3D models

The qualitative evaluation includes a visual comparison between the reconstructed buildings from the vertical Pictometry imagery and the BM building models. This comparison will provide a useful indication of the overall quality. It is important to mention here that only a selection of the most interesting models, which show some visual differences, will be illustrated in this section. The qualitative comparison for the reconstructed buildings in the University main park is given in figure 6.16 and figure 6.17.

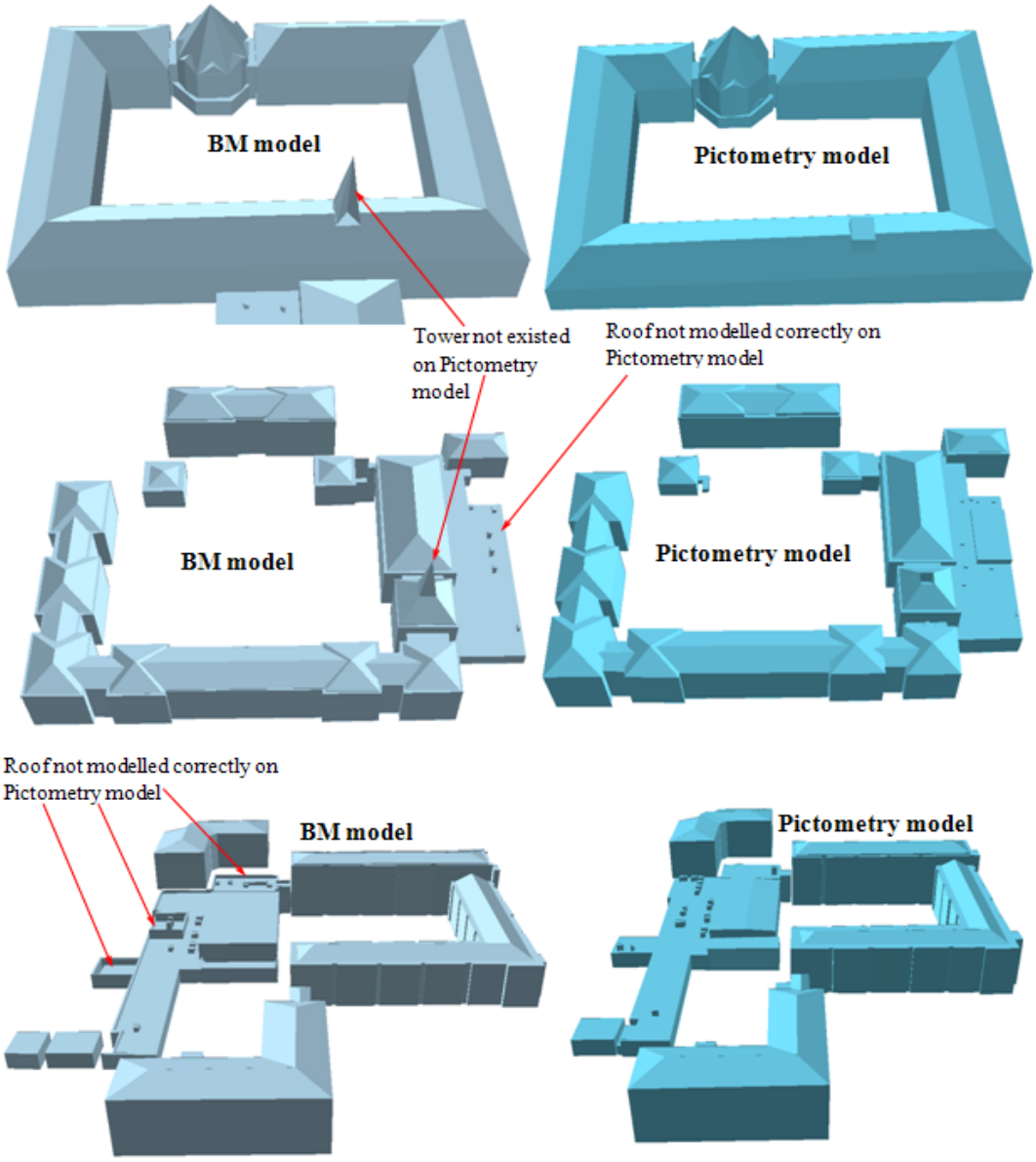

Figure 6.16: Qualitative comparison between the UltraCamD 3D models (BM) and the vertical Pictometry 3D models for Nottingham University main campus.

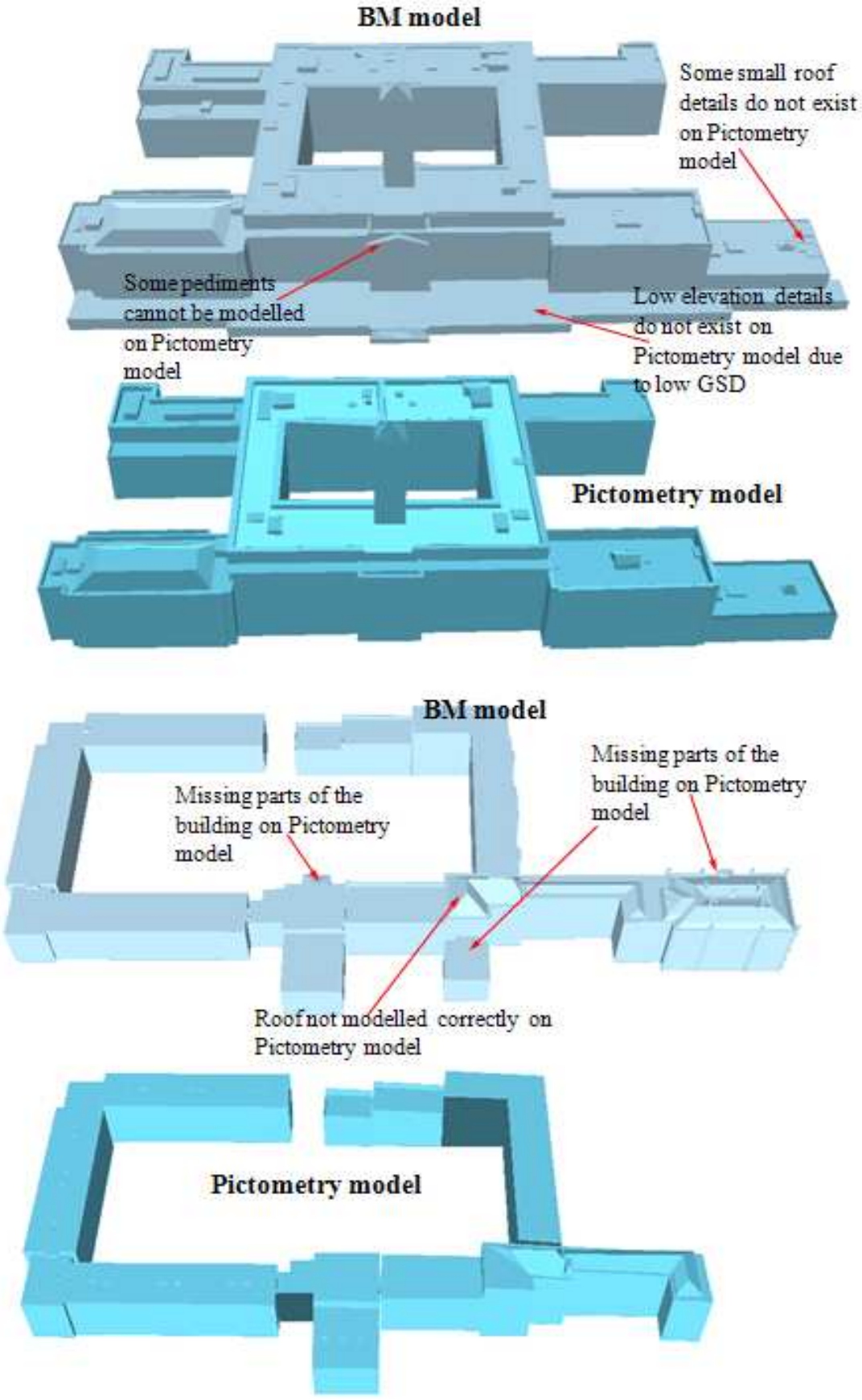

Figure 6.17: Qualitative comparison between the UltraCamD 3D models (BM) and the vertical Pictometry 3D models for Nottingham University main campus.

Figure 6.16 and figure 6.17 only show a selection of the reconstructed buildings that showed significant differences between BM models and Pictometry models. Most of the buildings in the study area showed minor differences that are not easy to be distinguished visually. Nonetheless, the qualitative assessment of the reconstructed building models depicted above (figure 6.16) indicates the impressive overall quality of the 3D models reconstructed from Pictometry imagery. The buildings were reconstructed to a higher level of detail and accurately with most roof details present, like dormer windows, ventilation units, and chimneys. Nevertheless, there are certain cases where the Pictometry models are missing some roof details especially the towers over some buildings which have very fine top ending. This is due to low contrast of the towers top parts. On the other hand, the bases of the towers were modelled correctly. In addition, there are some missing building parts due to not being able to model them because roof outlines were not clear on Pictometry images block. This is because of low GSD compared to UltraCamD.

Overall, the level of detail for the 3D models derived from the Pictometry images block is comparable with the level of detail acquired from the UltraCamD images block bearing in mind that the GSD of Pictometry images, although it is suitable for extraction of 3D building geometry with some fine details, is larger than that of UltraCamD images and therefore less efficient.

6.3.2 Quantitative evaluation of the Pictometry 3D models

The 3D building polygons extracted from Pictometry imagery will be compared with the benchmark (BM) polygons (extracted from UltraCamD) to better understand the planimetric accuracy of the building footprints and height accuracy of the roof planes of the relatively new imaging system.

A total of 977 points (vertices) in 99 buildings, which occur both in vertical Pictometry block and UltraCamD block, were used with their X and Y coordinates in the planimetric accuracy comparison. In addition, 762 vertices in 99 buildings were used with their Z coordinate in the height accuracy comparison. Figure 6.18 shows an example of roof outlines of buildings imposed over each other. These roof outlines were extracted from UltraCamD and Pictometry images. They were used to provide the Planimetric comparison

between the two data sets. Figure 6.19 shows a sample of some buildings' roofs with some vertical exaggeration to show the height differences.

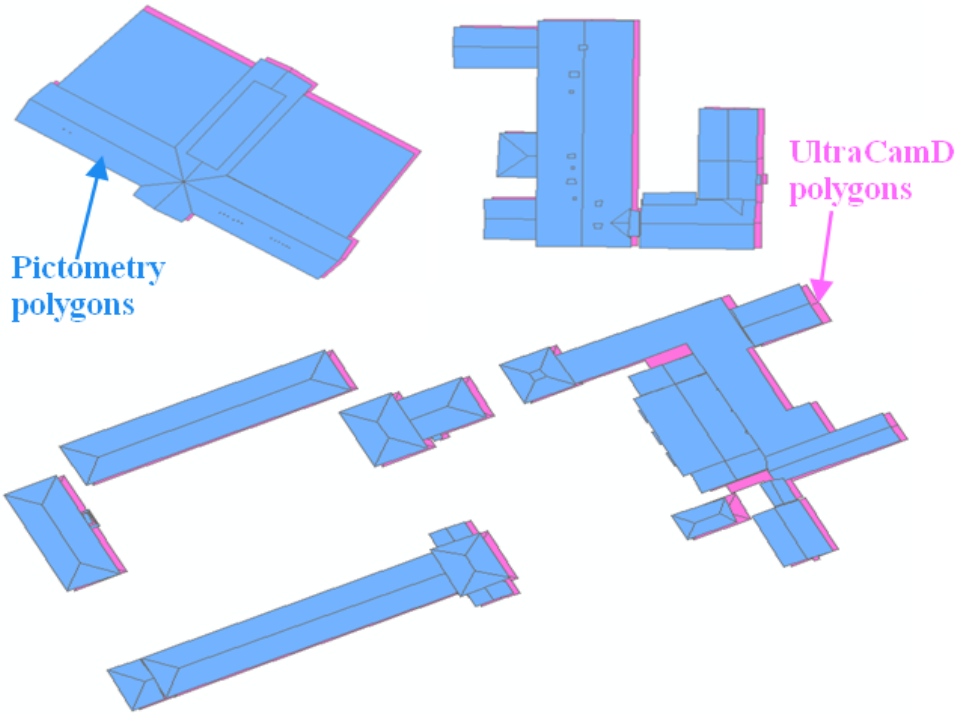

Figure 6.18: Two roof outlines imposed over each other to be used for Planimetric comparison.

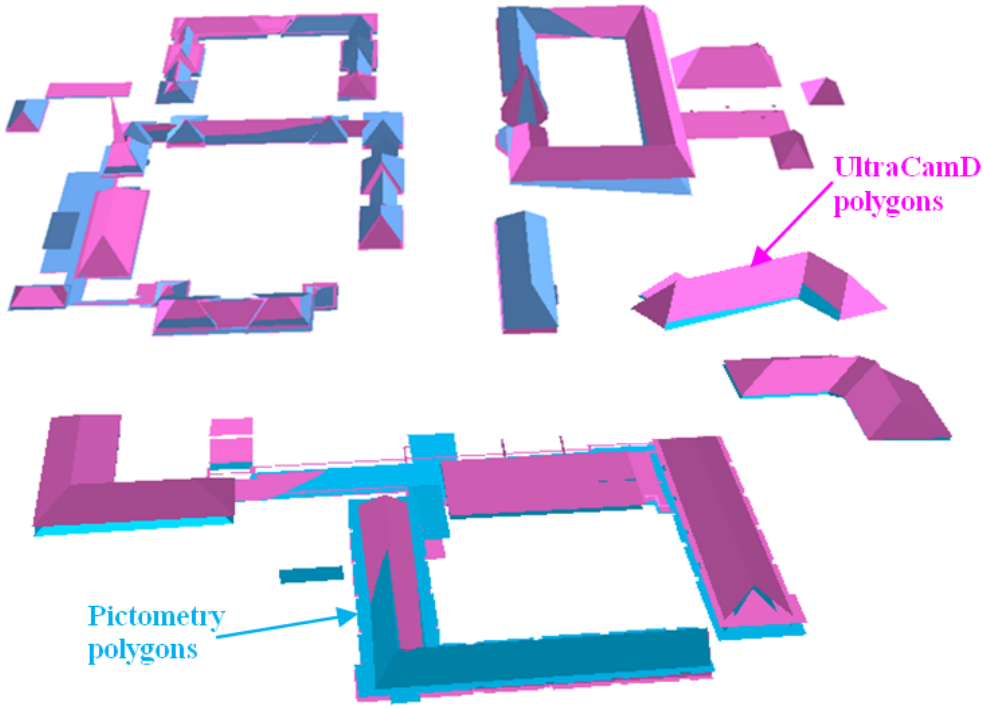

Figure 6.19: Buildings' roofs with some vertical exaggeration to show the height differences between the two camera systems.

Graphical representations of the planimetric differences between UltraCamD and Pictometry 3D polygons are shown in figures 6.20, and 6.21 for X, and Y respectively. Graphical representation of the height differences is shown in figure 6.22. Table 6.3 shows a summary of the statistical results achieved from the comparison.

Table 6.3: Results of comparing 3D polygons extracted from Pictometry and UltraCamD.

Component	X	Y	Avg. Z
Min.	-0.960	-0.800	-2.380
Max.	0.582	0.590	2.300
Mean	-0.057	-0.234	0.367
St.dev.	0.286	0.187	0.952

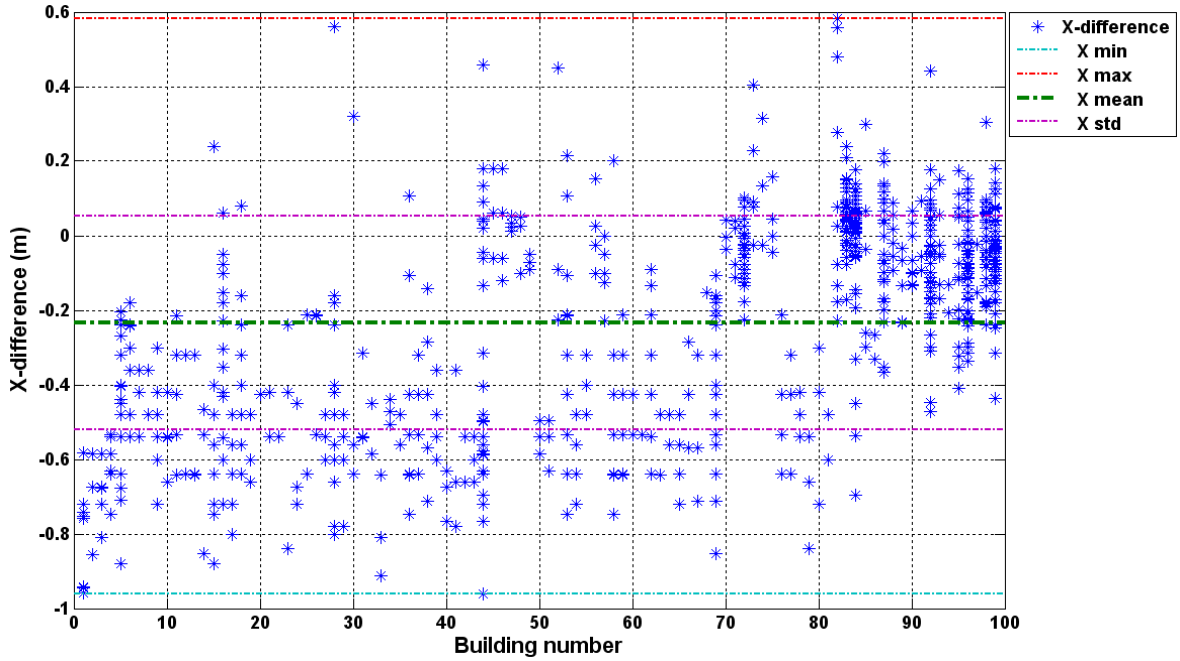

Figure 6.20: Differences in X-component between UltraCamD and Pictometry 3D polygons.

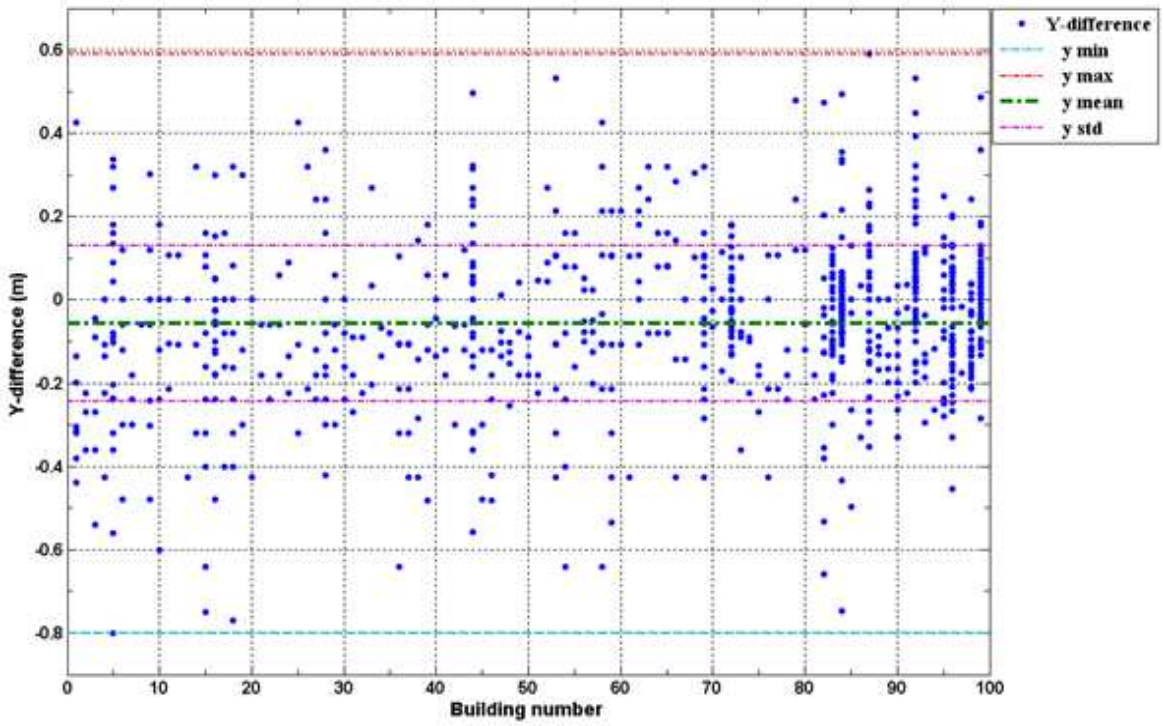

Figure 6.21: Differences in Y-component between UltraCamD and Pictometry 3D polygons.

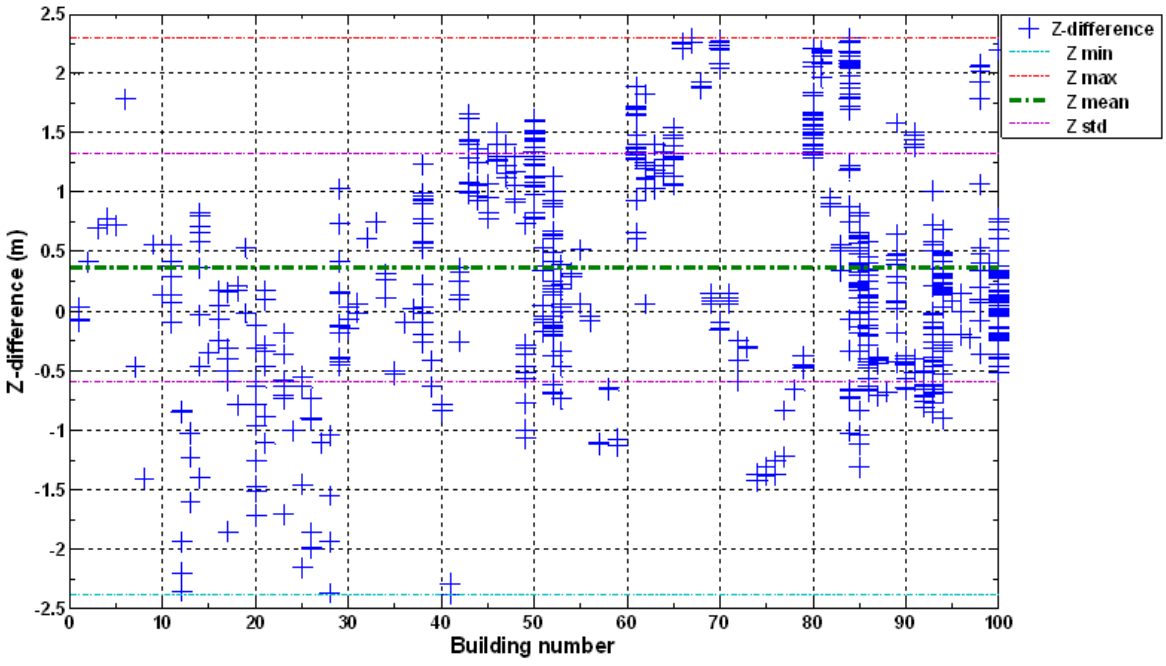

Figure 6.22: Differences in Z-component between UltraCamD and Pictometry 3D polygons.

ArcGIS tools (ArcScene, ArcMap, and ArcCatalogue) along with some Visual Basic scripts have been used to compare the areas of the building footprints extracted from Pictometry with those from UltraCamD. Figure 6.23 depicts the extracted building outlines from both camera systems overlaid on each other to be used in ArcGIS environment for the area comparison. 767 difference polygons resulted from comparing the footprints of the 99 buildings extracted.

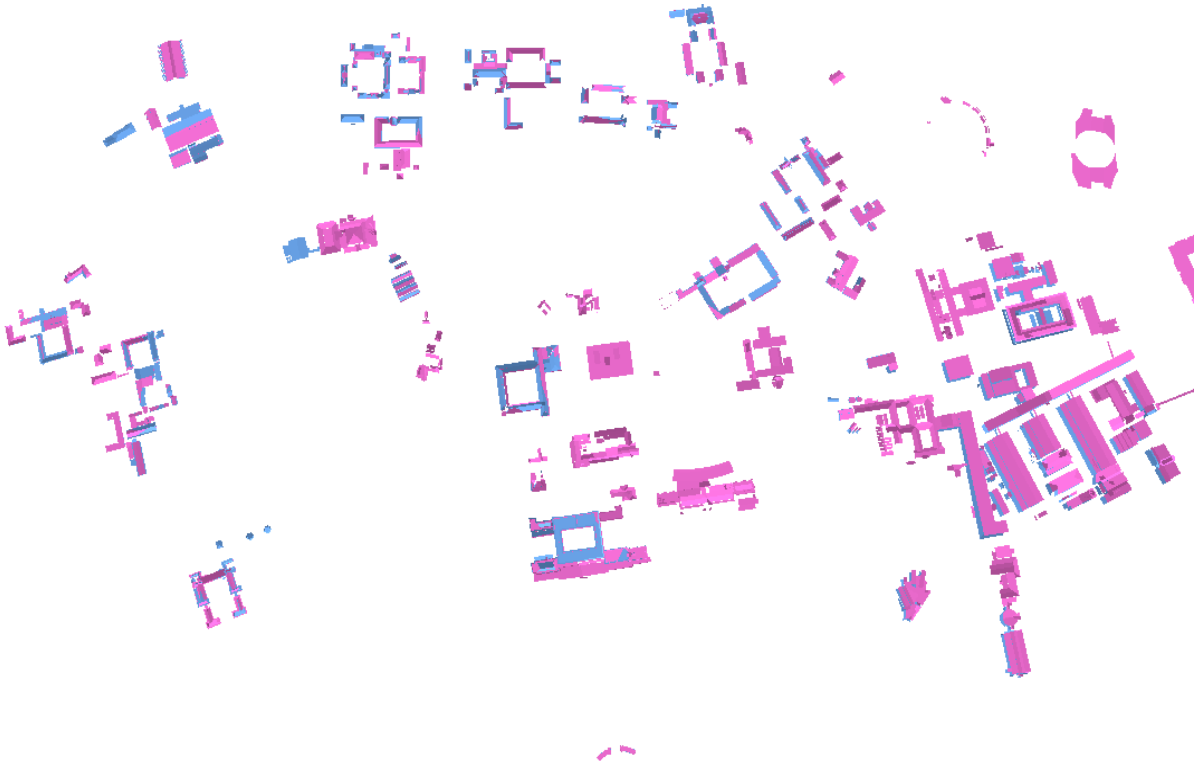

Figure 6.23: Building outlines from both camera systems imposed over each other to be used in ArcGIS for the area comparison.

Comparing the areas of the building footprints in ArcGIS requires many steps and tools such as buffering, erasing and multipart to single part tool. The buffer tool creates buffer polygons to a specified distance around the input coverage features. It is used to select features within a specified distance of a feature; for example, if a building consists of 2 parts or more, using erase function without buffering will take only one part of that building while using buffering will ensure the whole building will be included in the erase operation. Erasing operation is used to get the difference between any two building outlines. The first input in this operation is the UltraCamD feature

polygons (the ones whose features will be erased from). The Second parameter is the feature class with the features that will be erased (Pictometry polygons). The methodology involves creating a union between the erased feature class and the main feature class which needs to have the features removed from. An erased feature class is created based on the non-erased feature class structure. Then Visual Basic scripts are used to calculate the areas of the remaining features (the difference between the building two footprints). Figure 6.24 shows the footprints of the old IESSG building imposed over each other, the difference between the two polygons of one part of the building, and the resulting feature after performing the erase function.

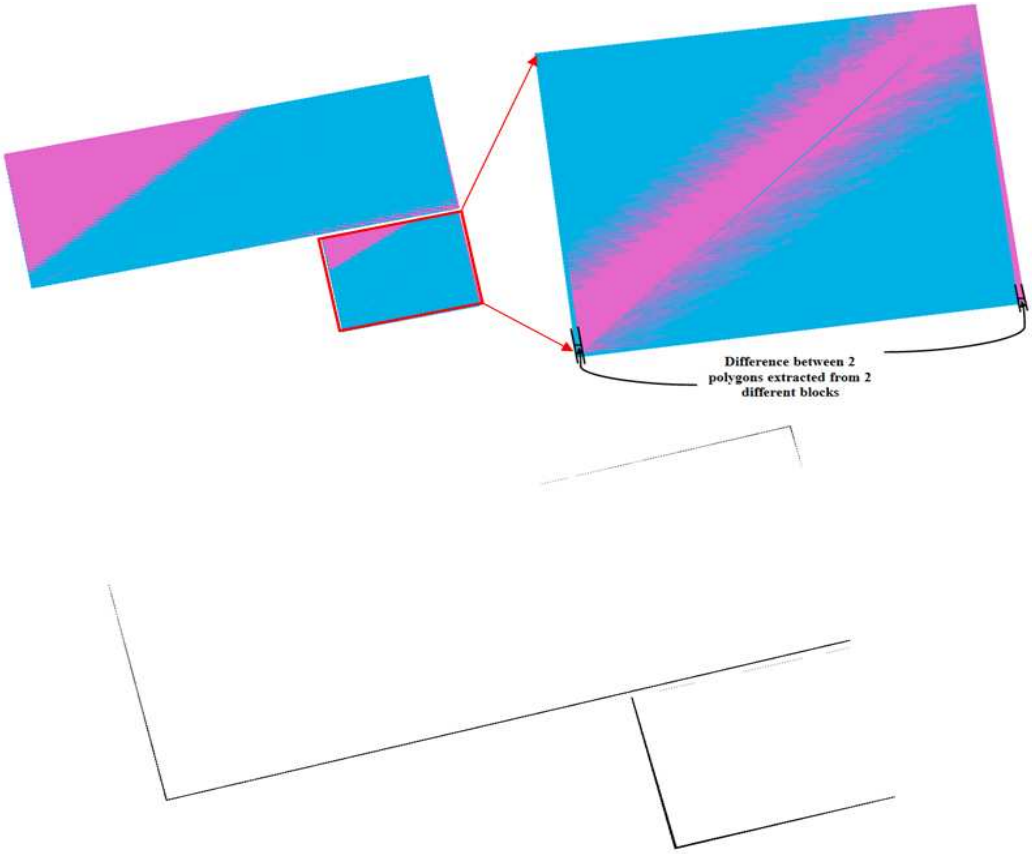

Figure 6.24: Footprints of the old IESSG building imposed over each other (top left), the two polygons of one part of the building zoomed in to show the difference in footprints (top right), and the resulting feature after performing the erase function (bottom).

After performing the erase function and before calculating the areas, multipart to singlepart function has to be used to separate multipart features into separate

singlepart features. This ensures the area calculation of every part of the difference features. For example, in figure 6.24 the area of the difference between the building two footprints (bottom figure) will normally be calculated as one area while when using multipart to singlepart function, the area will be calculated for every single part of the difference (here 3 parts and hence 3 areas). Figure 6.25 illustrates the multipart to singlepart function and graphical representation of the area differences between UltraCamD and Pictometry 3D polygons is shown in figure 6.26.

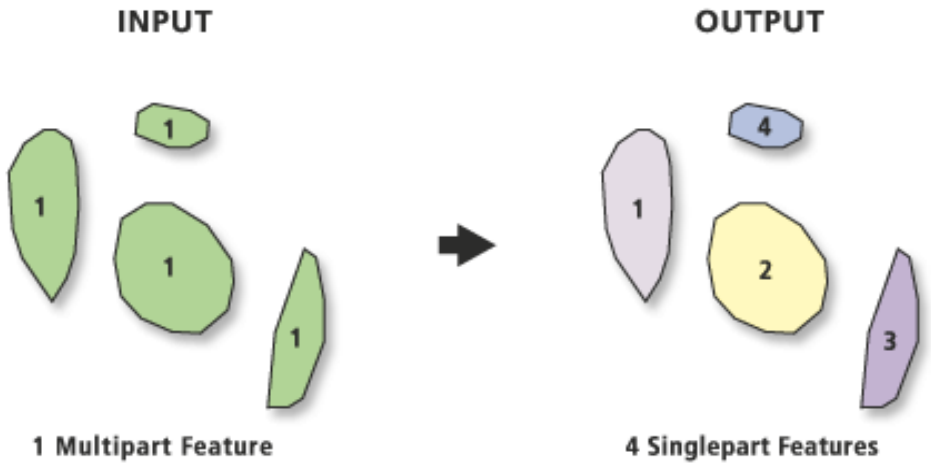

Figure 6.25: Multipart to singlepart function, adapted from ArcGIS manual.

The erase operation is performed only where the buildings overlap and therefore the calculation of the area differences does not take into account differences in the footprint of the buildings and buildings that do not exist in Pictometry block. Figure 6.27 shows some examples of the remaining building footprints after conducting the erase operation.

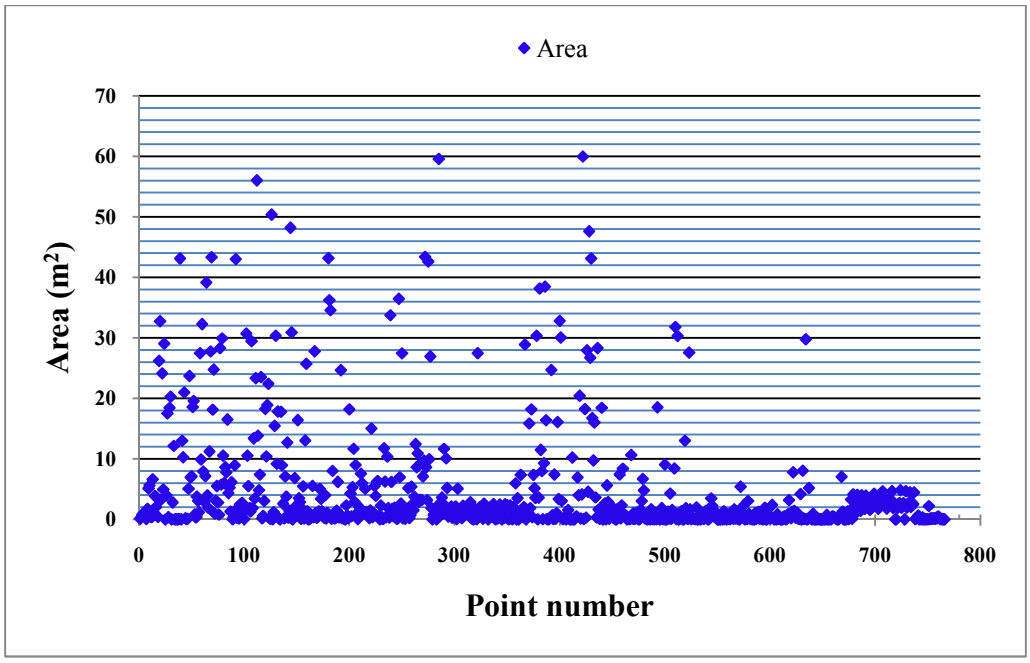

Figure 6.26: Differences in area between UltraCamD and Pictometry 3D polygons.

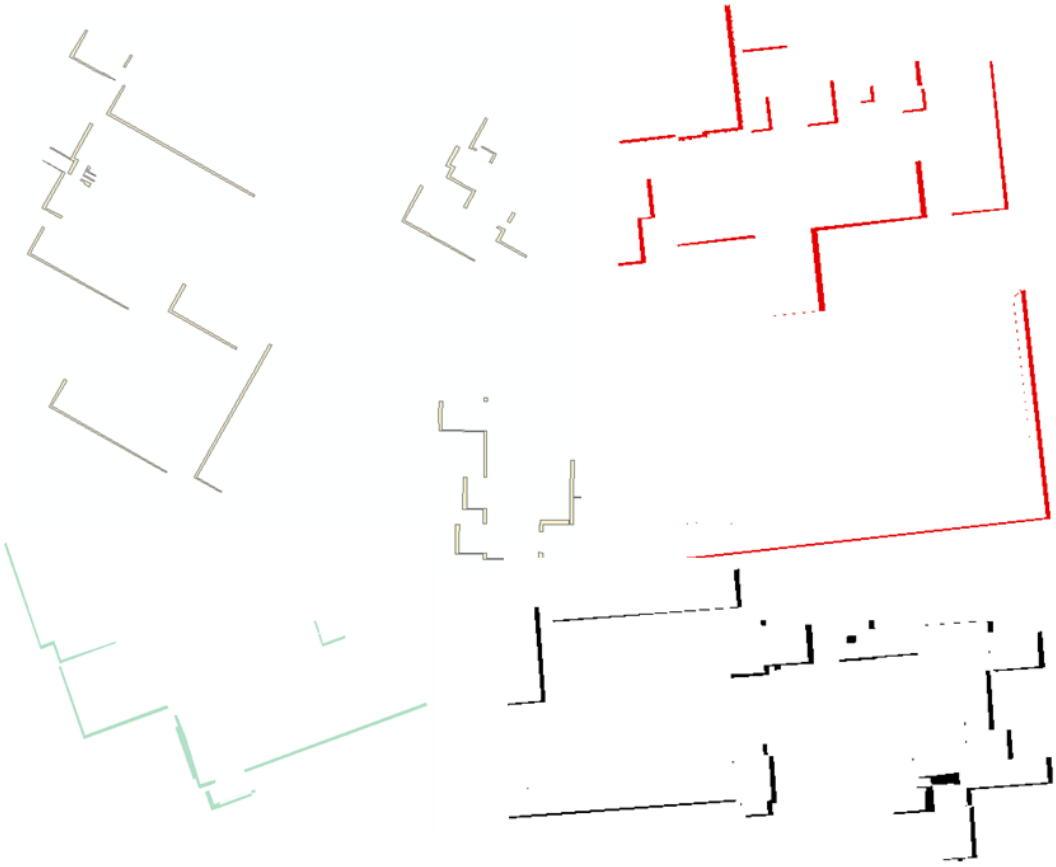

Figure 6.27: Examples of the remaining building footprints after conducting erase operation.

The differences in easting varied from -0.960 to 0.580m with a mean of -0.057 m and standard deviation of 0.286m while the differences in northing varied from -0.800 to 0.590m with a mean of -0.234m and standard deviation of 0.187m. The height differences between 3D polygons extracted from Pictometry and UltraCamD are worse than the planimetric components. They varied from -2.380 to 2.300m with a mean of 0.367 and standard deviation of 0.952m. Furthermore, the differences in area varied from 0.00 to 60m^2 with a mean of 4.86m^2 and a standard deviation of 9.33m^2 with 90% of the polygons have area differences of less than 10 m^2 which is very good taking into account the polygons lengths. As the polygons used in the comparison have different size, it was necessary to normalize the results of the area differences by dividing them by the area of the polygons to negate the effect of the size on the data. The mean of the normalized values is 0.034, the maximum is 0.198 and the standard deviation is 0.049.

These figures show that Pictometry produced good results especially in X and Y directions taking into consideration the GSD differences between the two imaging systems. The above differences may not be in the accuracy of measurement but could be in the interpretation and identification of features. The standard deviation for height measurements is approximately four times the standard deviation for northing and three times the standard deviation for easting. This difference is best explained by misinterpretation of ground level when extruding the roof outlines of Pictometry extracted outlines to the ground level in Stereo Analyst. Height accuracy is also directly related to the base to height (b/h) ratio and to the point measurement accuracy. The b/h ratio for both vertical Pictometry and UltraCamD imagery is the same (0.2), but the point measurement accuracy of UltraCamD images is better than that of Pictometry images as the GSD of UltraCamD is better (5cm versus 15cm) and the radiometric quality of UltraCamD images is much better (related to the camera type), hence, the large standard deviation for height measurements.

It is important to mention here that the calculation of height measurements was not performed using Pictometry software (EFS), because it is based on the DTM, the accuracy of which is not known. In addition, it was realized during the height measurements, using EFS, that the same height measured on

different images (vertical and different obliques) gave different results which indicates the poor quality of the DTM used for terrain height (did not adequately model the terrain).

These differences would be acceptable for the purpose of navigation, tourism, real estate, emergency services, etc. Moreover, the accuracy achieved from Pictometry data is quite good even for other application purposes where accuracy level may be more significant. It may be good for many engineering activities but may not be good enough for high accuracy work.

Building reconstruction using Pictometry vertical imagery produced impressive results with most building models visually correct. The imagery seems to be very reliable in producing 3D models. The amount of reconstructed roof details is impressive since most ventilation equipment, dormer windows and chimneys were reconstructed in almost all cases. The level of detail of the 3D building models is directly related to the GSD of the imagery used.

6.4 Texture mapping of the 3D models of the study areas

In texturing, normally colour images are mapped onto a 3D geometric surface. Knowing the parameters of the interior and exterior orientation of the images in the coordinate system of the geometric model, the corresponding image coordinates are calculated for each vertex of a triangle on the 3D surface. Then grey-scale or colour RGB values within the projected triangle are attached to the surface.

Texture mapping of the 3D models of both study areas was carried out in Texel Mapper. The Texel Mapper software allows the operator to map 2D textures onto Stereo Analyst-derived 3D models. The steps of texturing the models using Texel Mapper are as follows:

- Input the 3D Shapefile: type the path to the 3D shapefile to be textured.
- Input Block: type the path to the block file to use as texture on the shapefile. This step is performed if auto-texturing from photogrammetric block will be used rather than manual texturing. Auto-texturing allows the operator to automatically texture a shapefile by creating a Textured Vector Symbology (TVS) file from a 3D shapefile and a block file. TVS file stores the textures for each polygon on the shapefile for display in 3D visualization programs.

- Set the desired texture quality: this is related to the image quality level to be used when loading the textures. A lower texture quality provides faster load times and may be necessary when loading large data sets. Higher texture qualities provide better looking images, but may affect the video memory for large data sets which results in a very slow performance.
- Output Texture Symbology: choose the name of the TVS file to create. When a Shapefile has a corresponding TVS file, all of the mapped textures can be saved into the TVS file. This allows the operator to search through all of the possible images that can be used to texture the model and select the image that best suits it.
- The final step is to apply the texture to the current 3D model: this applies the estimated best image, at the selected texture resolution, to the current model. The software automatically estimates which image in the TVS file can provide the best texture for the selected model.

Texturing of the 3D polygons was performed using vertical Pictometry block, oblique Pictometry block, UltraCamD block, combined Pictometry block, and combined UltraCamD and Pictometry block.

6.4.1 Texturing the 3D models using vertical imagery

Automatic texturing of the 3D polygons was performed separately using the vertical Pictometry block only and then the UltraCamD block only following the workflow described in section 6.4. This is to check the suitability of using vertical Pictometry imagery in automatic texture mapping and compare the results with textured models using the high quality UltraCamD imagery, figure 6.28.


Textured using UltraCamD block

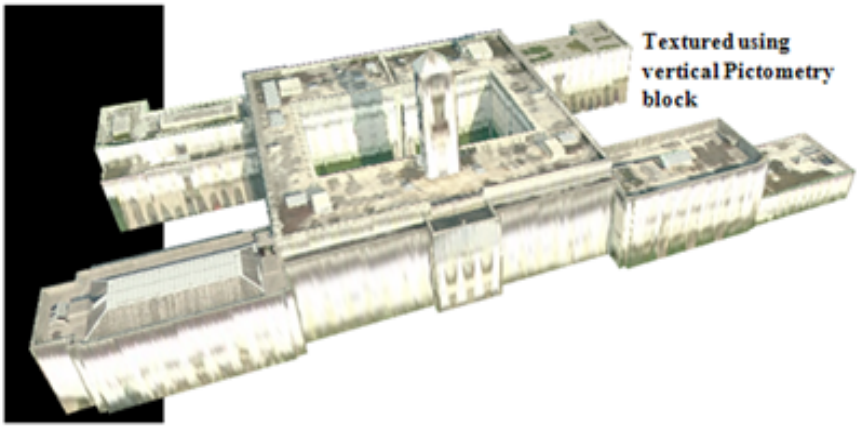
Textured using vertical Pictometry block

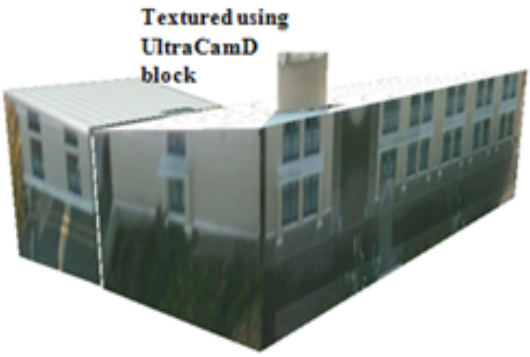
Textured using UltraCamD block

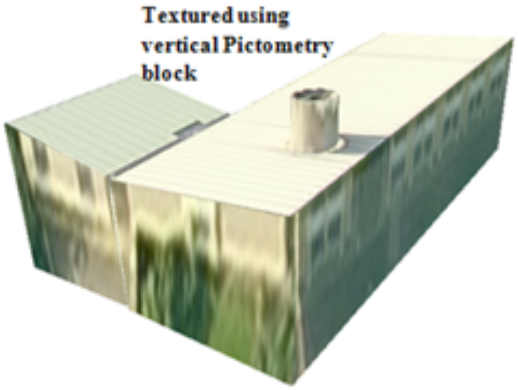
Textured using vertical Pictometry block

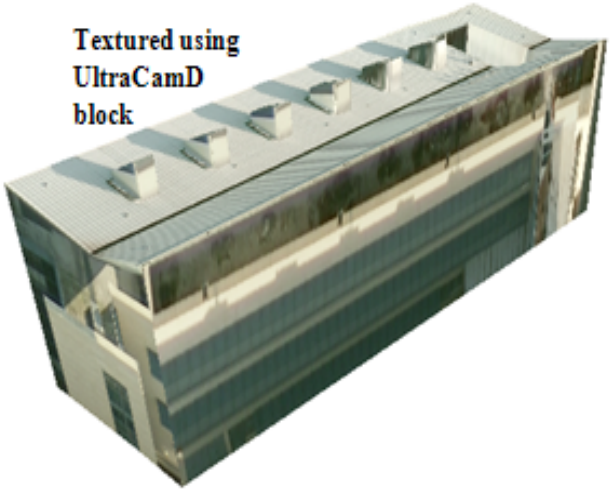
Textured using UltraCamD block

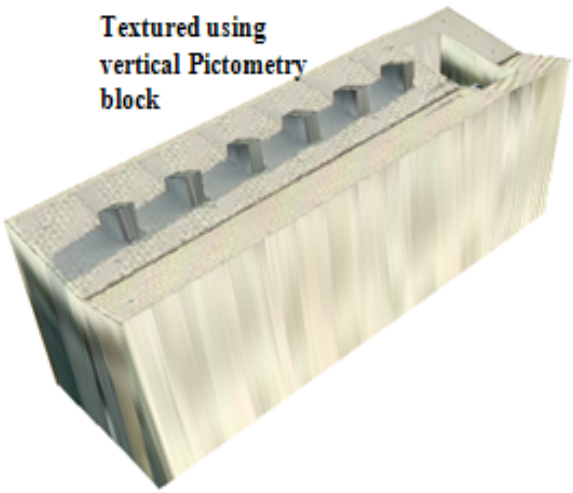
Textured using vertical Pictometry block

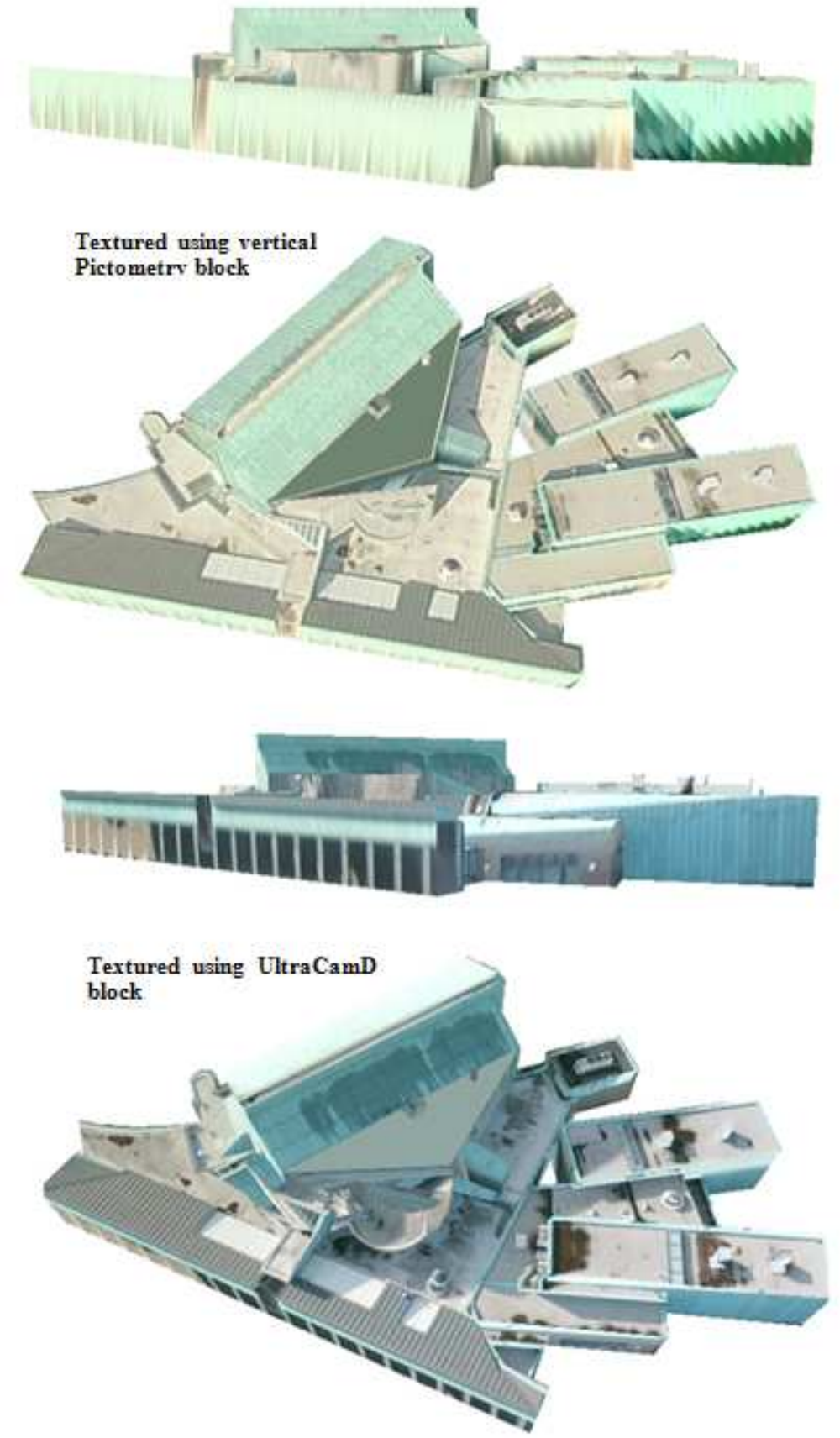

Figure 6.28: Comparison between texture mapping of some buildings in the University campus using vertical Pictometry and UltraCamD.

The visual inspection of the textured models show that using either vertical Pictometry block or UltraCamD block has given very good roof structure but when it comes to facade texturing the quality was not as good as roofs quality; the texture quality of the building facades is considerably degraded. This is because vertical images provide excellent views of roofs and depicts some of the building facades when located away from the nadir on the images only due to perspective effects. The resolution of image patches of walls is also too low in vertical images. There are usually too few vertical images available to cover all building sides. Although vertical Pictometry block has produced very good quality textures of roof tops, the quality produced by UltraCamD is better especially when it comes to facades. Figure 6.28 shows that both data sets produced high quality roof tops, but UltraCamD produced a little better texture for roofs which is related to the 3D geometry. The amount of details included in the 3D models is affected by the resolution of imagery which is much better in case of UltraCamD. The texture of facades when UltraCamD was used is better than that of vertical Pictometry. Texture quality is equivalent to the quality of the aerial photographs used. The vertical imagery even with 60% overlap (UltraCamD images) proves to be inadequate for facade texture mapping which in most cases is significantly distorted except for a few cases.

6.4.2 Texturing the 3D models using oblique Pictometry block

To enable visualization, particularly in urban areas with deep building canyons, the most appropriate viewing angle is often from the air looking obliquely at the ground and faces of the surrounding buildings. Oblique photos give an excellent view from the sky as the substantial tilt of oblique imagery leads to a high exposure of facades in the images making this kind of imagery well suited for texture mapping purposes. Moreover, the airborne cameras can fly over cities at a higher speed and not disturbed by the ground traffic.

Texture mapping buildings with the aid of aerial oblique imagery may be performed in many different ways. Wide-angle vertical images provide an oblique view at their edges, which may be used for automated texture extraction (Zebedin et al., 2007). Alternatively, modern 3-line scanners such as ADS40 provide oblique views with their forward and backward looking

channels, enabling an automated generation of 3D textured facades (Hirschmuller et al., 2005). However, to ensure that all sides of buildings in a city area are covered, it is necessary to utilize multiple images from different viewing angles; hence, the use of the oblique Pictometry imagery.

Furthermore, using Pictometry imagery offers a greater coverage than terrestrial imagery (digital camera, video, or panoramic images) as it ensures including facades that are not accessible from the ground. Moreover, the use of a single data set (Pictometry) in automatic texture mapping of 3D models has the potential to reduce the occurrence of radiometric differences, resolution differences, variations due to time of capturing and lighting conditions because adjacent textured faces from different data sets would appear disjointed, figure 6.30, while seams between different aerial images are mostly invisible. Using one data set will also ensure that the texture is homogeneous and the radiometric enhancement is no longer needed.

When only the block of oblique images was used for texturing the 3D models, the facade texturing was of very good quality, figure 6.29, but the texturing quality of some buildings' roofs was reduced compared with the vertical images, figure 6.30.

Figure 6.29: Some buildings textured using only oblique images block, (left) from Nottingham city centre and (right) from University campus.

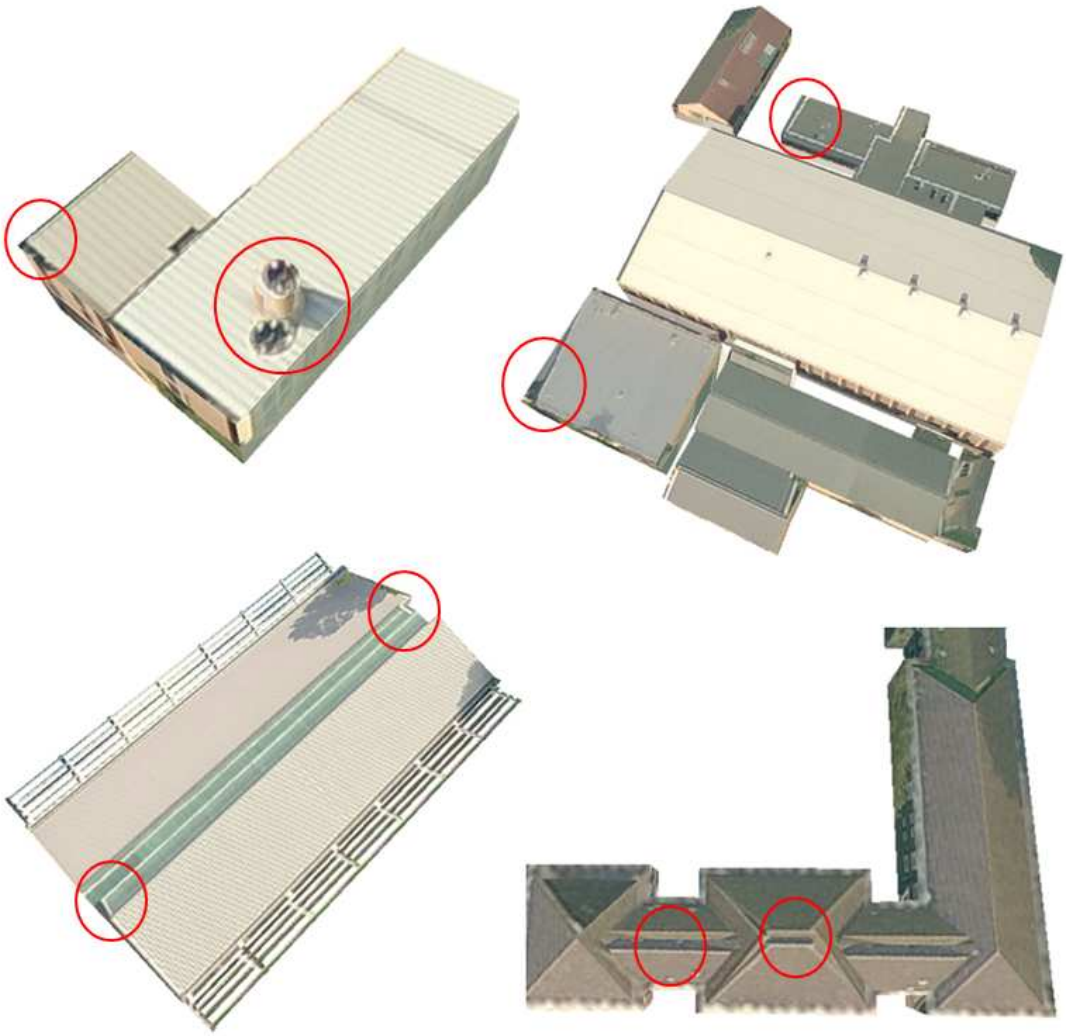

Figure 6.30: Some of the University campus buildings textured using oblique images block; the red circles show where the texturing went wrong.

6.4.3 Texturing the 3D models using combined Pictometry block

Despite providing multiple viewing angles, oblique airborne images are not always enough for texturing 3D models properly especially the rooftops. To ensure that all building facades and roof tops in an area are covered and properly textured, it is necessary to utilize multiple oblique and vertical aerial images with different viewing angles. Zhang et al. (2005) and Frueh et al. (2004) concluded that it is necessary in this case to cope with most parts of a model being visible in several images, under varied viewing angles, resolutions, and potentially different lighting conditions.

To achieve photo-realistic rendering, texture has to be acquired and mapped in a separate process. Previous methods have decoupled the problem into texturing building tops using vertical views of the roofs, and texturing facades by utilizing ground-based images. In this case, roofs and terrain are often texture mapped with top-down aerial images, and building sides that are not accessible from ground-level are not textured. However, the successful combining of both vertical and oblique images in one block gives the benefit of good quality textures for both the roofs and facades and provides an excellent opportunity to produce an efficient method of high quality urban model texturing.

Texturing theory when using combined vertical and oblique images block is as follows; after all buildings are successfully reconstructed and the precise camera parameters of each image (EOP) have been also determined from block AT, the reconstructed 3D models can be back-projected onto the image; thus textures of building facades can be retrieved. Where a facade appears in multiple images, an image with maximum projected area is selected for providing the corresponding texture. Texture for building rooftops is mapped from the vertical images. It is usually taken from the middle image among all the target images in which it is visible as in vertical images the shortest distance to the ground is usually directly at the centre of the image and the distance to the ground on two opposite edges of the image is roughly the same, figure 6.31. The use of images with large overlap enables the best nadir view of an area. However, in oblique images this changes according to how much the camera is tilted from nadir, figure 6.31. As can be seen from figure 6.31 the distance to the ground in the lower part of the oblique image is small, whereas the distance to the ground in the upper part is bigger. Since the geometric resolution of image patches of facades from vertical images is often lower than that in the oblique ones and as there is a wide range of resolutions within each oblique image, the best texture of the visible facade is auto-selected and mapped from the oblique images.

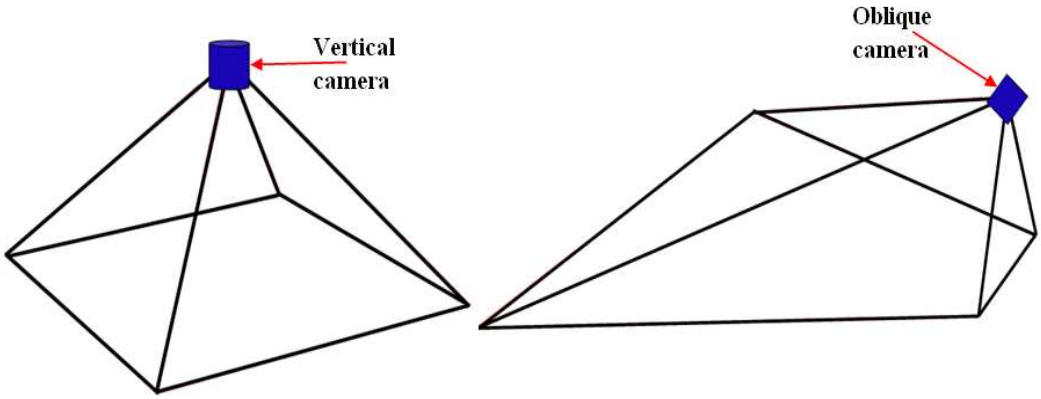

Figure 6.31: Visible surface (viewing frustum) from vertical camera viewpoint (left) and from oblique camera viewpoint (right).

Figure 6.32 depicts some of the 3D models in both study areas texture mapped using the combined vertical and oblique Pictometry images block. Combining both vertical and oblique images gives the benefit of very good quality textures for both the rooftops and facades as the texture is automatically chosen from the image that has the maximum projected area and ideally from the image that has approximately the same orientation as the 3D polygon (taken from a direct, perpendicular view). From the models presented in figure 6.32, with very few exceptions, the automatically textured building models using the combined images block achieved high quality for the roof and facade textures. Furthermore, areas texture mapped with different images (vertical and different obliques) align nicely with each other and seams are mostly invisible. This is due to the fact that all used images were acquired within a short period of time and hence under very similar lighting conditions.

Some of the University Park textured 3D building models

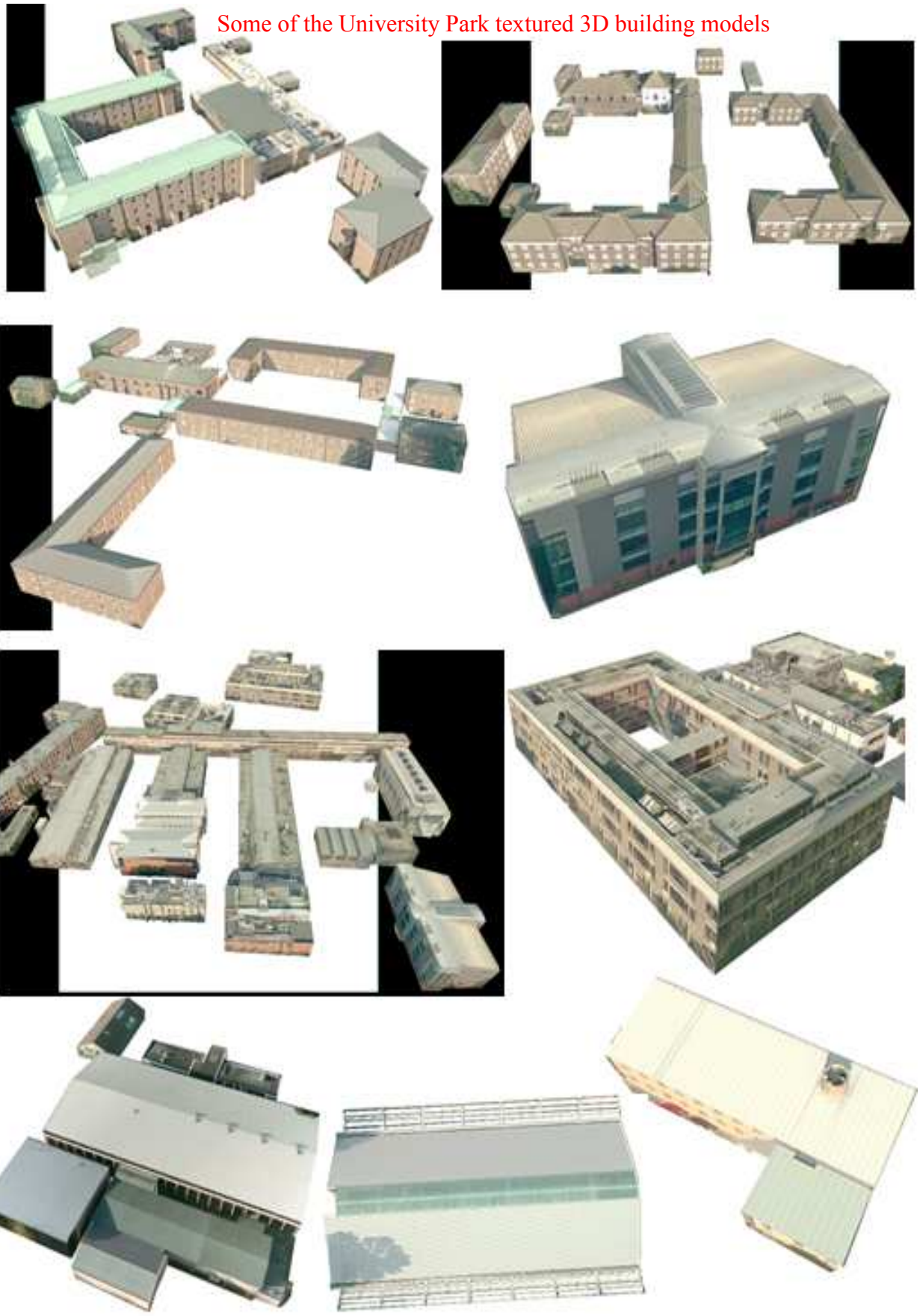

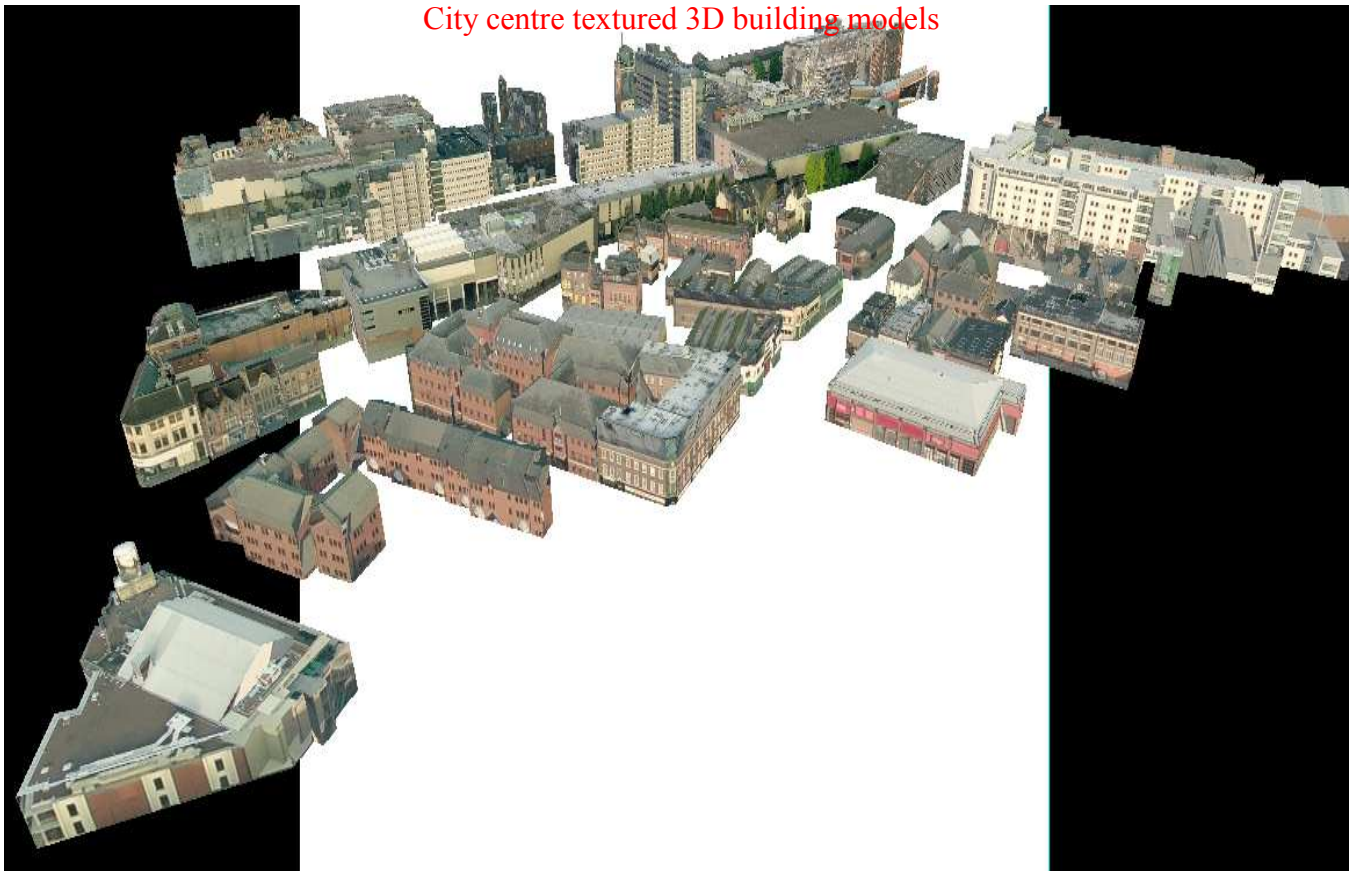

Figure 6.32: Some 3D building models textured using the combined vertical and oblique Pictometry images block. The upper part is for some of the University campus buildings while the lower bottom part is for Nottingham city centre. The bottom row of the upper buildings shows the same buildings as in figure 6.30 but with very good quality roof texture.

6.4.4 Texturing the 3D models using combined UltraCamD and oblique Pictometry block

Automatic texture mapping of the 3D polygons was also performed using the combined UltraCamD and oblique images block following the workflow described in section 6.4. This is to compare the results with textured models using the combined Pictometry images block. Figure 6.33 shows some 3D polygons that have been textured using the combined UltraCamD and oblique images block.

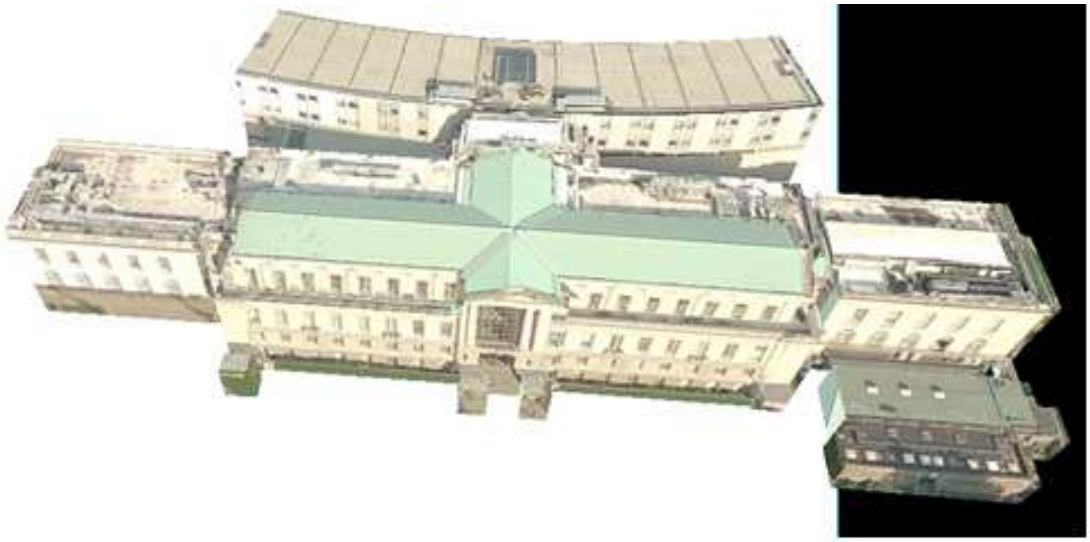

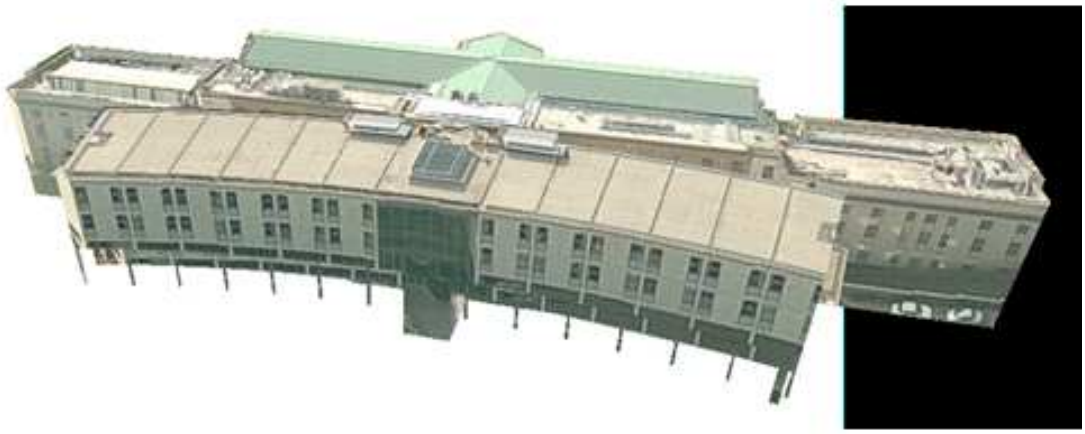

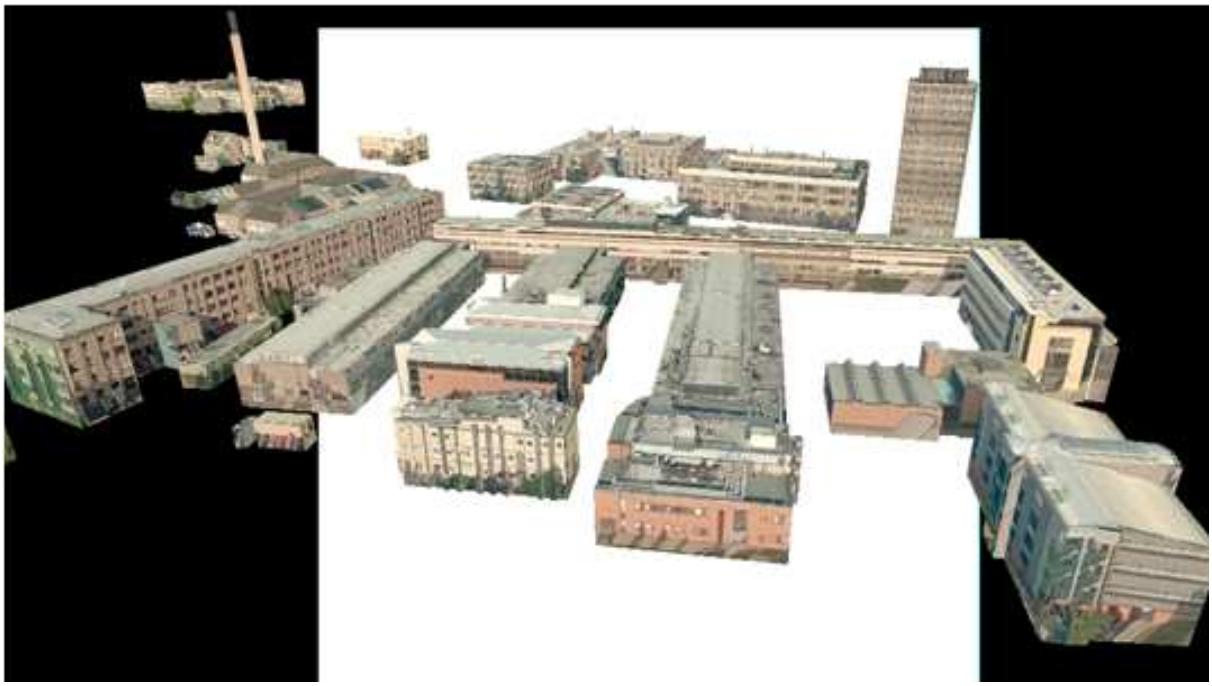

Figure 6.33: Some 3D building models textured using the combined UltraCamD and oblique images block.

As can be seen from figure 6.33, the combined UltraCamD and oblique images block gave superior texture quality for both facades and rooftops. Compared to the models textured using the combined vertical and oblique Pictometry images block, both blocks produced high quality roof and facade textures with a few exceptions where the combined UltraCamD and oblique images block gave better roof textures as might be expected. The amount of roof details that can be extracted from UltraCamD images is much more than that from vertical Pictometry images. This is due to the difference in GSD between the two data sets; hence, as stated in section 6.4.1, texture quality is equivalent to the quality of the aerial images used.

6.5 Analysis of results

Though it is an astounding experience to see this incredible amount of detail on the 3D building models especially when using one data set of vertical and oblique images together, some of the 3D models contain errors especially in terms of texturing. This section will highlight some problems that caused some textures to have lower quality.

- Features are mainly extruded based on roof footprint; this can miss features under overhanging roofs.
- The Atmospheric effects, such as haze, reduce the information content of aerial images. The overall quality of the Pictometry images is characterized in some instances by the presence of haze which affects the texture mapping quality. Figure 6.34 shows textured facades which are affected by the haze in the images used for texturing.
- Buildings with internal quadrangles, which are very challenging to texture from airborne images. Figure 6.35 shows an example of these buildings.
- The effect of dead ground; area that cannot be seen from the aerial images due to shadow or perspective view. Figure 6.36 shows an example of these buildings.

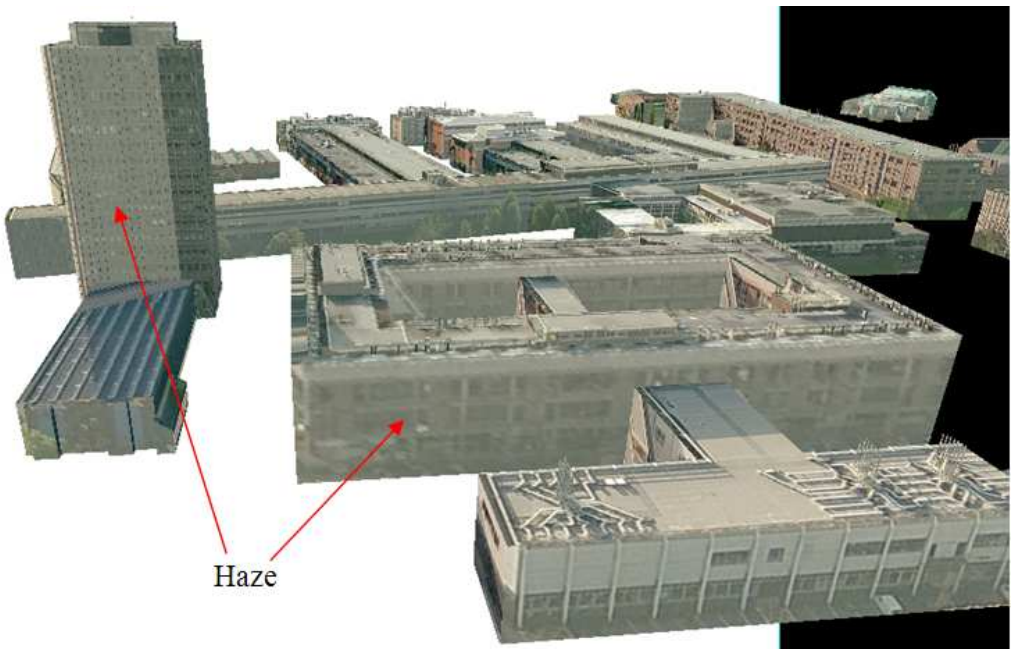

Figure 6.34: Texturing quality is affected by haze in some images.

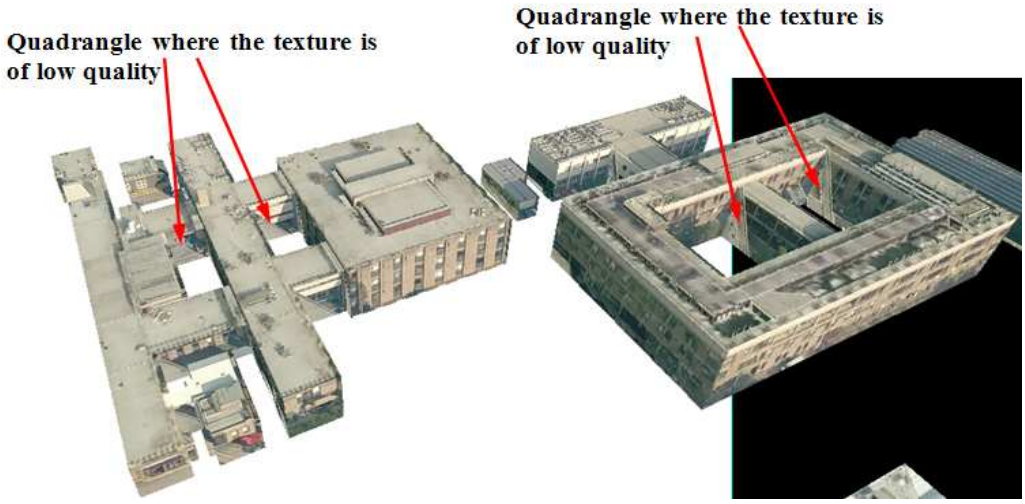

Figure 6.35: Texturing quality is affected by internal quadrangles in some buildings.

Figure 6.36: Texturing quality is affected by dead ground in images.

- One of the shortcomings of using images of actual buildings to texture the models is that one also gets artifacts in the images. In other words, one gets a picture of the lamp posts, power lines, and cars that happen to be parked in front of the building at the time the image was captured. Figure 6.37 illustrates example of these artifacts.

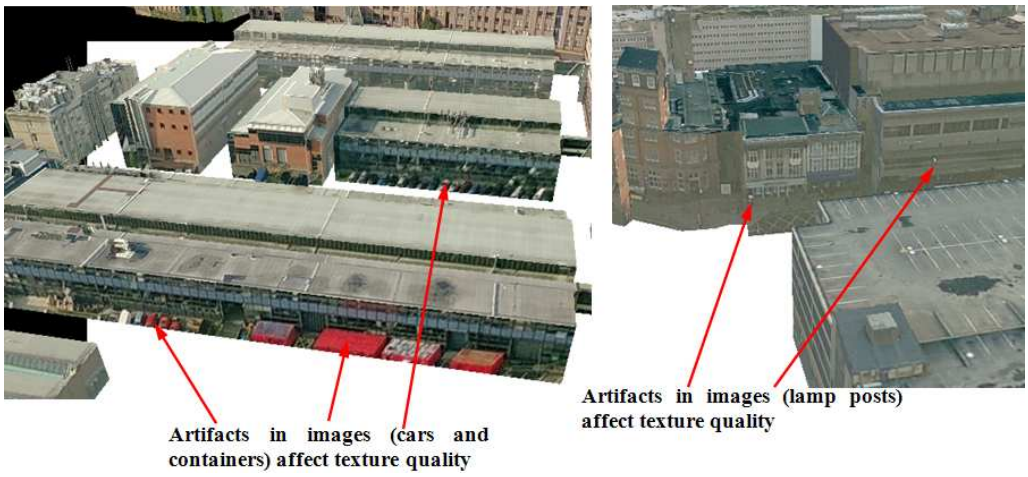

Figure 6.37: Examples of artifacts in images which affect the textures quality.

- Oblique sunlight with features casting shadows is typically a cumbersome scenario for photogrammetric imaging systems, particularly when shadows change between shots due to time delay, especially when capturing different strips, or in times of different cloud cover. Figure 6.38 depicts some textures that affected by shadows.

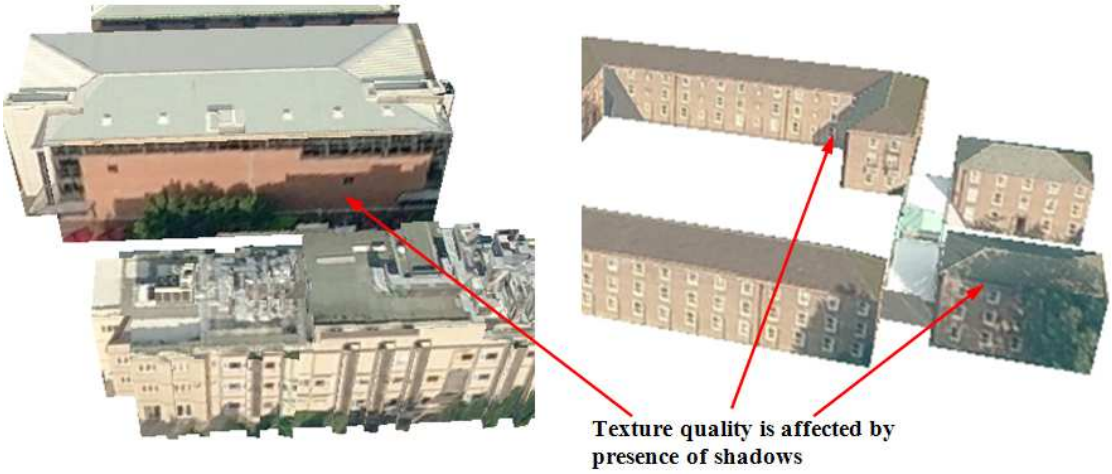

Figure 6.38: Texturing quality is affected by the presence of shadows in some images.

- The most important factor that affects the texturing quality is occlusion. Occlusion can be defined as part of a texture that is not visible from the image viewpoint. It is often difficult to select viewpoints where the complete facade is visible, especially in case of narrow streets. For stereo processing, at least two images are required which means more difficult situations to avoid occlusion.

There are different types of occlusion; self-occlusion which is caused by complex buildings and occlusions caused by other objects such as vegetation, other buildings (buildings might occlude each other causing a poor experience) or dynamic objects (e.g. moving people or vehicles). Figure 6.39 shows examples of self-occlusion and occlusion caused by adjacent buildings while figure 6.40 depicts examples of occlusion caused by vegetation and trees.

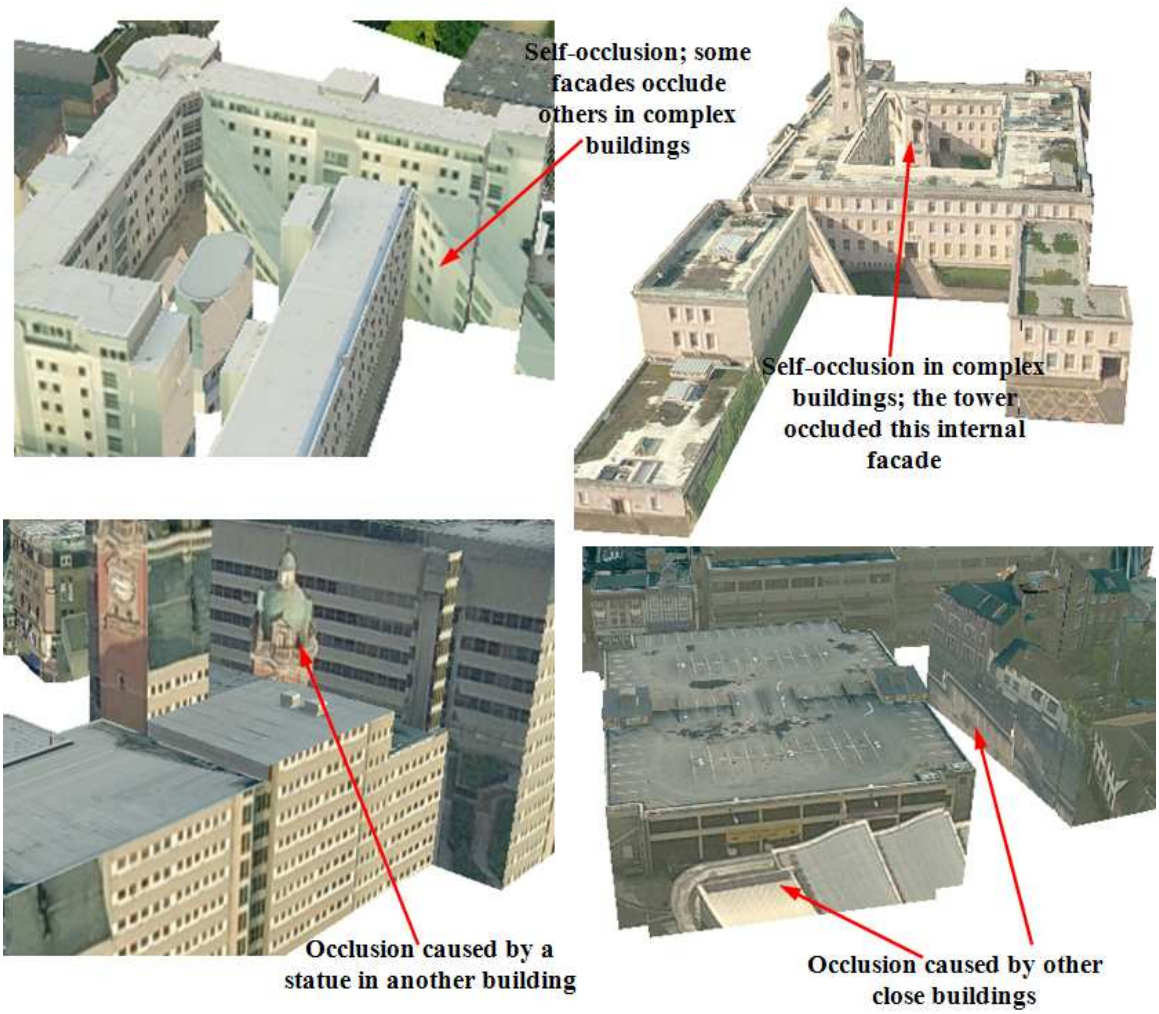

Figure 6.39: Self-occlusion in complex buildings and occlusion due to adjacent buildings.

Figure 6.40: Occlusion caused by vegetation and tall trees.

The 3D objects, which occlude the facades such as cars and trees, which are not included in the 3D model but visible in the images and thus textured onto the geometric model appear as flat features. While these flat features greatly contribute to the level of photo-realism of the 3D model for a wide range of viewing angles, they appear somewhat distorted if rendered from an extremely oblique view.

There are a number of factors that are related to the image quality or the capturing system used which affect the photo-realism of a textured 3D model;

- The orientation of the oblique images is often assumed accurate after performing the bundle block adjustment. This assumption is not always true in the real world where small errors in the estimation of the orientation of the oblique images cause inaccuracies in the texture mapping.
- Image radiometric effects: this effect comes from the use of different images acquired in different positions with different cameras (5 cameras used in this research) or in different daily moments (varying light conditions). This leads to the presence of discontinuities and artifacts in the 3D textured models along the edges of adjacent triangles textured with different images. Kim and Pollefeys (2004) applied blending methods based on weighted functions to avoid these distortions.
- Image dynamic range (The ratio of the lightest and darkest elements on a displayed image): digital images have always a lower dynamic range than the scene. Therefore bright areas are often saturated while dark parts contain low signal to noise (S/N) ratio. Debevec and Malik (1997) suggested that radiometric adjustment can be performed with common image processing tools to create high dynamic range images.
- Geometric distortion: this kind of error is generated from an incorrect camera calibration and orientation, an imprecise image registration, too large triangles or errors in the surface reconstruction. Ortin and Remondino (2008) said that 'all these sources do not preserve detailed contents like straight edges or big discontinuity changes of the surface. Accurate photogrammetric bundle adjustment, precise and complete camera calibration and polygons refinement must be employed to reduce or minimize possible geometric errors'. Weinhaus and Devich (1999) gave a detailed account of the geometric corrections that must be applied to remove distortions resulting from the transformation of the texture from the image plane to the triangle plane.

Figure 6.40 shows the effect of vegetation cover on the building facades. This can only really be overcome by the use of terrestrial images behind the vegetation or using patches of the visible facade to paste over the obscured

surface. Modelling these objects and the buildings behind correctly is often complex and time-consuming.

There are lots of approaches that can be used to remove the occlusion in pre-processing steps but all these methods deal with only terrestrial images. Such methods include what have been done, for example, by Ortin and Remondino (2008), Bekins and Aliaga (2005), Boehm (2004), and Wang et al. (2002) which will be highlighted in the next chapter.

Obstruction of neighbouring buildings in inner cities and other densely populated places is common with a fixed oblique view of, for example, about 50° in this research. Grenzdorffer et al. (2008) suggested that a possible solution for this problem is a variable multi-head camera system, enabling different view angles according to the average width of the streets and the average height of the buildings. However, Kurz et al. (2007) concluded that within direct georeferencing, the boresight alignment of such a multi head camera system with overlapping images requires special treatment.

In many cases occlusions can be removed from building facades by cloning parts of the same image. The alternative is to texture the building by copying architectural facade details, from other images that contain visible floors, to those facades that are not visible. If the desired facade is occluded in all oblique images and as the vertical images will not provide the required resolution, it can be represented with colour shading or with synthetic textures representative of the architecture (from existing library of textures). Alternatively, manual approach to texturing 3D models can be used to minimize the occlusion. Although the manual approach of texturing includes correction for the occlusion, by selecting the most suitable image for the required building face, it requires a manual operator which makes the process time consuming and the cost rapidly increases. This highlights the need for capturing terrestrial imagery to supplement the oblique imagery in texture mapping the models.

The most important thing that should be mentioned here is that no attempt of whatsoever was made to remove the occlusion or to enhance the textured facades using Pictometry imagery, as the purpose of this research is to explore the possibility of using this kind of relatively new imagery semiautomatically

in 3D modelling and automatically in texture mapping. Automating the texturing process can lead to both an increased profit and a market advantage by being able to provide the product in faster times and at a lower price than the competitors. In some instances, retaining the vegetation instead of removing it will potentially assist the user in recognizing and locating places especially if the model is to be used for city navigation.

6.6 Summary

Building reconstruction in dense urban areas is such a complex problem that it is impossible to look for a universal solution that could efficiently reconstruct every building, from a simple gabled roof to a whole complex building. The creation of geometrically correct, detailed and complete 3D models of complex objects therefore remains a difficult problem. If the goal is the creation of accurate, complete and photo-realistic 3D models of medium and large scale objects under practical situations, then full automation is still beyond reach. Object extraction and modelling from images is possible in semi-automated modes at best.

Extraction of 3D geometry for all buildings in both study areas has been performed using vertical Pictometry imagery block. An UltraCamD block was used to extract the 3D geometry for only the University campus test site as UltraCamD images for the city centre site are not available.

Extraction of 3D geometry from the oblique images was not possible because some roof outlines cannot be seen due to the tilt of the oblique images. However, the availability of oblique imagery during digitization provided additional information for the interpretation of geometry by allowing each building to be seen from different angles. Oblique images were of a great benefit in helping the interpretation of building outlines where differences in building height required digitizing of separate polygons.

Overall, the level of detail for the 3D models derived from the Pictometry images block is comparable with the level of detail acquired from the UltraCamD images block bearing in mind that the scale of Pictometry images, although it is suitable for extraction of 3D building geometry with some fine details, is much smaller than that of UltraCamD images.

Building reconstruction using Pictometry vertical imagery produced impressive results with most building models visually correct. The imagery seems to be very reliable in producing 3D models. In addition, the amount of reconstructed roof details is impressive since most of ventilation equipment, dormer windows and chimneys were reconstructed in almost all cases. The level of detail of the 3D building models is directly related to the GSD of the imagery used.

Depending on the angle from which a building is visualized, aerial or terrestrial images may be utilised as the source of textures. From a practical point of view, textures are required mostly for the facades of buildings that show, from a pedestrian view level, the way buildings look in reality. Having high vertical perspectives, aerial images are either not or rarely suitable for the extraction of textures for vertical faces of buildings. Therefore, the photo-realism of building facades can usually be achieved only if terrestrial images are acquired and mapped on their corresponding building faces. However, using Pictometry imagery offers a greater coverage than terrestrial imagery as it ensures including facades that are not accessible from the ground. Moreover, the use of a single data set (Pictometry) in automatic texture mapping of 3D models has the potential to reduce the occurrence of radiometric differences.

The visual inspection of the textured models show that using either vertical Pictometry block or UltraCamD block has given very good roof structure but when it comes to facade texturing, the quality was not as good as roof quality. The lower resolution of vertical imagery even with 60% overlap (UltraCamD images) proves to be inadequate for facade texture mapping which in most cases is significantly distorted except for a few occasions.

When only the block of oblique images was used for texturing the 3D models, the facade texturing was of very good quality but the texturing quality of some buildings' roofs was reduced compared with the vertical images.

To ensure that all building facades and roof tops in an area are covered and properly textured, it is necessary to utilize multiple oblique and vertical aerial images with different viewing angles. Using the combined UltraCamD and oblique images block or the combined vertical and oblique Pictometry images block gave high texture quality for both facades and rooftops.

Unfortunately the generation of detailed facade textures still poses a challenge due to the fact that there are usually many textures of building walls that are occluded either by other buildings or by vegetation in the street. Refining these textures to generate realistic 3D city models is usually done semi-automatically under the control and supervision of an operator which is a time consuming and costly process.

CHAPTER7: INTEGRATION OF TERRESTRIAL IMAGES WITH PICTOMETRY IMAGES

Although it is very easy to create a simple 3D model of an object, the generation of survey quality and photo-realistic models of complex scenes still requires great modelling efforts. From the preceding chapter, it's obvious that none of the texturing data sources used can satisfy all the requirements of large-scale modelling projects. Therefore, the integration of terrestrial imagery is inevitable to overcome this limitation of aerial imagery in such application scenarios.

7.1 Reasons and benefits of the integration

Aerial photogrammetry is able to economically capture the roof landscape and ground texture of a large built-up area. On the other hand, having high vertical perspective, vertical aerial images are either not or rarely suitable for the extraction of textures for vertical sides of buildings as they are mostly invisible from the air. For this reason, multiple-image photogrammetry using vertical and oblique aerial photos is considered a good alternative as this allows for texture extraction of both roof landscape and building faces. Furthermore, this can be a cost effective alternative to vertical aerial photos because the capital investment in equipment is comparatively small as small and medium format cameras can be used in this imaging system. On the other hand, using aerial imagery (vertical and oblique) as the only source for texture mapping did not give quality facade textures in some buildings especially for the lower part of building sides which are mostly affected by occlusion, figure 6.39 and figure 6.40. Therefore, where the oblique imagery does not provide sufficient alternative images for texturing of all facades correctly, the final 3D model may be supplemented with terrestrial imagery as a finishing process. However, acquiring this type of imagery is laborious and time consuming. Terrestrial images, therefore, are most useful in applications that require 3D models of only a few structures. Furthermore, it is usual, when acquiring both terrestrial and aerial images for texture mapping purposes, that not all images have equal

radiometric or colour properties. This is because of differences in resolution, image quality and weather conditions between different data sets. The demand of homogeneity in the textured facades requires that these differences should be effectively resolved, otherwise seams between aerial and terrestrial-based texture maps in one facade will be clearly noticed, figure 2.13. Therefore, all the above methods can be combined to construct high-fidelity and photorealistic 3D building models. Lerma et al. (2004) emphasized that the following three statements must be guaranteed all over the images that will be used in texture mapping to fulfil the client's expectations:

- Geometrical connection with the neighbouring images.
- Radiometric continuity of images.
- Colour and colour degradation of images.

7.2 Results of integrating terrestrial images with aerial images photogrammetric block

Automatic procedures for tie and control point measurements from terrestrial images are not available yet which means a considerable amount of human interaction. This is the main reason why the reconstruction of exterior orientation for terrestrial imagery is more time consuming and costly compared to aerial imagery. Moreover, Extracting and mapping textures manually, especially textures from perspective-distorted images is an inexact science. It involves trial and error which means that the steps performed may have to be repeated several times. Manual texture mapping using terrestrial imagery requires repetition of same procedures if there are any changes in the reconstructed building geometry, for example if a building was split, eliminated, or added. These changes are required to enable real time visualization of the new changed model. To enable automatic texture mapping from terrestrial imagery, automatic procedures to georeference this type of imagery should be available to minimize the manual interaction and hence the costs incurred.

Because of the above, a new method to automatically texture building facades from terrestrial images was used in this research. This method is based on integrating the terrestrial image that will be used for texture mapping of a

certain building facade with the photogrammetric block which will be used for texture mapping the other building facades and the roof tops. This approach also follows the workflow described in section 6.4.2 and in section 6.4.2.3 in which the texture is automatically chosen from the image that was taken from a direct, perpendicular view. The following points provide a summary of the method:

- The terrestrial image is added to the already triangulated photogrammetric combined block through the 'add frame' function in LPS.
- The IO of the camera used to capture the terrestrial image is entered. The camera used in this research was 'Canon EOS-1Ds Mark II' and it was calibrated on the same day of capturing the images using Australis software. The camera has a resolution of 4992 x 3328 pixels, a pixel size of 7.2 μm in both sides, a focal length of 28.4007 mm, and x_p and y_p (principal point shift) of -0.0562 mm and -0.2304 mm respectively.
- The EOP were used as unknowns since the position and orientation of the camera at the time of exposure are not available.
- A minimum of six tie points, between the terrestrial image and the oblique images that cover the facade which will be textured, have to be manually measured to position the terrestrial image correctly relative to the other images in the block. This was necessary since the minimum input requirements (X_0, Y_0, Z_0, ω, φ, and κ) to automatically generate the tie points for the terrestrial image are not available. Some tie points were on building facades and others were on the ground, figure 7.1.
- The bundle block adjustment is then re-performed to compute the EOP of the terrestrial image and thus to allow for the terrestrial image to be used in automatic texture mapping.
- After performing the AT and accepting its results, the block is now ready to be used in automatic texture mapping process in Texel Mapper software.

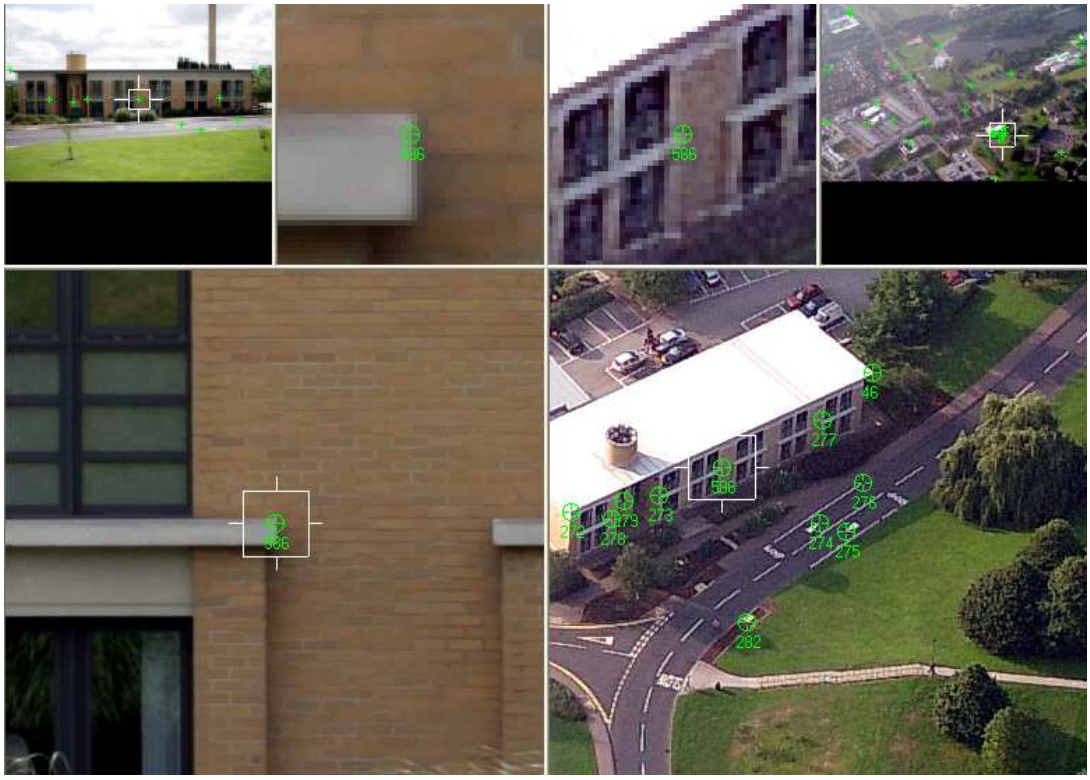

Figure 7.1: Tie points measurement between terrestrial image (left) and oblique image (right); some tie points are on the facade of old IESSG building and some on the ground.

The addition of the terrestrial image to the combined block did not significantly affect the AT results except for an insignificant increase in total image RMSE as can be seen from figure 7.2.

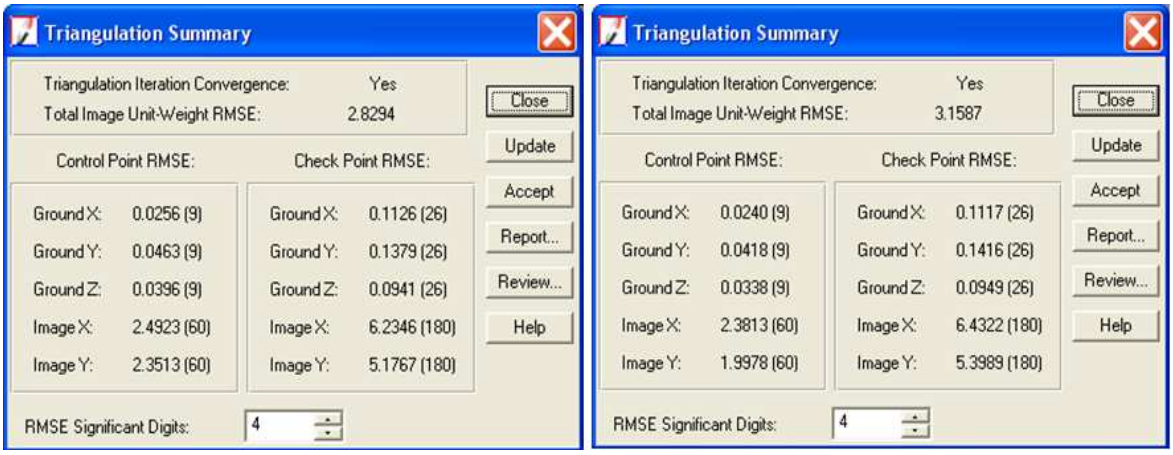

Figure 7.2: The result of AT before adding the terrestrial image (left) and after adding it (right).

Figure 7.3 shows the textured facade of the old IESSG building using the integrated block. As can be seen from the figure, the integration of the terrestrial image with the combined block worked very well. The results show the potential benefits of this approach. In addition to getting the best photo-realistic texture, the integration of terrestrial image in the photogrammetric combined block gives the benefit of using three types of imagery (terrestrial, aerial vertical and aerial oblique) in texture mapping automatically. This reduces the time needed for using terrestrial images in texture mapping significantly as the only manual interaction in this approach is the measurement of some tie points which is much less than the time required for manual texture mapping.

Using this method resulted in high quality facade textures except for the occlusion which is an unavoidable limitation of using photos of the actual building in texture mapping. There are lots of approaches that can be used to remove the occlusion in pre-processing steps. Such methods include what have been undertaken, for example, by Ortin and Remondino (2008), Bekins and Aliaga (2005), Boehm (2004), and Wang et al. (2002).

Figure 7.3: Old IESSG building automatically textured using the integrated block; top image shows the facade that is textured using the terrestrial image, middle image shows the roof top which is textured using the vertical aerial image, and the bottom image shows another facade that is textured using aerial oblique image.

Ortin and Remondino (2008) presented a method for the generation of occlusion-free artificial views for the realistic texturing of 3D models. The approach for occlusion removal from planar surfaces employs a simple method that exploits the fact that most facades can be locally well approximated by planar facets; the texture among different views can be transferred using a projective transformation. This produces alternative, independent estimates for the appearance of each facade. Rather than using a direct average of these values, the redundancy in the data is exploited to robustly determine the most likely texture of the wall. The required number of images is strictly related to the quantity of occlusions present in the image and if they are static or in movement. However, the proposed method is limited to planar features; figure 7.4 depicts the method proposed by Ortin and Remondino, 2008.

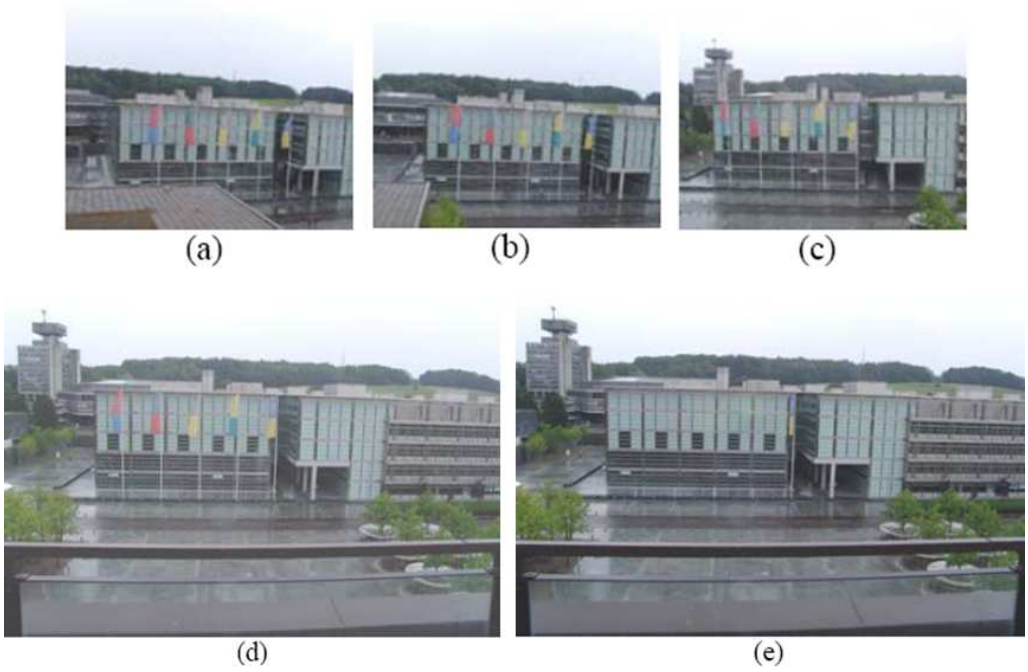

Figure 7.4: (a), (b), and (c) are sample views of the sequence; (d) is the reference view; and (e) is the synthetic view in which poles and flags have been removed, adapted from (Ortin and Remondino, 2008).

The approach proposed by Bekins and Aliaga (2005) is as follows: a model recovered from a sparse set of images is subdivided and grouped into feature regions that can be rearranged to texture the model in the style of the original. The redundancy found in architecture is used to derive procedural

rules describing the organization of the original building, which can then be used to automate the subdivision and texturing of buildings. This redundancy can also be used to automatically fill occluded and poorly sampled areas of the image set, as well as to equalize the colour and lighting between images and surfaces of the model. The scene is rendered using view-dependent texture mapping with a degree of realism comparable to that of the original scene.

Wang et al. (2002) described a method to obtain a realistic facade texture map, removing occlusions and effects of illumination variations as follows: a coarse geometric model of buildings and a set of images taken from nodes at different locations and associated with reasonably accurate camera pose information are taken as input for this approach. The light source for the urban images is assumed the normal sunlight (i.e. nearly white) and thus only the luminance in the colour space is considered in this approach. The input images are rectified into facade images, i.e. images under orthographic projection of a facade. For each image, the facade visibility and rectification is calculated based on the camera geometry at the node where the image is taken. To facilitate texture fusion for removing occlusions, the facade images are normalized by linear gray-level stretching. The resulting luminance normalized facade images (or LNF images) have the same average luminance and thus are comparable to one another.

Ortin and Remondino (2008) summarized some of the other successful methods for occlusion removal like this:

- Background learning and subtraction (Toyama et al., 1999): this method needs a very long sequence of images, acquired from the same standpoint. Methods like these are also applied to people detection and identification in forensic CCTV.
- Rectification of multiple images in image space and average estimation of the unoccluded pixel values (Boehm, 2004). Because of the involved projectivity, this method can be applied only to planar patches.
- Manual retouching of the occlusions in a single image (Ulm, 2005).

7.3 Comparison of integrated block textured model with other models

Automatic texture mapping using only aerial images has been undertaken in the previous chapter and using integrated block of terrestrial and aerial images has been done in the previous section. Manual texture mapping for one facade of IESSG building will be performed in this section, then the result will be compared to the previous results. The same terrestrial image that was used in the integrated block will be used to perform the manual texture mapping.

There are numerous ways to map textures onto the facades of any building model. The chosen method depends upon the type of imagery used and the orientation of this imagery. The method which will be used here is the affine map method which performs an affine transformation (defines the relationship between the pixel coordinate system and the image space coordinate system) to stretch a portion of the image onto selected model facades. This method is used to map a texture directly onto the facade by dragging the vertices of the selected facade to their corresponding positions on the active image. Since the terrestrial image has no or very little perspective distortion because it was captured opposite the facade, this method is very suitable as it works best with head-on images. Texel Mapper software was used to perform the manual texturing. After loading the 3D model and then the terrestrial image (the texture), texturing was performed following Texel Mapper manual. Figure 7.5 depicts the 3D model, the terrestrial image used for texturing, and the yellow vertices which must be dragged so that they roughly overlay the corresponding parts of the image. Sometimes one corner (or more) of the feature of interest is occluded in the image, as is the case of the bottom right and left vertices in this model. Where these corners lie must be estimated by making the best possible guess. The next step is to fine tune the position of each corner (vertex) to minimize the worst of the warping and stretching. Figure 7.6 illustrates the manual texture mapping result.

Figure 7.5: Vertices of 3D model and the terrestrial image used for texturing should overlay each other.

Figure 7.6: The manually textured 3D model of the old IESSG building.

It can be seen from figure 7.6 that some parts of the facade are distorted due to warping and stretching of the image during the process of manual texturing. Figure 7.7 depicts a closer view of some of the distorted parts.

Figure 7.7: Zoomed-in view to show the stretched and warped parts of the texture.

Since using photographs of actual buildings to texture the model gives also artifacts in the pictures, the Texel Mapper provides an Image Edit tool to edit these artifacts out of the image and get a cleaner texture on the building face. The main occlusion here is due to vegetation as depicted in figure 7.6. This partial occlusion will be removed manually by transferring the texture among different views in the facade. This method is similar to what has been done by Ortin and Remondino, (2008). The difference is that they did it automatically which required a sequence of images and manually marking of corresponding points between the views. For example 18 images were acquired to remove the occlusion and derive the clear appearance of the facade depicted in figure 7.4 as well as 8 corresponding points were measured in the views to determine the parameters of projective transformation. Whereas the manual removal of occlusion used here requires only one image and no corresponding points. When the editing process starts, the 3D textured model is hidden and the image displays with a yellow box (the source box) and a red box (the destination box). The portion of the image enclosed by the source box is used to replace the portion of the image in the destination box, figure 7.8.

Figure 7.8: The red destination box covers the occlusion to be removed and replaced by what is covered by the yellow source box.

The destination box is moved by dragging each of the vertices so that it covers the part of the image that is occluded. When the entire partial occlusion is covered by the destination box, drag the vertices of the source box so that they enclose an unobstructed portion of the facade that has the same view as the occluded part, for example the window in figure 7.8, until it is roughly the same size as the occluded view. This is to minimize stretching and warping. The preview radio button on the Image Edit menu can be selected to see a preview of what the edited image will look like. If the operator is satisfied with the preview, apply button can then be clicked to get the final result. Otherwise, adjusting the vertices should be continued until getting satisfied results. To see the results of the editing on the model, the Model Options mode is chosen by clicking its button on the Texel Mapper toolbar. This enables the model to be displayed. Note that the vegetation that was occluding the building facade is no longer visible on the textures front of the building, figure 7.9.

Figure 7.9: The final result of the manually textured facade after the removal of occlusion.

Comparing the results of texture mapping the old IESSG building facade using the integrated block, figure 7.3, and using the manual approach, figure 7.9, shows that:

- The manually textured model has a lot of stretched and warped patches which not only affect the realism and viewing of details on the model but also the accuracy of measurements on the facade. Whereas the automatically textured model is free of these distortions.
- The whole image has been used in the manual process which caused the presence of unwanted ground features in the texture, for example the sidewalk, the road, and the grass. On the other hand, when using the automatic approach, the software crops the unwanted features and leaves only the part that corresponds to the facade. Cropping of the image can be performed in manual texturing as well, but this will increase the time required to accomplish the task and hence the costs.
- The operator experience and skills play an important role in manual approach which makes the process more susceptible to any human mistakes and errors. Whereas in automatic method the operator has little or no affect on the results.
- The manual removal of occlusion is a tedious task to perform and it heavily depends upon the operator experience. Moreover, using views of the same image to replace the occluded parts is not always without limitations. For

instance, the contrast and brightness of different image patches may not be the same which affects the overall texturing quality, figure 7.10.

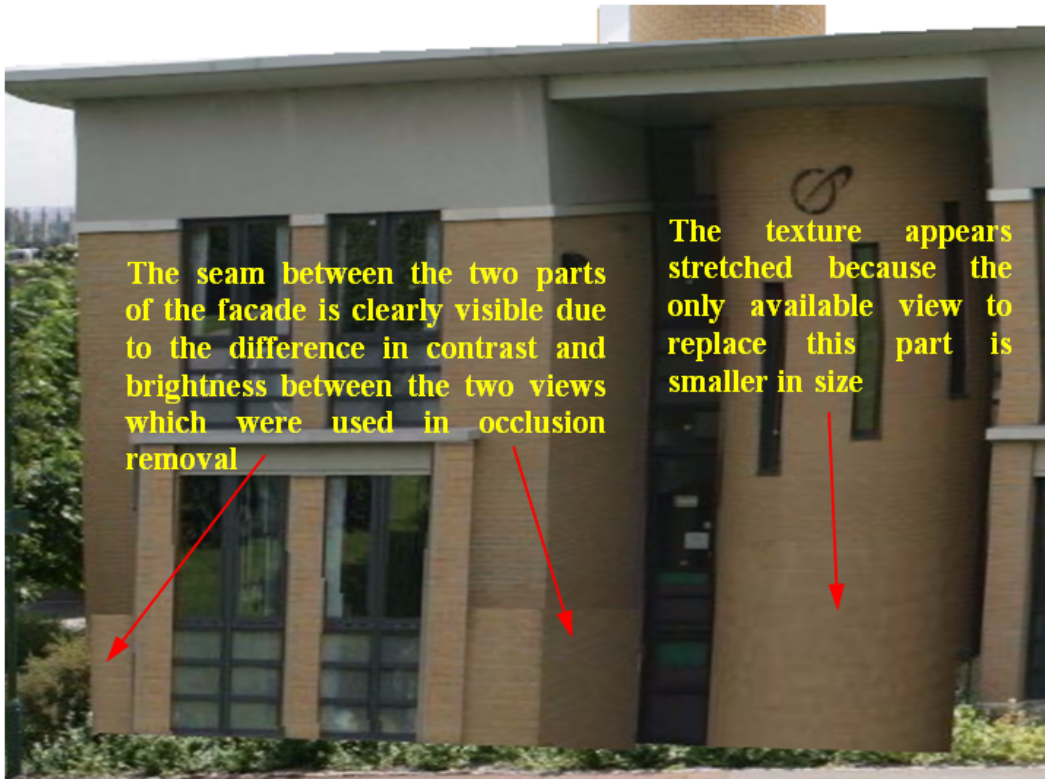

Figure 7.10: The effect of difference in contrast, brightness, and size of the used patches to replace the occluded views on the texturing quality.

7.4 Summary

There is no single data source that works for texture mapping of all building types and at the same time is fully automated and satisfies the requirements of every application. In addition, visualization based only on aerial images texturing is sufficient if nadir or oblique views were generated at medium distances to illustrate buildings. If the observer comes closer during a walk-through viewing, texturing solely based on aerial images is not adequate anymore. Since the building facades are one of the most important elements to be visualized, the integration of terrestrial imagery is inevitable to overcome this limitation of aerial imagery in such application scenarios. On the other hand, every acquisition technique has obviously some limitations. Although terrestrial images provide high fidelity ground, vegetation, and building

facades details, they lack building top information and occlusion limits their range as well as acquiring this type of imagery is laborious and time consuming. Terrestrial images, therefore, are most useful in applications that require 3D models of only a few structures.

The integration of terrestrial image of any building facade (whose texture needs enhancement) with the combined aerial imagery block has been successfully and automatically performed. AT of the integrated block was successfully performed and thus the terrestrial image parameters were calculated from the bundle block adjustment. Using this method resulted in high quality facade and roof top textures except for the partial occlusion which is an unavoidable limitation of using photos of the actual building in texture mapping. The occlusion can be removed using several existing approaches. The resulting quality of texture mapping using the integrated block outperforms the manually texture mapping quality. Manual texturing not only depends upon the experience and skill of the operator but also time consuming and laborious. Naturally, the more details there are in the model, the more costs incurred.

CHAPTER8: CONCLUSIONS AND RECOMMENDATIONS

3D city models have been increasingly used in a growing number of applications such as urban planning, tourism, archaeological sites reconstruction, civil engineering, mobile telecommunication, navigation, disaster simulation, and computer games. Although these applications share the common demand for 3D information, their special requirements considerably differ with regard to the accuracy and spatial coverage. The speed in which a building can be successfully identified, for example in case of disasters, is improved by increasing the accuracy of the 3D model by applying texture mapping. The texture mapping allows us to recognise a building not only from its silhouette but also from colour and objects such as windows or doors. The big recent improvement in 3D models quality is being driven by a vast collection of appropriate and efficient data acquisition tools and efficient data processing algorithms.

The inclination angle in combination with atmospheric scattering and the quality of the CCD and lens assembly of the consumer-type cameras are adversely affecting the overall quality of the oblique images. Despite the decreased quality, these data sets present an excellent opportunity to evaluate the use of these images in automatic texture mapping of building facades in combination with UltraCamD images.

The use of combined blocks of vertical and oblique images in AT showed that good point coordination can be achieved. The point coordination in AT can come from not just an intersection of a pair of image point's rays but also from multiple rays. The coordination quality is further improved by the use of oblique images providing strong intersection angles at the measured points. However, this does not necessarily give a good indication of the feature extraction/mapping that can be obtained as this is normally undertaken with a stereopair. Using oblique images with the same viewing direction for stereo viewing is possible but large differential tilts are not helpful for comfortable stereo viewing.

The results of this research show that Pictometry, vertical and oblique, images can be successfully and reliably used in 3D modelling of urban environment. Vertical imagery is required to extract building footprints and texture the roof tops and oblique imagery is needed to assist in identification of building outlines and texture the facades. The integration of terrestrial image of any building facade with the combined aerial imagery block has been successfully and automatically performed. This allows for automatically using terrestrial images in texturing which significantly enhances the facades and at the same time is faster, cheaper, more accurate, and easier to implement.

8.1 Evaluation of the Aim and Objectives

As stated in the introductory chapter, the overall aim of this research was to investigate the geometric potential for using Pictometry imagery to provide 3D city modelling and texturing. The key factors which were considered necessary for successful achievement of the research aim were the investigation of the basic image orientation and geometry, the combining of vertical and oblique images in one photogrammetric block, the use of the combined block in automatic texture mapping the 3D models, and the integration of terrestrial images with the combined photogrammetric block. The combination of these factors has facilitated the achievement of the research aim and has helped in introducing a novel methodology for texture mapping of 3D models using aerial vertical and oblique and terrestrial images.

Section 1.2 lists a number of objectives that require addressing in order to achieve the research aim. These will be summarized and recalled below and a summary of the main drawn conclusions about each one, resulting from the research based on the investigations and findings presented and described elsewhere in the thesis.

8.1.1 Basic image orientation and geometry through exploring the aerial triangulation on different photogrammetric blocks

- The AT was conducted, on the created photogrammetric blocks, using four different solutions. They are ‘float solution’, ‘constrained solution’, ‘integrated sensor orientation solution’ and finally ‘direct georeferencing or only in-flight GPS and IMU’ solution. The RMSE values of the CCPs compared to the truth

value (static GPS survey) was used to represent the external geometry of the blocks. Plots of CCPs residual vectors were presented to examine the possible existence of any remaining systematic errors after the solution. Moreover, y-parallax plots were also presented to investigate the problematic existence of y-parallax which affects the stereo viewing. Comparison between the raw EOP values and the calculated EOP values after performing the traditional AT showed that there were significant positional and attitude deviations of the order of up to 2m and 1degree for Pictometry imagery, hence the assignment of 1m and 1degree as a priori standard deviation for the in-flight position and attitude. This reflects the non-optimal GPS/IMU quality. The orientation of the oblique images block leads to a strong overlap of images with up to 14 images per object point. However, standard commercial programs are not able to handle such a block by automatic image matching so a manual measurement was needed although it is time consuming. Moreover, the distribution and number of tie points will not be ideal in case of manual measurement.

- The results of all blocks have shown that the use of indirect georeferencing produced very good quality coordination of ground points. In addition, high quality image measurements have been achieved. The check points show more realistic values of what might be achievable for mapping. Special care was given to the integrated sensor orientation and DG solutions as using these solutions compared to conventional photogrammetry demonstrates a significant decrease in time and thus cost for photogrammetric processes because the use of automatically measured tie points is a cost effective way of generating ground control points. The results of direct sensor orientation have shown that height accuracy of 0.06% of flying height and plan accuracy of 0.02% of flying height can be achieved for the vertical Pictometry images block. Combining of oblique images with vertical images in one block has given a very good improvement for the height quality which reached 0.02% of flying height. Furthermore, the introduction of the image coordinates of tie points in the solutions reduced the y-parallax to the acceptable levels. The total image RMSE of all blocks was less than third of the pixel size of the original imagery except for the DG solution which was about half of the pixel size.

- Quality of DG is fully dependent on the quality of directly measured EOP.

The quality of object point coordinates in DG is dependent on the number of image rays used for object point determination. A large image overlap providing strong block geometry positively influences the point accuracy since multiple image rays can compensate remaining errors in the orientation parameters. The use of integrated sensor orientation results in a significant accuracy improvement compared to results from DG with fixed EOP. Integrated sensor orientation should be applied whenever very high accuracy is crucial. It offers the most effective way to compensate any remaining errors even with no or very reduced number of ground control points. On the other hand, the reliability of the results remains a weak point of direct and integrated sensor orientation solutions due to lack of redundancy in absolute orientation. Systematic errors in the GPS/IMU measurements may go unnoticed, because they cannot be detected without the introduction of GCP coordinates. Thus, it is recommended to include at least a minimum number of GCPs in the actual project area wherever possible.

8.1.2 Evaluation of using vertical and oblique Pictometry images in extracting 3D geometry.

- Extraction of 3D geometry for all buildings in both study areas has been performed using vertical Pictometry imagery block. In addition, UltraCamD block was used to extract the 3D geometry for only the University campus test site as UltraCamD images for the city centre site are not available. Extraction of 3D geometry from the oblique images was not possible because some roof outlines cannot be seen due to the tilt of the oblique images. However, the availability of oblique imagery during digitization provided additional information for the interpretation of geometry by allowing each building to be seen from different angles. In addition, oblique images were of a great benefit in helping the interpretation of building outlines where differences in building heights required digitizing of separate polygons. Building reconstruction using Pictometry vertical imagery produced impressive results with most building models visually correct. The imagery seems to be very reliable in producing 3D models. In addition, the amount of reconstructed roof details is impressive

since most of ventilation equipment, dormer windows and chimneys were reconstructed in almost all cases.

8.1.3 Using vertical and oblique Pictometry images in texturing of 3D models.

- Using images as texture will not only increase the realism of the model but also enable the viewing of details and creates the false impression of a higher level of geometric detail. Due to high vertical perspectives, aerial vertical images are either not or rarely suitable for the extraction of textures for vertical facades of buildings. Therefore, the photo-realism of building facades can usually be achieved only if terrestrial imagery is acquired and mapped on their corresponding building facades. However, using Pictometry imagery offers a greater coverage than terrestrial imagery as it ensures including facades that are not accessible from the ground. Moreover, the use of a single data set (vertical and oblique Pictometry) in automatic texture mapping of 3D models has the potential to reduce the occurrence of radiometric differences. The visual inspection of the textured models show that using either vertical Pictometry block or UltraCamD block has given very good roof structure but when it comes to facade texturing the quality was not as good as roofs quality. On the other hand, using only oblique images resulted in very good quality facade texturing but the texturing quality of some buildings' roofs was reduced compared with the vertical images.
- To ensure that all building facades and roof tops in an area are covered and properly textured, it is necessary to utilize multiple oblique and vertical aerial images with different viewing angles. Thus, using the combined UltraCamD and oblique images block or the combined vertical and oblique Pictometry images block gave high texture quality for both facades and rooftops. Unfortunately the generation of detailed facade textures is still a challenge due to the fact that there are usually many textures of building walls that are occluded either by other buildings or by vegetation in the street. Refining these textures to generate realistic 3D city models is usually done semi-automatically under the control and supervision of an operator which is a time consuming and costly process.

8.1.4 Integrating terrestrial images with the combined aerial images block in automatic texture mapping.

- Since the building facades are one of the most important elements to be visualized, the integration of terrestrial imagery, although acquiring this type of imagery is laborious and time consuming, is inevitable to overcome the limitation of insufficient texture from aerial imagery.
- The integration of terrestrial image of any building facade (whose texture needs enhancement) with the combined aerial imagery block has been successfully and automatically performed. Using this method resulted in high quality facade and roof top textures except for the partial occlusion which is an unavoidable limitation of using photos of the actual building in texture mapping. The results are much better than the results obtained by manual texturing which not only depends upon the experience and skill of the operator but also time consuming and laborious.
- This method allows for automatically using terrestrial images in texturing which significantly enhances the facades and at the same time is faster, cheaper, more accurate, and easier to implement.

8.2 Recommendations for Future Research

Based on the research reported in this thesis and the conclusions deduced from the results of the study, the following recommendations are being made for possible future work to extend the potential of using combined photogrammetric blocks of vertical and oblique imagery in semi-automatic, possibly automatic in future, feature extraction and automatic texture mapping of 3D building models.

- Blocks of ideal overlap (60%) and high quality GPS/IMU derived EOP as well as lever arm and boresight misalignments should be tested. In addition, using up to 90% overlap is required and should be tested as this increases the number of images without increasing the project costs due to the automation of processing. The resulted redundancy increase will make the AT more robust and gives better results which will positively affect the 3D modelling.
- Obviously, not all topics related to the analysis of the Pictometry imaging system were investigated within this research. For example, issues related to

the economical use (time and cost required for preparation, processing, and post-processing) have not been considered. Moreover, the behaviour of AT for larger and non-regular blocks, the influence of control points, and the effect of number of tie points were not investigated. These factors should be examined to allow the transferability and generalization of the results obtained here.

- Performing height measurements on oblique images resulted in significant errors (relative to heights measured on stereopairs) due to the fact that geo-coding of oblique images is done by means of DEM. Therefore high accurate DEM should be used and tested.
- As an increasing demand for detailed 3D city models worldwide is expected in the next years, the automation of building extraction from vertical imagery with the aid of oblique imagery requires examination.
- The effect of occlusion can be minimized by having a good plan prior to data acquisition, especially in case of terrestrial imagery, to get an occlusion-free faces of buildings. Occlusion can be removed using artificial or image based facade patches and images of similar information to replace the occluded parts. However, using these approaches may result in unrealistic representation of facades and seams in the mapped texture due to different illumination, intensity and hue. Therefore, techniques to overcome these limitations are desired and need to be addressed in the future to minimize post-processing stage when the texture is of poor quality.

REFERENCES

ALAMÚS, R., KORNUS, W., PALÀ, V., PÉREZ, F., ARBIOL, R., BONET, R., COSTA, J., HERNÁNDEZ, J., MARIMON, J., ORTIZ, M. A., PALMA, E., PLA, M., RACERO, S. & TALAYA, J. (2005) Validation process of the ICC digital camera. International Archives of Photogrammetry, Remote Sensing and Spatial Information Sciences(Part I/W3)—on CD-ROM 36.

ALAMÚS, R., KORNUS, W. & TALAYA, J. (2006) Studies on DMC geometry. *ISPRS Journal of Photogrammetry and Remote Sensing,* 60 (6)**,** 375-386.

ARIAS, B. N. & GOMEZ-LAHOZ, J. (2009) Testing the stereoscopic precision of a large-format digital camera. *The Photogrammetric Record* 24(126)**,** 157–170.

ASM (2008) Virtual Earth Streets: Next-Generation 3D Modelling, in Asian Surveying and Mapping http://www.asmmag.com/news/virtual-earth-streets-next-generation-3d-modelling, August 2008.

AVERDUNG, C. (2004) Modeling of 3D city model with heterogeneous output data. *KS Volume 9 - The X factor - value to spatial data and maps, Bonn, 148-156.*

BALTSAVIAS, E. P. (1999) A comparison between photogrammetry and laser scanning. *ISPRS Journal of Photogrammetry and Remote Sensing,* 54 (2-3)**,** 83-94.

BECK, M. (2003) Real-time visualization of big 3D city models. *International Archives of Photogrammetry, Remote Sensing and Spatial information Sciences, Tarasp, Switzerland, vol. XXXIV-5/W10.*

BEKINS, D. & ALIAGA, D. G. (2005) Build-by-number: Rearranging the real world to visualize novel architectural spaces. In *IEEE Visualization*, October 23-28, 2005, Minneapolis, MN, USA, pages 143-150.

BERALDIN, J., PICARD, M., EL-HAKIM, S., GODIN, G., VALZANO, V. & BANDIERA, A. (2005) Combining 3D technologies for cultural heritage interpretation and entertainment. *Proceedings of SPIE-IS&T Electronic Imaging: Videometrics VIII.* San Jose, California, 18th to 20th January 2005.

BILDSTEIN, F. (2005) 3D city models for Simulation & Training - Requirements on Next Generation 3D city models. ISPRS WG III/4, Next Generation city models, Bonn, 21-22 June 2005.

BLAIS, F. (2004) Review of 20 years of range sensor development. ,. *Journal of Electronic Imaging,* 13 (1)**,** 231-243, January, 2004.

BOEHM, J. (2004) Multi-image Fusion for Occlusion-free facade texturing. IAPRS Vol. XXXV, part 5, pp.867-872.

BÖHLER, W. & MARBS, A. (2004) 3D Scanning & Photogrammetry for Heritage Recording: A Comparison. . *Proceedings of the 12th International Conference on Geoinformatics, June, Gävle, Sweden, pp. 291-298.*

BRENNER, C., DOLD, C. & JÜLGE, K. (2003) Fusion, Interpretation and Combination of Geodata for the Extraction of Topographic Objects. Proc. Workshop 3-D reconstruction from airborne laser scanner and InSAR data. The International Archives of the Photogrammetry,

Remote Sensing and Spatial Information Sciences. Maas, H.-G., Vosselman, G., Streilein, A. (Eds.), Vol. XXXIV, Part 3/W13, Dresden.

BRENNER, C. & HAALA, N. (1998) Fast production of virtual reality city models. International Archives of Photogrammetry and Remote Sensing, 32(4): 77-84.

BRENNER, C., HAALA, N. & FRITSCH, D. (2001) Towards fully automated 3D city model generation. In: E. P. Baltsavias, A. Grün and L. V, Gool. eds., Automatic Extraction of Man-Made Objects from Aerial and Space Images (III). A.A. Balkema, Ascona, Switzerland, pp. 47-58.

CASSETTARI, S. (2007) THE OBLIQUE VIEW. *GEOconnexion International Magazine,* February 2007**,** 34-35.

CAVAGNA, R., ROYAN, J., GIOIA, P., BOUVILLE, C., ABDALLAH, M. & BUYUKKAYA, E. (2009) Peer-to-peer visualization of very large 3D landscape and city models using MPEG-4. *Signal Processing: Image Communication,* 24 (1-2)**,** 115-121.

CHIKOMO, F. O., MILLS, J. P. & BARR, S. L. (2007) An integrated approach to level-of-detail building extraction and modelling using airborne lidar and optical imagery. *International Archives of Photogrammetry, Remote Sensing and Spatial Information Sciences,* 36(3/W49B), On CD-Rom, 6 pages.

CRAMER, M. (2005) Digital Airborne Cameras Status and Future. Proceedings ISPRS workshop 'High Resolution Earth Imaging for Geospatial Information' Unicersity of Hannover, HANNOVER, Germany. May 17-20, 2005

CRAMER, M. & HAALA, N. (2009) DGPF PROJECT: EVALUATION OF DIGITAL PHOTOGRAMMETRIC AERIAL BASED IMAGING SYSTEMS – OVERVIEW AND RESULTS FROM THE PILOT CENTRE. *ISPRS Hannover Workshop 2009, High-Resolution Earth Imaging for Geospatial Information.* Hannover, Germany, Tuesday, June 2 to Friday, June 5, 2009.

CYBERCITY (2009) Residential real state, http://www.cybercity3d.com/, last accessed May, 2009.

DEBEVEC, P. E. & MALIK, J. (1997) Recovering high dynamic range radiance maps from photographs, Proceedings of the 24th annual conference on Computer graphics and interactive techniques, p.369-378, August 1997

DEBEVEC, P. E., TAYLOR, C. J. & MALIK, J. (1996) Modeling and rendering architecture from photographs: a hybrid geometry- and image-based approach. *ACM Proceedings of SIGGRAPH '96.* New Orleans, Louisiana, 4th to 9th August 1996. 518 pages: 11–20.

DIETZE, L., NONN, U. & ZIPF, A. (2007) Metadata for 3D City Models: Analysis of the Applicability of the ISO 19115 Standard and Possibilities for further Amendments *10th AGILE International Conference on Geographic Information Science 2007 Aalborg University, Denmark.*

DIMAC (2009) http://www.dimacsystems.com/, last accessed December, 2009.

DÖRSTEL, C. (2003) DMC—practical experiences and photogrammetric system performance. In: Photogrammetric Week 2003 Fritsch D. (Ed.),

September 2003 Sttutgart (Germany), Wichmann Verlag, Heidelberg, pp. 59–65.

DOT (2006) Photogrammetry Surveys IN TRANSPORTATION, C. D. O. (Ed.). California.

EBNER, H. (1976) Self calibrating block adjustment. *Bildmessung und Luftbildwesen* 44: 128-139.

EL-HAKIM, S., GONZO, L., VOLTOLINI, F., GIRARDI, S., RIZZI, A., REMONDINO, F. & WHITING, E. (2007) Detailed 3D modeling of castles. *international journal of architectural computing,* issue 02, volume 05**,** PP 199-220.

EL-HAKIM, S. & REMONDINO, F. (2006) Image-based 3D modelling: A review. *Photogrammetric Record,* 21 (115)**,** pp. 269-291, (September 2006).

EL-HAKIM, S. F. (2002) Semi-automatic 3D reconstruction of occluded and unmarked surfaces from widely separated views. . *International Archives of the Photogrammetry, Remote Sensing and Spatial Information Sciences,*. Greece, Sept. 2-6, 2002.

EL-HAKIM, S. F., BERALDIN, J.-A., PICARD, M. & GODIN, G. (2004) Detailed 3D reconstruction of large-scale heritage sites with integrated techniques. *IEEE Computer Graphics and Applications,* 24 (3)**,** 21-29.

ERVING, A., RÖNNHOLM, P. & NUIKKA, M. (2009) DATA INTEGRATION FROM DIFFERENT SOURCES TO CREATE 3D VIRTUAL MODEL. IN FABIO REMONDINO, S. E.-H., LORENZO GONZO (Ed.) *3D-ARCH 2009: "3D Virtual Reconstruction and Visualization of Complex Architectures.* Trento, Italy, 25-28 February 2009,

FEMA (2005) Report: Providing structural elevation data - Appendix I: Pictometry accuracy analyses. *Available online at: http://www.fema.gov/pdf/nfip/alt_elevations/elevations_appi.pdf , accessed: July 2009*.

FLAMANC, D., MAILLET, G. & JIBRINI, H. (2003) 3D CITY MODELS: AN OPERATIONAL APPROACH USING AERIAL IMAGES AND CADASTRAL MAPS. *ISPRS Archives, Vol. XXXIV, Part 3/W8.* Munich, 17-19 Sept. 2003.

FRICKER, P. (2001) ADS40-Progress in digital aerial data collection, Photogrammetric Week 01, Wichmann Verlag, Heidelberg, 2001.

FRUEH, C., SAMMON, R. & ZAKHOR, A. (2004) Automated texture Mapping of 3D City Models with Oblique Aerial Imagery. In: Proceedings of 2nd International Symposium on 3D Data Processing, Visualization and Transmission, Thessaloniki, Greece, pp. 396-403.

FRUEH, C. & ZAKHOR, A. (2004) An Automated Method for Large-Scale, Ground-Based City Model Acquisition. *International Journal of Computer Vision,* 60 (1)**,** 5–24.

GETMAPPING (2009) http://www2.getmapping.com/, last accessed December, 2009.

GONZO, L., EL-HAKIM, S., PICARD, M., GIRARDI, S. & WHITING, E. (2004) Photo-Realistic 3-D Reconstruction of Castles with Multiple-Sources Image-Based Techniques. In: The International Archives of the Photogrammetry, Remote Sensing and Spatial Information Sciences, Vol. (35) B5, pp.120-125.

GRAHAM, R. & KOH, A. (2002) *Digital Aerial Survey: Theory and Practice. Caithness, Scotland: Whittles Publishing.*

GRENZDORFFER, G., GURETZKI, M. & FRIEDLANDER, I. (2008) PHOTOGRAMMETRIC IMAGE ACQUISITION AND IMAGE ANALYSIS OF OBLIQUE IMAGERY. *The Photogrammetric Record,* 23 (124)**,** 372–386.

GRÖGER, G., KOLBE, T., DREES, R., KOHLHAAS, A., MÜLLER, H., BUD, F., GRUBER, U. & KRAUSE, U. (2004) the interoperable 3D city model of the SIG 3D of GDI NRW. Version 2, http://www.ikg.uni-bonn.de/sig3d/.

GRUBER, M. & LADSTADTER, R. (2006) Geometric Issues of the Digital Large Format Aerial Camera UltraCamD. International Calibration and Orientation Workshop. EuroCow 2006. 25-27 January. Castelldefels, Spain.

GRUBER, M., PONTICELLI, M., BERNÖGGER, S. & LEBERL, F. (2008) ULTRACAMX, THE LARGE FORMAT DIGITAL AERIAL CAMERA SYSTEM BY VEXCEL IMAGING / MICROSOFT. *ISPRS Congress Beijing 2008, China, The International Archives of the Photogrammetry, Remote Sensing and Spatial Information Sciences. Vol. XXXVII. Part B1. Beijing 2008.*

GRUEN, A. (2000) Semi-automated approaches to site recording and modelling. *International Archives of Photogrammetry and Remote Sensing, Vol. XXXIII, Amsterdam 2000, 309–318.*

GRUEN, A. (2005) New technologies for efficient large site modelling. IN SABRY EL-HAKIM, F. R., LORENZO GONZO (Ed.) *3D-ARCH 2005, Virtual Reconstruction and Visualization of Complex Architectures.* Mestre-Venice, Italy, 22-24 August, 2005.

GRUEN, A. (2008) Reality-based generation of virtual environments for digital earth. *International Journal of Digital Earth,* Vol. 1, No. 1, March 2008**,** 88-106.

GRUSSENMEYER, P., LANDES, T., VOEGTLE, T. & RINGLE, K. (2008) COMPARISON METHODS OF TERRESTRIAL LASER SCANNING, PHOTOGRAMMETRY AND TACHEOMETRY DATA FOR RECORDING OF CULTURAL HERITAGE BUILDINGS. *ISPRS Congress, Beijing, China, The International Archives of the Photogrammetry, Remote Sensing and Spatial Information Sciences. Vol. XXXVII. Part B5. Beijing 2008.*

HABIB, A. F., GHANMA, M. S., AL-RUZOUQ, R. I. & KIM, E. M. (2004a) 3-D MODELLING OF HISTORICAL SITES USING LOW-COST DIGITAL CAMERAS. *XXth ISPRS Congress, Istanbul, Turkey, Commission 5, SS4-CIPA-Low-Cost Systems in Recording and Managing the Cultural Heritage.*

HABIB, A. F., PULLIVELLI, A. M. & MORGAN, M. (2004b) QUANTITATIVE MEASURES FOR THE EVALUATION OF CAMERA STABILITY. *XXth ISPRS. Congress.* Istanbul, Turkey.

HAMRUNI, A., SMITH M. & JAMIESON, A. (2008) Investigation into the geometry of Pictometry imagery,. *RSPSoc annual conference.* Falmouth, UK.

HEIPKE, C. (1997) Automation of interior, relative, and absolute orientation. *ISPRS Journal of Photogrammetry and Remote Sensing,* 52 (1)**,** 1-19.

HEIPKE, C., JACOBSEN, K. & WEGMANN, H. (2002) Analysis of the results of the OEEPE test "Integrated Sensor Orientation". IN HEIPKE, C., JACOBSEN, K. & WEGMANN, H. (Eds.) *Integrated Sensor Orientation, Test Reports and Worshop Proceedings, July, 2002.*

HIRSCHMULLER, H., SCHOLTEN, F. & HIRZINGER, G. (2005) Stereo Vision Based Reconstruction of Huge Urban Areas from an Airborne Pushbroom Camera (HRSC). *in Proc. 27th DAGM Symposium, (Vienna, Austria), pp. 58-66, LNCS 3663, Sept 2005.*

HUANG, X., KWOH, L. K., BO, Y. & TAN, Y. K. A. (2006) An Efficient Platform for 3D City Model Visualization. *Proc. IEEE International Geoscience and Remote Sensing Symposium, Denver, Colorado, USA, pp 297 – 300.*

HUSSAIN, M. & BETHEL, J. (2004) editors of section 15:Project and Mission Planning in Manual of Photogrammetry, fifth edition, American Society for Photogrammetry and Remote Sensing, Maryland, USA.

INTERGRAPH (2008) http://www.intergraph.com/sgi/products/default.aspx, last accessed June, 2009.

JACOBSEN, K. (2004) Direct/integrated sensor orientation-pros and cons, International Archives of the Photogrammetry, Remote Sensing and Spatial Information Sciences, 35 (B3), pp. 829-835.

JACOBSEN, K. (2008) CALIBRATION OF CAMERA SYSTEMS. *ASPRS 2008 Annual Conference.* Portland, Oregon, April 28 - May 2, 2008.

JACOBSEN, K. & WEGMAN, H. (2002) Dependencies and problems of direct sensor orientation, in Integrated Sensor Orientation, Test Reports and Worshop Proceedings, July, 2002.

JINHUI, H., YOU, S. & NEUMANN, U. (2003) Approaches to Large-Scale Urban Modeling. *IEEE Computer Graphics and Applications,* November/December 2003**,** 62-69.

JINHUI HU, YOU, S. & NEUMANN, U. (2003) Approaches to Large-Scale Urban Modeling. *IEEE Computer Graphics and Applications,* November/December 2003**,** 62-69.

KAARTINEN, H., J. HYYPPÄ, E. GÜLCH, G. VOSSELMAN, H. HYYPPÄ, L. MATIKAINEN, A.D. HOFMANN, U. MÄDER, Å. PERSSON, U. SÖDERMAN, M. ELMQVIST, A. RUIZ, M. DRAGOJA, D. FLAMANC, G. MAILLET, T. KERSTEN, J. CARL, R. HAU, E. WILD, L., FREDERIKSEN, J. HOLMGAARD & VESTER, K. (2005) ACCURACY OF 3D CITY MODELS: EuroSDR comparison. *ISPRS WG III/3, III/4, V/3 Workshop "Laser scanning 2005", Enschede, the Netherlands, September 12-14, 2005.*

KHOSHELHAM, K. & LI, Z. (2004) A MODEL-BASED APPROACH TO SEMIAUTOMATED RECONSTRUCTION OF BUILDINGS FROM AERIAL IMAGES. *The Photogrammetric Record,* 19 (108)**,** 342-359.

KIM, S. J. & POLLEFEYS, M. (2004) Radiometric Self-Alignment of Image Sequences. Proceedings of CVPR, pp. 645-651.

KOKKAS, N. (2008) AN INVESTIGATION INTO SEMI-AUTOMATED 3D CITY MODELLING. *Civil Engineering-IESSG.* Nottingham, University of Nottingham.

KOLBE, T. (2004) Interoperable 3D Visualization - 3D Web Map Server. KS Volume 9 - The XFaktor- Added value for spatial data and maps, Bonn 130-140.

KOLBE, T., GRÖGER, G. & PLÜMER, L. (2005) CityGML – Interoperable Access to virtual 3D City Models. *first international workshop on next generation 3D city models*. Bonn, Germany, 21-22 June,2005.

KRAUS, K. (2007) *Photogrammetry, Geometry from Images and Laser Scans. translated by Ian Harley and Stephen Kyle. Walter de Gruyter, Berlin, Germany, the 2nd edition*.

KREMER, J. & CRAMER, M. (2008) RESULTS OF A PERFORMANCE TEST OF A DUAL MID-FORMAT DIGITAL CAMERA SYSTEM. *ISPRS Congress Beijing 2008, China, The International Archives of the Photogrammetry, Remote Sensing and Spatial Information Sciences. Vol. XXXVII. Part B1, Commission I, ISSN 1682-1750, pp1051-1058, 3-11 Jul 2008*

KURZ, F., MÜLLER, R., STEPHANI, M., REINARTZ, P. & M. SCHROEDER (2007) Calibration of a wide-angle digital camera system for near real time scenarios *Proc. ISPRS Hannover Workshop 2007 - High Resolution Earth Imaging for Geospatial Information, Hannover, Germany, May 29 – June 1, 2007, ISSN 1682-1777.*

LABE, T. & FORSTNER, W. (2006) Automatic relative orientation of images. *. Proceedings of the 5th Turkish–German Joint Geodetic Days, Berlin, Germany. 6 pages. March 29th – 31st, 2006, Berlin, ISBN 3-9809030-4-4.*

LAFARGE, F., DESCOMBES, X., ZERUBIA, J. & PIERROT-DESEILLIGNY, M. (2008) Automatic building extraction from DEMs using an object approach and application to the 3D-city modeling. *ISPRS Journal of Photogrammetry and Remote Sensing,* 63 (3)**,** 365-381.

LEBERL, F. & SZABO, J. (2005) Novel Totally Digital Photogrammetric Workflow. Semana Geomatica, 10th August 2005 IGAC-Bogota, Columbia.

LEBERL F. & GRUBER, M. (2003) Flying the new large format digital aerial camera UltraCamD, Photogrammetric weeks Stuttgart 2003, Wichmann Verlag, Heidelberg 2003, pp. 67-76.

LEICA (2009a) http://www.leica.com/, last accessed, December, 2009.

LEICA (2009b) Stereo analyst manual.

LERMA, J. L., VIDAL, J. S. & PORTALE´S, C. (2004) THREE-DIMENSIONAL CITY MODEL VISUALISATION FOR REAL-TIME GUIDED MUSEUM TOURS. *The Photogrammetric Record* 19 (108)**,** 360-374.

LIEBOWITZ, D., CRIMINISI, A. & ZISSERMAN, A. (1999) Creating architectural models from images *Computer Graphics Forum, 18(3): 39–50.*

LORENZ, H. & DÖLLNER, J. (2006) Façade Texture Quality Estimation for Aerial Photography in 3D City Models. *Meeting of the ICA Commission on Visualization and Virtual Environments, Vancouver, WA, June 2006*

MAAS, H. & VOSSELMAN, G. (1999) Two algorithms for extracting building models from raw laser altimetry data. *ISPRS Journal of Photogrammetry & Remote Sensing* 54**,** 153-163.

MADANI, M. (2001) Importance of Digital Photogrammetry for a Complete GIS. 5th Global Spatial Data Infrastructure Conference. Catagena, Columbia. May 21-25, 2001.

MADANI, M. (2004) editor of section 14: photogrammetric applications in Manual of Photogrammetry, fifth edition, American Society for Photogrammetry and Remote Sensing, Maryland, USA. fifth edition ed.

MAYER, H. (1999) Automatic Object Extraction from Aerial Imagery –A Survey Focusing on Buildings. *Computer Vision and Image Understanding, 74(2):138–149*.

MENG, L. & FORBERG, A. (2007) 3D Building Generalisation. IN MACKANESS, W., RUAS, A. AND SARJAKOSKI, T. (Ed.) *Challenges in the Portrayal of Geographic Information: Issues of Generalisation and Multi Scale Representation.* . Elsevier Science Ltd.

MICROSOFT (2009) http://www.microsoft.com/ultracam/default.mspx, last accessed December,2009.

MIKHAIL, E. M., BETHEL, J. S. & MCGLONE, J. C. (2001) *Introduction to modern photogrammetry*, John Wiley and Sons.

MOFFITT, F. & MIKHAIL, E. (1980) *Photogrammetry. Third Edition. New York, Harper & Row Publishers.*

MOSTAFA, M. M. R. & HUTTON, J. (2001) DIRECT POSITIONING AND ORIENTATION SYSTEMS HOW DO THEY WORK? WHAT IS THE ATTAINABLE ACCURACY? *American Society of Photogrammetry and Remote Sensing Annual Meeting.* St. Louis, MO, USA,.

NEX, F. & RINAUDO, F. (2009) NEW INTEGRATION APPROACH OF PHOTOGRAMMETRIC AND LIDAR TECHNIQUES FOR ARCHITECTURAL SURVEYS. IN IN: BRETAR F, P.-D. M., VOSSELMAN G (EDS) LASER SCANNING 2009, IAPRS, VOL. XXXVIII, PART 3/W8 – PARIS, FRANCE, SEPTEMBER 1-2, 2009 (Ed.).

ORTIN, D. & REMONDINO, F. (2008) OCCLUSION-FREE IMAGE GENERATION FOR REALISTIC TEXTURE MAPPING. *ISPRS Congress Beijing 2008*. Beijing, The International Archives of the Photogrammetry, Remote Sensing and Spatial Information Sciences.

ORTIZ, P. & MATAS, M. (2009) EXPERIENCES ABOUT FUSIONING 3D DIGITALIZATION TECHNIQUES FOR CULTURAL HERITAGE DOCUMENTATION IN CÁCERES WALL (SPAIN). IN FABIO REMONDINO, S. E.-H., LORENZO GONZO (Ed.) *3D-ARCH 2009: "3D Virtual Reconstruction and Visualization of Complex Architectures"* Trento, Italy, International Archives of Photogrammetry, Remote Sensing and Spatial Information Sciences Volume XXXVIII-5/W1 ISSN 1682-1777

PAPARODITIS, N., SOUCHON, J.-P., MARTINOTY, G. & PIERROT-DESEILLIGNY, M. (2006) High-end aerial digital cameras and their impact on the automation and quality of the production workflow. *ISPRS Journal of Photogrammetry and Remote Sensing,* 60 (6)**,** 400-412.

PETRIE, G. (2006) Further advances in airborne digital imaging: several new imagers introduced at ASPRS. *GeoInformatics,* 9 (5) July/August 2006**,** 16-23.

PETRIE, G. (2009) Systematic Oblique Aerial Photography Using Multiple Digital Frame cameras *PHOTOGRAMMETRIC ENGINEERING & REMOTE SENSING, February, 2009, pages 102-107*.

PETRIE, G. & WALKER, A. S. (2007) AIRBORNE DIGITAL IMAGING TECHNOLOGY: A NEW OVERVIEW. *The Photogrammetric Record,* 22 (119)**,** 203–225.

PICTOMETRY (2008) pictometry.com, Last accessed November, 2009.

POLLEFEYS, M., KOCH, R., VERGAUWEN, M. & VAN GOOL, L. (2000) Automated reconstruction of 3D scenes from sequences of images. *ISPRS Journal of Photogrammetry and Remote Sensing,* 55 (4)**,** 251-267.

QTAISHAT, K. (2006) Assessing the photogrammetric performance of airborne digital cameras. *IESSG/ Civil Engineering.* Nottingham, The University of Nottingham.

RESSLA, C., HARINGA, A., BRIESEA, C. & ROTTENSTEINERB, F. (2006) Aconcept for adaptive mono-plotting using images and laserscanner data. *Proc. "Symposium of ISPRS Commission III - Photogrammetric Computer Vision - PCV '06", International Archives of the ISPRS XXXVI/3, 20-22 November, Bonn, Germany, p. 1682-1750.*

ROTTENSTEINER, F. (2001) Semi-automatic extraction of buildings based on hybrid adjustment using 3D surface models and management of building data in a TIS, PhD Thesis, Institute of Photogrammetry and Remote Sensing, Vienna, 189 pages

ROTTERNSTEINER, F. & JANSA, J. (2002) Automatic Extraction of Buildings from LiDAR Data and Aerial Images. *International Archives of Photogrammetry and Remote Sensing, Ottawa, Canada, Vol. 34, Part 4, pp. 569-574.*

RUTZINGER, M., ELBERINK, S. O., PU, S. & VOSSELMAN, G. (2009) AUTOMATIC EXTRACTION OF VERTICAL WALLS FROM MOBILE AND AIRBORNE LASER SCANNING DATA. IN IN: BRETAR F, P.-D. M., VOSSELMAN G (EDS) LASER SCANNING 2009, IAPRS, VOL. XXXVIII, PART 3/W8 – PARIS, FRANCE, SEPTEMBER 1-2, 2009 (Ed.).

SANDAU, R., BRAUNECKER, B., DRIESCHER, H., ECKARDT, A., HILBERT, S., HUTTON, J., KIRCHHOFER, W., LITHOPOULOS, E., REULKE, R. & WICKI, S. (2000) Design Prinsiples of the LH Systems ADS40 Airborne Digital Sensor. International Archives of Photogrammetry and Remote Sensing, Vol. 33, Part B1, Amsterdam, Netherlands, pp.258-265.

SCHENK, T. (1999) *Digital Photogrammetry: Volume 1. Ohio: TerraScience.*

SCHILCHER, M., ROSCHLAUB, R. & GUO, Z. (1998a) from 2D GIS to 3D city model Combination of GIS, CAD and animation techniques. ACS'98 Proceedings, Seminar Geographic information systems, 12 - 14 November 1998, Frankfurt, Germany.

SCHILCHER, M., ROSCHLAUB, R. & GUO, Z. (1998b) From 2D GIS to 3D city model using a combination of GIS, CAD and animation techniques. *Proceedings ACS '98, Fachseminar, Geoinformationssystem, 12. - 14. November 1998, Frankfurt, CD ROM.*

SCHNEIDER, S. & GRUBER, M. (2008) RADIOMETRIC QUALITY OF ULTRACAM-X IMAGES. *ISPRS Congress Beijing 2008 Beijing, CHINA, The International Archives of the Photogrammetry, Remote Sensing and Spatial Information Sciences.*

SCHULTZ, S. L., WEST HENRIETTA, N. U., GIUFFRIDA, F. D., HONEOYE FALLS, N. U., GRAY, R. L., CANANDAIGUA, N. U., CHARLES, M. & PITTSFORD, N. U. (2004) Pictometry patent. IN OFFICE, E. P. (Ed.) *European Patent Office.*

SIMMONS, G. & KARBO, N. (2007) Aerial imagery from different angles. *Professional Surveyor,* 27 (5)**,** 18–23.

SINNING-MEISTER, M., GRUEN, A. & DAN, H. (1996) 3D City models for CAAD-supported analysis and design of urban areas. *ISPRS Journal of Photogrammetry & Remote Sensing 51 (1996) 196-208*.

SKALOUD, J. & LEGAT, K. (2008) Theory and reality of direct georeferencing in national coordinates. *ISPRS Journal of Photogrammetry and Remote Sensing,* 63 (2)**,** 272-282.

SMITH, M. (2006) Photogrammetry Handouts. IESSG: The University of Nottingham.

SMITH, M., HAMRUNI, A. & JAMIESON, A. (2009) 3-D urban modelling using airborne oblique and vertical imagery *ISPRS Hannover Workshop 2009, High-Resolution Earth Imaging for Geospatial Information, The International Archives of the Photogrammetry, Remote Sensing and Spatial Information Sciences, Vol. 34, Part XXX.* Hannover, Germany

SMITH, M. J. (1989) A photogrammetric system for archaeological mapping using oblique non-metric photography. *Photogrammetric Record,* 13 (73)**,** 95-105.

SMITH, M. J., KOKKAS, N., HAMRUNI , A. M., CRITCHLEY , D. & JAMIESON, A. (2008) INVESTIGATION INTO THE ORIENTATION OF OBLIQUE AND VERTICAL DIGITAL IMAGES. *EuroCow08.* Barcelona, Spain.

SMITH, M. J., KOKKAS, N. & QTAISHAT, K. S. (2007) Investigation into Self-Calibration methods for the Vexcel UltraCam D Digital Aerial Camera. In: ISPRS Hannover Workshop, High Resolution Earth Imaging for Geospatial Information, 29 May - 1 June. pp. 6.

SMITH, M. J., QTAISHAT, K., PARK, D. & JAMIESON, A. (2005) Initial Results from the Vexcel UltraCam D Digital Aerial Camera. ISPRS Hannover Workshop on High resolution Earth imaging for geospatial information Proceedings, Volume XXXVI Part I/W3 ISSN No. 1682-1777.

SONG, Y. & SHAN, J. (2004) PHOTOREALISTIC BUILDING MODELING AND VISUALIZATION IN 3-D GEOSPATIAL INFORMATION SYSTEM. *XXth ISPRS Congress, Istanbul.* Turkey.

STAMOS, I. (2009) Automated 3D modeling of urban environments IN FABIO REMONDINO, S. E.-H., LORENZO GONZO (Ed.) *3D-ARCH 2009: "3D Virtual Reconstruction and Visualization of Complex Architectures".* Trento, Italy, International Archives of Photogrammetry, Remote Sensing and Spatial Information Sciences.

SUVEG, I. & VOSSELMAN, G. (2004) Reconstruction of 3D building models from aerial images and maps. *ISPRS Journal of Photogrammetry and Remote Sensing,* 58 (3-4)**,** 202-224.

THIEMANN, F. (2004) 3D building generalization. In: Theory 2003, cartographic blocks 26th Volume Koch, W.-G. (Ed.), Dresden 2004. 52-58.

TOYAMA, K., KRUMM, J., BRUMITT, B. & MEYERS, B. (1999) Wallflower: Principles and practice of background maintenance. In: ICCV99, pp. 255–261.

TUNC, E., KARSLI, F. & AYHAN, E. (2004) 3D CITY RECONSTRUCTION BY DIFFERENT TECHNOLOGIES TO MANAGE AND REORGANIZE THE CURRENT SITUATION. *ISPRS Congress* Istanbul, Turket, 12-23 July 2004 Commission 4.

ULM, K. (2005) 3D city models from aerial imagery – Integrating images and the landscape. GEOInformatics, January/February, Vol. 8, pp. 18-21.

VARSHOSAZ, M. (2003) TRUE REALISTIC 3D MODELS OF BUILDINGS IN URBAN AREAS. *WG V/6 International Workshop "Visualization and Animation of Reality-based 3D Models, International Archives of the Photogrammetry, Remote Sensing and Spatial Information Sciences, Vol. XXXIV-5/W10.* Tarasp, Switzerland.

VERMA, V., KUMAR, R. & HSU, S. (2006) 3D Building Detection and Modeling from Aerial LIDAR Data. *Proceedings of the 2006 IEEE Computer Society Conference on Computer Vision and Pattern Recognition (CVPR'06), Washington, DC, USA, 2006, IEEE Computer Society, pp. 2213–2220.*

VEXCEL (2007) Last accessed August, 2007, http://vexcel.com/downloads/photogram/ultracam/whitepapers/Perko. .

VOSSELMAN, G. (2002) Fusion of Laser Scanning Data, Maps,and Aerial Photographs for Building Reconstruction. *IEEE International Geoscience and Remote Sensing Symposium and the 24th Canadian Symposium on Remote Sensing, IGARSS'02,.* Toronto, Canada, June 24-28, 4 pages.

WANG, X., TOTARO, S., TAILLANDIER, F., HANSON, A. & TELLER, S. (2002) Recovering facade texture and microstructure from realworld images. In: Proc. 2nd International Workshop on Texture Analysis and Synthesis, pp. 145-149.

WANG, Y., SCHULTZ, S. & GIUFFRIDA, F. (2008) PICTOMETRY'S PROPRIETARY AIRBORNE DIGITAL IMAGING SYSTEM AND ITS APPLICATION IN 3D CITY MODELLING. *ISPRS Congress Beijing 2008* Beijing, CHINA, The International Archives of the Photogrammetry, Remote Sensing and Spatial Information Sciences.

WEINHAUS, F. & DEVICH, R. (1999) Photogrammetric Texture Mapping onto Planar Polygons *Graphical Models and Image Processing, Volume 61, Number 2, March 1999 , pp. 63-83(21).*

WOLF, P. R. (1983) *Elements of Photogrammetry: With Air Photo Interpretation and Remote Sensing. ,* New York, Second Edition. McGraw Hill.

WOLF, P. R. & DEWITT, B. A. (2000) Elements of Photogrammetry with applications in GIS. third ed., McGraw Hill.

YASTIKLI, N. & JACOBSEN, K. (2005) DIRECT SENSOR ORIENTATION FOR LARGE SCALE MAPPING—POTENTIAL, PROBLEMS, SOLUTIONS. *The Photogrammetric Record 20(111): 274–284 (September 2005)*.

YUAN, X., FU, J., SUN, H. & TOTH, C. (2009) The application of GPS precise point positioning technology in aerial triangulation. *ISPRS Journal of Photogrammetry and Remote Sensing, doi:10.1016/j.isprsjprs.2009.03.006,* In Press, Corrected Proof.

ZEBEDIN, L., KLAUS, A., GRUBER, B. & KARNER, K. (2007) Facade reconstruction from aerial images by multi-view plane sweeping. *In International Archives of the Photogrammetry, Remote Sensing and Spatial Information Sciences, 35-3, 31-36.*

ZHANG, Y., ZHANG, Z., ZHANG, J. & WU, J. (2005) 3D BUILDING MODELLING WITH DIGITAL MAP, LIDAR DATA AND VIDEO IMAGE SEQUENCES. *The Photogrammetric Record,* 20 (111)**,** 285-302.

ZHU, L., ERVING, A., KOISTINEN, K., NUIKKA, M., JUNNILAINEN, H., HEISKA, N. & HAGGRÉN, H. (2008) GEOREFERENCING MULTI-TEMPORAL AND MULTI-SCALE IMAGERY IN PHOTOGRAMMETRY. *ISPRS Congress Beijing 2008, China, The International Archives of the Photogrammetry, Remote Sensing and Spatial Information Sciences. Vol. XXXVII. Part B5*

APPENDICES

Appendix A: Corrections applied to improve measurements on oblique images

According to the Pictometry patent (2004), in order to compensate at least in part for changes in elevation and the resultant inaccuracies in the measurement of and between objects within an oblique image, the image display and analysis software references, as necessary, points within displayed image, for example 104a in figure 3.27, and on surface (31) to a pre-calculated tessellated or faceted ground plane. The tessellated ground plane includes a large number of individual facets, each of which are interconnected to each other and are defined by four vertices having respective elevations. Adjacent pairs of facets share two vertices. Each facet has a respective pitch and slope. The tessellated ground plane is created based upon various data and resources, such as topographical maps, and/or digital raster graphics, survey data, and various other sources. Generally, the geolocation of a point of interest on displayed oblique image is calculated by determining which of facets correspond to that point of interest. Thus, the location of the point of interest is calculated based on the characteristics, i.e., elevation, pitch and slope, of facets rather than based upon a flat or average-elevation ground plane. Error is introduced only in so far as the topography of the surface and the location of the point of interest deviate from the planar surface of the facet within which the point of interest lies. That error is reducible through a bilinear interpolation of the elevation of the point of interest within a particular one of the facets and using that interpolated elevation in the location calculation performed by the software.

Tessellated ground plane is preferably created outside the operation of image display and measurement computer system (user PC) and image display and analysis software. Rather, tessellated ground plane takes the form of a relatively simple data table or look-up table stored within the memory of and/or accessible to the user PC. The computing resources required to calculate the locations of all the vertices of the many facets of a typical ground plane do not

necessarily have to reside within the user PC. Thus, it is compatible for use with and executable by a conventional personal computer without requiring additional computing resources. Calculating tessellated ground plane outside of the user PC enables virtually any level of detail to be incorporated into tessellated ground plane, i.e., the size and/or area covered by or corresponding to each of facets, can be as large or as small as desired, without significantly increasing the calculation time, slowing the operation of, nor significantly increasing the resources required by the user PC and/or EFS. User PC can therefore be a relatively basic and uncomplicated computer system.

The facets are uniform in size throughout a particular displayed image. For example, if the displayed oblique image corresponds to an area that is approximately 750 m wide in the foreground by approximately 900 m deep, the image can be broken into facets that are approximately 50 m^2, thus yielding about 15 facets in width and 18 facets in depth. Alternatively, the size of facets are uniform in terms of the number of pixels contained therein, i.e., each facet is the same number of pixels wide and the same number of pixels deep. Facets in the foreground of oblique image, where the pixel density is greatest, would therefore be dimensionally smaller than facets in the background of the image where pixel density is lowest. Since it is desirable to take most measurements in the foreground of a displayed image where pixel density is greatest, creating facets that are uniform in terms of the number of pixels they contain has the advantages of providing more accurate measurements in the foreground of the displayed image relative to facets that are dimensionally uniform and simplicity of operation within the user PC (Pictometry patent, 2004).

Appendix B: UltraCamD calibration report

VEXCEL

UltraCam D, Serial Number UCD-SU-1-0012

Calibration Report

Geometric Calibration

Camera:	UltraCam D, S/N UCD-SU-1-0012
Manufacturer:	Vexcel Imaging GmbH, A-8010 Graz, Austria
Panchromatic Camera:	ck = 101.400mm
Multispectral Camera:	ck = 101.400mm
Date of Calibration:	July-19-2005
Date of Report:	Sep-04-2006
Camera Revision:	7.0
Revision of Report:	7.0

(2 of 13)

Vexcel Imaging GmbH, Münzgrabenstraße 11, A-8010 GRAZ, www.vexcel.co.at

VEXCEL

UltraCam D, Serial Number UCD-SU-1-0012

Panchromatic Camera

Large Format Panchromatic Output Image

Image Format	long track	67.5mm	7500 pixel
	cross track	103.5mm	11500 pixel
Image Extent		(-33.75, -51.75)mm	(33.75, 51.75)mm
Pixel Size		9.000µm*9.000µm	
Focal Length	ck	101.400mm	± 0.002mm
Principal Point	X_ppa	0.000mm	± 0.002mm
	Y_ppa	0.180mm	± 0.002mm
Lens Distortion	Remaining Distortion less than 0.002mm		

Multispectral Camera

Medium Format Multispectral Output Image
(Upscaled to panchromatic image format)

Image Format	long track	67.5mm	2400 pixel
	cross track	103.5mm	3680 pixel
Image Extent		(-33.75, -51.75)mm	(33.75, 51.75)mm
Pixel Size		28.125µm*28.125µm	
Focal Length	ck	101.400mm	
Principal Point	X_ppa	0.000mm	
	Y_ppa	0.000mm	
Lens Distortion	Remaining Distortion less than 0.002mm		

Vexcel Imaging GmbH, Münzgrabenstraße 11, A-8010 GRAZ, www.vexcel.co.at

Appendix C: Pictometry cameras calibration reports

C1: Calibration report of the vertical camera

Australis Bundle Adjustment Results: Camera Parameters

11 April, 2005 08:54:18

Project: I:\Calibration Images1506_65mm_1523.aus

Adjustment: Free-Network
Number of Points: 144
Number of Images: 9
RMS of Image coords: 0.54 (um)

Results for Camera 1 65mm Lens

Sensor Size Pixel Size (mm)
H 4000 0.009
V 2672 0.009

Camera Variable	Initial Value	Total Adjustment	Final Value	Initial Std. Error	Final Std. Error
C	65.0487	0.00000	65.0487	1.0e+003	5.253e-003 (mm)
XP	-0.3023	-0.00000	-0.3023	1.0e+003	1.860e-003 (mm)
YP	-0.2900	-0.00000	-0.2900	1.0e+003	2.098e-003 (mm)
K1	5.25636e-006	-1.750e-018	5.25636e-006	1.0e+003	3.588e-007
K2	-8.53456e-009	1.120e-020	-8.53456e-009	1.0e+003	1.912e-009
K3	-3.55605e-012	-2.127e-023	-3.55605e-012	1.0e+003	3.080e-012
P1	-1.20301e-024	-6.508e-025	-1.85377e-024	1.0e-016	1.345e-016
P2	-3.05516e-025	-1.708e-025	-4.76335e-025	1.0e-016	1.345e-016
B1	5.97439e-026	3.157e-026	9.13152e-026	1.0e-016	1.345e-016
B2	-3.93228e-026	-2.033e-026	-5.96486e-026	1.0e-016	1.345e-016

Maximum Observational Radial Distance Encountered: 20.3 mm

Exterior Orientation Summary (Xc, Yc, Zc are in project units, rotations are in decimal degrees)

Station	Image	Xc	Yc	Zc	Alpha	Elev.	Roll
1	Image001	-105.66185	-35.50200	220.97177	-75.005914	-59.087075	143.351962
2	Image002	-104.88277	-1.84721	220.19204	-88.707519	-58.302193	178.682798
3	Image003	-98.59550	23.47565	223.13675	-107.605171	-60.575436	126.674604
4	Image004	-0.66437	26.60133	247.05247	-179.441562	-83.526402	-91.441025
5	Image005	-0.44224	-1.85580	261.83711	-116.801511	-89.469800	-154.269894
6	Image006	0.93616	-28.24888	284.86177	-2.425452	-85.840810	2.967723
7	Image007	117.07269	-35.58529	246.57821	76.636437	-61.918992	-144.177935
8	Image008	110.45482	-2.21325	239.06294	89.063839	-60.433001	2.701528
9	Image009	114.61693	20.27511	237.73717	97.079162	-59.545962	68.562064

C2: Calibration report of the oblique cameras 1 and 2 (northern and southern cameras)

Australis Bundle Adjustment Results: Camera Parameters

08 April, 2005 13:02:14

Project: I:\Calibration Images\B\1509B_85mm_1524.aus

Adjustment: Free-Network
Number of Points: 158
Number of Images: 9
RMS of Image coords: 0.43 (um)

Results for Camera 1 85mm Lens

Sensor Size Pixel Size (mm)
H 4000 0.009
V 2672 0.009

Camera Variable	Initial Value	Total Adjustment	Final Value	Initial Std. Error	Final Std. Error
C	84.7629	0.00118	84.7640	1.0e+003	7.952e-003 (mm)
XP	0.0610	-0.00047	0.0606	1.0e+003	2.444e-003 (mm)
YP	-0.0763	-0.00042	-0.0767	1.0e+003	2.642e-003 (mm)
K1	8.77723e-006	-9.459e-009	8.76777e-006	1.0e+003	1.150e-007
K2	-1.18355e-008	3.928e-011	-1.17962e-008	1.0e+003	2.554e-010
K3	-1.58772e-020	-1.566e-020	-3.15386e-020	1.0e-016	1.074e-016
P1	-4.27914e-025	-4.247e-025	-8.52618e-025	1.0e-016	1.074e-016
P2	2.09941e-026	1.717e-026	3.81599e-026	1.0e-016	1.074e-016
B1	3.82952e-026	3.770e-026	7.59938e-026	1.0e-016	1.074e-016
B2	8.77489e-027	9.090e-027	1.78648e-026	1.0e-016	1.074e-016

Maximum Observational Radial Distance Encountered: 20.9 mm

Exterior Orientation Summary (Xc, Yc, Zc are in project units, rotations are in decimal degrees)

Station	Image	Xc	Yc	Zc	Alpha	Elev.	Roll
1	Image001	-147.32363	23.93627	274.99783	-98.209157	-58.203242	133.108791
2	Image002	-146.23120	-1.98388	283.10838	-87.812693	-58.960674	178.167478
3	Image003	-144.38633	-33.64613	285.90887	-79.457687	-58.940695	142.032818
4	Image004	-1.97944	-27.10538	354.06895	-4.319786	-87.270813	5.157652
5	Image005	-6.76976	-0.34470	359.69449	-102.128438	-86.303949	-170.722223
6	Image006	-5.76488	25.10545	361.38869	-173.246100	-84.057760	-99.580624
7	Image007	147.19840	14.11607	302.93235	99.157219	-62.363886	42.377893
8	Image008	146.71790	-0.85289	301.38162	89.163967	-62.204795	-3.663735
9	Image009	152.69823	-32.41288	307.70619	77.202214	-60.739874	-128.462914

C3: Calibration report of the oblique camera 3 (western)

Australis Bundle Adjustment Results: Camera Parameters

12 April, 2005 09:43:00

Project: I:\Calibration Images 1491_85mm_1478.aus

Adjustment: Free-Network
Number of Points: 139
Number of Images: 9
RMS of Image coords: 0.35 (um)

Results for Camera 1 85mm Lens

Sensor Size Pixel Size (mm)
H 4000 0.009
V 2672 0.009

Camera Variable	Initial Value	Total Adjustment	Final Value	Initial Std. Error	Final Std. Error
C	84.8396	-0.00102	84.8386	1.0e+003	4.960e-003 (mm)
XP	0.2547	0.00008	0.2548	1.0e+003	2.183e-003 (mm)
YP	-0.0653	0.00008	-0.0652	1.0e+003	2.207e-003 (mm)
K1	9.71671e-006	1.071e-009	9.71778e-006	1.0e+003	8.916e-008
K2	-1.22029e-008	3.640e-013	-1.22025e-008	1.0e+003	1.950e-010
K3	-2.28637e-020	-2.300e-020	-4.58673e-020	1.0e-016	8.812e-017
P1	-6.05391e-027	-5.509e-027	-1.15634e-026	1.0e-016	8.812e-017
P2	9.69909e-026	9.643e-026	1.93416e-025	1.0e-016	8.812e-017
B1	1.78733e-026	1.786e-026	3.57380e-026	1.0e-016	8.812e-017
B2	-1.75438e-027	-1.847e-027	-3.60111e-027	1.0e-016	8.812e-017

Maximum Observational Radial Distance Encountered: 21.4 mm

Exterior Orientation Summary (Xc, Yc, Zc are in project units, rotations are in decimal degrees)

Station	Image	Xc	Yc	Zc	Alpha	Elev.	Roll
1	Image001	-131.54978	-34.40638	262.57508	-75.402988	-56.806615	139.409841
2	Image002	-129.14385	-1.58493	263.22920	-89.300081	-58.215094	179.653257
3	Image003	-131.19606	32.75214	264.99711	-102.178414	-58.276918	125.485650
4	Image004	-2.00052	27.89340	319.13766	-175.854251	-83.936778	-93.972004
5	Image005	-2.06945	-2.00302	319.03169	-40.069786	-88.885410	130.248746
6	Image006	-2.33819	-28.11620	338.40739	-6.440467	-84.754474	8.335294
7	Image007	125.45753	-36.24244	265.89148	82.185757	-59.327960	-151.359808
8	Image008	124.66243	-1.76543	265.85680	88.686010	-59.512799	0.826319
9	Image009	127.09196	20.71991	266.68678	98.589999	-59.803688	61.159019

C4: Calibration report of the oblique camera 4 (eastern)

Australis Bundle Adjustment Results: Camera Parameters

05 April, 2005 10:23:36

Project: I:\Calibration Images\1507_85mm_1526.aus

Adjustment: Free-Network
Number of Points: 137
Number of Images: 9
RMS of Image coords: 0.36 (um)

Results for Camera 1 85mm Lens

Sensor Size Pixel Size (mm)
H 4000 0.009
V 2672 0.009

Camera Variable	Initial Value	Total Adjustment	Final Value	Initial Std. Error	Final Std. Error
C	84.5753	-0.00000	84.5753	1.0e+003	5.650e-003 (mm)
XP	-0.2303	0.00000	-0.2303	1.0e+003	1.968e-003 (mm)
YP	-0.0447	-0.00000	-0.0447	1.0e+003	2.304e-003 (mm)
K1	1.03885e-005	-1.196e-015	1.03885e-005	1.0e+003	9.927e-008
K2	-1.26498e-008	6.803e-018	-1.26498e-008	1.0e+003	2.200e-010
K3	-1.38591e-020	-1.078e-020	-2.46374e-020	1.0e-016	8.878e-017
P1	2.31686e-025	4.898e-026	2.80668e-025	1.0e-016	8.878e-017
P2	-9.10931e-025	-2.806e-025	-1.19156e-024	1.0e-016	8.878e-017
B1	3.49235e-026	2.325e-026	5.81717e-026	1.0e-016	8.878e-017
B2	-5.68796e-027	-7.187e-027	-1.28754e-026	1.0e-016	8.878e-017

Maximum Observational Radial Distance Encountered: 20.6 mm

Exterior Orientation Summary (Xc, Yc, Zc are in project units, rotations are in decimal degrees)

Station	Image	Xc	Yc	Zc	Alpha	Elev.	Roll
1	Image001	134.91747	-34.76778	281.10846	71.751002	-60.424077	-134.931436
2	Image002	130.30228	-1.57838	276.93819	89.670373	-59.850997	-0.351835
3	Image003	133.29390	20.57651	276.79708	97.200554	-59.356136	63.061113
4	Image004	-1.36145	28.39990	317.79087	-178.264773	-82.997876	-90.952049
5	Image005	-1.45898	-2.25110	317.76171	-53.098300	-89.387888	143.888270
6	Image006	-0.85167	-28.15328	326.77927	-1.739142	-85.080962	2.689255
7	Image007	-138.29909	-36.14009	272.19886	-76.875736	-57.220661	150.107257
8	Image008	-134.14346	-1.51807	272.42077	-89.994387	-58.748769	-179.962016
9	Image009	-127.79059	33.50251	275.25886	-104.239826	-60.751884	119.298110

Appendix D: Quality of multi-ray tie points

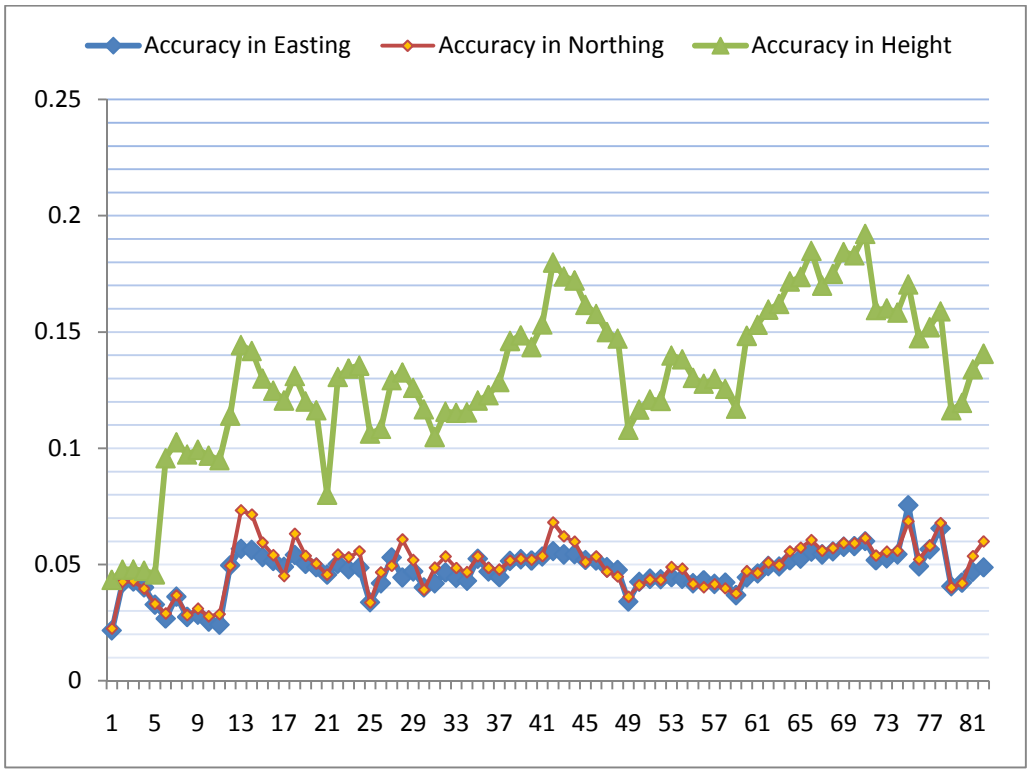

Figure D1: quality of 2-fold tie point of UltraCamD block.

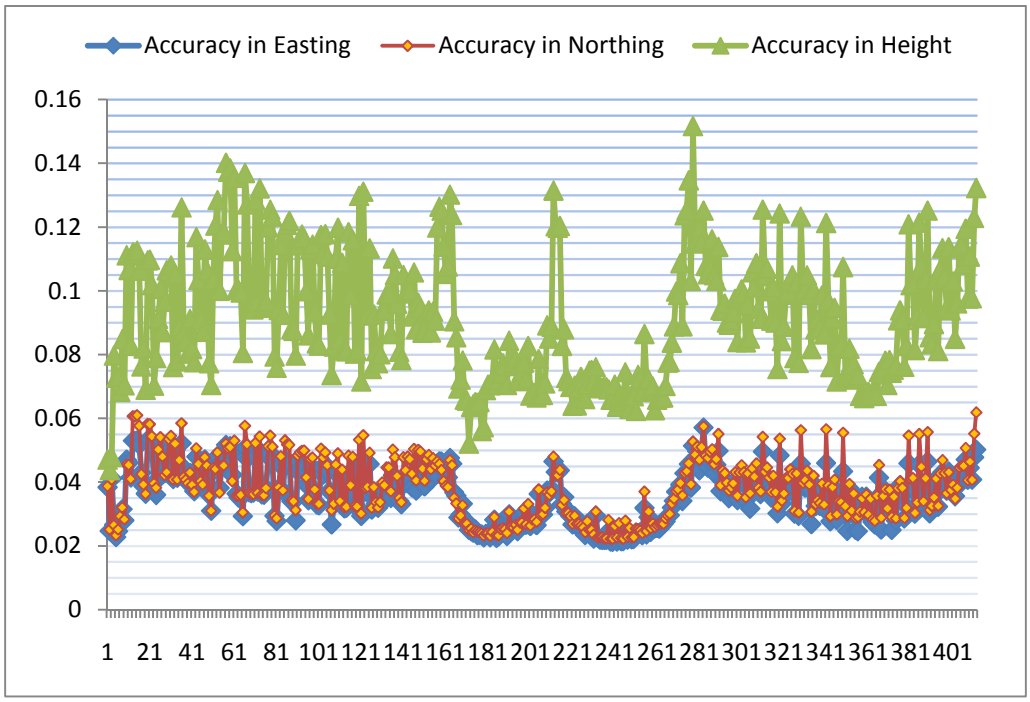

Figure D2: quality of 3-fold tie point of UltraCamD block.

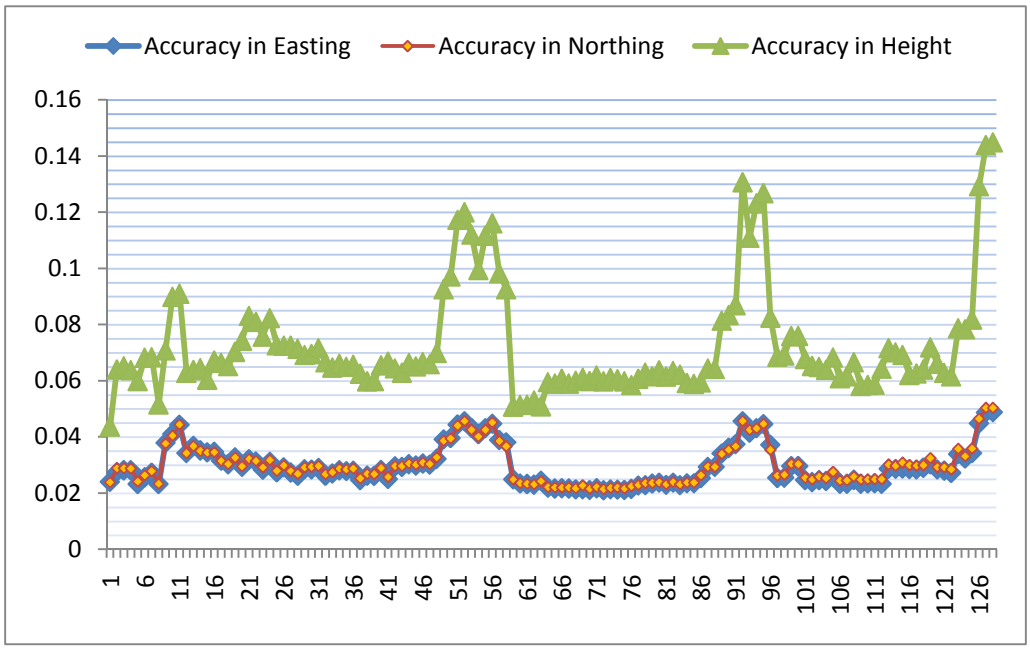

Figure D3: quality of 4-fold tie point of UltraCamD block.

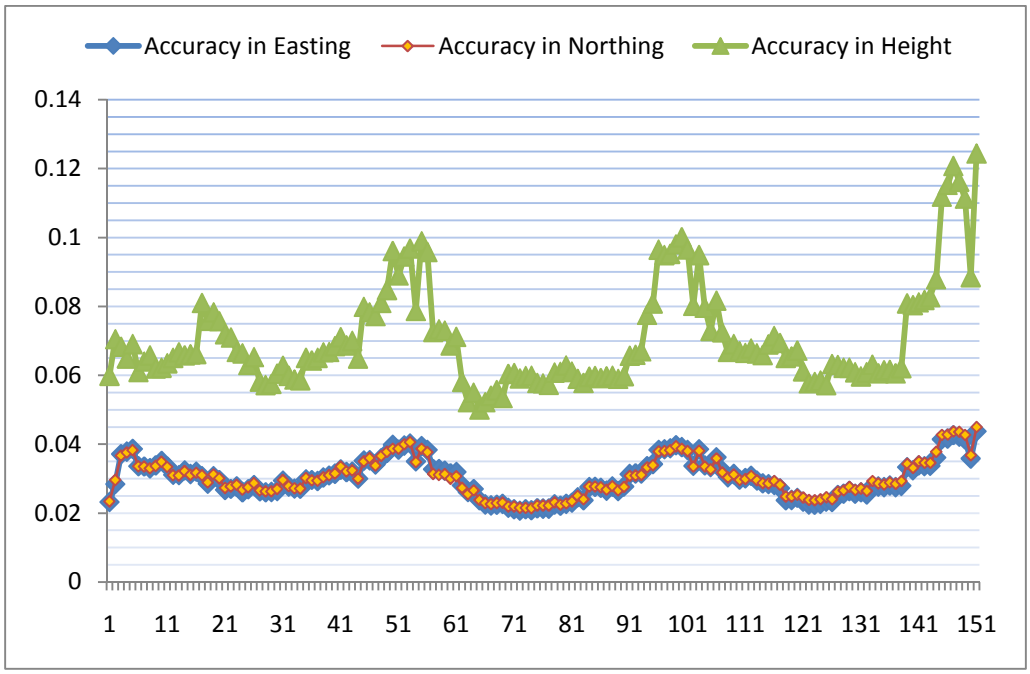

Figure D4: quality of 5-fold tie point of UltraCamD block.

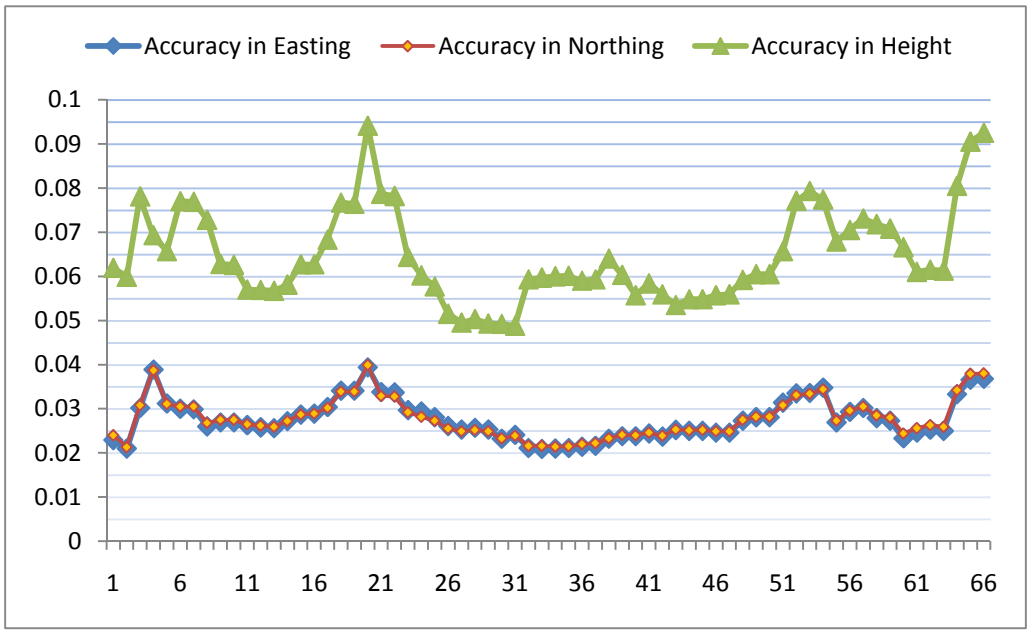

Figure D5: quality of 6-fold tie point of UltraCamD block.

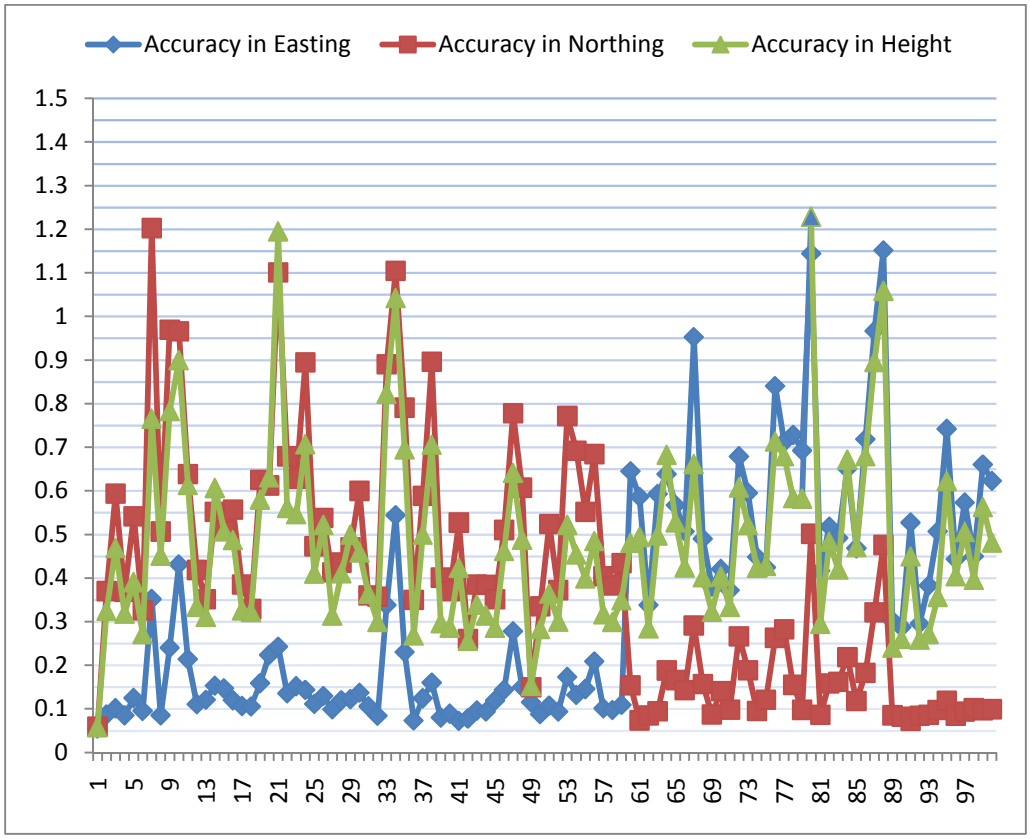

Figure D6: quality of 2-fold tie point of oblique images block.

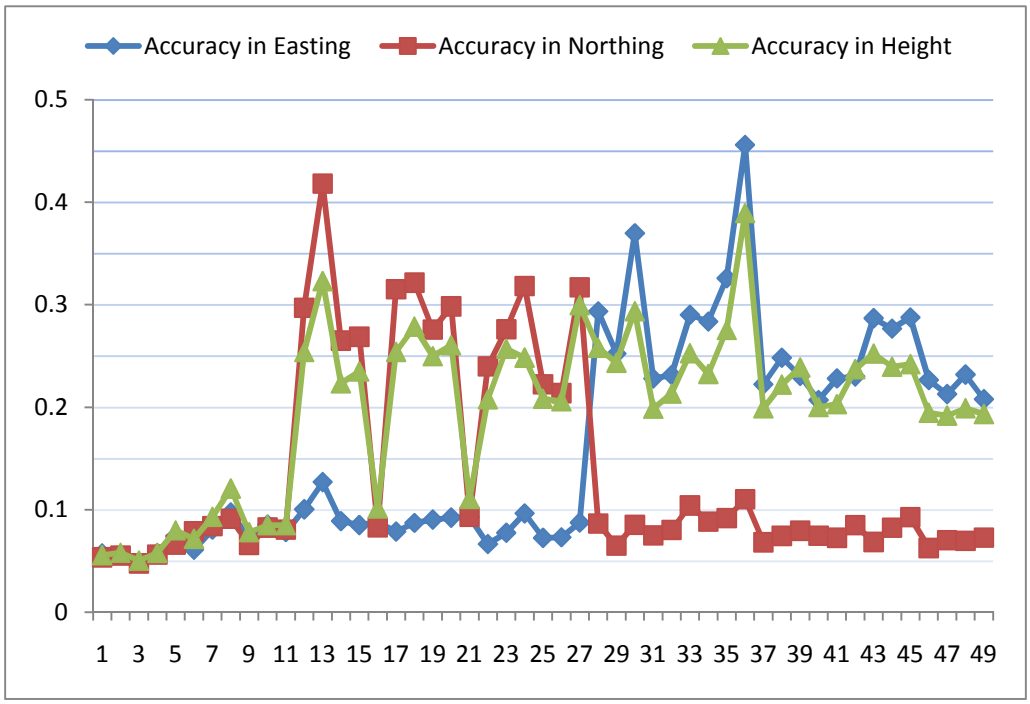

Figure D7: quality of 3-fold tie point of oblique images block.

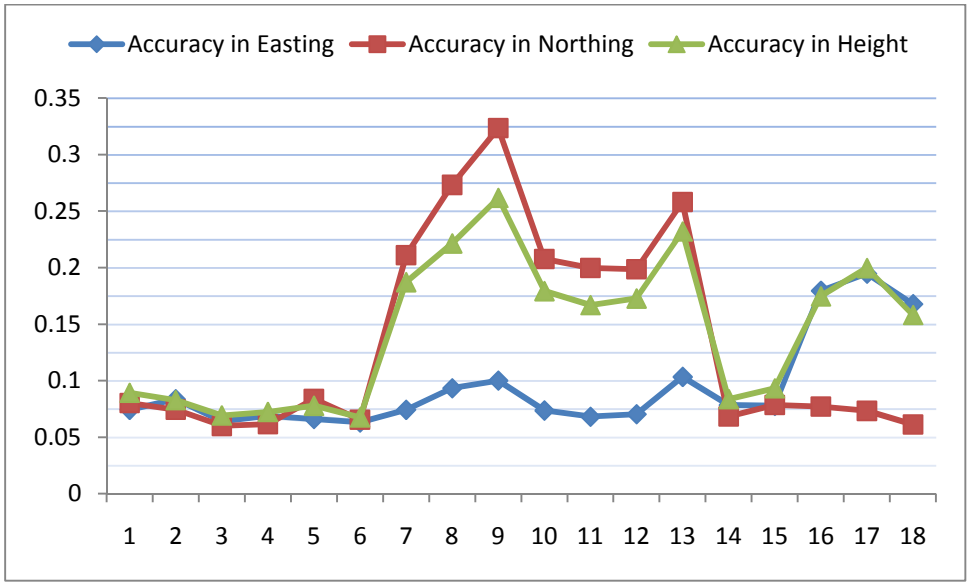

Figure D8: quality of 4-fold tie point of oblique images block.

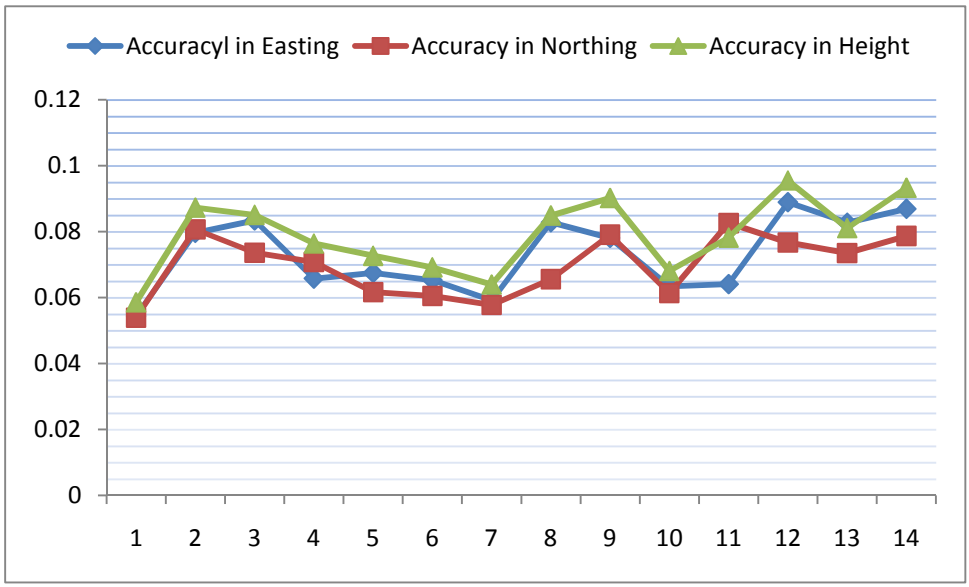

Figure D9: quality of 5-fold tie point of oblique images block.

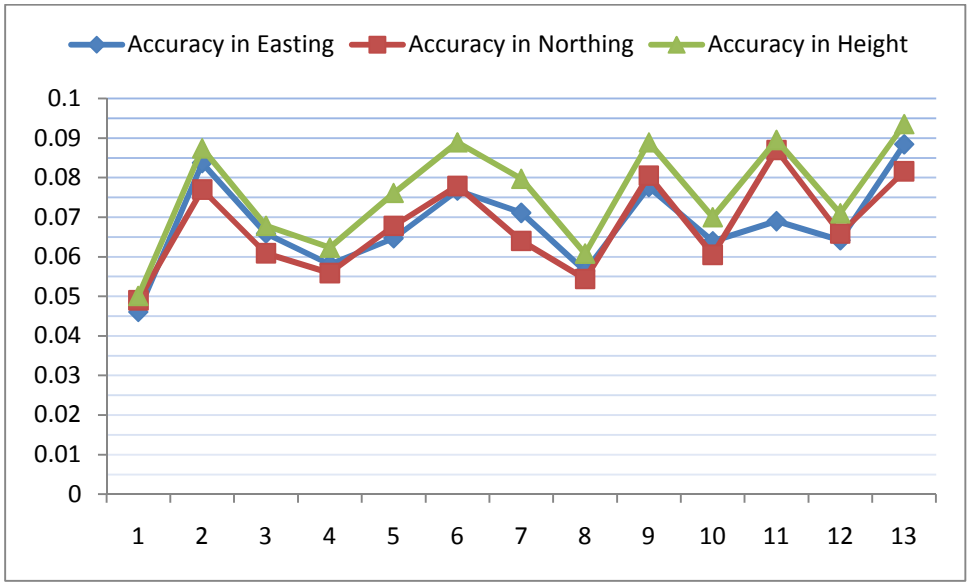

Figure D10: quality of 6-fold tie point of oblique images block.

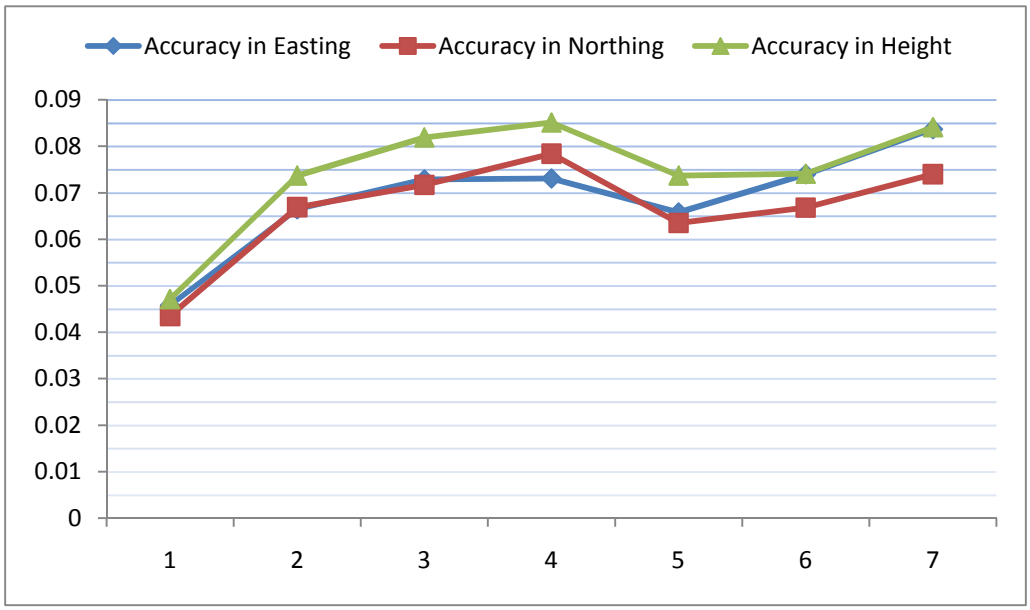

Figure D11: quality of 7-fold tie point of oblique images block.

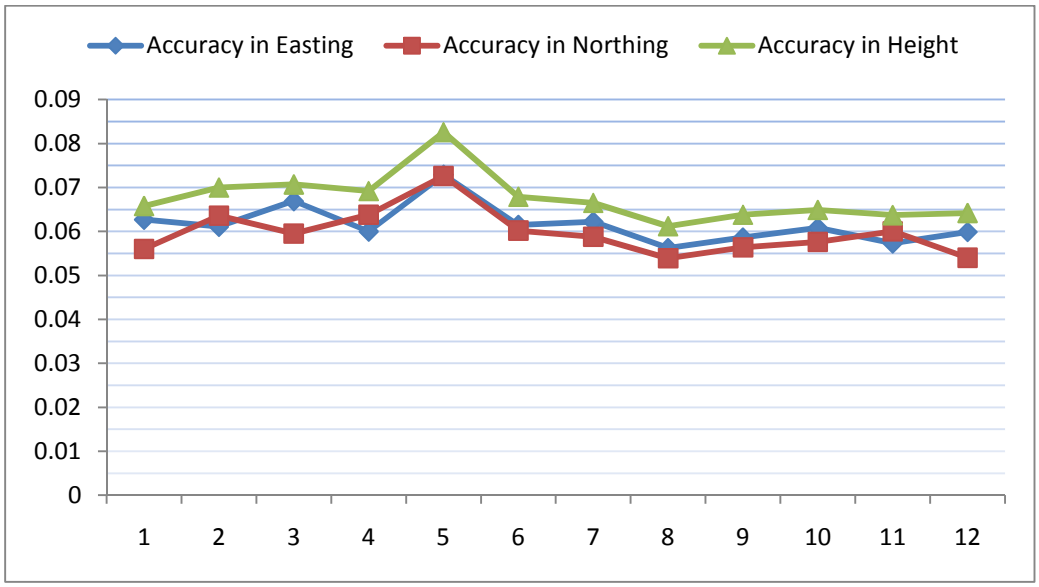

Figure D12: quality of 8-fold tie point of oblique images block.

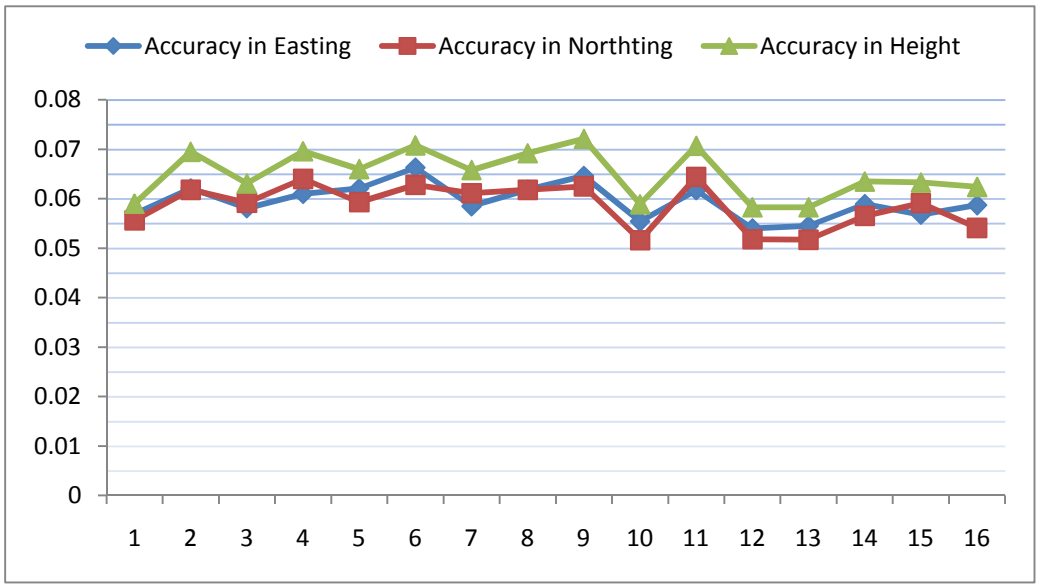

Figure D13: quality of 9 to 14-fold tie point of oblique images block.

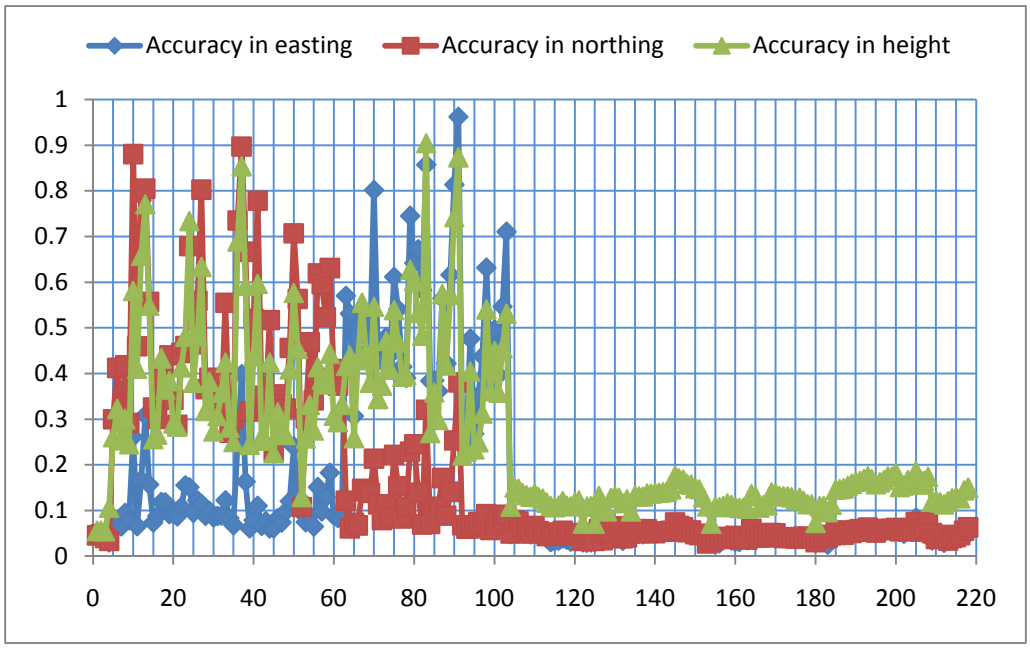

Figure D14: quality of 2-fold tie point of combined UltraCamD and oblique images block.

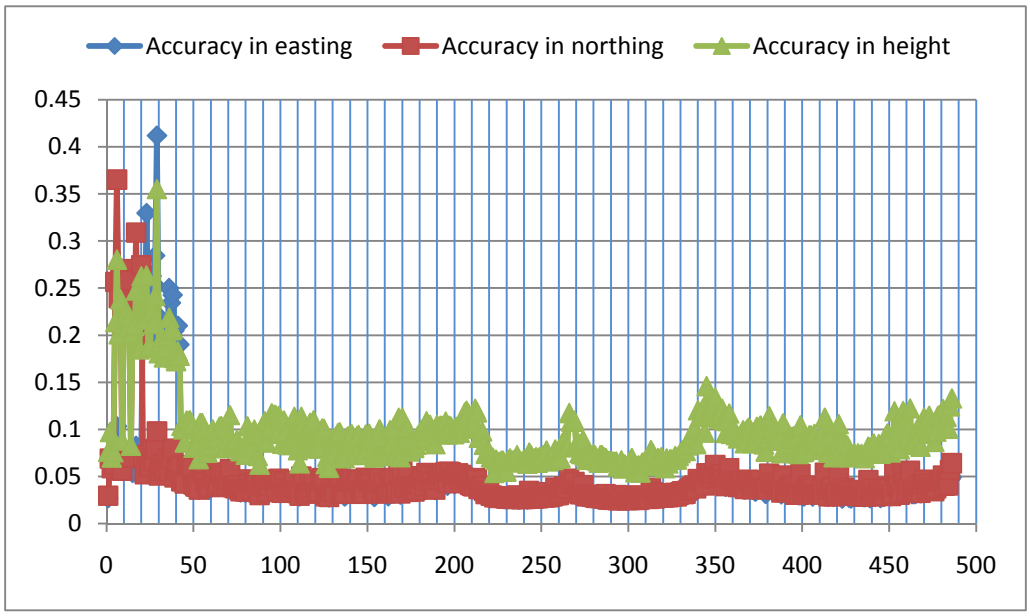

Figure D15: quality of 3-fold tie point of combined UltraCamD and oblique images block.

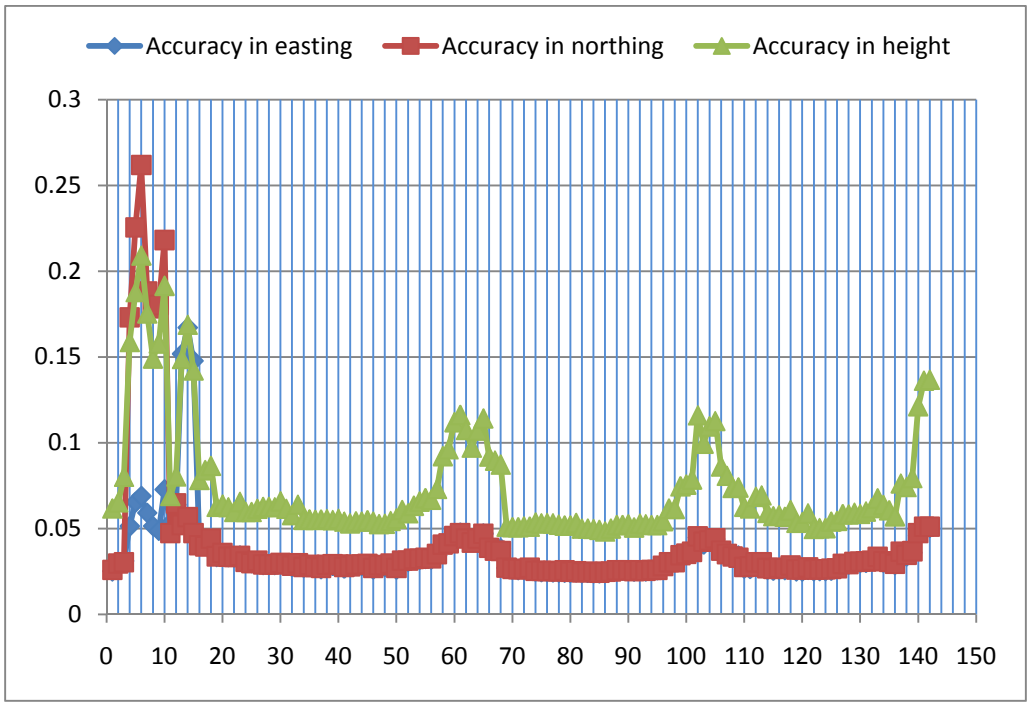

Figure D16: quality of 4-fold tie point of combined UltraCamD and oblique images block.

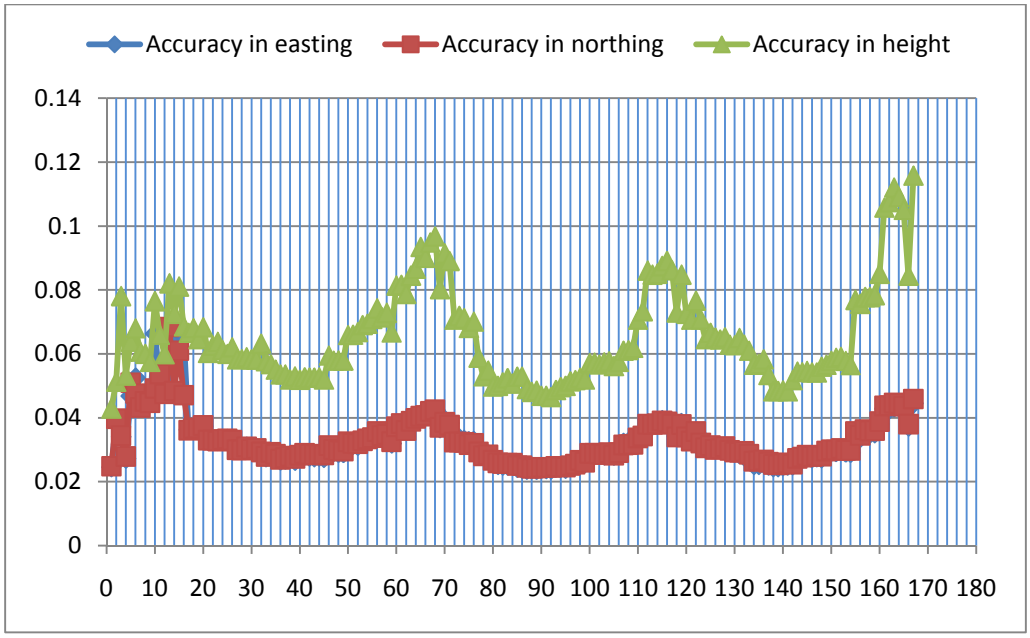

Figure D17: quality of 5-fold tie point of combined UltraCamD and oblique images block.

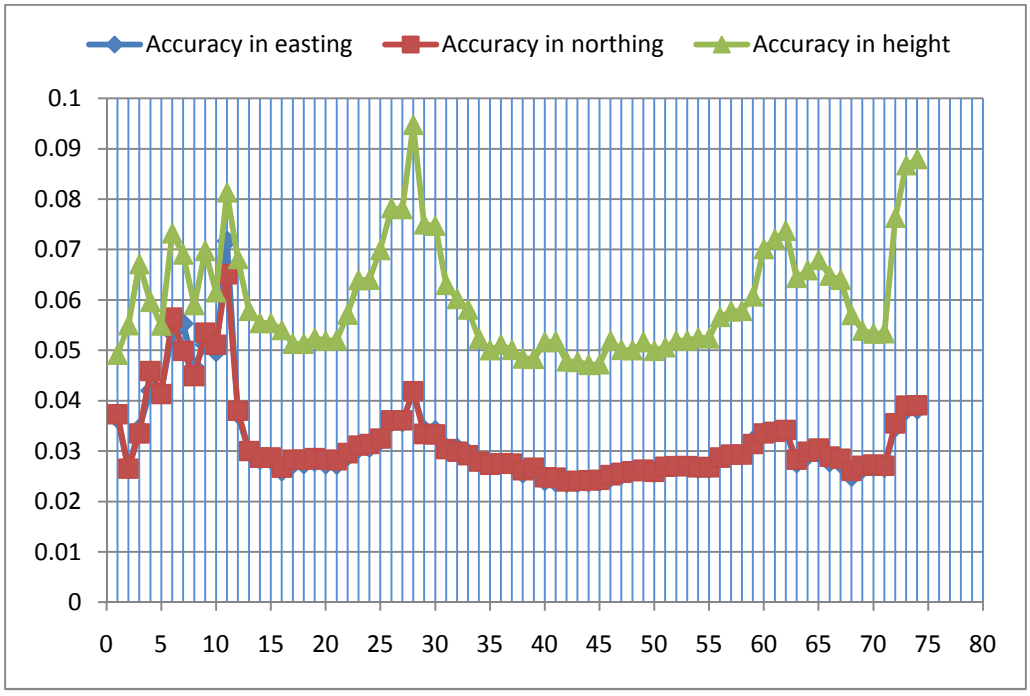

Figure D18: quality of 6-fold tie point of combined UltraCamD and oblique images block.

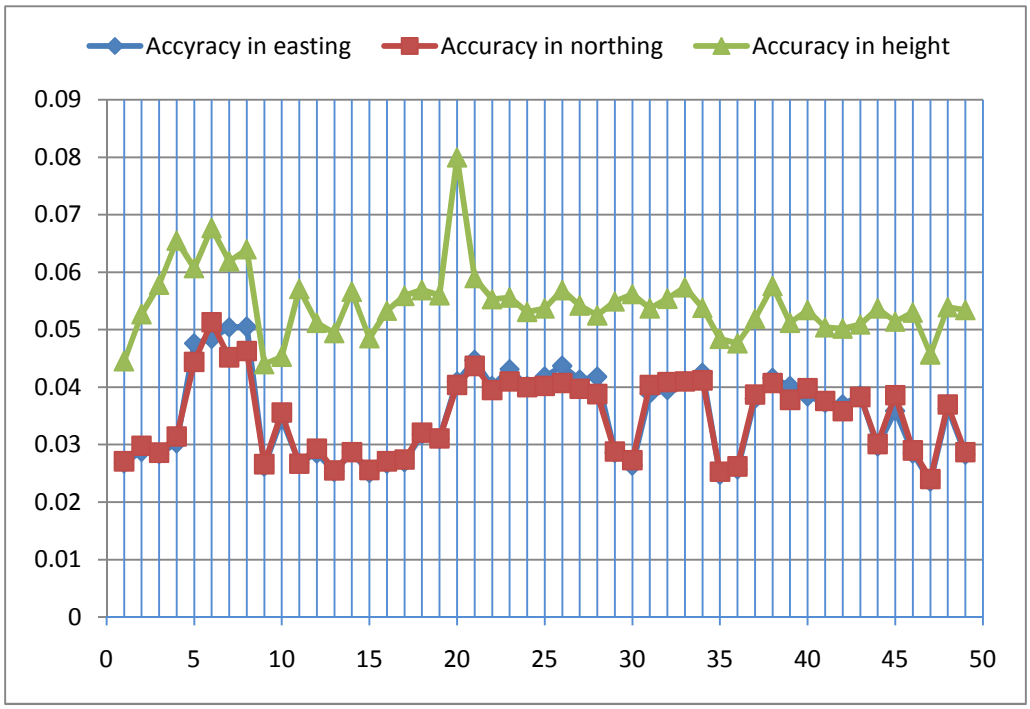

Figure D19: quality of 7 to 14-fold tie point of combined UltraCamD and oblique images block.